

DISSERTATION

MOMENT STABILITY ANALYSIS METHOD FOR DETERMINING SAFETY
FACTORS FOR ARTICULATED CONCRETE BLOCKS

Submitted by

Amanda L. Cox

Department of Civil and Environmental Engineering

In partial fulfillment of the requirements

For the Degree of Doctor of Philosophy

Colorado State University

Fort Collins, Colorado

Summer 2010

COLORADO STATE UNIVERSITY

June 17, 2010

WE HEREBY RECOMMEND THAT THE DISSERTATION PREPARED UNDER OUR SUPERVISION BY AMANDA L. COX ENTITLED MOMENT STABILITY ANALYSIS METHOD FOR DETERMINING SAFETY FACTORS FOR ARTICULATED CONCRETE BLOCKS BE ACCEPTED AS FULFILLING IN PART REQUIREMENTS FOR THE DEGREE OF DOCTOR OF PHILOSOPHY.

Committee on Graduate Work

Evan C. Vlachos

Steven R. Abt

Chester C. Watson

Advisor: Christopher I. Thornton

Department Head: Luis A. Garcia

ABSTRACT OF DISSERTATION
MOMENT STABILITY ANALYSIS METHOD FOR DETERMINING SAFETY
FACTORS FOR ARTICULATED CONCRETE BLOCKS

Articulated concrete block (ACB) revetment systems are widely used for channel lining and embankment protection. Current approaches for prediction of ACB system stability are based on a moment stability analysis and utilize shear stress to account for all hydrodynamic forces. Assumptions utilized in the moment stability analysis derivations were identified and the applicability to channelized and steep-slope conditions was investigated. The assumption of equal lift and drag forces was determined to be non-conservative and the most influential to computed safety factors.

A database of twenty-four tests encompassing both channelized and overtopping conditions was compiled from available data for three ACB systems. Safety factors were computed using the current state-of-the-practice design methodology for each test. The current design methodology proved accurate at predicting the point of instability for five out of the nine total tested ACB installations. A new safety factor design methodology was developed using a moment stability analysis coupled with the computation of hydrodynamic forces using both boundary shear stress and flow velocity. Lift coefficients were calibrated for each of the three ACB systems within the database. Safety factors were computed using the new safety factor method and the calibrated lift

coefficients. The new safety factor design method proved accurate at predicting stability for eight of the nine total tested ACB installations.

Amanda L. Cox
Department of Civil and Environmental Engineering
Colorado State University
Fort Collins, CO 80523
Summer 2010

ACKNOWLEDGMENTS

I would like to express my gratitude to Dr. Christopher Thornton, my advisor, for his dedication and support throughout my graduate studies. Without his professional direction, this dissertation would not have been completed. Additionally, I would like to express my appreciation to my committee members, Dr. Chester Watson, Dr. Steven Abt, and Dr. Evan Vlachos, for the time and expertise they have devoted to my doctoral studies. I would also like to thank Dr. Watson and Dr. Abt for the advice and guidance they have provided. I am humbled to have been given the opportunity to work under the direction of such distinguished advisors with renowned engineering experience.

A very special thank you goes to Gloria Garza for her reviewing and editing of this document. She is much appreciated for her friendship, resourcefulness, and reviewing expertise. Additionally, I would like to acknowledge Nathan Holste for his assistance in developing the database.

I would like to extend great appreciation to my loving husband, Kevin, and amazing daughters, Mariella and Clara. Without Kevin's support, encouragement, continual advice, and most of all love, I would not have completed this dissertation. He is the foundation of my accomplishments. Furthermore, Mariella and Clara's beautiful spirits are my inspiration and have given me the determination to complete my goals. I would also like to thank my father, Jim Lee, and mother, Doris Baker, for their constant support in my educational endeavors. Finally, I would like to sincerely thank all of my family members for their love and encouragement.

TABLE OF CONTENTS

ABSTRACT OF DISSERTATION	iii
ACKNOWLEDGMENTS	v
LIST OF FIGURES	viii
LIST OF TABLES	xi
LIST OF SYMBOLS	xiv
1 INTRODUCTION	1
1.1 Introduction and General Background.....	1
1.2 Research Objectives.....	3
2 LITERATURE REVIEW	5
2.1 Embankment Testing and Analysis of Articulated Concrete Block Systems	5
2.1.1 CIRIA Embankment Testing	6
2.1.2 FHWA Overtopping Research (Clopper and Chen, 1988).....	7
2.1.3 FHWA ACB Stability for Overtopping Flow (Clopper, 1989)	9
2.1.4 Leech <i>et al.</i> (1999b).....	12
2.1.5 Abt <i>et al.</i> (2001).....	14
2.1.6 ASTM D7277 (2008) ACB Test Standard	15
2.1.7 ASTM D7276 (2008) ACB Analysis Standard.....	17
2.2 Factor of Safety Design Methods	23
2.2.1 Stevens and Simons (1971).....	23
2.2.2 Clopper (1991)	35
2.2.3 Julien (1998)	46
2.2.4 Julien and Anthony (2002).....	58
2.2.5 National Concrete Masonry Association (2006).....	63
2.3 Summary	74
3 EXAMINATION OF ASSUMPTIONS IN SAFETY FACTOR DERIVATIONS	75
3.1 Identification of Assumptions	75
3.2 Investigation of Assumptions.....	79
3.3 Summary	89
4 ACB TESTING DATABASE	91
4.1 Introduction	91
4.2 30S Dataset.....	91
4.3 Petraflex Dataset.....	96

4.4	Corps Block Dataset	99
4.5	Summary	101
5	HYDRAULIC ANALYSIS OF ACB TEST DATA	104
5.1	Example ASTM D7276 (2008) Hydraulic Analysis	105
5.2	ASTM D7276 (2008) Hydraulic Analysis of 30S and Petraflex Data	112
5.3	Hydraulic Analysis of Corps Block Data.....	116
5.4	Summary	118
6	EVALUATION OF CLOPPER (1991) AND NCMA (2006) METHODS USING ACB TEST DATA	120
6.1	30S Clopper (1991) and NCMA (2006) <i>SF</i> Analysis.....	123
6.2	Petraflex Clopper (1991) and NCMA (2006) <i>SF</i> Analysis.....	127
6.3	Corps Block Clopper (1991) and NCMA (2006) <i>SF</i> Analysis	130
6.4	Summary	135
7	DERIVATION OF NEW SAFETY FACTOR METHOD.....	136
7.1	Derivation of Submerged Weight Force Components.....	138
7.2	Derivation of Side-slope Angle Perpendicular to Bed Slope.....	141
7.3	Derivation of Safety Factor Equations.....	144
7.3.1	Safety Factor Equation for Rotation about Block Corner (Point M)	146
7.3.2	Safety Factor Equation for Rotation in the Flow Direction (Point P)	151
7.3.3	Safety Factor Equation for Rotation Perpendicular to the Flow Direction (Point O).....	153
7.4	Safety Factor Equation for Blocks on a Channel Bed	154
7.5	Summary	156
8	ANALYSIS OF NEW SAFETY FACTOR EQUATIONS.....	160
8.1	30s New <i>SF</i> Analysis	161
8.2	Petraflex New <i>SF</i> Analysis	163
8.3	Corps Block New <i>SF</i> Analysis	164
8.4	Discussion of Considerations, Recommendations and Limitations	166
8.5	Summary	167
9	CONCLUSIONS AND RECOMMENDATIONS	168
9.1	Overview	168
9.2	Conclusions	171
9.3	Research Recommendations	172
	REFERENCES	174
	APPENDIX A HYDRAULIC DATA FROM CLOPPER AND CHEN (1988)	177
	APPENDIX B ACB BLOCK DIMENSIONS AND PHYSICAL PROPERTIES.....	206
	APPENDIX C HYDRAULIC DATA FOR CSU TESTING	210

LIST OF FIGURES

Figure 1.1: Sketches of an ACB Mat and Individual Blocks.....	2
Figure 2.1: Limiting Velocity versus Flow Duration for Plain and Reinforced Grass (adapted from Hewlett <i>et al.</i> (1987)).....	7
Figure 2.2: Sketches of the Five ACB Systems Tested during the Clopper (1989) FHWA Research (adapted from Clopper (1989)).....	11
Figure 2.3: Sketch of ASTM D7277 (2008) Test Setup.....	15
Figure 2.4: Flow Chart of Step-forewater Analysis Method (adapted from ASTM D7276 (2008))	20
Figure 2.5: Sketch of Variables used in Momentum Shear-stress Equation (adapted from ASTM D7276 (2008)).	22
Figure 2.6: Force Diagrams (adapted from Stevens and Simons (1971))	25
Figure 2.7: Force Diagrams (adapted from Clopper (1991)).....	37
Figure 2.8: Force Diagrams (adapted from Julien (1998))	47
Figure 2.9: Force Diagrams (adapted from Julien and Anthony (2002))	60
Figure 2.10: Force Diagrams (adapted from NCMA (2006)).....	65
Figure 3.1: Potential Relationships between the Stability Number and the Boundary Shear Stress to Critical Shear-stress Ratio	76
Figure 3.2: Calculated Safety Factors for Varying Shear Stress.....	81
Figure 3.3: Calculated Safety Factors for Varying Bed Slopes	81
Figure 3.4: Calculated Safety Factors for Varying Side Slopes.....	82
Figure 3.5: Comparison of Safety Factors without the Assumption of the Relationship between Stability Number and Shear Stress	83
Figure 3.6: Safety Factor Comparison with 10% Non-conservative Critical Shear Stress	84
Figure 3.7: Safety Factor Comparison without Trigonometric Simplifications	85
Figure 3.8: Safety Factor Comparison with β Equal to 48.3°	86
Figure 3.9: Safety Factor Comparison Using the Block Height for ℓ_3	87
Figure 3.10: Safety Factor Comparison without the Assumption of Equal Lift and Drag Forces (lift coefficient equal to 0.045)	88
Figure 3.11: Lift Force and Drag Force Relationship to Velocity	88

Figure 4.1: Photograph of Installed 30S Blocks	92
Figure 4.2: Photograph of Installed Petraflex Blocks.....	96
Figure 4.3: Photograph of Corps Blocks Installation.....	99
Figure 5.1: Comparison of Measured Flow Depths to Best-fit WSP	106
Figure 5.2: Flow Velocity and Shear Stress versus Horizontal Station.....	111
Figure 5.3: Energy Grade Line and Hydraulic Grade Line versus Horizontal Station	112
Figure 5.4: Comparison of Shear Stresses Computed from ASTM D7276 (2008) to Shear Stresses Reported in Clopper and Chen (1988).....	115
Figure 5.5: Percent Difference between ASTM D7276 (2008) Shear Stresses and Reported Values from Clopper and Chen (1988) versus Overtopping Flow Depth	115
Figure 6.1: 30S <i>SF</i> Computed from Clopper (1991) and NCMA (2006) Method with $\tau_c = 13.5 \text{ lbs/ft}^2$ Calibrated from Clopper and Chen (1988) Data with ASTM D7276 (2008) Analysis.....	126
Figure 6.2: 30S <i>SF</i> Computed from Clopper (1991) and NCMA (2006) Method with $\tau_c = 4.5 \text{ lbs/ft}^2$ Calibrated from CSU Data at 0.230 Embankment Slope	126
Figure 6.3: 30S <i>SF</i> Computed from Clopper (1991) and NCMA (2006) Method with $\tau_c = 4.7 \text{ lbs/ft}^2$ Calibrated from CSU Data at 0.431 Embankment Slope	127
Figure 6.4: Petraflex <i>SF</i> Computed from Clopper (1991) and NCMA (2006) Method with $\tau_c = 8.6 \text{ lbs/ft}^2$ Calibrated from Clopper and Chen (1988) Data and ASTM D7276 (2008) Analysis	129
Figure 6.5: Petraflex <i>SF</i> Computed from Clopper (1991) and NCMA (2006) Method with $\tau_c = 5.7 \text{ lbs/ft}^2$ Calibrated from CSU Petraflex Data.....	129
Figure 6.6: Corps Block <i>SF</i> Computed from Clopper (1991) and NCMA (2006) Methods with $\tau_c = 3.7 \text{ lbs/ft}^2$ Calibrated from 0.200 ft/ft Bed-slope Data.....	134
Figure 6.7: Corps Block <i>SF</i> Computed from Clopper (1991) and NCMA (2006) Methods with $\tau_c = 2.2 \text{ lbs/ft}^2$ Calibrated from 0.143 ft/ft Bed-slope Data.....	134
Figure 6.8: Corps Block <i>SF</i> Computed from Clopper (1991) and NCMA (2006) Methods with $\tau_c = 2.9 \text{ lbs/ft}^2$ Calibrated from Channelized Corps Data.....	135
Figure 7.1: Coordinate System for Factor of Safety Equation Derivations.....	137
Figure 7.2: View of Block Normal to Side-slope Plane with Identified Pivot Points	137
Figure 7.3: Weight Force Components Normal and Perpendicular to the Direction of the Bed Slope.....	139

Figure 7.4: Channel Cross Section Normal to the Bed-slope View	140
Figure 7.5: Definition of θ_2	141
Figure 7.6: Cross-section V-V' View (vertical).....	143
Figure 7.7: Cross-section N-N' View (normal to the bed slope)	143
Figure 7.8: Channel Profile View Including Lengths O and O' for θ_1 and θ_2 , Respectively.....	144
Figure 7.9: View of Block Normal to Side-slope Plane with Identified Cross- section A-A' and Angle β	147
Figure 7.10: View of Block Normal to Side-slope Plane with Identified Force Components	148
Figure 7.11: Free-body Diagram for Rotation about Point M	149
Figure 7.12: Free-body Diagram for Rotation about Point P.....	152
Figure 7.13: Free-body Diagram for Rotation about Point O	154
Figure 8.1: 30S SF Computed from the New SF Method with $C_L = 0.0972$ Calibrated from CSU 30S 0.230 ft/ft Bed-slope Data.....	162
Figure 8.2: Petraflex SF Computed from the New SF Method with $C_L = 0.0207$ Calibrated from Clopper and Chen (1988) Data and ASTM D7276 (2008) Analysis.....	164
Figure 8.3: Corps Block SF Computed from the New SF Method with $C_L = 0.115$ Calibrated from Channel Data.....	166
Figure A.1: FHWA Petraflex 4.0-ft Overtopping Water-surface Profile (Clopper and Chen, 1988).....	180
Figure A.2: FHWA 30S 1.0-ft Overtopping Water-surface Profile (Clopper and Chen, 1988)	187
Figure A.3: FHWA 30S 2.0-ft Overtopping Water-surface Profile (Clopper and Chen, 1988)	196
Figure A.4: FHWA 30S 4.0-ft Overtopping Water-surface Profile (Clopper and Chen, 1988)	202
Figure A.5: FHWA 30S 96-cfs Overtopping Water-surface Profile (Clopper and Chen, 1988)	205
Figure B.1: 30S Block Dimensions and Physical Properties	207
Figure B.2: Petraflex Block Dimensions and Physical Properties	208
Figure B.3: Corps Block Dimensions and Physical Properties.....	209

LIST OF TABLES

Table 2.1: Limiting Values of Shear Stress Reported in Clopper and Chen (1988)	9
Table 2.2: Critical Flow-velocity and Shear-stress Values Reported in Clopper (1989)	12
Table 2.3: Safety Factor Calculation Method According to Stevens and Simons (1971)	34
Table 2.4: Safety Factor Calculation Method According to Clopper (1991)	46
Table 2.5: Safety Factor Calculation Method According to Julien (1998).....	57
Table 2.6: Safety Factor Calculation Method According to Julien and Anthony (2002)	63
Table 2.7: Safety Factor Calculation Method According to the NCMA (2006).....	73
Table 3.1: Summary of the Sensitivity of Assumptions with Respect to the Example	89
Table 4.1: Hydraulic Results for 30S FHWA Testing Reported in Clopper and Chen (1988)	93
Table 4.2: Robeson <i>et al.</i> (2002) 30S Testing.....	94
Table 4.3: 2009 CSU 30S Testing	94
Table 4.4: Combined 30S Testing Dataset	95
Table 4.5: Hydraulic Results for Petraflex FHWA Testing Reported in Clopper and Chen (1988).....	97
Table 4.6: Robeson <i>et al.</i> (2002) Petraflex Testing	98
Table 4.7: Combined Petraflex Testing Dataset.....	98
Table 4.8: Corps Block Overtopping Testing Data	100
Table 4.9: Corps Block Channelized Testing Data	101
Table 4.10: Entire ACB Database	102
Table 5.1: Hydraulic Data for CSU Petraflex Test (Robeson <i>et al.</i> , 2002) on 0.501 Bed Slope at 10.0 cfs (8-21-2000).....	105
Table 5.2: Water-surface Profile Data and Computed Hydraulics for Optimal Manning's n (0.020).....	107
Table 5.3: ASTM D7276 (2008) Hydraulic Results for 30S Testing.....	114
Table 5.4: ASTM D7276 (2008) Hydraulic Results for Petraflex Testing.....	114

Table 5.5: Results of the Corps Block Hydraulic Analysis	118
Table 5.6: Hydraulic Analysis Results for ACB Database	119
Table 6.1: Computed Critical Shear-stress Values for the 30S on a Horizontal Plane	123
Table 6.2: Computed 30S <i>SF</i> for Clopper (1991) and NCMA (2006) Method.....	125
Table 6.3: Computed Critical Shear-stress Values for the Petraflex on a Horizontal Plane.....	127
Table 6.4: Computed Petraflex <i>SF</i> for Clopper (1991) and NCMA (2006) Method.....	128
Table 6.5: Computed Critical Shear-stress Values for the Corps Block on a Horizontal Plane.....	130
Table 6.6: Computed Corps Block <i>SF</i> for Overtopping Tests for Clopper (1991) and NCMA (2006) Method	132
Table 6.7: Computed Corps Block <i>SF</i> for Channel Tests for Clopper (1991) Method	132
Table 6.8: Computed Corps Block <i>SF</i> for Channel Tests for NCMA (2006) Method	133
Table 7.1. Summary of New Safety Factor Equations	158
Table 8.1: Computed 30S <i>SF</i> for the New <i>SF</i> Method.....	162
Table 8.2: Computed Petraflex <i>SF</i> for the New <i>SF</i> Method.....	164
Table 8.3: Computed Corps Block <i>SF</i> for the New <i>SF</i> Method	165
Table A.1: Available Data for FHWA Petraflex Testing (Clopper and Chen, 1988)	178
Table A.2: Available Velocity Data for FHWA Petraflex Testing (Clopper and Chen, 1988)	179
Table A.3: FHWA 30S 1.0-ft Overtopping Data (Clopper and Chen, 1988)	181
Table A.4: FHWA 30S 1.0-ft Overtopping Velocity Data (Clopper and Chen, 1988)	186
Table A.5: FHWA 30S 2.0-ft Overtopping Data (Clopper and Chen, 1988)	188
Table A.6: FHWA 30S 2.0-ft Overtopping Velocity Data (Clopper and Chen, 1988)	193
Table A.7: FHWA 30S 4.0-ft Overtopping Data (Clopper and Chen, 1988)	197
Table A.8: FHWA 30S 4.0-ft Overtopping Velocity Data (Clopper and Chen, 1988)	200
Table A.9: FHWA 30S 96-cfs Overtopping Data (Clopper and Chen, 1988).....	203
Table A.10: FHWA 30S 96-cfs Overtopping Velocity Data (Clopper and Chen, 1988)	204
Table C.1: Hydraulic Data for CSU 30S Test (Robeson <i>et al.</i> , 2002) on 0.499 Bed Slope at 10.0 cfs (8-11-2000)	211

Table C.2: Hydraulic Data for CSU 30S Test on 0.431 Bed Slope at 8.0 cfs (6-25-2009)	211
Table C.3: Hydraulic Data for CSU 30S Test on 0.431 Bed Slope at 12.0 cfs (6-25-2009)	212
Table C.4: Hydraulic Data for CSU 30S Test on 0.230 Bed Slope at 10.0 cfs (6-14-2009)	213
Table C.5: Hydraulic Data for CSU 30S Test on 0.230 Bed Slope at 20.0 cfs (6-15-2009)	214
Table C.6: Hydraulic Data for CSU 30S Test on 0.230 Bed Slope at 30.0 cfs (6-15-2009)	215
Table C.7: Hydraulic Data for CSU Petraflex Test (Robeson <i>et al.</i> , 2002) on 0.501 Bed Slope at 10.0 cfs (8-21-2000).....	216
Table C.8: Hydraulic Data for CSU 30S Test (Robeson <i>et al.</i> , 2002) on 0.501 Bed Slope at 28.4 cfs (8-21-2000)	216

LIST OF SYMBOLS

a_θ	=	coefficient of the weight force acting in the direction normal to the side-slope plane
A-A	=	cross section along particle rotation path
A-A'	=	cross section along particle rotation path
A	=	cross-section flow area (ft ²)
A	=	length adjacent of angles θ_1 and θ_2
A_B	=	block area parallel to direction of flow (ft ²)
A_N	=	area of the particle normal to the direction of flow (ft ²)
b	=	block width normal to the flow direction (ft)
C_D	=	drag force coefficient
C_L	=	lift force coefficient
d	=	flow depth (ft)
d_m	=	maximum flow depth at uniform flow (ft)
d_s	=	particle diameter (ft)
f	=	Darcy-Weisbach friction factor
F_D	=	drag force (lbs)
F_D'	=	additional drag force caused by block protrusion (lbs)
F_L	=	lift force (lbs)

F_L'	=	additional lift force caused by block protrusion (lbs)
F_S	=	submerged weight of the particle (lbs)
g	=	acceleration due to gravity (ft/s ²)
G_P	=	specific weight of Particle P
h_1	=	upstream water-surface elevations at station 1 (ft)
h_2	=	downstream water-surface elevations at station 2 (ft)
h_i	=	water-surface elevation at station i (ft)
h_{obs}	=	observed water-surface elevation at station i_i (ft)
h_{pred}	=	predicted water-surface elevation at station i_i (ft)
H	=	hypotenuse of right triangle created by θ_1
H'	=	hypotenuse of right triangle created by θ_2
i_1	=	initial station for analysis
i_n	=	ending station for analysis
K_u	=	units conversion coefficient, equal to 1.486 for U.S. Customary Units and 1.0 for SI units
ℓ_1	=	moment arm for submerged weight force component parallel to the embankment plane (ft)
ℓ_1'	=	moment arm for submerged weight force component within the plane normal to Cross-section A-A (ft)
ℓ_2	=	moment arm for submerged weight force component normal to the side-slope plane (ft)
$\ell_{2U}, \ell_{3U}, \ell_{4U}$	=	moment arms for the untested block (ft)

$\ell_{2T}, \ell_{3T}, \ell_{4T}$	=	moment arms for the tested block (ft)
ℓ_3	=	moment arm for the drag force component along the path of motion (ft)
ℓ_3'	=	moment arm for the drag force component within the plane normal to Cross-section A-A (ft)
ℓ_4	=	moment arm for the lift force (ft)
ℓ_n	=	block length normal to the bed slope (ft)
ℓ_p	=	block length parallel to the bed slope (ft)
L	=	length of control volume along the embankment (ft)
L	=	embankment length (ft)
M	=	lift force variable grouping
n	=	Manning's resistance coefficient
N	=	drag force variable grouping
N-N'	=	cross-section normal to the bed slope
O	=	length opposite of angle θ_1
O'	=	length opposite of angle θ_2
P	=	wetted (roughened) perimeter (ft)
Particle P	=	cohesionless particle resting on a channel side slope
Point M	=	rotation point about the block corner
Point O	=	rotation point about the block edge laterally into the channel
Point P	=	rotation point about the block edge in the downstream direction
q	=	unit discharge (ft ² /s)

Q	=	discharge (cfs)
$Q_{p,n}$	=	continuity discharge (cfs)
R	=	hydraulic radius (ft)
S_0	=	embankment slope (ft/ft)
S_f	=	slope of the energy grade line (friction slope) (ft/ft)
S_{f1}	=	upstream friction slope at station 1 (ft/ft)
S_{f2}	=	downstream friction slope at station 2 (ft/ft)
S_{fi}	=	friction slope at station i (ft/ft)
SF	=	factor of safety
SF_{BED}	=	safety factor for rotation of a block on the channel bed
SF_M	=	safety factor for rotation about block corner (Point M)
SF_O	=	safety factor for rotation about Point O
SF_P	=	safety factor for rotation of a block on the channel bed
v_1	=	flow velocity at upstream end of control volume at station 1 (ft/s)
v_2	=	flow velocity at downstream end of control volume at station 2 (ft/s)
V	=	flow velocity (ft/s)
$V-V'$	=	vertical cross section
V_i	=	flow velocity at station i (ft/s)
V_m	=	maximum velocity at uniform flow (ft/s)
$V_{p,n}$	=	average of point flow velocities collected at 20%, 60%, and 80% of flow depth (ft/s)
w	=	width of the projecting surface normal to the direction of flow (ft)

W_S	=	block submerged weight (lbs)
W_{ST}	=	submerged weight of the tested blocks (lbs)
W_{SU}	=	submerged weight of the untested blocks (lbs)
W_{SX}	=	block submerged weight force component parallel to the side-slope plane along the x axis (lbs)
W_{SY}	=	block submerged weight force component normal to the side-slope plane along the y axis (lbs)
W_{SZ}	=	block submerged weight force component parallel to the side-slope plane along the z axis (lbs)
y	=	flow depth measured perpendicular to embankment (ft)
y_1	=	flow depth at upstream end of control volume (ft)
y_2	=	flow depth at downstream end of control volume (ft)
y_i	=	flow depth at station i (perpendicular to the embankment) (ft)
z	=	side slope (ft/ft)
z_i	=	bed elevation at station i (ft)
<i>Greek</i>		
α	=	bed-slope angle
β	=	angle of particle or block rotation measured in the side-slope plane (radians)
γ	=	unit weight of water (lbs/ft ³)
δ	=	angle between the drag force and the particle or block rotation path measured in the side-slope plane (radians)

ΔZ	= height of the projecting surface (block protrusion) normal to the direction of flow (ft)
λ	= angle between horizontal and the streamline velocity vector measured in the side-slope plane (radians)
η	= stability number (Stevens and Simons, 1971)
η'	= stability number for particles or blocks on a side slope (Stevens and Simons, 1971)
η_0	= stability number (Julien, 1998; Julien and Anthony, 2002)
η_1	= stability number for particles on a side slope (Julien, 1998; Julien and Anthony, 2002)
θ	= resulting angle of the combined submerged weight force components acting in the side-slope plane (radians) (Julien, 1998; Julien and Anthony, 2002)
θ	= side-slope angle (radians) (Stevens and Simons, 1971)
θ_0	= bed-slope angle (radians)
θ_1	= side-slope angle measured from a vertical cross section (radians)
θ_2	= side-slope angle measured perpendicular to the bed-slope plane (radians)
θ_U	= untested bed-slope angle (radians)
θ_T	= tested bed-slope angle (radians)
ξ	= optimizing variable for determining best-fit Manning's n (ft)
ρ	= density of water (slugs/ft ³)

τ_0	=	boundary shear stress (lbs/ft ²)
τ_{*c}	=	critical Shields parameter
τ_c	=	block critical shear stress on a horizontal plane (lbs/ft ²)
$\tau_{c\theta}$	=	critical shear stress for the tested bed slope (lbs/ft ²)
τ_{CT}	=	critical shear stress for the tested block (lbs/ft ²)
τ_{CU}	=	critical shear stress for an untested block (lbs/ft ²)
ϕ	=	angle of repose (radians)

1 INTRODUCTION

1.1 INTRODUCTION AND GENERAL BACKGROUND

With non-stationary technology and a continually changing environment, there is a constant need to evaluate design methods and associated hypotheses. Articulated concrete block (ACB) revetment systems are commonly used for erosion protection for multiple applications. An ACB system, or mat, is a flexible interlocking matrix composed of individual concrete blocks. The term “interlocking” refers to interlocking block geometries or other connecting devices such as cables or ropes. Additionally, the term “articulating” designates that the system can conform to changes in the subgrade while staying interconnected. Figure 1.1 provides a sketch of an ACB system and individual blocks. Typical applications of ACB systems include channel lining, riverbank protection, dikes and levy protection, dam crest and spillways, and bridge abutment protection. The history of ACB development and use within engineering dates back to the mid-1970s when the former Soviet Union was testing and constructing concrete block erosion revetment systems (Clopper, 1991). Use of ACB systems has since been employed throughout the United States.

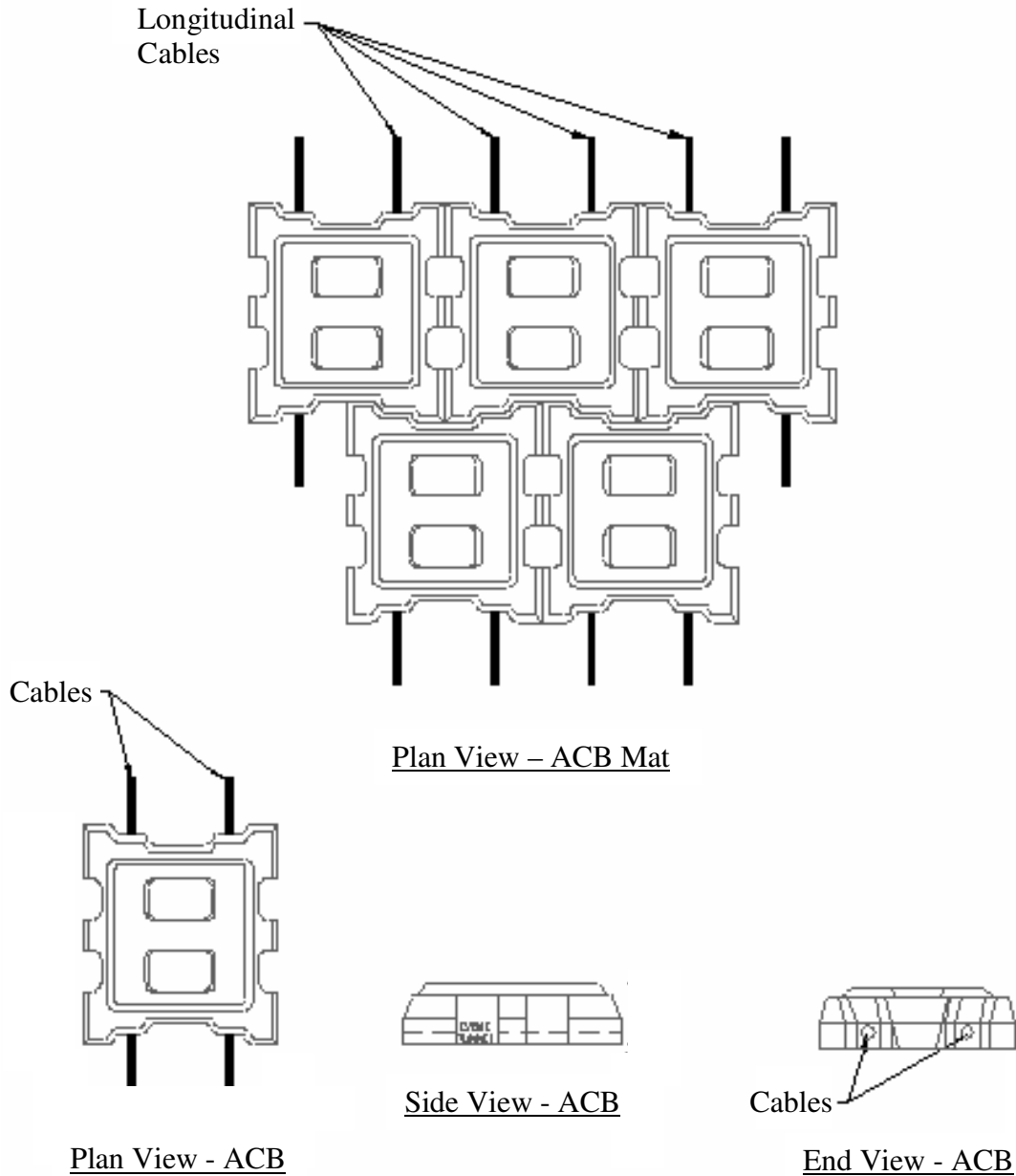


Figure 1.1: Sketches of an ACB Mat and Individual Blocks

Available design methods provided by Clopper (1991) and the National Concrete Masonry Association (NCMA, 2006) for ACB systems have not been verified with full-scale data. The Clopper (1991) and NCMA (2006) design methods compute a safety factor using a moment stability analysis approach. Chapter 2 presents a literature review that was conducted to identify: 1) the origin of the Clopper (1991) and NCMA (2006)

design methods, 2) ACB test data for analysis, and 3) hydraulic analysis techniques for ACB performance testing data. An investigation of the assumptions used in the development of the Clopper (1991) and NCMA (2006) design equations is presented in Chapter 3 and the most influential assumptions are identified.

A database is presented in Chapter 4 which was developed from full-scale laboratory tests. Three ACB systems were included in the database and testing conditions provided a range of overtopping flow depths, embankment lengths, in addition to both channelized and overtopping test conditions. Chapter 5 details the hydraulic analysis of the developed database.

An assessment of the Clopper (1991) and NCMA (2006) design equations using the database is provided in Chapter 6. The assessment demonstrates that the Clopper (1991) and NCMA (2006) design equations were ineffective at predicting stability conditions for the database. Chapter 7 details the derivation of a new safety factor design method which was based on a moment stability analysis and eliminated numerous assumptions associated with the Clopper (1991) and NCMA (2006) methods. An assessment of the new safety factor methodology is presented in Chapter 8. The new safety factor method proved successful at predicting stability for twenty-three of the twenty-four total tests.

1.2 RESEARCH OBJECTIVES

The objectives of this research were to:

1. Investigate the applicability of existing design methods to predict ACB system stability;

2. Identify assumptions used to formulate the equations utilized in the existing design methods;
3. Determine the influence of the identified assumptions on the computed safety factor value; and
4. Develop and verify a design methodology to predict ACB system stability for channelized and steep-slope, high-velocity applications.

2 LITERATURE REVIEW

Literature is detailed herein that addresses embankment testing and analysis of ACB revetment systems, and existing moment stability safety factor design methodologies. Section 2.1 details ACB testing conducted by the Construction Industry and Research Information Association (CIRIA), the Federal Highway Administration (FHWA), and the United States Army Corps of Engineers (USACE) (Hewlett *et al.*, 1987; Clopper and Chen, 1988; Clopper, 1989; Abt *et al.*, 2001). Furthermore, Section 2.1 addresses available testing and analysis protocols presented by Leech *et al.* (1999b), American Society for Testing and Materials (ASTM) D7276 (2008), and ASTM D7277 (2008). Moment stability analysis safety factor design methods by Stevens and Simons (1971), Clopper (1991), Julien (1998), Julien and Anthony (2002), and the NCMA (2006) are reviewed in Section 2.2.

2.1 EMBANKMENT TESTING AND ANALYSIS OF ARTICULATED CONCRETE BLOCK SYSTEMS

Due to the proprietary nature of ACB systems, it is difficult to identify the exact origin of ACB research. Clopper (1991) documented that in the mid-1970s, the former Soviet Union investigated the installation of ACB systems for embankment protection for steep-slope applications (66 to 197 ft in height). The earliest documented block testing

studies were conducted in 1986 by the CIRIA in the United Kingdom at Jackhouse Reservoir (Hewlett *et al.*, 1987). The FHWA followed the CIRIA closely with controlled laboratory testing of embankment protection systems in 1987 and 1988 (Clopper and Chen, 1988; Clopper, 1989).

Leech *et al.* (1999b) developed test protocols for ACB protection systems. Abt *et al.* (2001), following the protocols developed by Leech *et al.* (1999b), evaluated the performance of a generic block for overtopping and channelized hydraulic conditions. In 2008, the ASTM published a standard for ACB performance testing (ASTM D7277, 2008), in addition to a standard for analysis and interpretation of ACB performance test data (ASTM D7276, 2008). Subsequent sections detail relevant literature pertaining to testing and analysis of ACB protection systems.

2.1.1 CIRIA EMBANKMENT TESTING

Hewlett *et al.* (1987) documented the CIRIA embankment testing conducted in the United Kingdom at Jackhouse Reservoir. The CIRIA testing examined reinforced grass erosion protection systems including geotextile reinforcement, concrete reinforcement, and plain grass with no reinforcement. ACBs were classified as a concrete-reinforced system. Hewlett *et al.* (1987) provided results of the CIRIA field trials and conclude that the ArmortecTM 30S system, with established grass, was unstable at flow velocities between 23 and 26 ft/s and the PetraflexTM system with established grass was stable up to a flow velocity of 26 ft/s. Recommendations for limiting velocity values for various reinforced grass protection systems, including ACBs, are provided in Hewlett *et al.* (1987). Figure 2.1 provides the limiting velocities versus flow duration for

plain and reinforced grass presented in Hewlett *et al.* (1987). Based on the CIRIA test conditions, Hewlett *et al.* (1987) recommended limiting the maximum design velocity for ACB systems with “good interblock restraint” to 26 ft/s (8.0 m/s).

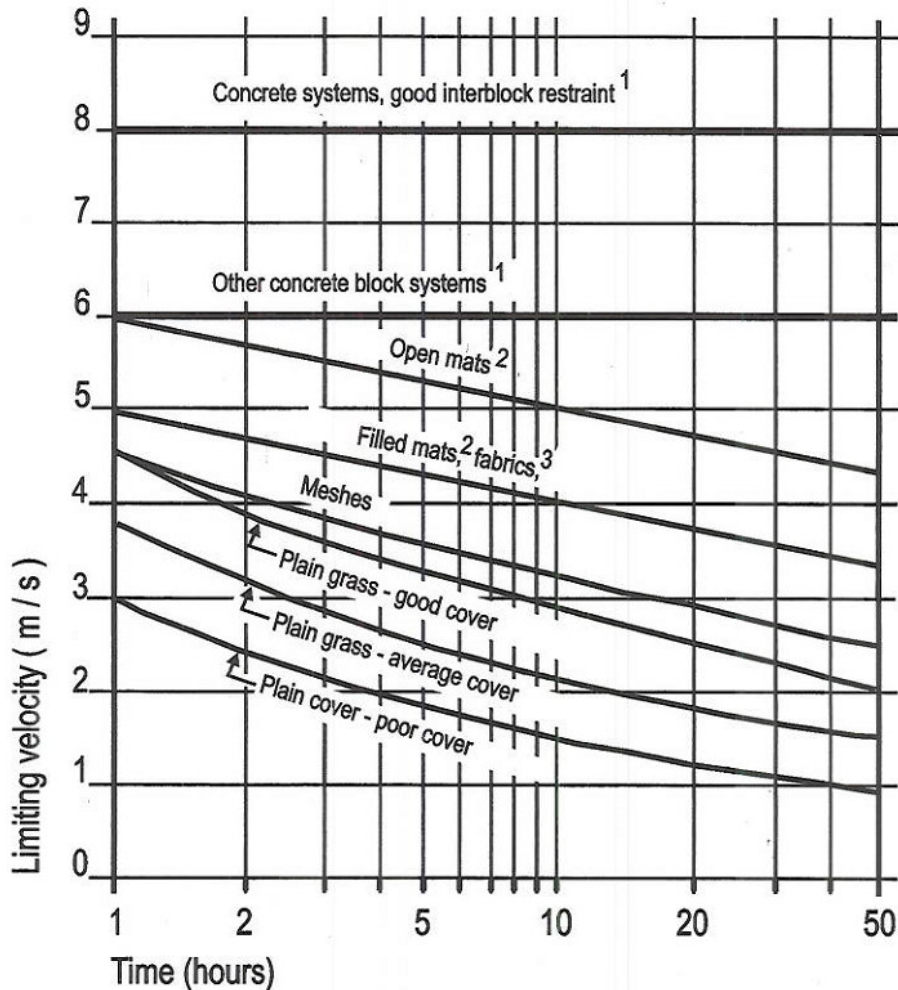


Figure 2.1: Limiting Velocity versus Flow Duration for Plain and Reinforced Grass (adapted from Hewlett *et al.* (1987))

2.1.2 FHWA OVERTOPPING RESEARCH (CLOPPER AND CHEN, 1988)

To develop preliminary design recommendations for the protection of embankments against erosion induced by overtopping flow was the primary objective of

the FHWA research detailed in Clopper and Chen (1988). To meet that objective, Clopper and Chen (1988) investigated previous studies including testing conducted by the CIRIA (Hewlett *et al.*, 1987) and available data on hydraulics of overtopping flow and erosion damage of unprotected embankments. Additionally, hydraulic performance testing of available protection systems was conducted. Embankment testing during the Clopper and Chen (1988) FHWA research included two soil types (CL and SC-SM), soil cement, gabion mattresses, Geoweb, Enkamat (7020), Enkamat (7020) with asphalt, and cable-tied concrete block revetment systems. The resulting data were analyzed, and flow-velocity and shear-stress values associated with each test condition were reported along with the stability of each protection system. Appendix A provides the available ACB data from testing reported in Clopper and Chen (1988).

Clopper and Chen (1988) concluded with recommendations for design of protection systems. Table 2.1 provides the limiting value of shear stress reported by Clopper and Chen (1988) for each protection system. Clopper and Chen (1988) provided two methods for computing shear stress and stated that the larger of the two computed shear stresses should be used for design. The first shear-stress computation method is computed from Equation 2.1 using the maximum flow depth at uniform flow:

$$\tau_0 = \gamma d_m S_0 \quad \text{Equation 2.1}$$

where

τ_0 = shear stress (lbs/ft²);

γ = unit weight of water (lbs/ft³);

d_m = maximum flow depth at uniform flow (ft); and

S_0 = embankment slope (ft/ft).

The second shear-stress method presented by Clopper and Chen (1988) computes shear stress from Equation 2.2, which incorporates the uniform flow velocity:

$$\tau_0 = \frac{1}{8} f \rho V_m^2 \quad \text{Equation 2.2}$$

where

f = Darcy-Weisbach friction factor;

ρ = density of water (slugs/ft³); and

V_m = maximum velocity at uniform flow (ft/s).

Table 2.1: Limiting Values of Shear Stress Reported in Clopper and Chen (1988)

Protection System	Limiting Shear Stress (lbs/ft ²)
Soil cement (8 percent) ^a	> 45
Gabions (6-in. thick)	35
Gabions (4-in. thick)	10
Enkamat with 1-in. asphalt	< 5
Enkamat with 3-in. asphalt	15
Armorflex Class 30 blocks	15
Petraflex-Vick blocks ^a	> 30
Dycel 100 blocks	< 7

^a Maximum capacity of facility was reached with no indication of failure

2.1.3 FHWA ACB STABILITY FOR OVERTOPPING FLOW (CLOPPER, 1989)

Results from the 1988 FHWA research on embankment protection systems indicated that ACB systems were capable of protecting embankments with overtopping conditions. However, the performance of the three systems investigated varied

considerably with the Petraflex-Vick block successful at preventing erosion during a 4-ft overtopping test and the Dycel 100 block proving incapable of protecting adequately during a 1-ft overtopping test. FHWA identified the need to further investigate the efficacy of ACB systems for protecting embankments during overtopping flow. The primary objective of the Clopper (1989) FHWA research was to provide detailed testing and analysis to quantify the processes causing failure of ACB protection systems.

Overtopping tests were conducted on five ACB systems: 1) Armorflex Class 30 block, 2) Dycel 100, 3) Petraflex-Vick block, 4) concrete construction blocks, and 5) concrete wedge-shaped overlapping blocks. Figure 2.2 provides sketches of the five ACB systems tested during the Clopper (1989) research. Overtopping tests were conducted utilizing either a rigid concrete embankment or an erodible soil embankment (SC-SM). In addition to water-surface elevation and flow-velocity data, pressure transducers were used in four locations to measure hydrodynamic pressure between the geotextile and the subgrade. Variations in embankment geometry including a chamfered crest were investigated.

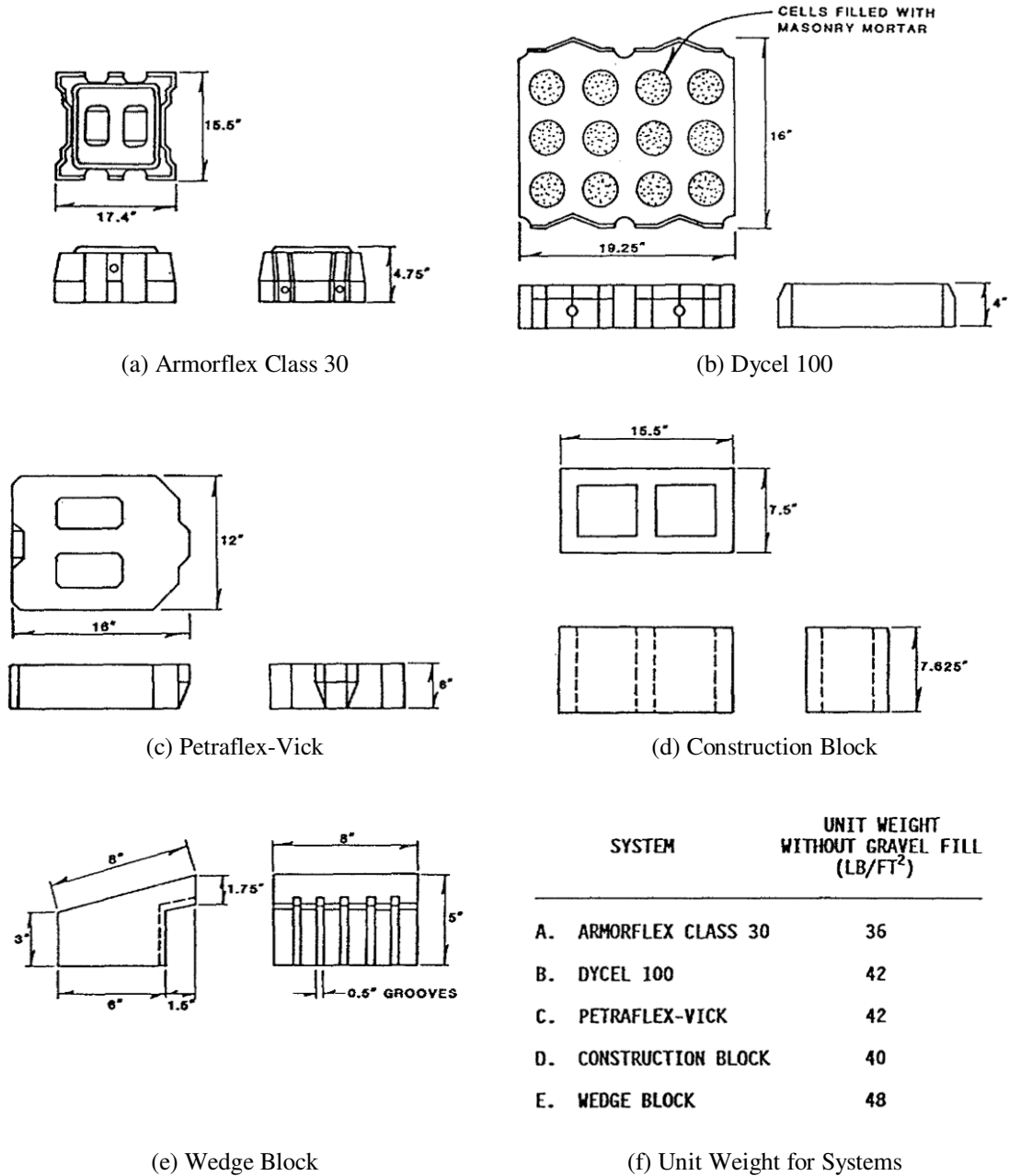


Figure 2.2: Sketches of the Five ACB Systems Tested during the Clopper (1989) FHWA Research (adapted from Clopper (1989))

Results from the Clopper (1989) FHWA research are presented in Table 2.2. The Armorflex 30S block proved to be stable for the 4-ft overtopping test with the chamfered crest; whereas, it was not stable for the 4-ft overtopping condition without the chamfered

crest in the Clopper and Chen (1988) test. Since the Petraflex-Vick block did not fail during the Clopper and Chen (1988) testing, it was not tested on the erodible embankment during the Clopper (1989) tests.

Table 2.2: Critical Flow-velocity and Shear-stress Values Reported in Clopper (1989)

Protection System	Critical Flow Velocity (ft/s)	Critical Shear Stress (lbs/ft²)
Armorflex Class 30 blocks	>15	>34
Dycel 100 blocks	<9	<12
Concrete construction blocks	>17	>20
Wedge-shaped blocks	>17	>25

2.1.4 LEECH *ET AL.* (1999B)

While hydraulic testing of block systems had been previously conducted, Leech *et al.* (1999b) introduced a set of testing protocols for block systems intended to provide comparable performance data to designers. Two block-testing protocols are detailed in Leech *et al.* (1999b): one for overtopping system performance testing and one for channelized system performance testing. Leech *et al.* (1999b) described overtopping flow as lateral flow conditions typically associated with flow over dams, through spillways and down embankments. Channelized flow is described by Leech *et al.* (1999b) as flow conveyed through a channel resulting in flow parallel to the embankment.

The presented overtopping test protocol was founded on the FHWA studies documented in Clopper and Chen (1988) and Clopper (1989). Leech *et al.* (1999b) indicated minimum test facility requirements of 4.0 ft channel width, 6.0 ft high embankment, and a horizontal crest approach of 20.0 ft. Leech *et al.* (1999b) further

stated that the facility should be capable of variable embankment slopes (*i.e.*, 2-horizontal-to-1-vertical (2H:1V), 3H:1V, etc.). One key discrepancy in the testing protocol from the FHWA testing was the specification for the use of a sand or silty sand embankment material. Since locating a specific soil mixture can be difficult for multiple testing facilities, specifying sand or silty-sand embankment material allows test results to be comparable.

Leech *et al.* (1999b) described system installation, test procedures, and how to evaluate block system stability. According to Leech *et al.* (1999b), each tested discharge should be maintained for a 4-hr duration, and flow depths and velocities should be collected hourly along the centerline of the slope at predetermined cross sections. Leech *et al.* (1999b) provided the following definitions for block system failure:

1. Loss of a block or group of blocks that directly exposes the underlayer to the flow or the separation of the block system from the subgrade. Separation may result from erosion, settlement or liquefaction of the embankment soil, movement or settlement of the drainage bedding system, suction or lifting of a block(s) from the flow, or hydrodynamic loading of the system from the flow.
2. Loss of contact with the embankment soil beneath the block system by gradual erosion along the slope, washout through joints, or washout through open cells.
3. Loss of system integrity through block oscillation or loss of intimate contact of the block with the filter.

The second protocol presented by Leech *et al.* (1999b) is for channelized hydraulic testing of block systems. For channelized testing conditions, flow is conveyed parallel to the embankment. Leech *et al.* (1999b) indicated that the channelized protocol presented should be considered preliminary and stated that further research should be conducted before a detailed standard is developed.

2.1.5 ABT ET AL. (2001)

Abt *et al.* (2001) detailed a study sponsored by the USACE to evaluate testing protocols presented in Leech *et al.* (1999b). A generic block, identified as the Corps Block, was developed by the USACE (Leech *et al.*, 1999a) and tested in accordance to both the overtopping and channelized test protocols. Overtopping tests were conducted on 5H:1V and 7H:1V embankments composed of silty-sand material (SM, Universal Soil Classification System). Channelized testing was conducted in a half-trapezoidal channel with a bottom width of 1.2 ft and 2H:1V side slopes. The soil used for channelized testing was classified as a well-graded sand (SW, Universal Soil Classification System). A critical flow velocity of approximately 13.5 ft/s was identified for the Corps Blocks for both the overtopping and channelized conditions. Additionally, for both testing conditions, a critical shear stress of approximately 4.5 lbs/ft² was reported. Abt *et al.* (2001) concluded that both the overtopping and channelized flow testing protocols yielded similar results. Ultimately, Abt *et al.* (2001) recommended the overtopping testing protocol as the requirement for evaluating block systems due the efficiency of testing compared to channelized testing and associated cost savings.

2.1.6 ASTM D7277 (2008) ACB TEST STANDARD

ASTM D7277 (2008) is a standard test method for full-scale performance testing of ACB revetment systems for hydraulic stability in open channels. Within ASTM D7277 (2008), testing protocols are provided for system installation, test procedures, measurement techniques, analysis techniques, and reporting requirements. The test method presented is specific to steep-slope, high-velocity flow conditions.

Installation requirements include a silty-sand soil subgrade compacted to between 90 and 95% of standard effort density (ASTM D698, 2007). A minimum horizontal crest length is specified as 6 ft followed by the sloped embankment. ASTM D7277 (2008) identified a 2H:1V as the benchmark embankment slope, but indicated that other embankment slopes may be used. ASTM D7277 (2008) specified that an appropriately designed filter for the soil subgrade should be utilized and the ACB installed according to the manufacturer's recommendations. Figure 2.3 provides a sketch of a test setup from ASTM D7277 (2008).

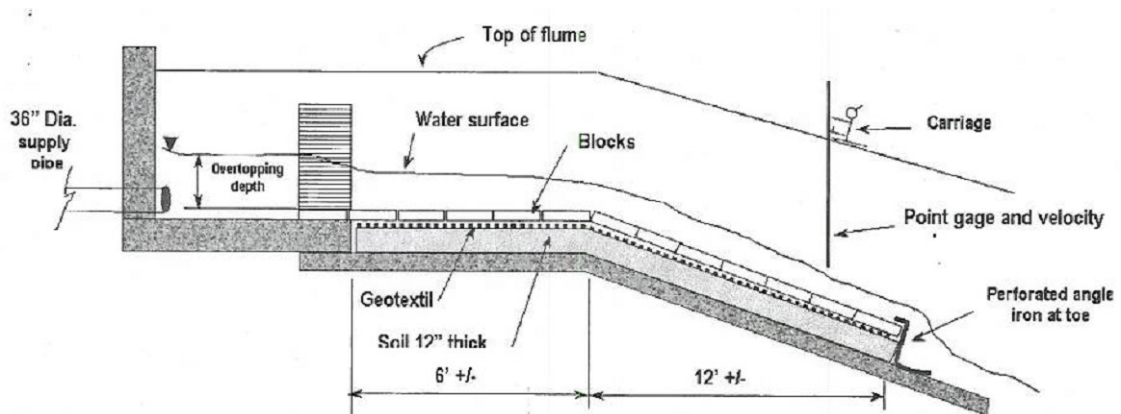


Figure 2.3: Sketch of ASTM D7277 (2008) Test Setup

ASTM D7277 (2008) defined a test as a 4-hr continuous uniform flow over a revetment system. Hourly measurements of water-surface elevations and point velocities are specified to be collected at 2- and 4-ft intervals, respectively.

Three methods of stability threshold assessment are identified in ASTM D7277 (2008):

1. Vertical displacement or loss of a block or group of blocks;
2. Loss of soil beneath the geotextile, resulting in voids; and
3. Liquefaction and mass slumping/sliding of the subsoil.

ASTM D7277 (2008) defined the stability threshold as any observations that one or more blocks have lost solid contact with the subgrade. Required reported data include measured data and calculated hydraulic conditions for each test. Measured data include discharge, overtopping depth, bed elevations, water-surface elevations, and point flow velocities. Computed data include discharge from continuity and flow depths. Continuity discharge is computed using Equation 2.3 (ASTM D7277 (2008)):

$$Q_{p,n} = A(V_{p,n}) \quad \text{Equation 2.3}$$

where

$Q_{p,n}$ = continuity discharge (cfs);

A = cross-sectional flow area measurement normal to embankment surface (ft²); and

$V_{p,n}$ = average of point flow velocities collected at 20%, 60%, and 80% of flow depth (ft/s).

Flow depths are computed accounting for slope correction by Equation 2.4 (ASTM D7277 (2008)):

$$y_i = (h_i - z_i) * \cos(\arctan(S_0)) \quad \text{Equation 2.4}$$

where

y_i = flow depth at station i (perpendicular to the embankment) (ft);

h_i = water-surface elevation at station i (ft);

z_i = bed elevation at station i (ft); and

S_0 = embankment slope (ft/ft).

2.1.7 ASTM D7276 (2008) ACB ANALYSIS STANDARD

ASTM D7276 (2008) is a standard for analysis and interpretation of ACB revetment system hydraulic test data collected under steep-slope, high-velocity conditions in a rectangular open channel. ASTM D7276 (2008) is intended to be used in conjunction with the ASTM D7277 (2008) standard for performance testing of ACB revetment systems. Methods for computation of discharge, flow depths, friction slope, cross-sectional averaged flow velocity, and boundary shear stress are detailed within ASTM D7276 (2008). Furthermore, guidelines for qualitative assessment of stability are also presented and are identical to those provided in ASTM D7277 (2008).

Calculation of continuity discharge and flow depth presented in ASTM D7276 (2008) are identical to those provided in ASTM D7277 (2008) which are detailed in Equation 2.3 and Equation 2.4, respectively. ASTM D7276 (2008) presents Equation 2.5, Manning's equation, for computation of friction slope at each measurement station:

$$S_{fi} = \left[\frac{n(V_i)}{K_u} \right]^2 \frac{1}{y_i^{4/3}} \quad \text{Equation 2.5}$$

where

S_{fi} = friction slope at station i (ft/ft);

n = Manning's resistance coefficient;

V_i = flow velocity at station i (ft/s); and

K_u = units conversion coefficient, equal to 1.486 for U.S. Customary Units and 1.0 for SI units.

ASTM D7276 (2008) indicated that the roughness of the flume walls is negligible compared to the ACB roughness of the flume bed and consequently uses the flow depth in place of the hydraulic radius within the Manning's equation to compute friction slope.

ASTM D7276 (2008) specified the computation of an optimal value of Manning's roughness, n , using a step-forewater analysis. Equation 2.6 is provided by ASTM D7276 (2008) for the step-forewater analysis:

$$h_2 = h_1 + \frac{1}{2g}(v_1 + v_2)(v_1 - v_2) - \frac{L}{2}(S_{f1} + S_{f2}) \quad \text{Equation 2.6}$$

where

h_1, h_2 = upstream and downstream water-surface elevations at stations 1 and 2, respectively (ft);

g = acceleration due to gravity (ft/s²);

v_1, v_2 = upstream and downstream velocities at stations 1 and 2, respectively (ft/s);

L = slope length between stations 1 and 2 (ft); and

S_{f1}, S_{f2} = upstream and downstream friction slopes at stations 1 and 2, respectively, as defined by Equation 2.5 (ft/ft).

Using the step-forewater analysis, water-surface profiles are generated for a range of Manning's roughness values. The optimal Manning's roughness value is identified from the profile which generates the lowest ξ value as defined by Equation 2.7:

$$\xi = \sum_{i=i_1}^{i_n} |h_{pred} - h_{obs}| \quad \text{Equation 2.7}$$

where

ξ = optimizing variable for determining best-fit Manning's n (ft);

i_1 = initial station for analysis;

i_n = ending station for analysis;

h_{pred} = predicted water-surface elevation at station i_i (ft); and

h_{obs} = observed water-surface elevation at station i_i (ft).

Figure 2.4 provides a flow chart of the ASTM D7276 (2008) step-forewater analysis method.

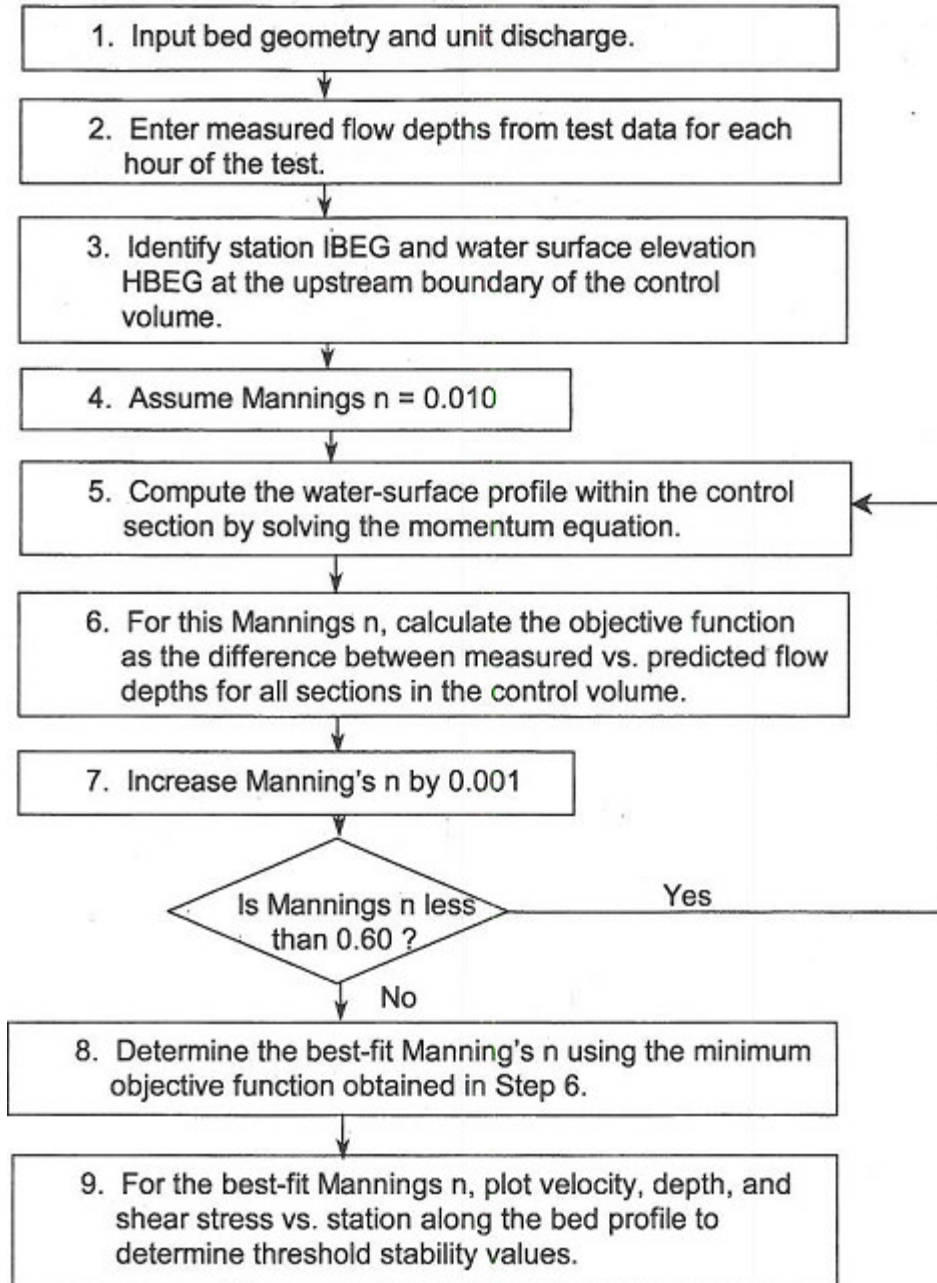


Figure 2.4: Flow Chart of Step-forewater Analysis Method (adapted from ASTM D7276 (2008))

Following the determination of the best-fit water-surface profile, cross-sectional averaged flow-velocity and control volume averaged shear-stress values are computed. Cross-sectional averaged flow velocities are computed at each station as the discharge

divided by the cross-sectional flow area, A , normal to the embankment surface. ASTM D7276 (2008) states that if gradually-varied flow conditions exist, then boundary shear stress, τ_0 , is computed using Equation 2.8:

$$\tau_0 = \gamma(y)(S_f) \quad \text{Equation 2.8}$$

where

γ = unit weight of water (62.4 lbs/ft³);

y = flow depth measured perpendicular to embankment (ft); and

S_f = friction slope (ft/ft).

A method for boundary shear-stress computation from the momentum equation is also provided by ASTM D7276 (2008). Equation 2.9 computes a shear-stress value over a representative control volume of finite embankment length, L :

$$\tau_0 = \frac{\gamma}{2}(y_1 + y_2)\sin\theta + \frac{1}{L}\left[\frac{\gamma}{2}(y_1^2 - y_2^2)\cos\theta - \rho q^2\left(\frac{1}{y_2} - \frac{1}{y_1}\right)\right] \quad \text{Equation 2.9}$$

where

γ = unit weight of water (62.4 lbs/ft³);

y_1, y_2 = flow depths at upstream and downstream ends of control volume, respectively (ft);

v_1, v_2 = flow velocity at upstream and downstream ends of control volume, respectively (ft/s);

L = length of control volume along the embankment (ft);

ρ = unit mass of water (1.94 slugs/ft³); and

q = unit discharge (ft²/s).

A sketch of the variables used in Equation 2.9 to compute shear stress is presented in Figure 2.5. ASTM D7276 (2008) identified reporting requirements including the requirement to quantify the hydraulic conditions, peak flow velocity and shear stress at the location of the stability threshold.

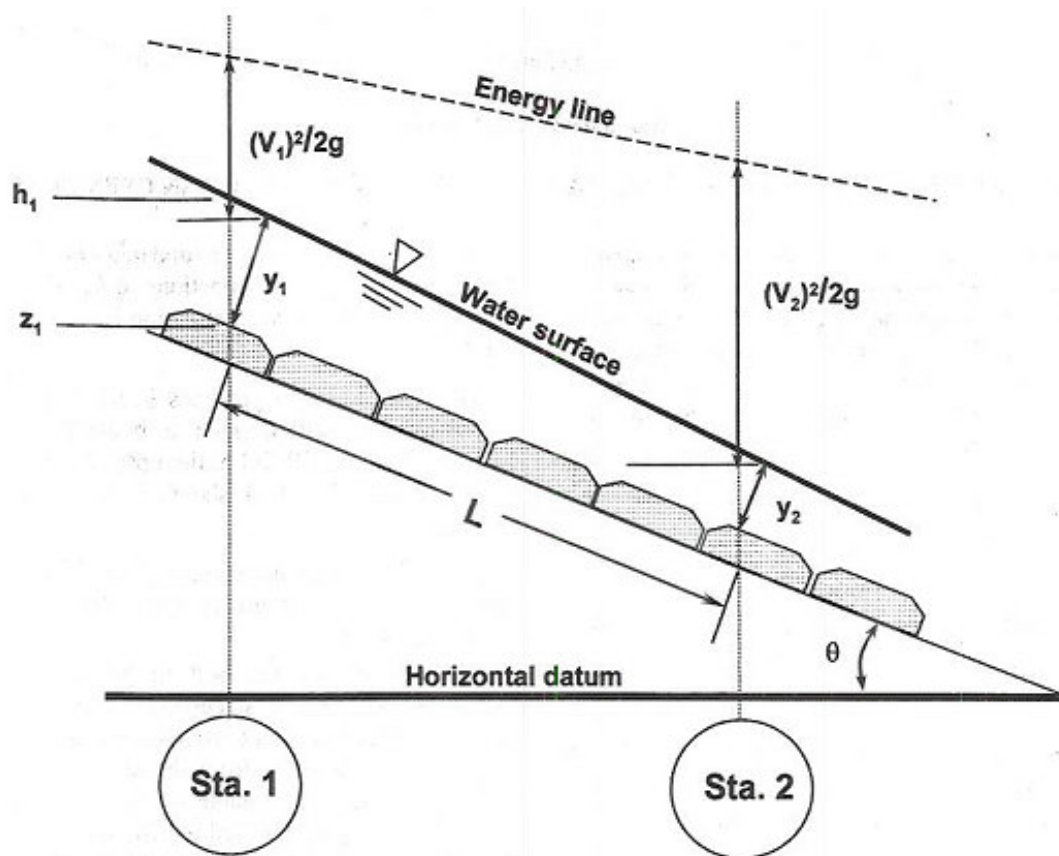


Figure 2.5: Sketch of Variables used in Momentum Shear-stress Equation (adapted from ASTM D7276 (2008)).

2.2 FACTOR OF SAFETY DESIGN METHODS

Over the course of the past two decades, moment stability analysis methods developed by Stevens and Simons (1971), Julien (1998), and Julien and Anthony (2002) have been adapted and modified to generate design procedures applicable to engineered armor units. The original application for the identified safety factor methods is to produce safety factors for cohesionless particles, which exhibit a quasi-spherical shape, on a channel side slope. Stevens and Simons (1971), Julien (1998), and Julien and Anthony (2002) safety factor methods have been adapted to obtain design guidelines for engineered armor units and are endorsed by the Harris County Flood Control District (HCFCD) and the NCMA (Clopper, 1991; HCFCD, 2001; NCMA, 2006). Several assumptions and simplifications were applied throughout the original and extrapolated derivations which generate uncertainty in the computed safety factors. Clopper (1991) and NCMA (2006) are the two primary safety methods used for design of ACB protection systems. Each method for calculating a safety factor value is detailed in the following sections.

2.2.1 STEVENS AND SIMONS (1971)

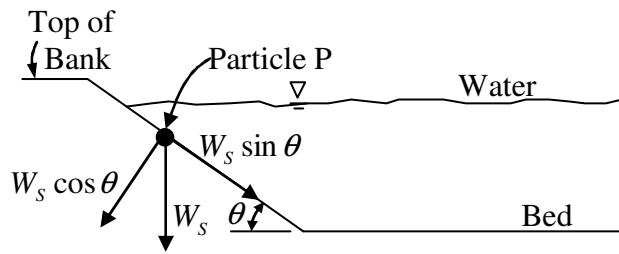
A method for determining safety factors for particles rotating out of a bank was presented in Stevens and Simons (1971). The method was based on a moment stability analysis and accounts only for contributions from the side slope when determining the submerged weight force distribution. Stevens and Simons (1971) incorporated a normalized Shields parameter to quantify incipient motion on a side slope. Furthermore,

the assumption that the moments created by the lift force and drag force are equal is applied. This section presents the derivation for the Stevens and Simons (1971) method.

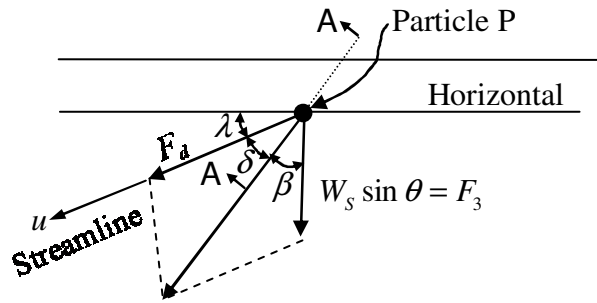
Figure 2.6(a) illustrates the forces acting on a cohesionless particle, P, resting on a channel side slope, which are visible within a channel cross-section view. The angle θ is the side-slope angle and W_s is the submerged weight of the particle as defined by the particle weight minus the buoyancy force. The side-slope angle is related to the side slope, z , by Equation 2.10:

$$\theta = \tan^{-1}(1/z) \qquad \text{Equation 2.10}$$

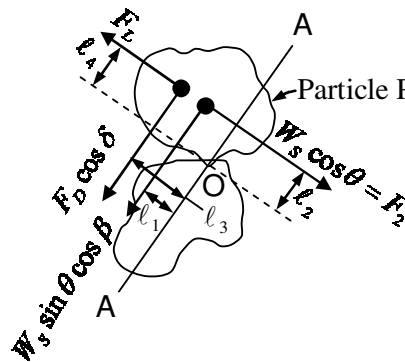
When accounting only for the side slope and assuming the bed slope is horizontal, the submerged weight force component parallel to the side slope is $W_s \sin \theta$ and the submerged weight force component normal to the side-slope plane is $W_s \cos \theta$ as depicted in Figure 2.6(a).



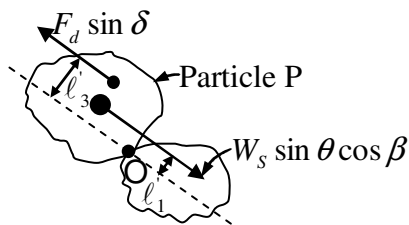
(a) Vertical Channel Cross-section View



(b) View Normal to Side Slope



(c) Section A-A



(d) Section Normal to Section A-A

Figure 2.6: Force Diagrams (adapted from Stevens and Simons (1971))

where		
A-A	=	cross section along particle rotation path
F_d	=	drag force (lbs)
F_L	=	lift force (lbs)
ℓ_1	=	moment arm for submerged weight force component parallel to the side-slope plane (ft)
ℓ_2	=	moment arm for submerged weight force component normal to the side-slope plane (ft)
ℓ_3	=	moment arm for the drag force component along the path of motion (ft)
ℓ_4	=	moment arm for the lift force (ft)
Particle P	=	cohesionless particle
O	=	point of rotation
u	=	streamline velocity vector
W_s	=	particle submerged weight (lbs)
β	=	particle rotation angle measured in the side-slope plane (radians)
δ	=	angle between the drag force and particle rotation path measured in the side-slope plane (radians)
θ	=	side-slope angle (radians)
λ	=	bed-slope angle (radians)

Figure 2.6 (continued): Force Diagrams (adapted from Stevens and Simons (1971))

Figure 2.6(b) illustrates the forces acting on Particle P including hydrodynamic forces, which are visible from a view normal to the side-slope plane. These forces include the drag force, F_D , and a component of the submerged weight force, W_s . Additionally, represented in Figure 2.6(b) is the streamline velocity vector, u , which deviates from horizontal at an angle λ .

When motion occurs, the particle follows a path at an angle β from a vertical line projected on the side-slope plane. This direction is illustrated in Figure 2.6(b) as the combined drag force and weight force vectors within the side-slope plane. Figure 2.6(c) presents the forces acting within a Cross-section A-A which is taken along the particle movement path. These forces include: the weight force acting in the normal direction into the side-slope plane, $W_s \cos \theta$; the lift force acting in the normal direction out of the side-slope plane, F_L ; the component of the drag force along Cross-section A-A,

$F_D \cos \delta$; and the weight force component along Cross-section A-A parallel to the side-slope plane, $W_s \sin \theta \cos \beta$.

A moment stability analysis was used to obtain an expression for the safety factor which was defined as the ratio of resisting moments (moments that work to stabilize the particle) to overturning moments (moments that work to set the particle in motion). Equation 2.11 presents the safety factor (SF) equation for moment stability about Point O within Cross-section A-A:

$$SF = \frac{\ell_2 W_s \cos \theta}{\ell_1 W_s \sin \theta \cos \beta + \ell_3 F_D \cos \delta + \ell_4 F_L} \quad \text{Equation 2.11}$$

where

ℓ_1 = moment arm for submerged weight force component parallel to the side-slope plane (ft);

ℓ_2 = moment arm for submerged weight force component normal to the side-slope plane (ft);

ℓ_3 = moment arm for the drag force component along the path of motion (ft);

and

ℓ_4 = moment arm for the lift force (ft).

where all other variables have been previously defined. Dividing Equation 2.11 by $\ell_1 W_s$ produces Equation 2.12:

$$SF = \frac{(\ell_2 / \ell_1) \cos \theta}{\sin \theta \cos \beta + \frac{\ell_3 F_D \cos \delta}{\ell_1 W_s} + \frac{\ell_4 F_L}{\ell_1 W_s}} \quad \text{Equation 2.12}$$

where all the variables have been previously defined.

The expression $\tan \phi = \ell_2 / \ell_1$ under static fluid conditions can be derived from the safety factor equation (Equation 2.12) by setting the side-slope angle θ equal to the angle of repose, ϕ , and the safety factor to 1.0. Equation 2.13 and Equation 2.14 present the derivation for the expression $\tan \phi = \ell_2 / \ell_1$:

$$1 = \frac{(\ell_2 / \ell_1) \cos \phi}{\sin \phi \cos(0) + \frac{\ell_3(0) \cos \delta}{\ell_1 W_S} + \frac{\ell_4(0)}{\ell_1 W_S}} = \frac{(\ell_2 / \ell_1) \cos \phi}{\sin \phi} = \frac{(\ell_2 / \ell_1)}{\tan \phi} \quad \text{Equation 2.13}$$

$$\tan \phi = \ell_2 / \ell_1 \quad \text{Equation 2.14}$$

Equation 2.15 is obtained by substituting $\tan \phi = \ell_2 / \ell_1$ into the safety factor equation, Equation 2.12:

$$SF_0 = \frac{\cos \theta \tan \phi}{\sin \theta \cos \beta + \tan \phi \left(\frac{\ell_3 F_D}{\ell_2 W_S} \cos \delta + \frac{\ell_4 F_L}{\ell_2 W_S} \right)} \quad \text{Equation 2.15}$$

For simplification, Stevens and Simons (1971) express the variable groupings associated with the lift force and the drag force as single variables M and N , respectively. Equation 2.16 and Equation 2.17 identify the single variables M and N , which represent the lift force and drag force variable groupings:

$$M = \frac{\ell_4 F_L}{\ell_2 W_S} \quad \text{Equation 2.16}$$

$$N = \frac{\ell_3 F_D}{\ell_2 W_S} \quad \text{Equation 2.17}$$

In addition, Stevens and Simons (1971) define a variable identified as the stability number for particles on a side slope, η' , by Equation 2.18 to simplify the safety factor expression:

$$\eta' = M + N \cos \delta \quad \text{Equation 2.18}$$

After making the substitutions from Equation 2.16, Equation 2.17, and Equation 2.18 into Equation 2.15, the main form of the Stevens and Simons (1971) safety factor equation is attained:

$$SF = \frac{\cos \theta \tan \phi}{\sin \theta \cos \beta + \eta' \tan \phi} \quad \text{Equation 2.19}$$

where all the variables have been previously defined.

The stability number for particles on a horizontal plane, η , (*i.e.*, $\theta = \delta = 0$), can be obtained by setting $\delta = 0$ in Equation 2.18 as presented in Equation 2.20:

$$\eta = M + N \quad \text{Equation 2.20}$$

Multiplying Equation 2.18 by $\frac{\eta}{M + N}$, which equals 1 by definition of Equation 2.20, generates Equation 2.21:

$$\eta' = \eta \frac{M + N \cos \delta}{M + N} \quad \text{Equation 2.21}$$

After dividing the numerator and denominator by N and recognizing that $\cos \delta = \sin(\lambda + \beta)$, Equation 2.22 can be obtained as an expression relating the stability

number for particles on a side slope, η' , to the stability number for particles on a horizontal plane, η :

$$\eta' = \eta \left[\frac{(M/N) + \sin(\lambda + \beta)}{1 + (M/N)} \right] \quad \text{Equation 2.22}$$

Incipient motion corresponds to a safety factor of 1 when the flow is fully turbulent over a hydraulically-rough horizontal surface (*i.e.*, $\theta = 0$ and $\delta = 0$). Equation 2.23 can be derived by substituting these appropriate values corresponding to incipient motion of a particle exposed to flow across a horizontal surface into the safety factor Equation 2.19:

$$SF = 1 = \frac{\tan \phi}{\eta \tan \phi} \quad \text{Equation 2.23}$$

Equation 2.23 reduces to identify that $\eta = 1$ for incipient motion of a particle exposed to flow across a horizontal surface. Also, by recognizing that when the flow is fully turbulent along the bed, the Shields parameter for incipient motion has a value of 0.047 (Gessler, 1971; Meyer-Peter and Müller, 1948) as illustrated in Equation 2.24:

$$\tau_{*c} = \frac{\tau_c}{(G_P - 1)\gamma d_s} = 0.047 \quad \text{Equation 2.24}$$

where

τ_{*c} = critical Shields parameter;

τ_c = critical shear stress (lbs/ft²);

G_P = specific weight of Particle P;

γ = unit weight of water (lbs/ft³); and

d_s = particle diameter (ft).

which can also be expressed in the form of Equation 2.25:

$$\frac{\tau_c}{0.047(G_p - 1)\gamma d_s} = 1 \quad \text{Equation 2.25}$$

A relationship between η and the Shields parameter can be obtained for incipient motion for particles exposed to flow across a horizontal bed as depicted by Equation 2.26:

$$\eta = \frac{\tau_c}{0.047(G_p - 1)\gamma d_s} = 1 \quad \text{Equation 2.26}$$

Stevens and Simons (1971) subsequently presumed that for flow conditions other than incipient motion, η can be determined by Equation 2.27, which uses the boundary shear stress, τ_0 , to replace the critical shear stress and can also be expressed in the form of a ratio of the boundary shear stress to the critical shear stress:

$$\eta = \frac{\tau_0}{0.047(G_p - 1)d_s} = \frac{\tau_0}{\tau_c} \quad \text{Equation 2.27}$$

To obtain an expression for β , Stevens and Simons (1971) assumed that the moment components of the drag force and submerged weight component, $W_s \sin \theta$, normal to Cross-section A-A are balanced. Figure 2.6(d) presents a view of the cross-section normal to Cross-section A-A in which components of the drag force and of the weight force are present. Equation 2.28 presents the expression for the equal moment components:

$$\ell_3' F_D \sin \delta = \ell_1' W_S \sin \theta \sin \beta \quad \text{Equation 2.28}$$

where ℓ_1' and ℓ_3' are the moment arms corresponding to the drag force component and the weight force component (ft), respectively, within the plane normal to Cross-section A-A as illustrated in Figure 2.6(d). Stevens and Simons (1971) apply the assumption that $\ell_3'/\ell_1' \approx \ell_3/\ell_1$ to Equation 2.28. From which, Equation 2.29 can be obtained by replacing $\sin \delta$ with $\cos(\beta + \lambda)$ within Equation 2.28 since $\delta + \beta + \lambda = 90^\circ$, and dividing both sides of the equation by $\ell_2 W_S$:

$$\frac{\ell_3 F_D}{\ell_2 W_S} \cos(\beta + \lambda) = \frac{\ell_1}{\ell_2} \sin \theta \sin \beta \quad \text{Equation 2.29}$$

Equation 2.29 can be further reduced by substituting N for the drag force variable grouping on the left-hand side of the equation (from Equation 2.17) and substituting $\tan \phi$ for ℓ_2 / ℓ_1 (from Equation 2.14), producing Equation 2.30:

$$N \cos(\beta + \lambda) = \frac{\sin \theta}{\tan \phi} \sin \beta \quad \text{Equation 2.30}$$

Acknowledging that $\cos(\beta + \lambda) = \cos(\beta)\cos(\lambda) - \sin(\beta)\sin(\lambda)$ and substituting within Equation 2.30 produces Equation 2.31:

$$\cos(\beta)\cos(\lambda) - \sin(\beta)\sin(\lambda) = \frac{\sin \theta}{N \tan \phi} \sin \beta \quad \text{Equation 2.31}$$

Dividing both sides of Equation 2.31 by $\sin \beta$ and solving for β generates Equation 2.32:

$$\beta = \tan^{-1} \left[\cos(\lambda) / \left(\frac{\sin \theta}{N \tan \phi} + \sin(\lambda) \right) \right] \quad \text{Equation 2.32}$$

Finally, multiplying the bottom left term of the right-hand side of Equation 2.32 by $(M + N)/\eta$, which is equal to 1 by the definition of η , produces Equation 2.33:

$$\beta = \tan^{-1} \left[\cos(\lambda) / \left(\frac{(M + N) \sin \theta}{N \eta \tan \phi} + \sin(\lambda) \right) \right] \quad \text{Equation 2.33}$$

Stevens and Simons (1971) stated that assuming $\ell_4/\ell_2 \approx 2$ and $F_L/F_D \approx 1/2$ is reasonable. Thereby, establishing the relationship $M/N \approx 1$, which imposes the assumption that the moments created by the drag force, $\ell_3 F_D$, and the lift force, $\ell_4 F_L$, are equivalent. With this assumption, Equation 2.22 reduces to Equation 2.34:

$$\eta' = \eta \left[\frac{1 + \sin(\lambda + \beta)}{2} \right] \quad \text{Equation 2.34}$$

and Equation 2.33 to Equation 2.35:

$$\beta = \tan^{-1} \left[\cos(\lambda) / \left(\frac{2 \sin \theta}{\eta \tan \phi} + \sin(\lambda) \right) \right] \quad \text{Equation 2.35}$$

For calculation of safety factors of particles on the channel bed, where the bed-slope angle is α , the downstream direction is equivalent to the oblique flow on a side slope with $\theta = \alpha$ and $\lambda = 90^\circ$. Substituting these values into Equation 2.35 produces a value of 0° for β . Accordingly, Equation 2.34 reduces to Equation 2.36, and Equation 2.19 reduces to Equation 2.37:

$$\eta' = \eta \left(\frac{1 + \sin(90^\circ + 0^\circ)}{2} \right) = \eta \quad \text{Equation 2.36}$$

$$SF = \frac{\cos \alpha \tan \phi}{\sin \alpha + \eta \tan \phi} \quad \text{Equation 2.37}$$

In summary, Stevens and Simons (1971) present a method for determining a safety factor for riprap stability by consecutively solving Equation 2.27, Equation 2.35, Equation 2.34, and Equation 2.19. Table 2.3 summarizes the Stevens and Simons (1971) safety factor equations and computation order. The Stevens and Simons (1971) method was derived from a moment stability analysis and requires values for bed slope, side slope, design shear stress, and particle diameter.

Table 2.3: Safety Factor Calculation Method According to Stevens and Simons (1971)

Order of Calculation	Equation	Equation Number
1	$\eta = \frac{\tau_0}{\tau_c}$	Equation 2.27
2	$\beta = \tan^{-1} \left[\cos(\lambda) / \left(\frac{2 \sin \theta}{\eta \tan \phi} + \sin(\lambda) \right) \right]$	Equation 2.35
3	$\eta' = \eta \left[\frac{1 + \sin(\lambda + \beta)}{2} \right]$	Equation 2.34
4	$SF = \frac{\cos \theta \tan \phi}{\sin \theta \cos \beta + \eta' \tan \phi}$	Equation 2.19

2.2.2 CLOPPER (1991)

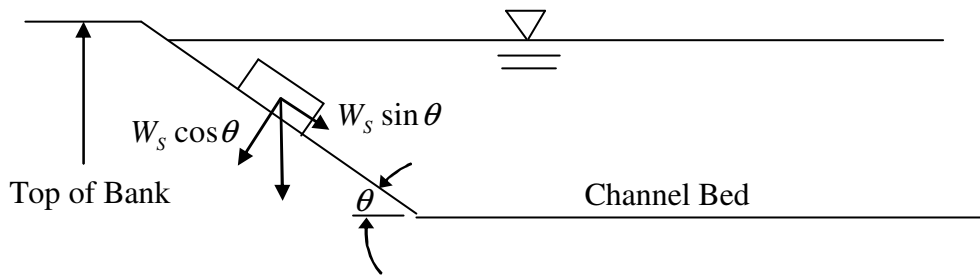
Clopper (1991) presented a method to calculate safety factors for individual rectangular armor units. This method was based on the Stevens and Simons (1971) safety factor method with modifications to account for particle geometry. The derivation for the safety factor calculation method given by Clopper (1991) is presented in this section.

Figure 2.7(a) illustrates the forces acting on a rectangular armor unit resting on a channel side slope, which are visible within a channel cross-section view. The angle θ is the side-slope angle and W_s is the submerged weight of the block as defined by the block weight minus the buoyancy force. When accounting only for the side slope and assuming the bed slope is horizontal, the weight force component parallel to the side slope is $W_s \sin \theta$ and the weight force component normal to the side-slope plane is $W_s \cos \theta$ as depicted in Figure 2.7(a).

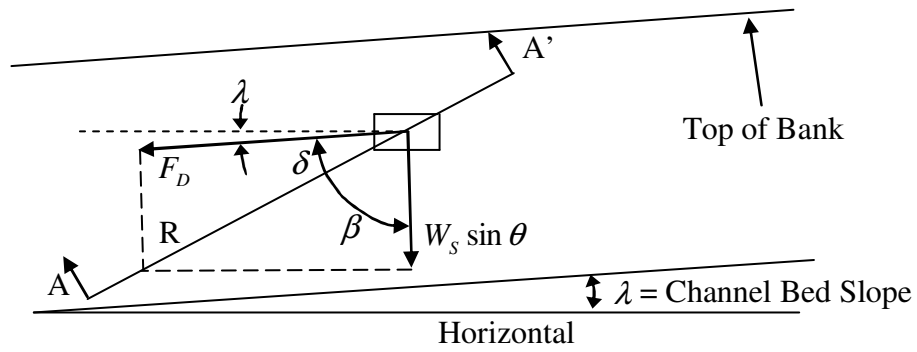
Figure 2.7(b) illustrates the forces acting on the block including hydrodynamic forces that are visible from a view normal to the side-slope plane. These forces include the drag force, F_D , and a component of the submerged weight force, W_s . The drag force acts in the direction of the streamline velocity vector, which deviates from horizontal at an angle λ .

Clopper (1991) identified that motion initiates along the vector R , which is located at an angle β from a vertical line projected on the side-slope plane. This direction is illustrated in Figure 2.7(b) as the combined drag force and weight force vectors within the side-slope plane. Figure 2.7(c) presents the forces acting within a Cross-section A-A, which is taken along vector R . These forces include: the weight force acting in the

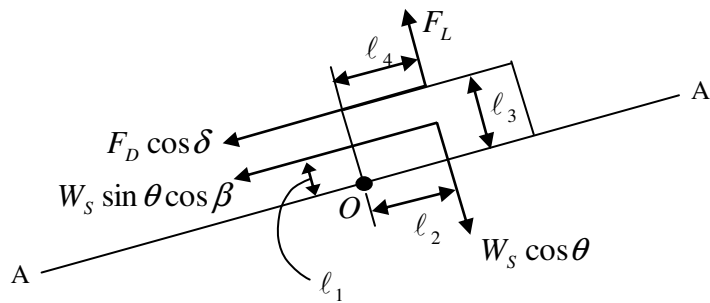
normal direction into the side-slope plane, $W_s \cos \theta$; the lift force acting in the normal direction out of the side-slope plane, F_L ; the component of the drag force along Cross-section A-A, $F_D \cos \delta$; and the weight force component along Cross-section A-A parallel to the side-slope plane, $W_s \sin \theta \cos \beta$.



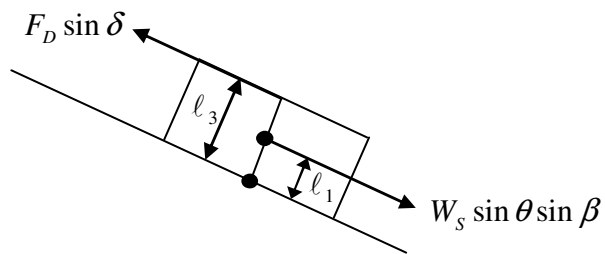
(a) Cross-section View



(b) View Normal to Side Slope



(c) Section A-A'



(d) View Normal to Section A-A'

Figure 2.7: Force Diagrams (adapted from Clopper (1991))

where	
A-A'	= cross section along block rotation path
F_D	= drag force (lbs)
F_L	= lift force (lbs)
ℓ_1	= moment arm for submerged weight force component parallel to the side-slope plane (ft)
ℓ_2	= moment arm for submerged weight force component normal to the side-slope plane (ft)
ℓ_3	= moment arm for the drag force component along the path of motion (ft)
ℓ_4	= moment arm for the lift force (ft)
O	= point of rotation
R	= vector located along the direction of block rotation
W_S	= block submerged weight (lbs)
β	= block rotation angle measured in the side-slope plane (radians)
δ	= angle between drag force and the particle rotation path measured in the side-slope plane (radians)
θ	= side-slope angle (radians)
λ	= channel-bed angle (radians)

Figure 2.7 (continued): Force Diagrams (adapted from Clopper (1991))

A moment stability analysis was used to obtain an expression for the safety factor where the safety factor was defined as the ratio of resisting moments to overturning moments. Equation 2.38 presents the safety factor equation for moment stability about Point O within Cross-section A-A:

$$SF = \frac{\ell_2 W_S \cos \theta}{\ell_1 W_S \sin \theta \cos \beta + \ell_3 F_D \cos \delta + \ell_4 F_L} \quad \text{Equation 2.38}$$

where

ℓ_1 = moment arm for submerged weight force component parallel to the side-slope plane (ft);

ℓ_2 = moment arm for submerged weight force component normal to the side-slope plane (ft);

l_3 = moment arm for the drag force component along the path of motion (ft);

and

l_4 = moment arm for the lift force (ft).

Dividing Equation 2.38 by $l_1 W_s$ produces Equation 2.39:

$$SF = \frac{(\ell_2 / \ell_1) \cos \theta}{\sin \theta \cos \beta + \frac{\ell_3 F_D \cos \delta}{\ell_1 W_s} + \frac{\ell_4 F_L}{\ell_1 W_s}} \quad \text{Equation 2.39}$$

where all the variables have been previously defined. Subsequently, Clopper (1991) defined the stability number on a channel side slope, η' , by Equation 2.40:

$$\eta' = \frac{\ell_3 F_D \cos \delta}{\ell_2 W_s} + \frac{\ell_4 F_L}{\ell_2 W_s} \quad \text{Equation 2.40}$$

Equation 2.40 is substituted into Equation 2.39 to obtain the primary form of the safety factor equation presented in Clopper (1991):

$$SF = \frac{(\ell_2 / \ell_1) \cos \theta}{\sin \theta \cos \beta + (\ell_2 / \ell_1) \eta'} \quad \text{Equation 2.41}$$

where all the variables have been previously defined.

The stability number for particles on a horizontal plane, η , can be obtained by setting $\delta = 0$ in Equation 2.40 as presented by Equation 2.42:

$$\eta = \frac{\ell_3 F_D}{\ell_2 W_s} + \frac{\ell_4 F_L}{\ell_2 W_s} \quad \text{Equation 2.42}$$

Equation 2.43 can be obtained by dividing Equation 2.40 by Equation 2.42:

$$\frac{\eta'}{\eta} = \frac{\frac{\ell_3 F_D}{\ell_2 W_S} \cos \delta + \frac{\ell_4 F_L}{\ell_2 W_S}}{\frac{\ell_3 F_D}{\ell_2 W_S} + \frac{\ell_4 F_L}{\ell_2 W_S}} \quad \text{Equation 2.43}$$

For simplification, Clopper (1991) expresses the variable groupings associated with the lift force and the drag force as single variables M and N , respectively. Equation 2.44 and Equation 2.45 identify the single variables M and N , which represent the lift force and drag force variable groupings:

$$M = \frac{\ell_4 F_L}{\ell_2 W_S} \quad \text{Equation 2.44}$$

$$N = \frac{\ell_3 F_D}{\ell_2 W_S} \quad \text{Equation 2.45}$$

Equation 2.43 is modified to include the variables M and N as presented in Equation 2.46:

$$\frac{\eta'}{\eta} = \frac{N \cos \delta + M}{N + M} \quad \text{Equation 2.46}$$

Solving Equation 2.46 for η' produces Equation 2.47:

$$\eta' = \eta \frac{M + N \cos \delta}{M + N} \quad \text{Equation 2.47}$$

After dividing the numerator and denominator of the right-hand side of Equation 2.47 by N and recognizing that $\cos \delta = \sin(\lambda + \beta)$, Equation 2.48 is obtained as an expression relating η' to the stability number η :

$$\eta' = \eta \left[\frac{(M/N) + \sin(\lambda + \beta)}{1 + (M/N)} \right] \quad \text{Equation 2.48}$$

Incipient motion corresponds to a safety factor of 1 when the flow is fully turbulent over a hydraulically-rough horizontal surface (*i.e.*, $\theta = 0$ and $\delta = 0$). Equation 2.49 is obtained by substituting these appropriate values corresponding to incipient motion of a block exposed to flow across a horizontal surface into the safety factor Equation 2.41:

$$SF = 1 = \frac{(\ell_2/\ell_1)}{(\ell_2/\ell_1)\eta} \quad \text{Equation 2.49}$$

Equation 2.49 reduces to identify that $\eta = 1$ for incipient motion of a block exposed to flow across a horizontal surface. When flow is fully turbulent along the bed, the Shields parameter for incipient motion has a value of 0.047 (Gessler, 1971; Meyer-Peter and Müller, 1948) as illustrated in Equation 2.50:

$$\tau_{*c} = \frac{\tau_c}{(G_p - 1)\gamma d_s} = 0.047 \quad \text{Equation 2.50}$$

where

- τ_{*c} = critical Shields parameter;
- τ_c = critical shear stress (lbs/ft²);
- G_p = specific weight of Particle P;
- γ = unit weight of water (lbs/ft³); and
- d_s = particle diameter (ft).

which can also be expressed in the form of Equation 2.51:

$$\frac{\tau_c}{0.047(G_p - 1)\gamma d_s} = 1 \quad \text{Equation 2.51}$$

A relationship between η and the Shields parameter can be formed for incipient motion for a block exposed to flow across a horizontal bed as depicted by Equation 2.52:

$$\eta = \frac{\tau_c}{0.047(G_p - 1)\gamma d_s} = 1 \quad \text{Equation 2.52}$$

Clopper (1991) maintained the same assumption as Stevens and Simons (1971) that for flow conditions other than incipient motion, η can be determined by Equation 2.53 which uses the boundary shear stress, τ_0 , to replace the critical shear stress and can also be expressed in the form of a ratio of the boundary shear stress to the critical shear stress:

$$\eta = \frac{\tau_0}{0.047(G_p - 1)\gamma d_s} = \frac{\tau_0}{\tau_c} \quad \text{Equation 2.53}$$

To obtain an expression for β , Clopper (1991) assumed that the moment components of the drag force and submerged weight component, $W_s \sin \theta$, normal to Cross-section A-A are balanced. Figure 2.7(d) presents a view of the cross-section normal to Cross-section A-A in which components of the drag force and of the weight force are present. Equation 2.54 presents the expression for these equal moment components:

$$\ell_3 F_D \sin \delta = \ell_1 W_s \sin \theta \sin \beta \quad \text{Equation 2.54}$$

where ℓ_1 and ℓ_3 are the moment arms corresponding to the drag force component and the weight force component (ft), respectively, within the plane normal to Cross-section

A-A. Equation 2.55 is developed by replacing $\sin \delta$ with $\cos(\beta + \lambda)$ within Equation 2.54 since $\delta + \beta + \lambda = 90^\circ$, and dividing both sides of the equation by $\ell_2 W_S$:

$$\frac{\ell_3 F_D}{\ell_2 W_S} \cos(\beta + \lambda) = \frac{\ell_1}{\ell_2} \sin \theta \sin \beta \quad \text{Equation 2.55}$$

Equation 2.55 is further reduced by substituting N for the drag force variable grouping on the left-hand side of the equation (from Equation 2.45), producing Equation 2.56:

$$N \cos(\beta + \lambda) = \frac{\ell_1}{\ell_2} \sin \theta \sin \beta \quad \text{Equation 2.56}$$

Acknowledging that $\cos(\beta + \lambda) = \cos(\beta)\cos(\lambda) - \sin(\beta)\sin(\lambda)$ and substituting within Equation 2.56 produces Equation 2.57:

$$\cos(\beta)\cos(\lambda) - \sin(\beta)\sin(\lambda) = \frac{\ell_1 \sin \theta \sin \beta}{\ell_2 N} \quad \text{Equation 2.57}$$

Dividing both sides of Equation 2.57 by $\sin \beta$ and solving for β generates Equation 2.58:

$$\beta = \tan^{-1} \left[\cos(\lambda) / \left(\frac{\ell_1 \sin \theta}{\ell_2 N} + \sin(\lambda) \right) \right] \quad \text{Equation 2.58}$$

Finally, multiplying the bottom left term of the right-hand side of Equation 2.58 by $(M/N + 1)N/\eta$, which is equal to 1 by the definition of η , produces Equation 2.59 which is the final expression for β given in Clopper (1991):

$$\beta = \tan^{-1} \left[\cos(\lambda) / \left(\frac{\ell_1 (M/N + 1) \sin \theta}{\ell_2 \eta} + \sin(\lambda) \right) \right] \quad \text{Equation 2.59}$$

Clopper (1991) stated that because it is difficult to determine the lift force, it should be assumed to have the same value as the drag force, which is a conservative estimate. With this assumption, the ratio of M and N rely solely on the corresponding moment arms as demonstrated by Equation 2.60:

$$M/N = \frac{\ell_4 F_L}{\ell_2 W_S} \frac{\ell_2 W_S}{\ell_3 F_D} = \ell_4 / \ell_3 \quad \text{Equation 2.60}$$

This assumption varies from the assumption made by Stevens and Simons (1971) that the moments created by the lift and drag forces are equal.

Included in the Clopper (1991) safety factor formula are terms that account for additional forces which occur when blocks are not perfectly installed. Under these imperfect conditions, additional lift and drag forces, F_L' and F_D' , respectively, are incurred from the impact of flow against the projecting face. Equation 2.61 displays the formula for the additional lift and drag forces:

$$F_D' = F_L' = 0.5\rho(\Delta z)wV^2 \quad \text{Equation 2.61}$$

where

ρ = density of water (slugs/ft³);

Δz = height of the projecting surface normal to the direction of flow (ft);

w = width of the projecting surface normal to the direction of flow (ft); and

V = flow velocity (ft/s).

Equation 2.61 is derived from the drag force equation displayed in Equation 2.62 assuming the drag force coefficient, C_D , has a value of 0.5 and the lift force is equal to the drag force:

$$F_D' = \rho C_D A_N V^2 \quad \text{Equation 2.62}$$

where A_N is the area of the particle normal to the direction of flow. Using a value of 0.5 for the drag force coefficient is a conservative method which assumes no energy losses between the upstream approach velocity and the face of the projecting block. Adding these forces to the safety factor equation produces Equation 2.63, which is the safety factor formula for projecting blocks given by Clopper (1991):

$$SF = \frac{(\ell_2 / \ell_1) \cos \theta}{\sin \theta \cos \beta + (\ell_2 / \ell_1) \eta' + \frac{\ell_3 F_D'}{\ell_1 W_s} \sin(\lambda + \beta) + \frac{\ell_3 F_L'}{\ell_1 W_s}} \quad \text{Equation 2.63}$$

In summary, Clopper (1991) presented a method for determining a safety factor by consecutively solving Equation 2.60, Equation 2.53, Equation 2.59, Equation 2.48, Equation 2.61, and Equation 2.63. Table 2.4 summarizes the Clopper (1991) safety factor equations and computation order. Values for bed slope, side slope, block geometry, block weight, specific gravity of block material, design velocity, design shear stress, and critical shear stress are required to use the Clopper (1991) method.

Table 2.4: Safety Factor Calculation Method According to Clopper (1991)

Order of Calculation	Equation	Equation Number
1	$M/N = \ell_4/\ell_3$	Equation 2.60
2	$\eta = \frac{\tau_0}{\tau_c}$	Equation 2.53
3	$\beta = \tan^{-1} \left[\cos(\lambda) / \left(\frac{\ell_1(M/N+1)\sin\theta}{\ell_2\eta} + \sin(\lambda) \right) \right]$	Equation 2.59
4	$\eta' = \eta \left[\frac{(M/N) + \sin(\lambda + \beta)}{1 + (M/N)} \right]$	Equation 2.48
5	$F_D' = F_L' = 0.5\rho(\Delta z)wV^2$	Equation 2.61
6	$SF = \frac{(\ell_2/\ell_1)\cos\theta}{\sin\theta\cos\beta + (\ell_2/\ell_1)\eta' + \frac{\ell_3 F_D'}{\ell_1 W_S} \sin(\lambda + \beta) + \frac{\ell_3 F_L'}{\ell_1 W_S}}$	Equation 2.63

2.2.3 JULIEN (1998)

A method to determine safety factors for cohesionless particles on channel side slopes is given in Julien (1998). This method was based on the Stevens and Simons (1971) method; however, it accounts for bed slope within the submerged weight force distribution. A moment stability analysis is at the origin of the derivation, and with some assumptions and simplifications, a practical safety factor method was derived. The Julien (1998) method, like Stevens and Simons (1971), incorporated the element of a normalized Shields parameter to quantify incipient motion on a side slope. This section presents the derivation for the Julien (1998) safety factor method.

Figure 2.8(a) illustrates the forces acting on a cohesionless Particle, P, resting on a channel side slope which are visible within a channel cross-section view, where θ_1 is the side-slope angle; F_S is the submerged weight of the particle; and a_θ is geometrically defined by Equation 2.64 (Julien, 1998):

$$a_\theta = \sqrt{\cos^2 \theta_1 - \sin^2 \theta_0} \quad \text{Equation 2.64}$$

where θ_0 is the bed-slope angle. A complete derivation of Equation 2.64 is presented following the introduction of all the force components.

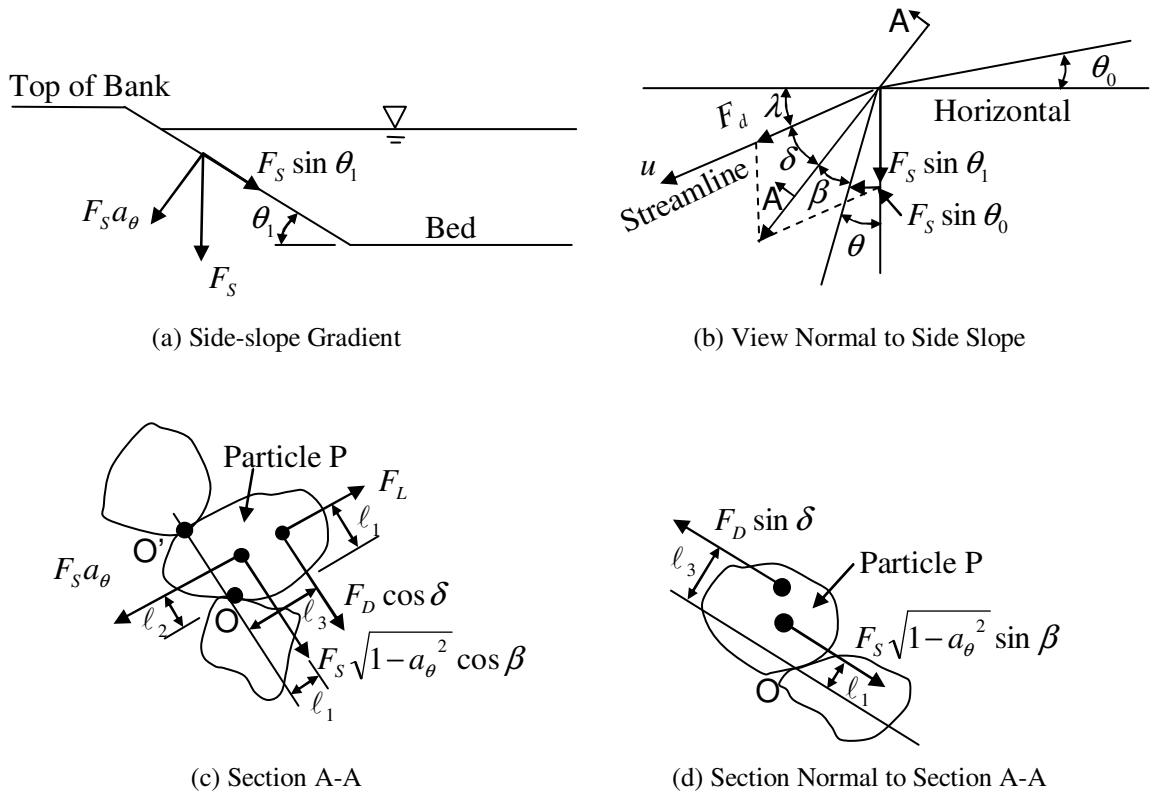


Figure 2.8: Force Diagrams (adapted from Julien (1998))

where		
a_θ	=	coefficient of the weight force acting in the direction normal to the side-slope plane
A-A	=	cross section along particle rotation path
F_d	=	drag force (lbs)
F_L	=	lift force (lbs)
F_s	=	particle submerged weight (lbs)
l_1	=	moment arm for submerged weight force component parallel to the side-slope plane (ft)
l_2	=	moment arm for submerged weight force component normal to the side-slope plane (ft)
l_3	=	moment arm for the drag force component along the path of motion (ft)
l_4	=	moment arm for the lift force (ft)
O	=	point of rotation
Particle P	=	cohesionless particle resting on a channel side slope
u	=	streamline velocity vector
β	=	particle rotation angle measured in the side-slope plane (radians)
δ	=	angle between the drag force and the particle rotation path measured in the side-slope plane (radians)
θ	=	resulting angle of the combined weight force components acting in the side-slope plane measured from a vertical line projected onto the side-slope plane (radians)
θ_0	=	bed-slope angle (radians)
θ_1	=	side-slope angle (radians)
λ	=	angle between horizontal and the streamline velocity vector measured in the side-slope plane (radians)

Figure 2.8 (continued): Force Diagrams (adapted from Julien (1998))

Figure 2.8(b) illustrates the forces acting on Particle P including hydrodynamic forces, which are visible from a view normal to the side-slope plane. These forces include the drag force, F_D , and components of the submerged weight, F_s . Additionally represented in Figure 2.8(b) is the streamline velocity vector, u , which deviates from the horizontal at an angle λ . Two weight force components are acting in this plane, $F_s \sin \theta_1$ and $F_s \sin \theta_0$, where the combination of these weight forces produces a single weight force component within the side-slope plane, which acts at an angle θ from a vertical line projected on the side-slope plane as illustrated in Figure 2.8(b). This angle θ is geometrically defined by Equation 2.65:

$$\theta = \tan^{-1}\left(\frac{F_s \sin \theta_0}{F_s \sin \theta_1}\right) = \tan^{-1}\left(\frac{\sin \theta_0}{\sin \theta_1}\right) \quad \text{Equation 2.65}$$

The expression for the coefficient of the weight force acting in the direction normal to the side-slope plane, a_θ , (Equation 2.64) as illustrated in Figure 2.8(b), is derived using the two weight force components acting in the side-slope plane, $F_s \sin \theta_1$ and $F_s \sin \theta_0$. Each of the weight force components in the three orthogonal axes must collectively produce the single weight force component which acts solely in the vertical direction. This concept is represented mathematically by Equation 2.66:

$$F_s = \sqrt{(F_s \sin \theta_1)^2 + (F_s \sin \theta_0)^2 + (F_s a_\theta)^2} \quad \text{Equation 2.66}$$

F_s can be removed from both sides of Equation 2.66 as presented in Equation 2.67:

$$1 = \sqrt{\sin^2 \theta_1 + \sin^2 \theta_0 + a_\theta^2} \quad \text{Equation 2.67}$$

Solving Equation 2.67 for a_θ produces Equation 2.68:

$$a_\theta = \sqrt{1 - \sin^2 \theta_1 - \sin^2 \theta_0} \quad \text{Equation 2.68}$$

After substituting the trigonometric identity $\cos^2 \theta_1 = 1 - \sin^2 \theta_1$, into Equation 2.68, Equation 2.69 is obtained as an expression for the coefficient of the weight force acting in the direction normal to the side-slope plane, a_θ :

$$a_\theta = \sqrt{\cos^2 \theta_1 - \sin^2 \theta_0} \quad \text{Equation 2.69}$$

When motion occurs, the particle follows a path at an angle β from a vertical line projected on the side-slope plane. This direction is illustrated in Figure 2.8(b) as the combined force vectors within the side-slope plane: F_D , $F_S \sin \theta_1$, and $F_S \sin \theta_0$. Figure 2.8(c) presents the forces acting within Cross-section A-A which is taken along the particle movement path. These forces include: the weight force acting in the normal direction into the side-slope plane, $F_S a_\theta$; the lift force acting in the normal direction out of the side-slope plane, F_L ; the component of the drag force along Cross-section A-A, $F_D \cos \delta$; and the weight force component along Cross-section A-A parallel to the side-slope plane, $F_S \sqrt{1 - a_\theta^2} \cos \beta$. The weight force along Cross-section A-A parallel to the side-slope plane is attained by adding the two weight force vectors within the side-slope plane, $F_S \sin \theta_1$ and $F_S \sin \theta_0$ as illustrated by Equation 2.70:

$$F_S \sqrt{\sin^2 \theta_1 + \sin^2 \theta_0} = F_S \sqrt{1 - a_\theta^2} \quad \text{Equation 2.70}$$

where a_θ was defined in Equation 2.64.

A moment stability analysis was used to obtain an expression for the safety factor where the safety factor was defined as the ratio of resisting moments to overturning moments. Equation 2.71 presents the safety factor equation for moment stability about Point O within Cross-section A-A:

$$SF_O = \frac{\ell_2 F_S a_\theta}{\ell_1 F_S \sqrt{1 - a_\theta^2} \cos \beta + \ell_3 F_D \cos \delta + \ell_4 F_L} \quad \text{Equation 2.71}$$

where

ℓ_1 = moment arm for submerged weight force component parallel to the side-slope plane (ft);

ℓ_2 = moment arm for submerged weight force component normal to the side-slope plane (ft);

ℓ_3 = moment arm for the drag force component along the path of motion (ft);

and

ℓ_4 = moment arm for the lift force (ft).

Dividing Equation 2.71 by $\ell_1 F_S$ produces Equation 2.72:

$$SF_O = \frac{(\ell_2 / \ell_1) a_\theta}{\sqrt{1 - a_\theta^2} \cos \beta + \frac{\ell_3 F_D \cos \delta}{\ell_1 F_S} + \frac{\ell_4 F_L}{\ell_1 F_S}} \quad \text{Equation 2.72}$$

where all the variables have been previously defined.

According to Julien (1998), the safety factor equals unity when the angle θ equals the angle of repose, ϕ , under static fluid conditions, *i.e.*, $F_D = F_L = \beta = 0$, from which $\tan \phi = \ell_2 / \ell_1$ can be derived. Equation 2.73 can be obtained by substituting $\tan \phi = \ell_2 / \ell_1$ into Equation 2.72:

$$SF_O = \frac{a_\theta \tan \phi}{\sqrt{1 - a_\theta^2} \cos \beta + \tan \phi \left(\frac{\ell_3 F_D \cos \delta}{\ell_2 F_S} + \frac{\ell_4 F_L}{\ell_2 F_S} \right)} \quad \text{Equation 2.73}$$

For simplification, Julien (1998) expressed the variable groupings associated with the lift force and the drag force as single variables M and N , respectively. Equation 2.74 and

Equation 2.75 identify the single variables M and N which represent the lift force and drag force variable groupings:

$$M = \frac{\ell_4 F_L}{\ell_2 F_S} \quad \text{Equation 2.74}$$

$$N = \frac{\ell_3 F_D}{\ell_2 F_S} \quad \text{Equation 2.75}$$

In addition, Julien (1998) defined a variable identified as the stability number for particles on a side slope, η_1 , by Equation 2.76 to simplify the safety factor expression:

$$\eta_1 = M + N \cos \delta \quad \text{Equation 2.76}$$

After making substitutions from Equation 2.76, Equation 2.75, and Equation 2.74 into Equation 2.73, the primary form of the Julien (1998) safety factor equation is attained as presented in Equation 2.77:

$$SF_o = \frac{a_\theta \tan \phi}{\sqrt{1 - a_\theta^2} \cos \beta + \eta_1 \tan \phi} \quad \text{Equation 2.77}$$

where all the variables have been previously defined.

The stability number for particles on a horizontal plane can be developed by setting $\delta = 0$ in Equation 2.76 as presented in Equation 2.78:

$$\eta_0 = M + N \quad \text{Equation 2.78}$$

where η_0 is the stability number for particles on a horizontal plane. Multiplying the

right-hand side of Equation 2.76 by $\frac{\eta_0}{M + N}$, which equals 1, generates Equation 2.79:

$$\eta_1 = \eta_0 \frac{M + N \cos \delta}{M + N} \quad \text{Equation 2.79}$$

After dividing the numerator and denominator on the right-hand side of Equation 2.79 by N and recognizing that $\cos \delta = \sin(\lambda + \beta + \theta)$, Equation 2.80 can be obtained as an expression relating the stability number for particles on a side slope, η_1 , to the stability number for particles on a horizontal plane, η_0 :

$$\eta_1 = \eta_0 \left[\frac{(M/N) + \sin(\lambda + \beta + \theta)}{1 + (M/N)} \right] \quad \text{Equation 2.80}$$

Incipient motion corresponds to a safety factor of 1 when the flow is fully turbulent over a hydraulically-rough horizontal surface (*i.e.*, $\theta_0 = 0$, $\theta_1 = 0$, $\delta = 0$, and $a_\theta = 1$). Equation 2.81 can be obtained by substituting these appropriate values corresponding to incipient motion of a particle exposed to flow across a horizontal surface into the safety factor equation (Equation 2.77):

$$SF_o = 1 = \frac{\tan \phi}{\eta_0 \tan \phi} \quad \text{Equation 2.81}$$

Equation 2.81 reduces to identify that $\eta_0 = 1$ for incipient motion of a particle exposed to flow across a horizontal surface. When flow is fully turbulent along the bed, the Shields parameter for incipient motion has a value of 0.047 (Gessler, 1971; Meyer-Peter and Müller, 1948) as illustrated in Equation 2.82:

$$\tau_{*c} = \frac{\tau_c}{(G_p - 1)\gamma d_s} = 0.047 \quad \text{Equation 2.82}$$

where

τ_{*c} = critical Shields parameter;

τ_c = critical shear stress (lbs/ft²);

G_p = specific weight of Particle P;

γ = unit weight of water (lbs/ft³); and

d_s = particle diameter (ft).

This can also be expressed in the form of Equation 2.83:

$$\frac{\tau_c}{0.047(G_p - 1)\gamma d_s} = 1 \quad \text{Equation 2.83}$$

A relationship between η_0 and the Shields parameter can be obtained for incipient motion for particles exposed to flow across a horizontal bed as depicted by Equation 2.84:

$$\eta_0 = \frac{\tau_c}{0.047(G_p - 1)\gamma d_s} = 1 \quad \text{Equation 2.84}$$

Julien (1998) subsequently presumed that for flow conditions other than incipient motion, η_0 can be determined by Equation 2.85 which uses the boundary shear stress, τ_0 , to replace the critical shear stress and can also be expressed in the form of a ratio of the boundary shear stress to the critical shear stress:

$$\eta_0 = \frac{\tau_0}{0.047(G_p - 1)\gamma d_s} = \frac{\tau_0}{\tau_c} \quad \text{Equation 2.85}$$

Julien (1998) presented alternative methods for calculating η_0 , which come from replacing the boundary shear stress with the reference velocity, the velocity against the particle, or the average flow velocity.

To obtain an expression for β , Julien (1998) assumed that the moment components of the drag force and submerged weight component, $F_S \sqrt{1 - a_\theta^2}$, normal to Cross-section A-A are balanced. Figure 2.8(d) presents a view of the cross-section normal to Cross-section A-A in which components of the drag force and of the weight force are present. Equation 2.86 presents the expression for these equal moment components:

$$\ell_3 F_D \sin \delta = \ell_1 F_S \sqrt{1 - a_\theta^2} \sin \beta \quad \text{Equation 2.86}$$

Equation 2.87 is developed by replacing $\sin \delta$ with $\cos(\beta + \lambda + \theta)$ in Equation 2.86 since $\delta + \beta + \lambda + \theta = 90^\circ$, and dividing both sides of the equation by $\ell_2 F_S$:

$$\frac{\ell_3 F_D}{\ell_2 F_S} \cos(\beta + \lambda + \theta) = \frac{\ell_1}{\ell_2} \sqrt{1 - a_\theta^2} \sin \beta \quad \text{Equation 2.87}$$

Equation 2.87 can be further reduced by substituting N for the drag force variable grouping on the left-hand side of the equation and substituting $\tan \phi$ for ℓ_2 / ℓ_1 , producing Equation 2.88:

$$N \cos(\beta + \lambda + \theta) = \frac{\sqrt{1 - a_\theta^2}}{\tan \phi} \sin \beta \quad \text{Equation 2.88}$$

Acknowledging that $\cos(\beta + \lambda + \theta) = \cos(\beta)\cos(\lambda + \theta) - \sin(\beta)\sin(\lambda + \theta)$ and substituting within Equation 2.88 produces Equation 2.89:

$$\cos(\beta)\cos(\lambda + \theta) - \sin(\beta)\sin(\lambda + \theta) = \frac{\sqrt{1 - a_\theta^2}}{N \tan \phi} \sin \beta \quad \text{Equation 2.89}$$

Dividing both sides of Equation 2.89 by $\sin \beta$ and solving for β provides Equation 2.90:

$$\beta = \tan^{-1} \left[\cos(\lambda + \theta) / \left(\frac{\sqrt{1 - a_\theta^2}}{N \tan \phi} + \sin(\lambda + \theta) \right) \right] \quad \text{Equation 2.90}$$

Finally, multiplying the bottom left term of the right-hand side of Equation 2.90 by $(M + N)/\eta_0$, which is equal to 1 by the definition of η_0 , produces Equation 2.91 which is the expression given for β in Julien (1998):

$$\beta = \tan^{-1} \left[\cos(\lambda + \theta) / \left(\frac{(M + N)\sqrt{1 - a_\theta^2}}{N\eta_0 \tan \phi} + \sin(\lambda + \theta) \right) \right] \quad \text{Equation 2.91}$$

Julien (1998) stated that the stability factor is not very sensitive to the ratio M / N and suggests using a value of 1 (*i.e.*, $M = N$), which thereby reduces Equation 2.80 to Equation 2.92:

$$\eta_1 = \eta_0 \left[\frac{1 + \sin(\lambda + \beta + \theta)}{2} \right] \quad \text{Equation 2.92}$$

and Equation 2.91 to Equation 2.93:

$$\beta = \tan^{-1} \left[\cos(\lambda + \theta) / \left(\frac{2\sqrt{1-a_\theta^2}}{\eta_0 \tan \phi} + \sin(\lambda + \theta) \right) \right] \quad \text{Equation 2.93}$$

This simplification implies that the moments created by the lift force, $\ell_4 F_L$, and the drag force, $\ell_3 F_D$, are equivalent.

In summary, by using the Julien (1998) method, a safety factor can be attained by calculating consecutively Equation 2.64, Equation 2.65, Equation 2.85, Equation 2.93, Equation 2.92, and Equation 2.77. Table 2.5 summarizes the Julien (1998) safety factor equations and computation order. Values for bed slope, side slope, design shear stress, and critical shear stress are required to use the Julien (1998) method.

Table 2.5: Safety Factor Calculation Method According to Julien (1998)

Order of Calculation	Equation	Equation Number
1	$a_\theta = \sqrt{\cos^2 \theta_1 - \sin^2 \theta_0}$	Equation 2.64
2	$\theta = \tan^{-1} \left(\frac{\sin \theta_0}{\sin \theta_1} \right)$	Equation 2.65
3	$\eta_0 = \frac{\tau_0}{0.047(G_p - 1)\gamma d_s} = \frac{\tau_0}{\tau_c}$	Equation 2.85
4	$\beta = \tan^{-1} \left[\cos(\lambda + \theta) / \left(\frac{2\sqrt{1-a_\theta^2}}{\eta_0 \tan \phi} + \sin(\lambda + \theta) \right) \right]$	Equation 2.93
5	$\eta_1 = \eta_0 \left[\frac{1 + \sin(\lambda + \beta + \theta)}{2} \right]$	Equation 2.92
6	$SF_o = \frac{a_\theta \tan \phi}{\sqrt{1-a_\theta^2} \cos \beta + \eta_1 \tan \phi}$	Equation 2.77

2.2.4 JULIEN AND ANTHONY (2002)

Julien and Anthony (2002) presented a similar moment stability analysis as Julien (1998); however, they provided more complex expressions for the weight force distribution coefficient, a_θ , and the angle θ . These variables are illustrated in Figure 2.9(a) and Figure 2.9(b). According to Julien and Anthony (2002), the non-simplified form of the weight force components $F_s \sin \theta_1$ and $F_s \sin \theta_0$ (Figure 2.8) from Julien (1998) are $F_s \cos \theta_0 \sin \theta_1$ and $F_s \cos \theta_1 \sin \theta_0$, respectively. The combination of these weight forces produces a single weight force component within the side-slope plane which acts at an angle θ from a vertical line projected on the side-slope plane as illustrated in Figure 2.9(b). This angle θ is geometrically defined by Equation 2.94:

$$\theta = \tan^{-1} \left(\frac{F_s \cos \theta_1 \sin \theta_0}{F_s \cos \theta_0 \sin \theta_1} \right) = \tan^{-1} \left(\frac{\cos \theta_1 \sin \theta_0}{\cos \theta_0 \sin \theta_1} \right) \quad \text{Equation 2.94}$$

Furthermore, it can be determined that the fraction of the submerged weight normal to the side slope, a_θ , is related to the bed slope and side slope by Equation 2.95:

$$a_\theta = \sqrt{1 - \cos^2 \theta_0 \sin^2 \theta_1 - \cos^2 \theta_1 \sin^2 \theta_0} \quad \text{Equation 2.95}$$

This expression can be derived using the two weight force components acting in side-slope plane, $F_s \sin \theta_1 \cos \theta_0$ and $F_s \sin \theta_0 \cos \theta_1$. Each of the weight force components in the three orthogonal axes must collectively produce the single weight force component which acts solely in the vertical direction. This concept is represented mathematically by Equation 2.96:

$$F_s = \sqrt{(F_s \cos \theta_0 \sin \theta_1)^2 + (F_s \cos \theta_1 \sin \theta_0)^2 + (F_s a_\theta)^2} \quad \text{Equation 2.96}$$

F_s can be removed from both sides of Equation 2.96 as presented in Equation 2.97:

$$1 = \sqrt{\cos^2 \theta_0 \sin^2 \theta_1 + \cos^2 \theta_1 \sin^2 \theta_0 + a_\theta^2} \quad \text{Equation 2.97}$$

By solving Equation 2.97 for a_θ , Equation 2.98 is obtained as the expression for the coefficient of the weight force acting in the direction normal to the side-slope plane:

$$a_\theta = \sqrt{1 - \cos^2 \theta_0 \sin^2 \theta_1 - \cos^2 \theta_1 \sin^2 \theta_0} \quad \text{Equation 2.98}$$

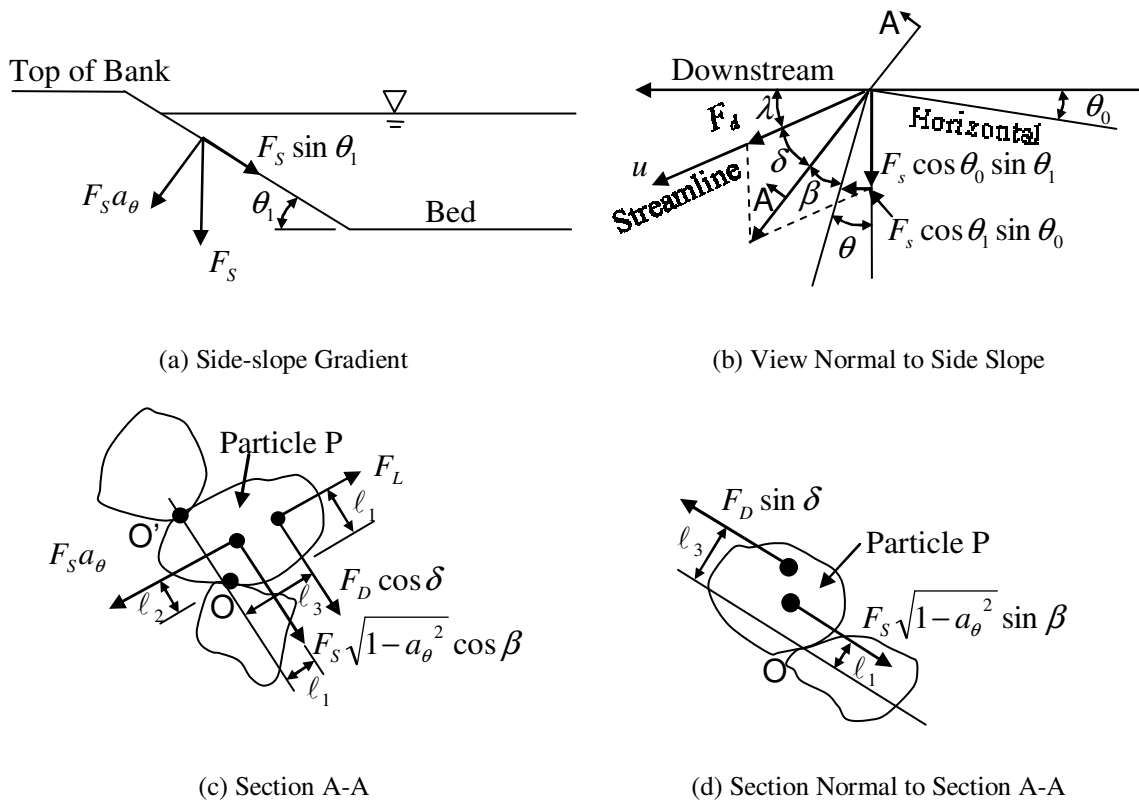
According to Julien and Anthony (2002), if the side-slope angle and the bed-slope angle are small (less than 20°), then a_θ can be approximated by Equation 2.99:

$$a_\theta = \sqrt{\cos^2 \theta_1 - \sin^2 \theta_0} \quad \text{Equation 2.99}$$

and θ can be approximated by Equation 2.100:

$$\theta = \tan^{-1} \left(\frac{\sin \theta_0}{\sin \theta_1} \right) \quad \text{Equation 2.100}$$

These are the expressions for a_θ and θ which are used in the Julien (1998) method.



where	
a_θ	= coefficient of the weight force acting in the direction normal to the side-slope plane
A-A	= cross section along particle rotation path
F_d	= drag force (lbs)
F_L	= lift force (lbs)
F_S	= particle submerged weight (lbs)
ℓ_1	= moment arm for submerged weight force component parallel to the side-slope plane (ft)
ℓ_2	= moment arm for submerged weight force component normal to the side-slope plane (ft)
ℓ_3	= moment arm for the drag force component along the path of motion (ft)
ℓ_4	= moment arm for the lift force (ft)
O	= point of rotation
Particle P	= cohesionless particle resting on a channel side slope
u	= streamline velocity vector
β	= particle rotation angle measured in the side-slope plane (radians)
δ	= angle between the drag force and the particle rotation path measured in the side-slope plane (radians)
θ	= resulting angle of the combined weight force components acting in the side-slope plane measured from a vertical line projected onto the side-slope plane (radians)
θ_0	= bed-slope angle (radians)
θ_1	= side-slope angle (radians)
λ	= angle between horizontal and the streamline velocity vector measured in the side-slope plane (radians)

Figure 2.9: Force Diagrams (adapted from Julien and Anthony (2002))

Following the derivation for the Julien (1998) method presented in Section 2.2.3, the safety factor equation can be obtained as presented in Equation 2.101:

$$SF_o = \frac{a_\theta \tan \phi}{\sqrt{1 - a_\theta^2} \cos \beta + \eta_1 \tan \phi} \quad \text{Equation 2.101}$$

where the stability number for particles on a side slope, η_1 , can be calculated from Equation 2.102:

$$\eta_1 = \eta_0 \left[\frac{(M/N) + \sin(\lambda + \beta + \theta)}{1 + (M/N)} \right] \quad \text{Equation 2.102}$$

The angle in the direction of particle movement, β , can be computed by Equation 2.103:

$$\beta = \tan^{-1} \left[\cos(\lambda + \theta) / \left(\frac{(M + N)\sqrt{1 - a_\theta^2}}{N\eta_0 \tan \phi} + \sin(\lambda + \theta) \right) \right] \quad \text{Equation 2.103}$$

The stability number for particles on a horizontal surface, η_0 , can be calculated by Equation 2.104:

$$\eta_0 = \frac{\tau_0}{0.047(G_p - 1)\gamma d_s} = \frac{\tau_0}{\tau_c} \quad \text{Equation 2.104}$$

and the variables M and N are defined by Equation 2.105 and Equation 2.106, respectively:

$$M = \frac{\ell_4 F_L}{\ell_2 W_s} \quad \text{Equation 2.105}$$

$$N = \frac{\ell_3 F_D}{\ell_2 W_s} \quad \text{Equation 2.106}$$

Analogous to the Julien (1998) derivation, the Julien and Anthony (2002) derivation used the concept that $\tan \phi = \ell_2 / \ell_1$. Additionally, the derivation utilized the assumption that the stability number, η_0 , for flow conditions other than incipient motion is linearly related to the boundary shear stress. A safety factor can be attained using the Julien and Anthony method by calculating consecutively Equation 2.95, Equation 2.94, Equation 2.104, Equation 2.103, Equation 2.102, and Equation 2.101. Table 2.6 summarizes the Julien and Anthony (2002) safety factor equations and computation order. Values for bed slope, side slope, design shear stress, and critical shear stress are required to use the Julien and Anthony (2002) method.

Table 2.6: Safety Factor Calculation Method According to Julien and Anthony (2002)

Order of Calculation	Equation	Equation Number
1	$a_{\theta} = \sqrt{1 - \cos^2 \theta_0 \sin^2 \theta_1 - \cos^2 \theta_1 \sin^2 \theta_0}$	Equation 2.95
2	$\theta = \tan^{-1} \left(\frac{\cos \theta_1 \sin \theta_0}{\cos \theta_0 \sin \theta_1} \right)$	Equation 2.94
3	$\eta_0 = \frac{\tau_0}{0.047(G_p - 1)\gamma d_s} = \frac{\tau_0}{\tau_c}$	Equation 2.104
4	$\beta = \tan^{-1} \left[\cos(\lambda + \theta) / \left(\frac{(M + N)\sqrt{1 - a_{\theta}^2}}{N\eta_0 \tan \phi} + \sin(\lambda + \theta) \right) \right]$	Equation 2.103
5	$\eta_1 = \eta_0 \left[\frac{(M / N) + \sin(\lambda + \beta + \theta)}{1 + (M / N)} \right]$	Equation 2.102
6	$SF_o = \frac{a_{\theta} \tan \phi}{\sqrt{1 - a_{\theta}^2} \cos \beta + \eta_1 \tan \phi}$	Equation 2.101

2.2.5 NATIONAL CONCRETE MASONRY ASSOCIATION (2006)

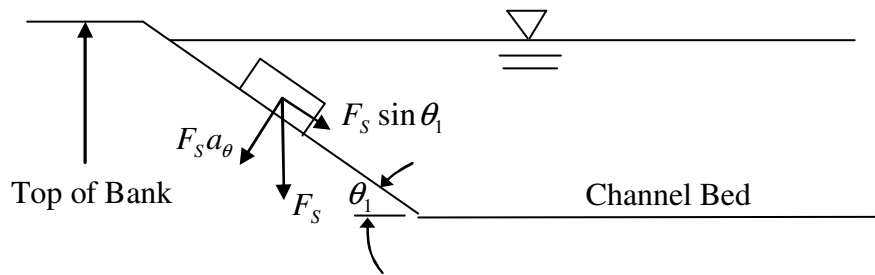
The NCMA (2006) presented a similar method to determine safety factors for individual blocks within a system. This method combined components of both the Julien and Anthony (2002) and the Julien (1998) safety factor methods with modifications to account for block geometry. The derivation for the safety factor calculation method provided in NCMA (2006) is presented in this section.

Figure 2.10(a) illustrates the forces acting on a block resting on a channel side slope which are visible within a channel cross-section view. The angle θ_1 is the side-

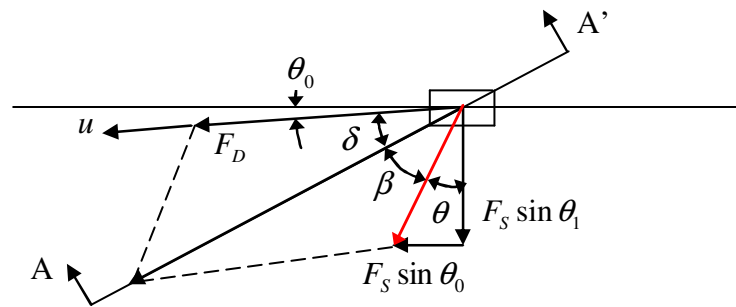
slope angle and F_s is the submerged weight of the particle as defined by the block weight minus the buoyancy force. The variable a_θ is geometrically defined by Equation 2.107 (Julien, 1998):

$$a_\theta = \sqrt{\cos^2 \theta_1 - \sin^2 \theta_0} \quad \text{Equation 2.107}$$

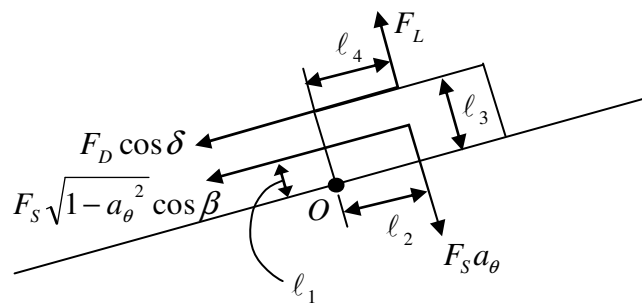
where θ_0 is the bed-slope angle. A complete derivation of Equation 2.107 is presented in Section 2.2.3.



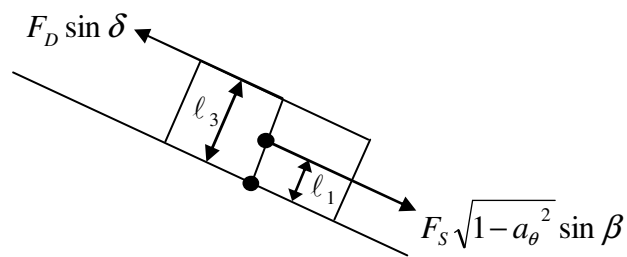
(a) Cross-section View



(b) View Normal to Side Slope



(c) Section A-A'



(d) View Normal to Section A-A'

Figure 2.10: Force Diagrams (adapted from NCMA (2006))

where	
a_θ	= coefficient of the weight force acting in the direction normal to the side-slope plane
A-A'	= cross section along particle rotation path
F_D	= drag force (lbs)
F_L	= lift force (lbs)
F_S	= block submerged weight (lbs)
ℓ_1	= moment arm for submerged weight force component parallel to the side-slope plane (ft)
ℓ_2	= moment arm for submerged weight force component normal to the side-slope plane (ft)
ℓ_3	= moment arm for the drag force component along the path of motion (ft)
ℓ_4	= moment arm for the lift force (ft)
O	= point of rotation
u	= streamline velocity vector
β	= angle of block rotation measured in the side-slope plane (radians)
δ	= angle between the drag force and the block rotation path measured in the side-slope plane (radians)
θ	= resulting angle of the combined weight force components acting in the side-slope plane measured from a vertical line projected onto the side-slope plane (radians)
θ_0	= bed-slope angle (radians)
θ_1	= side-slope angle (radians)

Figure 2.10 (continued): Force Diagrams (adapted from NCMA (2006))

Figure 2.10(b) illustrates the forces acting on the block, including hydrodynamic forces, which are visible from a view normal to the side-slope plane. These forces include the drag force, F_D , and components of the submerged weight, F_S . Additionally represented in Figure 2.10(b) is the streamline velocity vector, u , which deviates from horizontal at an angle θ_0 . Two weight force components are acting in this plane where the combination of these weight forces produces a single weight force component within the side-slope plane that acts at an angle θ from a vertical line projected on the side-slope plane as illustrated in Figure 2.10(b). Julien (1998) defined the forces as $F_S \sin \theta_1$ and $F_S \sin \theta_0$ as displayed in Figure 2.10(b) whereas Julien and Anthony (2002) defined the forces as $F_S \sin \theta_1 \cos \theta_0$ and $F_S \sin \theta_0 \cos \theta_1$. The method presented by NCMA (2006) used the Julien (1998) definition to calculate the value of a_θ and the Julien and

Anthony definition to compute the angle θ . Equation 2.108 presents the expression relating the angle θ to the side-slope angle, θ_1 , and the bed-slope angle, θ_0 :

$$\theta = \tan^{-1} \left(\frac{\sin \theta_0 \cos \theta_1}{\sin \theta_1 \cos \theta_0} \right) \quad \text{Equation 2.108}$$

When motion occurs, the block follows a path at an angle β from a vertical line projected on the side-slope plane. This direction is illustrated in Figure 2.10(b) as the combined force vectors within the side-slope plane: F_D , $F_S \sin \theta_1$, and $F_S \sin \theta_0$. Figure 2.10(c) presents the forces acting within a Cross-section A-A which is taken along the block movement path. These forces include: the weight force acting in the normal direction into the side-slope plane, $F_S a_\theta$; the lift force acting in the normal direction out of the side-slope plane, F_L ; the component of the drag force along Cross-section A-A, $F_D \cos \delta$; and the weight force component along Cross-section A-A parallel to the side-slope plane, $F_S \sqrt{1 - a_\theta^2} \cos \beta$. The weight force along Cross-section A-A parallel to the side-slope plane is attained by adding the two weight force vectors within the side-slope plane, $F_S \sin \theta_1$ and $F_S \sin \theta_0$, as illustrated by Equation 2.109:

$$F_S \sqrt{\sin^2 \theta_1 + \sin^2 \theta_0} = F_S \sqrt{1 - a_\theta^2} \quad \text{Equation 2.109}$$

where a_θ was defined in Equation 2.107.

A moment stability analysis is used to obtain an expression for the safety factor where the safety factor is defined as the ratio of resisting moments to overturning moments. Equation 2.110 presents the safety factor equation for moment stability about a block within Cross-section A-A:

$$SF_o = \frac{\ell_2 F_S a_\theta}{\ell_1 F_S \sqrt{1 - a_\theta^2} \cos \beta + \ell_3 F_D \cos \delta + \ell_4 F_L} \quad \text{Equation 2.110}$$

where

ℓ_1 = moment arm for submerged weight force component parallel to the side-slope plane (ft);

ℓ_2 = moment arm for submerged weight force component normal to the side-slope plane (ft);

ℓ_3 = moment arm for the drag force component along the path of motion (ft);

and

ℓ_4 = moment arm for the lift force (ft).

Dividing Equation 2.110 by $\ell_1 F_S$ produces Equation 2.111:

$$SF_o = \frac{(\ell_2 / \ell_1) a_\theta}{\sqrt{1 - a_\theta^2} \cos \beta + \frac{\ell_3 F_D \cos \delta}{\ell_1 F_S} + \frac{\ell_4 F_L}{\ell_1 F_S}} \quad \text{Equation 2.111}$$

where all the variables have been previously defined. For simplification, the variable groupings associated with the lift force and the drag force are expressed as single variables M and N , respectively. Equation 2.112 and Equation 2.113 identify the single variables M and N which represent the lift force and drag force variable groupings, respectively:

$$M = \frac{\ell_4 F_L}{\ell_2 F_S} \quad \text{Equation 2.112}$$

$$N = \frac{\ell_3 F_D}{\ell_2 F_S} \quad \text{Equation 2.113}$$

In addition, the variable identified by Julien (1998) as the stability number for particles on a side slope, η_1 , is utilized to simplify the safety factor expression. η_1 is defined in relation to the variable groupings M and N by Equation 2.114:

$$\eta_1 = M + N \cos \delta \quad \text{Equation 2.114}$$

After making the substitutions from Equation 2.114, Equation 2.113, and Equation 2.112 into Equation 2.111, the primary form of the NCMA (2006) safety factor equation is obtained as presented in Equation 2.115:

$$SF_O = \frac{(\ell_2 / \ell_1) a_\theta}{\sqrt{1 - a_\theta^2} \cos \beta + (\ell_2 / \ell_1) \eta_1} \quad \text{Equation 2.115}$$

where all the variables have been previously defined.

The stability number for blocks on a horizontal plane, η_0 , can be obtained by setting $\delta = 0$ in Equation 2.114 as presented in Equation 2.116:

$$\eta_0 = M + N \quad \text{Equation 2.116}$$

Multiplying Equation 2.116 by $\frac{\eta_0}{M + N}$, which equals 1, produces Equation 2.117:

$$\eta_1 = \eta_0 \frac{M + N \cos \delta}{M + N} \quad \text{Equation 2.117}$$

After dividing the numerator and denominator of the right-hand side of Equation 2.117 by N and recognizing that $\cos \delta = \sin(\theta_0 + \beta + \theta)$, Equation 2.118 can be obtained as an

expression relating the stability number for particles on a side slope, η_1 , to the stability number η_0 :

$$\eta_1 = \eta_0 \left[\frac{(M/N) + \sin(\theta_0 + \beta + \theta)}{1 + (M/N)} \right] \quad \text{Equation 2.118}$$

As described in Section 2.2.1, the stability number for a discrete particle on a side-slope plane, η_0 , can be related to the boundary shear stress by Equation 2.119:

$$\eta_0 = \frac{\tau_0}{\tau_c} \quad \text{Equation 2.119}$$

To obtain an expression for β , NCMA (2006) made the same assumption as Julien (1998) and Stevens and Simons (1971) that the moment components of the drag force and submerged weight component, $F_S \sqrt{1 - a_\theta^2}$, normal to Cross-section A-A are balanced. Figure 2.10(d) presents a view of the cross-section normal to Cross-section A-A in which components of the drag force and of the weight force are present. Equation 2.120 presents the expression for these equal moment components:

$$\ell_3 F_D \sin \delta = \ell_1 F_S \sqrt{1 - a_\theta^2} \sin \beta \quad \text{Equation 2.120}$$

Equation 2.121 can be obtained by replacing $\sin \delta$ with $\cos(\beta + \theta_0 + \theta)$ in Equation 2.120 since $\delta + \beta + \theta_0 + \theta = 90^\circ$, and dividing both sides of the equation by $\ell_2 F_S$:

$$\frac{\ell_3 F_D}{\ell_2 F_S} \cos(\beta + \theta_0 + \theta) = \frac{\ell_1}{\ell_2} \sqrt{1 - a_\theta^2} \sin \beta \quad \text{Equation 2.121}$$

Equation 2.121 can be further reduced by substituting N for the drag force variable grouping on the left-hand side of the equation producing Equation 2.122:

$$N \cos(\beta + \theta_0 + \theta) = \frac{\ell_1}{\ell_2} \sqrt{1 - a_\theta^2} \sin \beta \quad \text{Equation 2.122}$$

Acknowledging that $\cos(\beta + \theta_0 + \theta) = \cos(\beta)\cos(\theta_0 + \theta) - \sin(\beta)\sin(\theta_0 + \theta)$ and substituting within Equation 2.122 produces Equation 2.123:

$$\cos(\beta)\cos(\theta_0 + \theta) - \sin(\beta)\sin(\theta_0 + \theta) = \frac{\ell_1 \sqrt{1 - a_\theta^2}}{\ell_2 N} \sin \beta \quad \text{Equation 2.123}$$

Dividing both sides of Equation 2.123 by $\sin \beta$ and solving for β provides Equation 2.124:

$$\beta = \tan^{-1} \left[\cos(\theta_0 + \theta) / \left(\frac{\ell_1 \sqrt{1 - a_\theta^2}}{\ell_2 N} + \sin(\theta_0 + \theta) \right) \right] \quad \text{Equation 2.124}$$

Multiplying the bottom left term of the right-hand side of Equation 2.124 by $(M + N)/\eta_0$, which is equal to 1 by the definition of η_0 , produces Equation 2.125:

$$\beta = \tan^{-1} \left[\cos(\theta_0 + \theta) / \left(\frac{(M + N)\ell_1 \sqrt{1 - a_\theta^2}}{\eta_0 \ell_2 N} + \sin(\theta_0 + \theta) \right) \right] \quad \text{Equation 2.125}$$

Lastly, multiplying the bottom left term of the right-hand side of Equation 2.125 by $\frac{1/N}{1/N}$

generates Equation 2.126, the expression used for β in NCMA (2006):

$$\beta = \tan^{-1} \left[\cos(\theta_0 + \theta) / \left(\frac{(M/N + 1)\sqrt{1 - a_\theta^2}}{(\ell_2/\ell_1)\eta_0} + \sin(\theta_0 + \theta) \right) \right] \quad \text{Equation 2.126}$$

NCMA (2006) assumed that the drag and lift forces have the same value. With this assumption the ratio of M and N relies solely on the corresponding moment arms as demonstrated by Equation 2.127:

$$M/N = \frac{\ell_4 F_L \ell_2 F_S}{\ell_2 F_S \ell_3 F_D} = \ell_4 / \ell_3 \quad \text{Equation 2.127}$$

The assumption that the drag and lift forces are equal varies from the assumption made by Julien (1998) that the moments created by the lift and drag forces are equal.

Like the method given by Clopper (1991), NCMA (2006) included the terms displayed in Equation 2.61 that account for additional drag and lift forces which occur when blocks are not perfectly installed. Adding the additional lift and drag forces to the safety factor equation produces Equation 2.128, which is the safety factor formula given in NCMA (2006):

$$SF_o = \frac{(\ell_2/\ell_1)a_\theta}{\sqrt{1 - a_\theta^2} \cos \beta + (\ell_2/\ell_1)\eta_1 + \frac{\ell_3 F_D'}{\ell_1 F_S} \sin(\theta_0 + \beta) + \frac{\ell_3 F_L'}{\ell_1 F_S}} \quad \text{Equation 2.128}$$

In summary, NCMA (2006) presented a method for determining a safety factor by calculating consecutively Equation 2.127, Equation 2.119, Equation 2.107, Equation 2.108, Equation 2.126, Equation 2.118, Equation 2.61, and Equation 2.128. Table 2.7 summarizes the NCMA (2006) safety factor equations and computation order. Values for bed slope, side slope, block geometry, block weight, specific gravity of block material,

design velocity, design shear stress, and critical shear stress are required to use the NCMA (2006) method.

Table 2.7: Safety Factor Calculation Method According to the NCMA (2006)

Order of Calculation	Equation	Equation Number
1	$M/N = \ell_4/\ell_3$	Equation 2.127
2	$\eta_0 = \frac{\tau_0}{\tau_c}$	Equation 2.119
3	$a_\theta = \sqrt{\cos^2 \theta_1 - \sin^2 \theta_0}$	Equation 2.107
4	$\theta = \tan^{-1} \left(\frac{\sin \theta_0 \cos \theta_1}{\sin \theta_1 \cos \theta_0} \right)$	Equation 2.108
5	$\beta = \tan^{-1} \left[\cos(\theta_0 + \theta) / \left(\frac{(M/N + 1)\sqrt{1 - a_\theta^2}}{(\ell_2/\ell_1)\eta_0} + \sin(\theta_0 + \theta) \right) \right]$	Equation 2.126
6	$\eta_1 = \eta_0 \left[\frac{(M/N) + \sin(\theta_0 + \beta + \theta)}{1 + (M/N)} \right]$	Equation 2.118
7	$F_D' = F_L' = 0.5\rho(\Delta z)wV^2$	Equation 2.61
8	$SF_o = \frac{(\ell_2/\ell_1)a_\theta}{\sqrt{1 - a_\theta^2} \cos \beta + (\ell_2/\ell_1)\eta_1 + \frac{\ell_3 F_D'}{\ell_1 F_S} \sin(\theta_0 + \beta) + \frac{\ell_3 F_L'}{\ell_1 F_S}}$	Equation 2.128

2.3 SUMMARY

Testing and evaluation of ACB protection systems has been conducted by CIRIA, FHWA, USACE, and Colorado State University (CSU) dating back to the late 1980s. Overtopping hydraulic conditions is the primary form of testing ACB armored embankments with the exception of Abt *et al.* (2001) which included testing of channelized flow conditions. The current state-of-the-practice for testing and evaluation of ACB protection systems is the ASTM D7277 (2008) testing standard and corresponding ASTM D7276 (2008) standard for analysis and interpretation of ACB test data.

To obtain design guidelines for ACB protection systems, safety factor methods developed for riprap design have been tailored to engineered armor units. From the literature review, two safety factor methods for ACB protection systems were identified: 1) Clopper (1991) and 2) NCMA (2006). Within both derivations, a moment stability analysis was used in conjunction with a stability number for hydrodynamic forces. The current state-of-the practice for ACB system hydraulic design is NCMA (2006).

3 EXAMINATION OF ASSUMPTIONS IN SAFETY

FACTOR DERIVATIONS

Throughout the safety factor (SF) derivations presented in Section 2.2, a significant number of assumptions were used to develop the safety factor computation methods. As with many areas of engineering, simplifications can be necessary to describe the mechanics of a phenomenon simply due to the large number of variables and availability of appropriate input values for computation. Given that the moment stability analysis methods were extrapolated outside of the original application, the employed assumptions need to be identified and investigated for the appropriate use for ACB design. Chapter 3 identifies each of the assumptions applied in the safety factor derivations and provides an investigation of the relevance of each assumption.

3.1 IDENTIFICATION OF ASSUMPTIONS

One assumption identified for Clopper (1991) and NCMA (2006) is that for flow conditions other than incipient motion, η can be expressed in the form of a ratio of the boundary shear stress to the critical shear stress. Since the critical shear stress is a constant, this assumption implies a linear relationship between the stability number and the boundary shear stress. Recalling that the stability number, η , is related to the drag

force and lift force, Equation 3.1 expresses the relationship imposed between these forces and the boundary shear stress:

$$\eta = \frac{\ell_4 F_L}{\ell_2 W_S} + \frac{\ell_3 F_D}{\ell_2 W_S} = \frac{\tau_0}{\tau_c} \quad \text{Equation 3.1}$$

This relationship assumes that the lift and drag forces are solely dependent upon the boundary shear stress. When the boundary shear stress is 0, the value of the stability number, η , is 0; and, as previously established, when the boundary shear stress is equal to the critical shear stress, the value of the stability number is unity. Figure 3.1 illustrates the assumed linear relationship, but also presents other potential relationships that satisfy these specific known values.

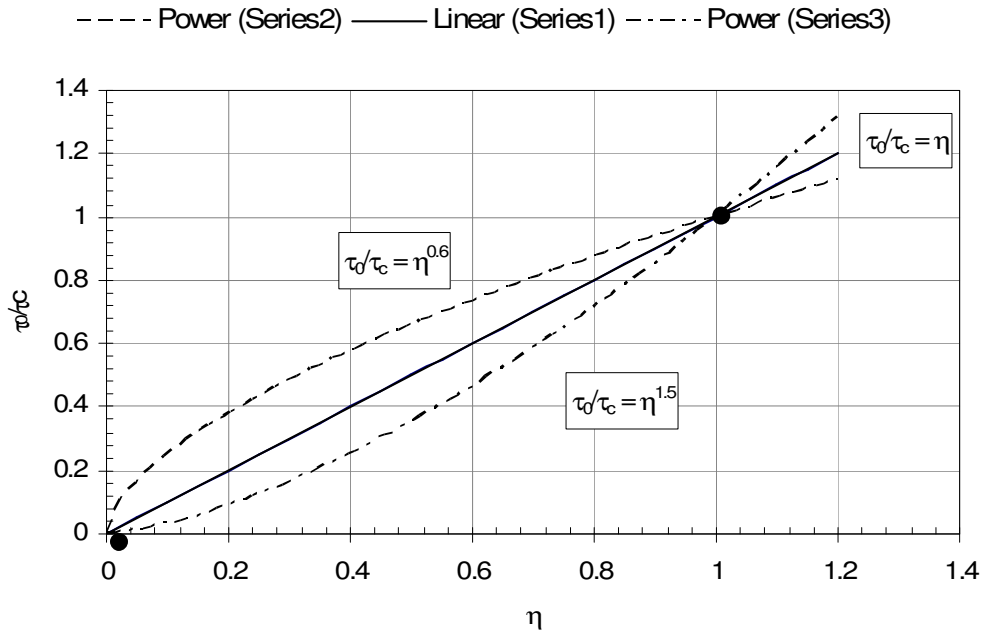


Figure 3.1: Potential Relationships between the Stability Number and the Boundary Shear Stress to Critical Shear-stress Ratio

Critical shear-stress values are required to use both calculation methods. Having an accurate value for the critical shear stress is crucial considering it is used for the

computation of the stability number, η . An extrapolation method is given to obtain the critical shear-stress value for a block on a given slope from a known value for the same block on a different slope. Equation 3.2 provides the extrapolation formula to obtain the critical shear stress for a block on an untested slope, $\tau_{C\theta_U}$ (NCMA, 2006):

$$\tau_{C\theta_U} = \tau_{C\theta_T} \left(\frac{\ell_2 \cos \theta_U - \ell_1 \sin \theta_U}{\ell_2 \cos \theta_T - \ell_1 \sin \theta_T} \right) \quad \text{Equation 3.2}$$

where

$\tau_{C\theta_T}$ = critical shear stress for the tested bed slope (lbs/ft²);

θ_U = untested bed slope (radians);

θ_T = tested bed slope (radians);

ℓ_2 = moment arm corresponding to the weight force component normal to the bed surface (ft); and

ℓ_1 = moment arm corresponding to the weight force component parallel to the bed surface (ft).

In addition, an extrapolation formula is given to obtain the critical shear stress for an untested block, τ_{CU} , from a value known for a similar tested block. This formula is provided in Equation 3.3 (NCMA, 2006):

$$\tau_{CU} = \tau_{CT} \left(\frac{W_{SU} \ell_{2U} (\ell_{3T} + \ell_{4T})}{W_{ST} \ell_{2T} (\ell_{3U} + \ell_{4U})} \right) \quad \text{Equation 3.3}$$

where

τ_{CT} = critical shear stress for the tested block (lbs/ft²);

W_{SU}, W_{ST} = submerged weight of the untested and tested blocks (lbs),
respectively;

$\ell_{2U}, \ell_{3U}, \ell_{4U}$ = moment arms for the untested block (ft); and

$\ell_{2T}, \ell_{3T}, \ell_{4T}$ = moment arms for the tested block (ft).

Clopper (1991) and NCMA (2006) safety factor methods use trigonometric simplifications for the weight force distributions, which are only suitable for small bed slopes. Clopper (1991) derived expressions for the weight force distributions do not account for the bed slope. As a result, the Clopper (1991) method produces non-conservative safety factor predictions at higher bed slopes. Conversely, the NCMA (2006) method over accounts for the bed slope and generates conservative predictions at higher bed slopes.

An additional shared assumption is that the lift force and drag force are equivalent. This is considered a conservative assumption by Clopper (1991); however, there is no evidence to verify that this assumption is conservative. Without a known lift coefficient for the block, calculating the lift force is not feasible.

For Clopper (1991) and NCMA (2006), a value is calculated for the block movement direction angle, β ; however, the corresponding movement arms for the forces acting along the cross section taken at the angle β are specified as half of the block diagonal. Rotation about a computed direction angle, β , other than the angle to the block corner or the edge of a block is impossible. Furthermore, the moment arms employed imply that the block rotates about the block corner which has a defined angle, β , from the

block geometry. Dependent on conditions, rotation may initiate about the downstream edge of the block or the inside edge of the block facing the center of the channel. Calculating safety factors for rotation about each of the three potential rotation points is necessary to determine the critical rotation mode.

To obtain an expression for β , Clopper (1991) and NCMA (2006) assume that the moment components of the drag force and submerged weight component normal to the direction of flow are balanced. This excludes the lift force and a component of the weight force which also create moments for rotation in this cross section. Since the angle β is defined by the armor unit geometry, this assumption is unnecessary.

A value of eight-tenths of the armor unit height is specified to be appropriate for the moment arm corresponding to the drag force in both calculation methods. According to NCMA (2006), this value is a good estimate which accounts for both the drag force on the top surface of the block and the drag force on the body of the block. Accounting for the drag force acting on the side of the block assumes there is significant interstitial flow within the revetment system.

3.2 INVESTIGATION OF ASSUMPTIONS

An example scenario was developed to investigate the assumptions outlined in the preceding chapter. The example revetment is composed of a rectangular-shaped block with an assumed perfect installation. It has a submerged weight of 37.3 lbs; a critical shear stress of 22.4 lbs/ft² for a horizontal plane; and values of l_1 , l_2 , l_3 , and l_4 as 0.198 ft, 0.971 ft, 0.317 ft, and 0.971 ft, respectively. For this example, the shear stress is 5.26 lbs/ft², the side slope is 3 ft/ft and the bed slope is 0.50 ft/ft. An evaluation of the

stability of the example block under these normal flow conditions produces a safety factor value of 3.37 using the method presented in Clopper (1991), and a value of 2.42 using the method presented in NCMA (2006). Figure 3.2 presents Clopper (1991) and NCMA (2006) safety factor values computed for the example with varying shear stresses between 0.5 to 10.5 lbs/ft², while keeping all other variables constant. Figure 3.3 presents Clopper (1991) and NCMA (2006) safety factor values computed for the example with varying bed slopes between 0.005 to 1.0 ft/ft, while keeping all other variables constant. Figure 3.4 presents Clopper (1991) and NCMA (2006) safety factor values computed for the example with varying side slopes between 1 to 10 ft/ft, while keeping all other variables constant. This section discusses each of the assumptions and evaluates the resulting influence on the safety factor prediction for the given example.

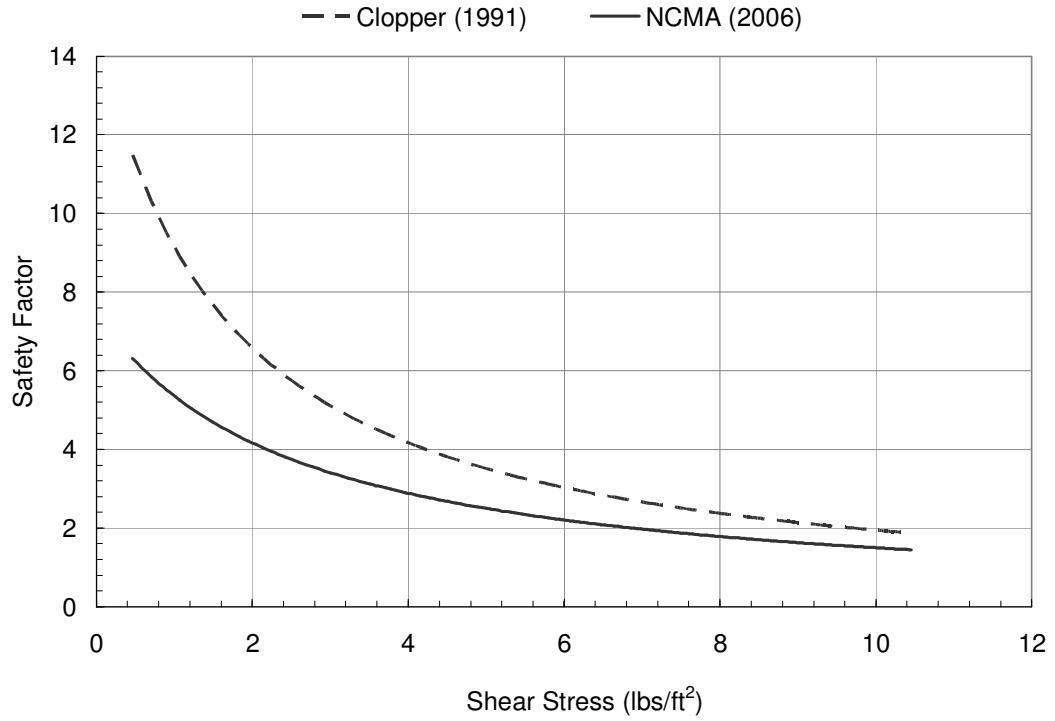


Figure 3.2: Calculated Safety Factors for Varying Shear Stress

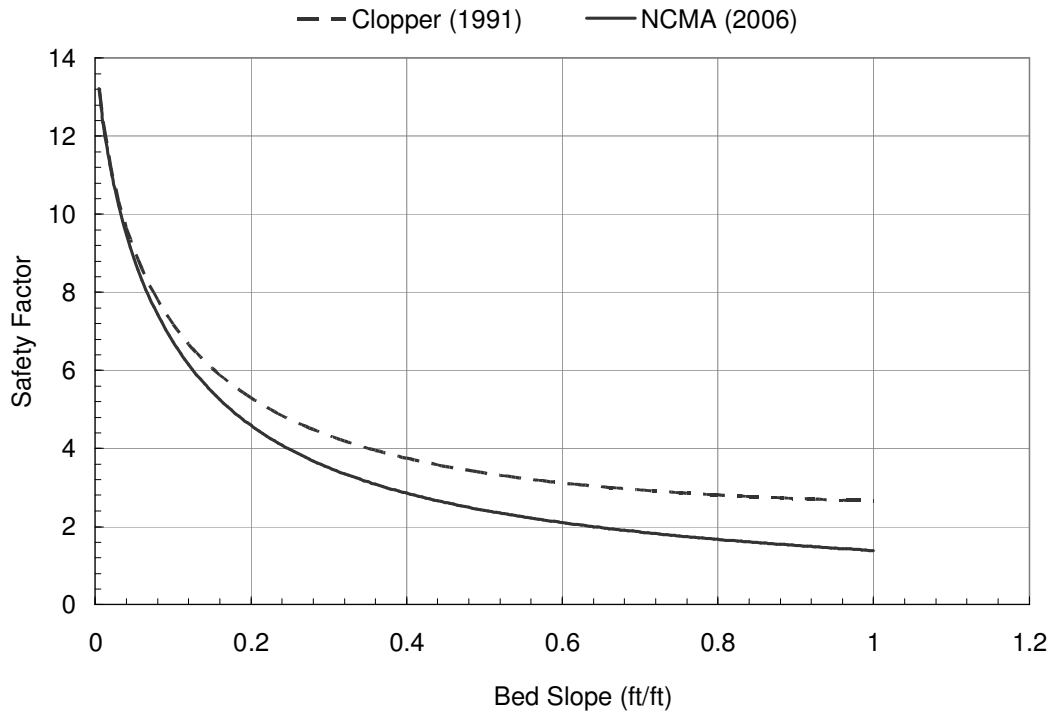


Figure 3.3: Calculated Safety Factors for Varying Bed Slopes

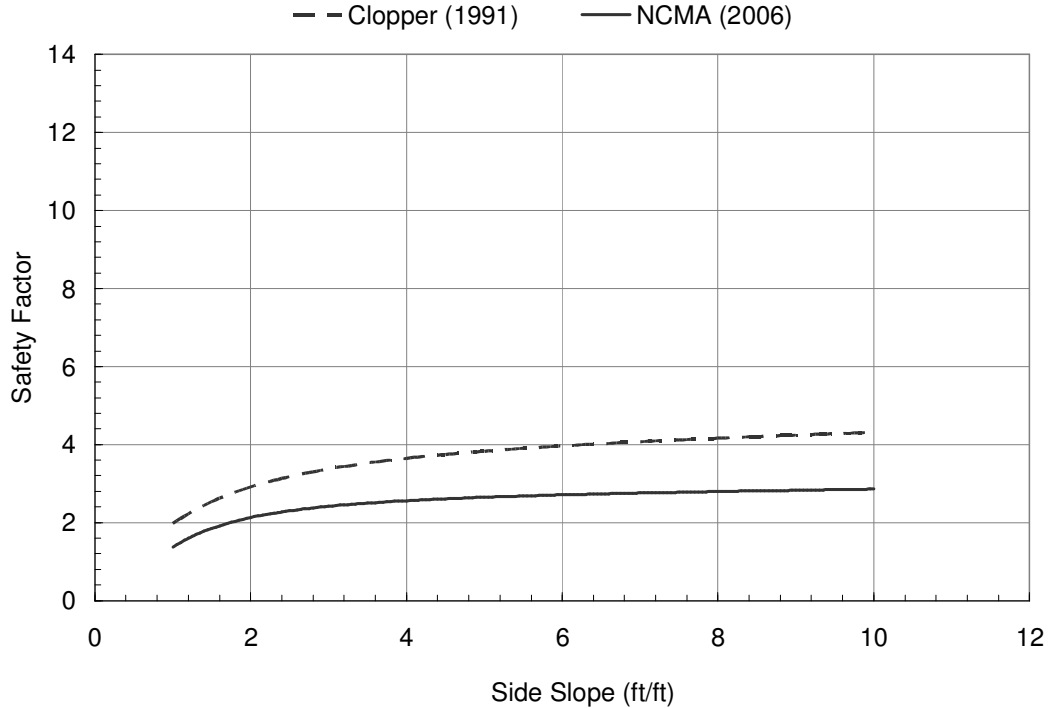


Figure 3.4: Calculated Safety Factors for Varying Side Slopes

Removing the assumption that the stability number is equal to the ratio of the boundary shear stress to the critical shear stress in the example results in safety factors of 3.19 and 2.30 for the Clopper (1991) method and the NCMA (2006) method, respectively. The value of the stability number was computed maintaining the assumption that the lift and drag forces are equal and calculating the drag force using the product of the shear stress and block surface area parallel to the flow direction. Using the stability number assumption produces a 6% difference, which is non-conservative, for the Clopper (1991) method and 5% difference, which is non-conservative, for the NCMA (2006) method. Figure 3.5 illustrates the influence of this assumption for a range of shear-stress values from 0.5 to 10.5 lbs/ft².

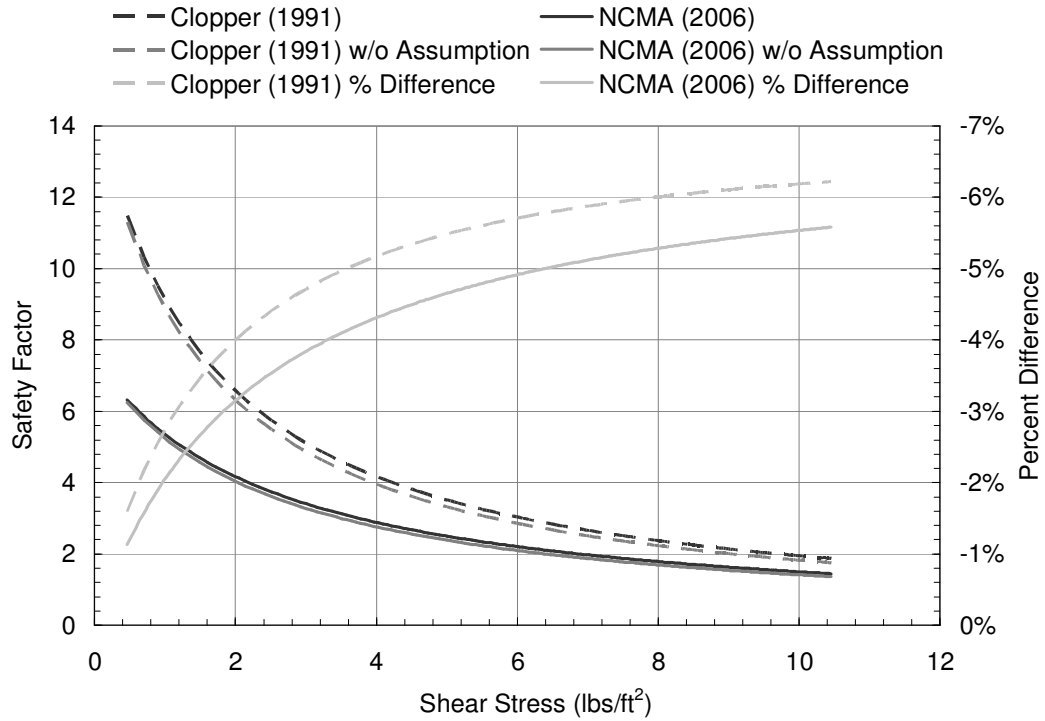


Figure 3.5: Comparison of Safety Factors without the Assumption of the Relationship between Stability Number and Shear Stress

Assuming the critical shear stress is actually 10% less than the extrapolated value for the example block, the safety factor would be 3.10 (8% difference) and 2.25 (7% difference) for the Clopper (1991) and NCMA (2006) methods, respectively. Figure 3.6 illustrates the influence of this assumption for a range of shear-stress values from 0.5 to 10.5 lbs/ft².

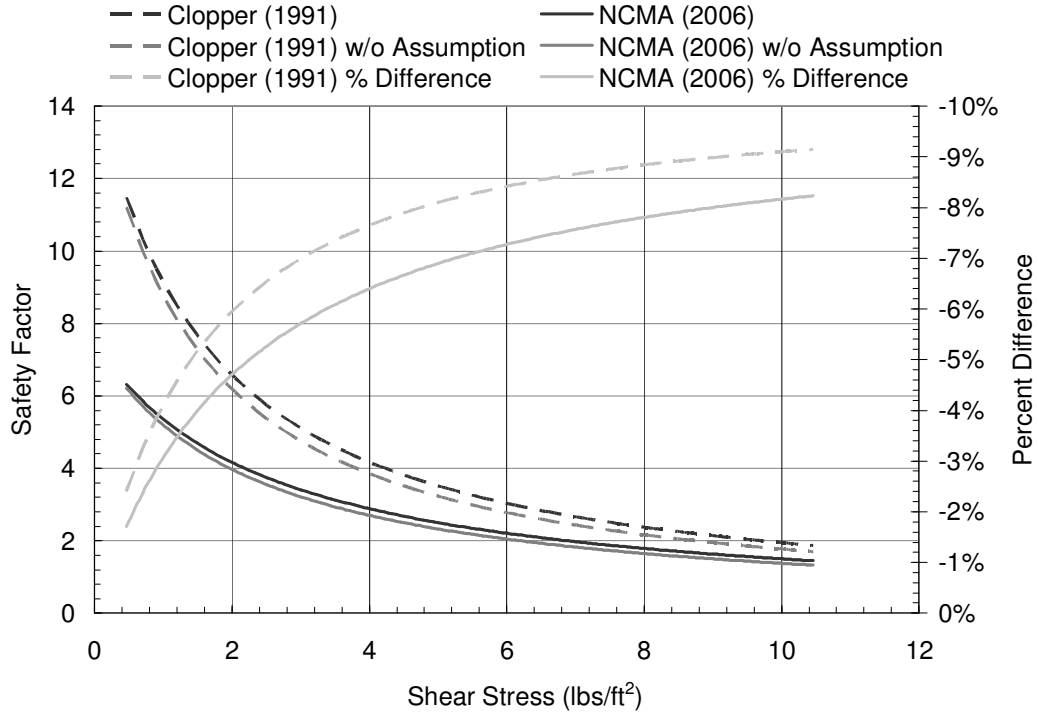


Figure 3.6: Safety Factor Comparison with 10% Non-conservative Critical Shear Stress

Without trigonometric simplifications for the weight force distribution, the safety factor values are 2.67 and 2.67 for the Clopper (1991) method and the NCMA (2006) method, respectively. Therefore, using trigonometric simplifications for the example results in a non-conservative 21% difference for the Clopper (1991) method and a conservative 10% difference for the NCMA (2006) method. Figure 3.7 illustrates the influence of this assumption for a range of bed slopes from 0.005 to 1.0 ft/ft.

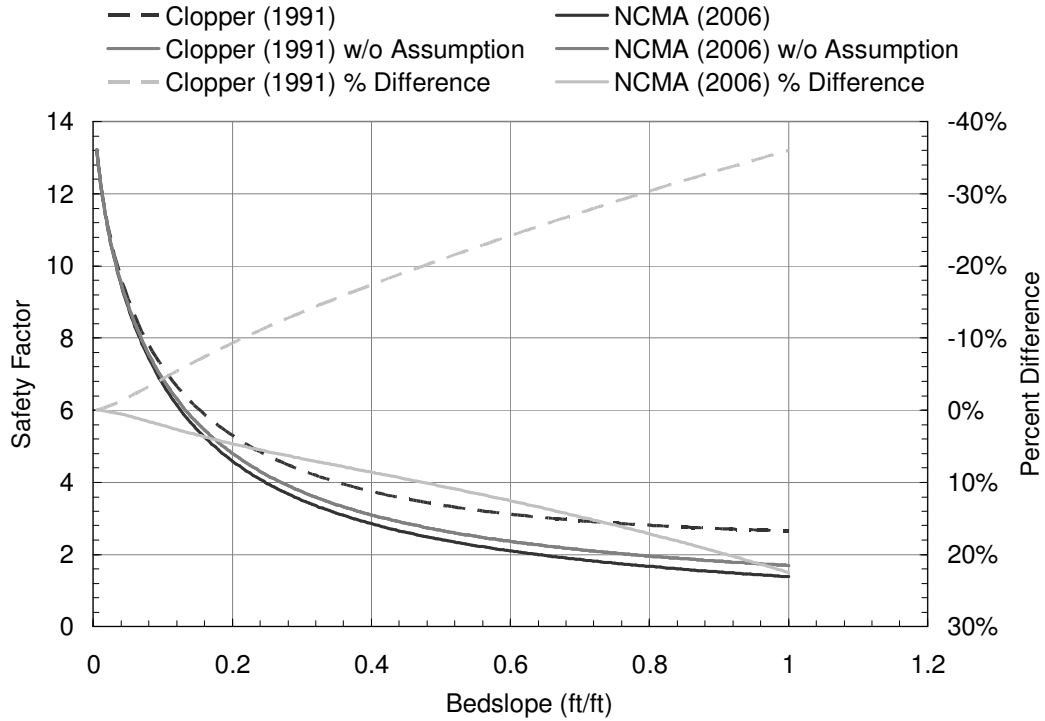


Figure 3.7: Safety Factor Comparison without Trigonometric Simplifications

When using a value of 48.3° for β , which is the angle to the block corner for the example block, safety factor values were calculated to be 3.40 and 2.81 for the Clopper (1991) method and NCMA (2006) method, respectively. Using the calculated value for β produces a conservative 2% and 17% difference for the Clopper (1991) method and the NCMA (2006) method, respectively. The degree of error associated with calculating the angle β using the given formulas varies with hydraulics. Figure 3.8 displays a comparison of the calculated safety factors for a range of shear stresses between 0.5 to 10.5 lbs/ft² computed using a value of 48.3° for the angle β .

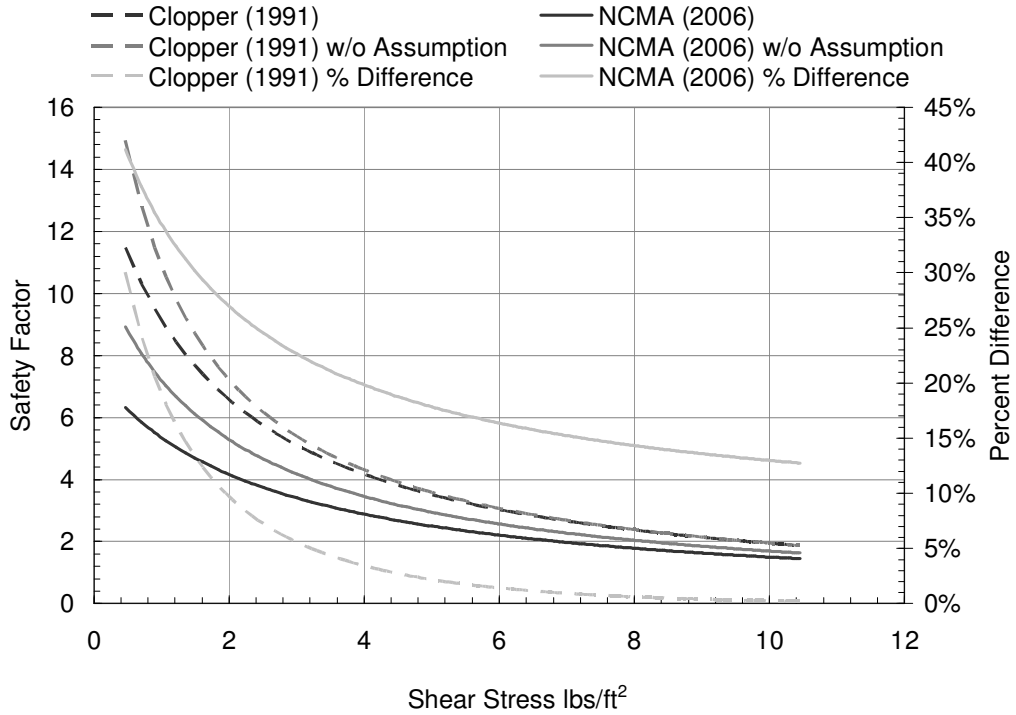


Figure 3.8: Safety Factor Comparison with β Equal to 48.3°

Using the block height for the moment arm corresponding to the drag force should produce a more conservative prediction given the mechanics of the moment stability analysis; however, using the two methods with a moment arm equal to the block height produced safety factor values of 3.39 (0.6% difference) and 2.42 (0.0% difference) for the Clopper (1991) method and the NCMA (2006) method, respectively. The conservative prediction associated with using eight-tenths of the block height comes from the mechanics of the combined formulas. While changing ℓ_3 has very little effect on the stability number, η , it increases β thereby decreasing $\cos \beta$ and ultimately increasing the safety factor. Although the assumption proved slightly conservative, it illustrates the flawed mechanics of the combined formulas given the original form of the safety factor

equation (Equation 2.38). Figure 3.9 provides a comparison of the safety factor values computed using the block height for ℓ_3 .

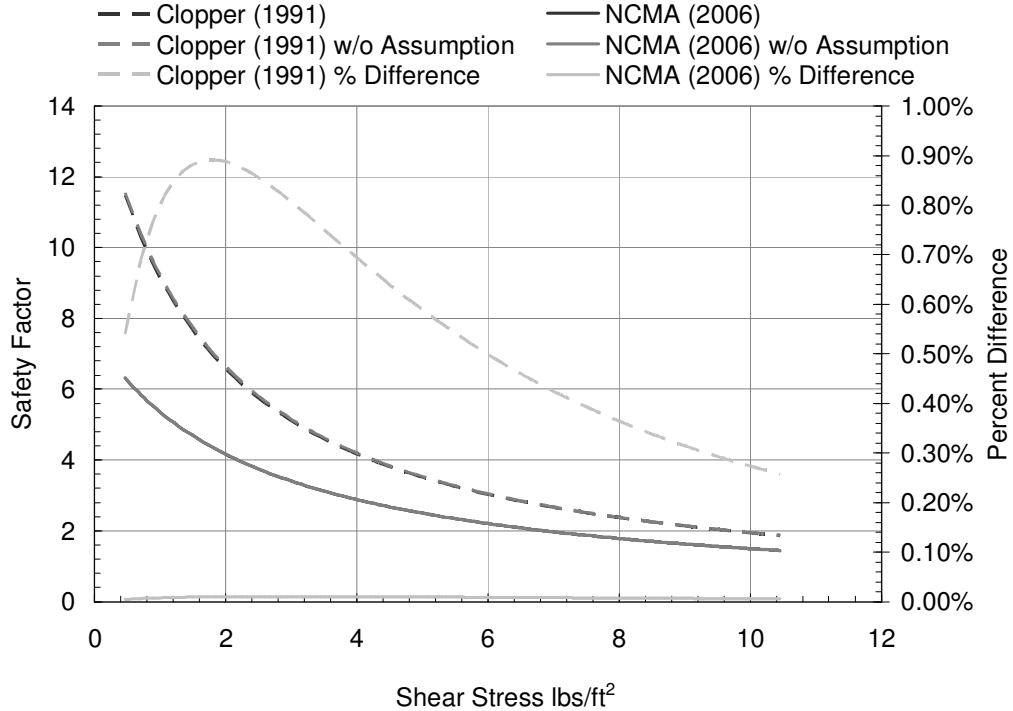


Figure 3.9: Safety Factor Comparison Using the Block Height for ℓ_3

Calculating a safety factor for the example assuming a lift coefficient of 0.045, results in a value of 2.06 (-39% difference) for the Clopper (1991) method and a value of 1.58 (-35% difference) for the NCMA (2006) method. A comparison of the safety factors computed without the assumption of equal lift and drag forces for a constant shear-stress value and a range of velocities of 2.98 to 23.70 ft/s is given by Figure 3.10. Furthermore, Figure 3.11 presents the relationship between the lift and drag forces for a range of flow velocities from 3 to 24 ft/s for the example. The theoretical analysis indicates that assuming the lift and drag forces are equal is a reasonable assumption for cases with velocities less than approximately 10 ft/s.

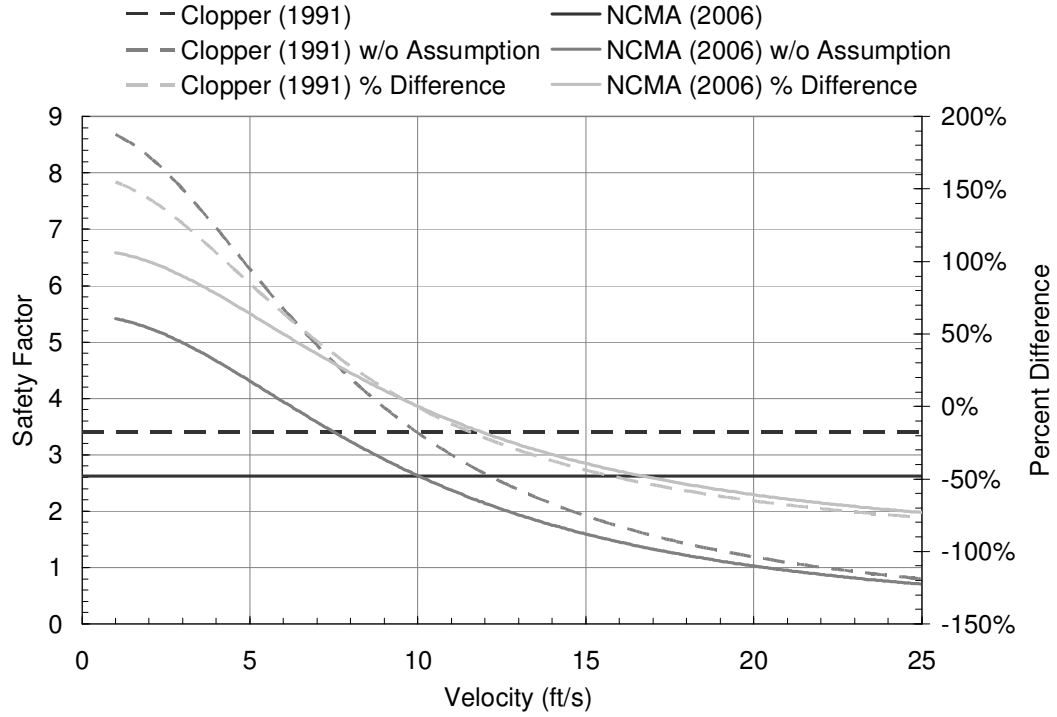


Figure 3.10: Safety Factor Comparison without the Assumption of Equal Lift and Drag Forces (lift coefficient equal to 0.045)

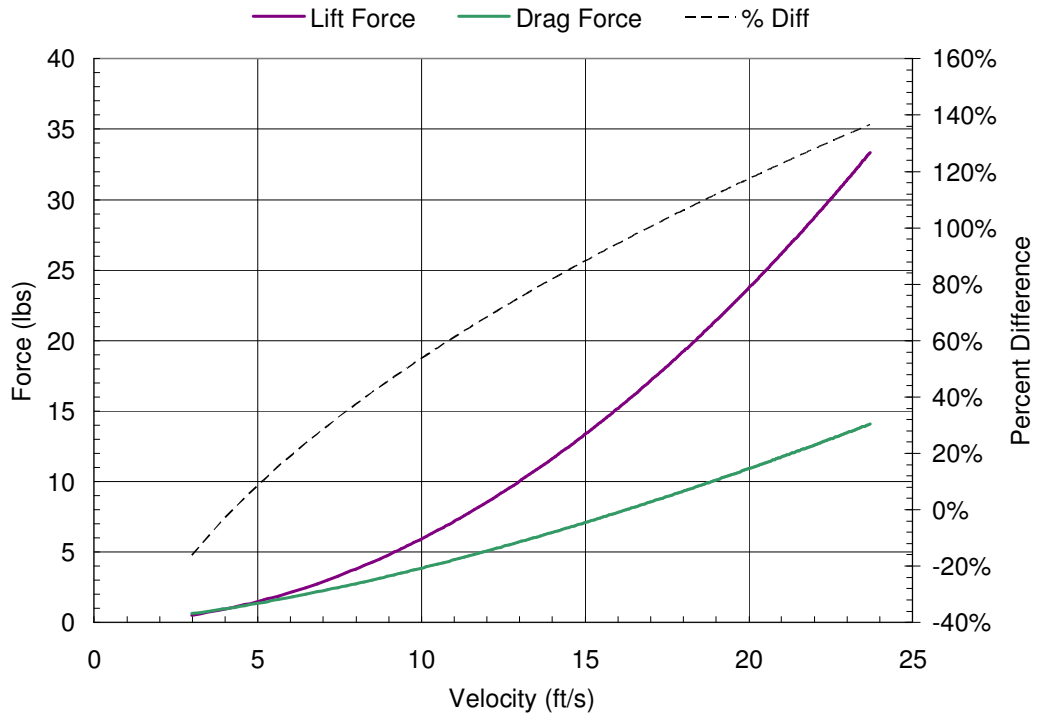


Figure 3.11: Lift Force and Drag Force Relationship to Velocity

The relative influence on computed safety factors for each assumption has been investigated. Table 3.1 provides a summary of the results from the comparisons to the example scenario. The assumption of equal lift and drag forces has been identified as the most influential for this high-velocity, steep-slope bed example. Furthermore, this assumption is non-conservative, which can have drastic consequences if misapplied. Other unsuitable assumptions include the trigonometric simplifications and the computation of the angle β .

Table 3.1: Summary of the Sensitivity of Assumptions with Respect to the Example

Description	Comparison with Example ^a			
	Clopper (1991)		NCMA (2006)	
	Safety Factor	Percent Difference	Safety Factor	Percent Difference
Original Methods	3.37	-	2.42	-
Assuming the lift coefficient is 0.045	2.06	-38.9%	1.58	-34.7%
Without trigonometric simplifications	2.67	-20.8%	2.67	10.3%
Assuming critical shear stress is 10% less than the extrapolated value	3.10	-8.0%	2.25	-7.0%
Using a value of 48.3° for β	3.44	2.1%	2.84	17.4%
Without assumption of relationship between stability number and shear stress	3.19	-5.3%	2.30	-5.0%
Using the block height for the moment arm corresponding to the drag force	3.39	0.6%	2.42	0.0%

^a Shear stress of 5.26 lbs/ft², side slope of 3 ft/ft, and bed slope of 0.50 ft/ft

3.3 SUMMARY

From the literature review, two primary safety factor methods were identified: Stevens and Simons (1971) and Julien (1998). Within both derivations, the moment stability analysis was used in conjunction with the stability number for hydrodynamic

forces. The original application for both methods was to produce safety factors for cohesionless particles, which exhibit a quasi-spherical shape, on a channel side slope.

The Stevens and Simons (1971) and Julien (1998) safety factor methods have been adapted and modified to generate design procedures applicable to engineered armor units (Clopper, 1991; HCFCD, 2001; NCMA, 2006). As detailed in Section 3.1, additional assumptions and simplifications were incorporated which add uncertainty to the level of accuracy and conservatism for the block safety factor design method. For example, Clopper (1991) presents an extrapolation of the safety factor method developed by Stevens and Simons (1971) for mild-slope, low-velocity hydraulic conditions to the high-velocity, steep-slope conditions associated with dam overtopping environments. In addition, NCMA (2006) endorses a particle stability analysis method developed for subcritical flow regimes (Julien, 1998; Julien and Anthony, 2002) for channels designed to convey supercritical flow.

Through the investigation of assumptions presented in Section 3.2, the most unsuitable assumption for the high-velocity, steep-slope example was identified as the assumption of equal lift and drag forces. Trigonometric simplifications and the computation of the angle β were also identified as inapt assumptions affecting the computed safety factor for the example by as much as 20.8% and 17.4%, respectively. Based on the theoretical investigation of assumptions used in the Clopper (1991) and NCMA (2006) safety factor method derivation, the need to evaluate the Clopper (1991) and NCMA (2006) safety factor method using full-scale data was identified.

4 ACB TESTING DATABASE

4.1 INTRODUCTION

Datasets from ACB testing were necessary to evaluate the ability of the Clopper (1991) and NCMA (2006) safety factor design methods to predict stable and unstable conditions. Three datasets were developed from testing of three ACB systems: 1) 30S, 2) Petraflex-Vick (hereafter referred to as Petraflex), and 3) the Corps Block. In addition to the 30S and Petraflex data available in Clopper and Chen (1988), 30S, Petraflex, and Corps Block data were available from testing previously conducted at CSU (Abt *et al.*, 2001; Robeson *et al.*, 2002). Since the majority of overtopping tests were conducted on a 2H:1V embankment slope, two additional installations were tested on the 30S block at a bed slope of 0.230 ft/ft and 0.431 ft/ft to develop a more comprehensive dataset. All hydraulic testing performed at CSU was conducted in accordance to ASTM D7277 (2008).

4.2 30S DATASET

The 30S dataset included testing reported in Clopper and Chen (1988), testing reported in Robeson *et al.* (2002), and two supplemental tests conducted at the CSU Hydraulics Laboratory in the summer of 2009. 30S block properties are provided in

Appendix B and Figure 4.1 presents a photograph of the 30S block installed in an overtopping test channel.



Figure 4.1: Photograph of Installed 30S Blocks

Testing of the 30S system was conducted for the FHWA in 1987 and reported in Clopper and Chen (1988). The 30S system was installed with cables on a 13-ft long soil embankment with a slope of 0.442 ft/ft. Clopper and Chen (1988) tested the 30S system at 1-ft, 2-ft, and 4-ft overtopping depths. Table 4.1 presents the hydraulic results from the 30S overtopping testing reported in Clopper and Chen (1988). Additionally, Appendix A provides the available water-surface elevation, bed-elevation, and flow-velocity data for the Clopper and Chen (1988) 30S tests. As reported in Clopper and Chen (1988), system instability was observed during the 4-ft overtopping test. Based on the results of the Clopper and Chen (1988) analysis, a limiting shear-stress value of 15 lbs/ft² was reported for the 30S system on the tested embankment. No limiting value for velocity was reported in Clopper and Chen (1988).

Table 4.1: Hydraulic Results for 30S FHWA Testing Reported in Clopper and Chen (1988)

Test ID No.	Block Name	Over-topping Depth (ft)	Test Date	S_0 (ft/ft)	Q (cfs)	V^a (ft/s)	τ_0^a (lbs/ft ²)	Manning's n^a	System Condition
1	30S	1.0	9/1/1987	0.442	13.8	12.9	7.0	0.044	Stable
2	30S	2.0	9/9/1987	0.442	34.0	15.1	12.0	0.073	Stable
3	30S	4.0	9/11/1987	0.442	90.5	16.2	36.0	0.064	Unstable

^a Maximum values reported in Clopper and Chen (1988)

Testing was performed in 2000 by CSU on one installation of the 30S system on a 20-ft long, 2H:1V soil embankment (Robeson *et al.*, 2002). One test at a 1-ft overtopping depth was conducted for the CSU 30S installation. Table 4.2 provides testing information pertaining to the 2000 CSU 30S test. Additionally, Appendix C provides the flow-depth, bed-elevation, and flow-velocity data for the Robeson *et al.* (2002) 30S test. Shear stress and velocity values were not reported by Robeson *et al.* (2002) and therefore

are not presented in Table 4.2. System instability was observed during the 1-ft overtopping test. 30S blocks were physically removed from the test section during the 1-ft overtopping test.

Table 4.2: Robeson *et al.* (2002) 30S Testing

Test ID No.	Block Name	Overtopping Depth (ft)	Test Date	S_0 (ft/ft)	Q (cfs)	Notes	System Condition
4	30S	1.0	8/11/2000	0.499	10.0	Cabled	Unstable

Two supplemental 30S installations were tested at the CSU Hydraulics Laboratory in 2009 to provide 30S overtopping performance data for a wider range of embankment slopes. Testing was conducted in two flumes, a 40-ft long, 6-ft wide flume which was reconfigured to a 4-ft wide rectangular channel and a 30-ft long, 4-ft wide rectangular flume. Table 4.3 provides testing information pertaining to the 2009 CSU 30S tests. Additionally, Appendix C provides the flow-depth, bed-elevation, and flow-velocity data for the 2009 CSU 30S tests.

Table 4.3: 2009 CSU 30S Testing

Test ID No.	Block Name	Overtopping Depth (ft)	Test Date	S_0 (ft/ft)	Q (cfs)	Notes	System Condition
5	30S	1.0	6/14/2009	0.230	10.0	Not Cabled	Stable
6	30S	1.6	6/15/2009	0.230	20.0	Not Cabled	Stable
7	30S	2.0	6/15/2009	0.230	30.0	Not Cabled	Unstable
8	30S	0.9	6/25/2009	0.431	8.0	Not Cabled	Stable
9	30S	1.2	6/25/2009	0.431	12.0	Not Cabled	Unstable

For the 40-ft long channel, 30S blocks were installed on a soil embankment with a slope of 0.230 ft/ft. Testing was conducted at 1.0-ft, 1.6-ft, and 2.0-ft overtopping

depths. During the 2.0-ft overtopping test, one 30S block was physically removed from the test section. Therefore, the 2.0-ft overtopping test was identified as unstable.

For the 30-ft long channel, 30S blocks were installed on a soil embankment with a slope of 0.431 ft/ft. Testing was conducted at 0.9-ft and 1.2-ft overtopping depths. During the 1.2-ft overtopping test, 30S blocks were physically removed from the test section. Therefore, the 1.2-ft overtopping test was identified as unstable.

A combined dataset was developed from the available 30S test data. A total of nine tests were conducted, of which, five were identified as stable and four were identified as unstable. The 30S dataset is presented in Table 4.4. Discharges (Q) ranged from 8.0 to 90.5 cfs for the combined dataset and embankment slopes ranged from 0.230 to 0.499 ft/ft. Furthermore, embankment lengths ranged from 13 ft to 40 ft.

Table 4.4: Combined 30S Testing Dataset

Test ID No.	Block Name	Overtopping Depth (ft)	Test Date	S_0 (ft/ft)	Q (cfs)	Notes	System Condition
1	30S	1.0	9/1/1987	0.442	13.8	Cabled	Stable
2	30S	2.0	9/9/1987	0.442	34.0	Cabled	Stable
3	30S	4.0	9/11/1987	0.442	90.5	Cabled	Unstable
4	30S	1.0	8/11/2000	0.499	10.0	Cabled	Unstable
5	30S	1.0	6/14/2009	0.230	10.0	Not Cabled	Stable
6	30S	1.6	6/15/2009	0.230	20.0	Not Cabled	Stable
7	30S	2.0	6/15/2009	0.230	30.0	Not Cabled	Unstable
8	30S	0.9	6/25/2009	0.431	8.0	Not Cabled	Stable
9	30S	1.2	6/25/2009	0.431	12.0	Not Cabled	Unstable

4.3 PETRAFLEX DATASET

The Petraflex dataset included testing reported in Clopper and Chen (1988) and Robeson *et al.* (2002). Petraflex block properties are provided in Appendix B and Figure 4.2 presents a photograph of the Petraflex block installed in an overtopping test channel.



Figure 4.2: Photograph of Installed Petraflex Blocks

Testing of the Petraflex system was conducted for the FHWA in 1987 and reported in Clopper and Chen (1988). Petraflex blocks were installed with cables on a 13-ft long soil embankment with a slope of 0.437 ft/ft. Clopper and Chen (1988) tested the Petraflex system at 1.0-ft, 2.0-ft, and 4.0-ft overtopping depths. Table 4.5 presents the hydraulic results from the Petraflex overtopping testing reported in Clopper and Chen (1988). Additionally, Appendix A provides the available water-surface elevation, bed-elevation, and flow-velocity data for the Clopper and Chen (1988) Petraflex tests. System instability was not observed during the FHWA Petraflex testing. Based on the results of the Clopper and Chen (1988) analysis, a limiting shear-stress of greater than 30 lbs/ft² was reported for the Petraflex system on the tested embankment. No limiting value for velocity was reported in Clopper and Chen (1988).

Table 4.5: Hydraulic Results for Petraflex FHWA Testing Reported in Clopper and Chen (1988)

Test ID No.	Block Name	Overtopping Depth (ft)	Test Date	S_0 (ft/ft)	Q (cfs)	V^a (ft/s)	τ_0^a (lbs/ft ²)	Manning's n^a	System Condition
10	Petraflex	1.0	n/a	0.437	13.5	10.0	10.0	0.053	Stable
11	Petraflex	2.0	n/a	0.437	34.0	14.7	12.0	0.068	Stable
12	Petraflex	4.0	9/22/1987	0.437	96.0	16.9	32.0	0.080	Stable

n/a = not available

^a Maximum values reported in Clopper and Chen (1988)

Overtopping testing was performed in 2000 by CSU on the Petraflex system installed on a 20-ft long, 2H:1V soil embankment (Robeson *et al.*, 2002). CSU tested the Petraflex system at 1.0-ft and 2.0-ft overtopping depths in a 4-ft wide rectangular flume. Table 4.6 provides testing information pertaining to the 2000 CSU Petraflex tests. Additionally, Appendix C provides the water-surface elevation, bed-elevation, and flow-velocity data for the Robeson *et al.* (2002) Petraflex tests. Shear stress and velocity

values were not reported by Robeson *et al.* (2002) and therefore are not presented in Table 4.6. During the 2.0-ft overtopping test, gullies had formed under the Petraflex blocks resulting in loss of intimate contact between the blocks and the subgrade. Therefore, the 2.0-ft overtopping test was identified as unstable.

Table 4.6: Robeson *et al.* (2002) Petraflex Testing

Test ID No.	Block Name	Overtopping Depth (ft)	Test Date	S_0 (ft/ft)	Q (cfs)	Notes	System Condition
13	Petraflex	1.0	8/21/2000	0.501	10.0	Cabled	Stable
14	Petraflex	2.0	8/21/2000	0.501	28.4	Cabled	Unstable

A combined dataset was developed from the available Petraflex test data. A total of five tests were conducted, of which, four were identified as stable and one was identified as unstable. The Petraflex dataset is presented in Table 4.7. Discharges ranged from 10.0 to 96.0 cfs for the combined dataset and embankment slopes ranged from 0.437 to 0.501 ft/ft. Furthermore, embankment lengths ranged from 13 ft to 20 ft.

Table 4.7: Combined Petraflex Testing Dataset

Test ID No.	Block Name	Overtopping Depth (ft)	Test Date	S_0 (ft/ft)	Q (cfs)	Notes	System Condition
10	Petraflex	1.0	n/a	0.437	13.5	Cabled	Stable
11	Petraflex	2.0	n/a	0.437	34.0	Cabled	Stable
12	Petraflex	4.0	9/22/1987	0.437	96.0	Cabled	Stable
13	Petraflex	1.0	8/21/2000	0.501	10.0	Cabled	Stable
14	Petraflex	2.0	8/21/2000	0.501	28.4	Cabled	Unstable

n/a = not available

4.4 CORPS BLOCK DATASET

Additional testing data were available from the USACE Corps Block testing presented in Abt *et al.* (2001). Testing of the Corps Block included both overtopping and channelized conditions. Corps Block properties are provided in Appendix B and Figure 4.3 presents a photograph of the Corps Block being installed in the overtopping test channel. Overtopping tests were conducted in a 40-ft long, 4-ft wide flume that was configured with a crest length of 20 ft and a sloped section of 20 ft. Channelized testing was conducted in a half-trapezoidal channel with a bottom width of 1.2 ft and 2H:1V side slopes.



Figure 4.3: Photograph of Corps Blocks Installation

Overtopping tests reported by Abt *et al.* (2001) included two embankment slopes: 5H:1V and 7H:1V. Table 4.8 presents the hydraulic results from the Corps Block overtopping testing reported in Abt *et al.* (2001). Testing was conducted on the 5H:1V installation at 1.0-ft and 2.0-ft overtopping depths. Abt *et al.* (2001) identified the 2.0-ft overtopping test as a failure condition for the 5H:1V embankment slope. Testing was conducted on the 7H:1V Corps Block installation at 1.0-ft, 1.2-ft and 2.0-ft overtopping depths. Both the 1.2-ft and 2.0-ft overtopping tests were reported as failure conditions by Abt *et al.* (2001) for the 7H:1V embankment slope.

Table 4.8: Corps Block Overtopping Testing Data

Test ID No.	Block Name	Over-topping Depth (ft)	S_0 (ft/ft)	Q (cfs)	Flow Depth (ft)	Flow Velocity (ft/s)	Shear Stress (lbs/ft ²)	System Condition
15	Corps Block	1.0	0.200	11.0	0.28	13.6	3.46	Stable
16	Corps Block	2.0	0.200	28.5	0.49	17.3	4.92	Failure
17	Corps Block	1.0	0.143	9.75	0.25	12.8	2.07	Stable
18	Corps Block	2.0	0.143	25.0	0.65	16.5	4.79	Failure
19	Corps Block	1.2	0.143	13.0	n/a	14.5	n/a	Failure

n/a = not available

Channelized tests reported in Abt *et al.* (2001) included six tests with progressively increasing discharges. Table 4.9 presents the hydraulic results from the Corps Block channelized testing reported in Abt *et al.* (2001). Abt *et al.* (2001) identified the 112.0 cfs and 125.0 cfs tests as “failure transition” and “failure,” respectively. Test ID 25 was not used within the dataset since flow depth and shear stress values were not available and instability was identified at the conclusion of the previous test, Test ID 24.

Table 4.9: Corps Block Channelized Testing Data

Test ID No.	Block Name	S₀ (ft/ft)	Side Slope (H/V)	Q (cfs)	Flow Depth (ft)	Flow Velocity (ft/s)	Shear Stress (lbs/ft²)	System Condition
20	Corps Block	0.030	2.0	29.0	2.0	6.5	3.74	Stable
21	Corps Block	0.030	2.0	50.0	2.1	7.9	3.93	Stable
22	Corps Block	0.030	2.0	80.0	2.3	11.5	4.21	Stable
23	Corps Block	0.030	2.0	100.0	2.3	13.2	4.31	Stable Transition
24	Corps Block	0.030	2.0	112.0	2.5	14.0	4.68	Failure Transition
25	Corps Block	0.030	2.0	125.0	n/a	14.8	n/a	Failure

4.5 SUMMARY

A database of twenty-four tests was developed from available testing data for the purpose of evaluating the NCMA (2006) safety factor design method. Table 4.10 provides a summary of the entire ACB database. Three ACB systems were included in the database: 1) 30S, 2) Petraflex, and 3) the Corps block. Both overtopping and channel hydraulic conditions are represented in the database.

Table 4.10: Entire ACB Database

Test ID No.	Block Name	Test Condition	Over-topping Depth (ft)	S_0 (ft/ft)	Side Slope (H/V)	Q (cfs)	System Condition
1	30S	Overtopping	1.0	0.442	n/a	13.8	Stable
2	30S	Overtopping	2.0	0.442	n/a	34.0	Stable
3	30S	Overtopping	4.0	0.442	n/a	90.5	Unstable
4	30S	Overtopping	1.0	0.499	n/a	10.0	Unstable
5	30S	Overtopping	1.0	0.230	n/a	10.0	Stable
6	30S	Overtopping	1.6	0.230	n/a	20.0	Stable
7	30S	Overtopping	2.0	0.230	n/a	30.0	Unstable
8	30S	Overtopping	0.9	0.431	n/a	8.0	Stable
9	30S	Overtopping	1.2	0.431	n/a	12.0	Unstable
10	Petraflex	Overtopping	1.0	0.437	n/a	13.5	Stable
11	Petraflex	Overtopping	2.0	0.437	n/a	34.0	Stable
12	Petraflex	Overtopping	4.0	0.437	n/a	96.0	Stable
13	Petraflex	Overtopping	1.0	0.501	n/a	10.0	Stable
14	Petraflex	Overtopping	2.0	0.501	n/a	28.4	Unstable
15	Corps Block	Overtopping	1.0	0.200	n/a	11.0	Stable
16	Corps Block	Overtopping	2.0	0.200	n/a	28.5	Unstable
17	Corps Block	Overtopping	1.0	0.143	n/a	9.8	Stable
18	Corps Block	Overtopping	2.0	0.143	n/a	25.0	Unstable
19	Corps Block	Overtopping	1.2	0.143	n/a	13.0	Unstable
20	Corps Block	Channel	n/a	0.030	2.0	29.0	Stable
21	Corps Block	Channel	n/a	0.030	2.0	50.0	Stable
22	Corps Block	Channel	n/a	0.030	2.0	80.0	Stable
23	Corps Block	Channel	n/a	0.030	2.0	100.0	Stable
24	Corps Block	Channel	n/a	0.030	2.0	112.0	Unstable

n/a = not applicable

Nine total overtopping tests on four different installations composed the 30S dataset. Discharges ranged from 8.0 to 90.5 cfs, embankment slopes ranged from 0.230 to 0.499 ft/ft, and embankment lengths ranged from 13 to 40 ft for the combined 30S dataset.

The Petraflex dataset was composed of five total overtopping tests on two different installations. Discharges ranged from 10.0 to 96.0 cfs, embankment slopes

ranged from 0.437 to 0.501 ft/ft, and embankment lengths ranged from 13 ft to 20 ft for the combined Petraflex dataset.

The Corps Block dataset was composed of eleven total tests including five overtopping tests and six channelized tests. Discharges ranged from 9.75 to 28.5 cfs, embankment slopes ranged from 0.143 to 0.200 ft/ft, and a constant 20-ft embankment length for the Corps Block overtopping dataset. The Corps Block channelized dataset had discharges ranging from 29.0 to 125.0 cfs.

5 HYDRAULIC ANALYSIS OF ACB TEST DATA

Data from the database detailed in Chapter 4 were analyzed using ASTM D7276 (2008), *Guide for Analysis and Interpretation of Test Data for Articulating Concrete Block (ACB) Revetment Systems in Open Channel Flow*. Section 2.1.7 provided a review of the ASTM D7276 (2008) standard guide and details the analysis methods for computation of hydraulic parameters. Although flow-velocity and shear-stress values were reported for the FHWA 30S and Petraflex tests in Clopper and Chen (1988), all available data for FHWA 30S and Petraflex tests were reanalyzed according to the ASTM D7276 (2008) standard to maintain a consistent analytical method for evaluating the Clopper (1991) and NCMA (2006) safety factor equations. Water-surface elevation and bed-elevation data were not provided in Abt *et al.* (2001). Abt *et al.* (2001) reported hydraulic analysis was retained for the overtopping testing and the channelized testing hydraulic analysis was slightly modified such that shear stress was computed using hydraulic radius instead of flow depth. Using the hydraulic radius associated with the roughened perimeter is a more accurate method for computing boundary shear stress. Chapter 5 provides: 1) an example of shear-stress and flow-velocity calculations using the ASTM D7276 (2008) method, 2) hydraulic results from the ASTM D7276 (2008) analysis of the database, and 3) a hydraulic assessment and additional analysis of the Abt *et al.* (2001) data.

5.1 EXAMPLE ASTM D7276 (2008) HYDRAULIC ANALYSIS

An example of shear-stress and flow-velocity computations using ASTM D7276 with the Petraflex 1.0-ft overtopping test data on the 0.501 ft/ft embankment slope is provided in this section. Bed elevations, water-surface elevations, channel geometry, and discharge are required to conduct the forewater analysis used to determine the optimum Manning's n value representing the collected data. Table 5.1 presents the bed and water-surface elevations collected during the 1.0-ft overtopping test. Following the steps outlined in Figure 2.4, an optimum Manning's n value of 0.020 was determined. Figure 5.1 provides a graphical comparison of the water-surface profile (WSP) generated by the 0.020 Manning's n value and the collected water-surface data. A value of 0.875 was computed for the coefficient of determination, R^2 , for the WSP fit to the collected flow-depth data.

Table 5.1: Hydraulic Data for CSU Petraflex Test (Robeson *et al.*, 2002) on 0.501 Bed Slope at 10.0 cfs (8-21-2000)

Station along Slope (ft)	Horizontal Station (ft)	Bed Elevation (ft)	Flow Depth (ft)	Vertical Depth (ft)	Continuity Velocity (ft/s)
20.85	17.80	101.50	0.28	0.32	6.05
22.86	19.51	100.64	0.23	0.27	7.30
25.04	21.38	99.67	0.16	0.19	10.41
27.05	23.09	98.82	0.16	0.19	10.27
29.23	24.95	97.89	0.17	0.20	9.76
31.24	26.67	97.03	0.16	0.19	10.41
33.42	28.53	96.11	0.17	0.20	9.64
35.43	30.25	95.28	0.15	0.18	11.00
37.61	32.11	94.35	0.15	0.18	10.85
39.62	33.83	93.47	0.17	0.19	10.10
41.80	35.69	92.47	0.15	0.18	10.85

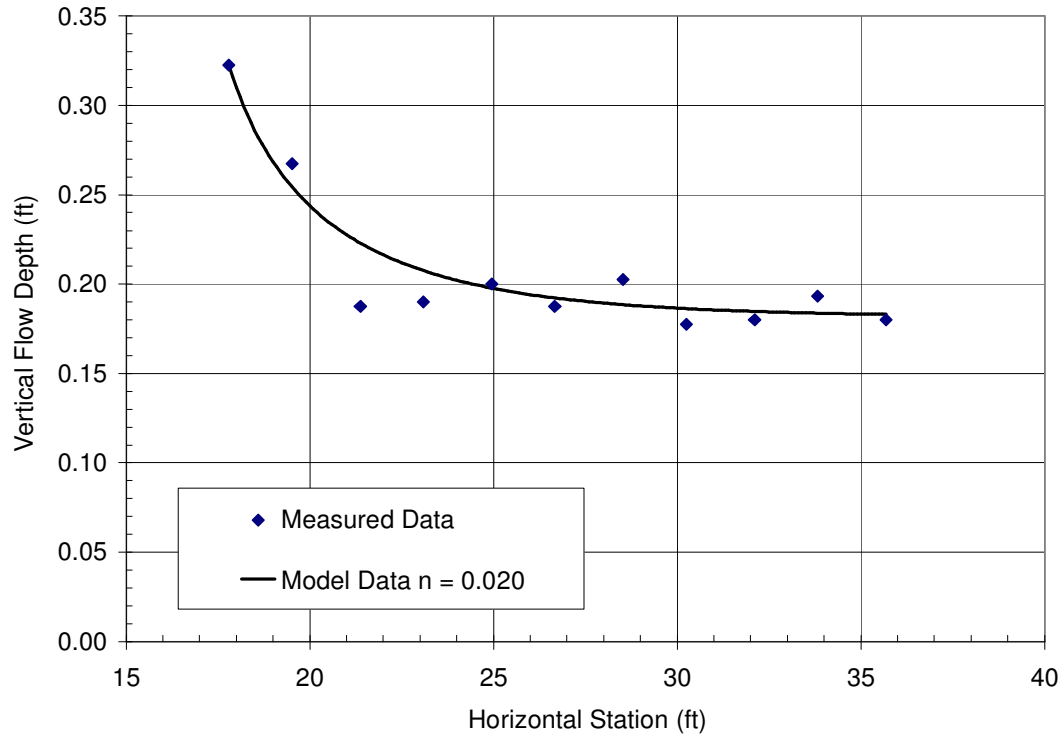


Figure 5.1: Comparison of Measured Flow Depths to Best-fit WSP

Local cross-sectional averaged flow velocities and shear stresses were computed using the best-fit theoretical WSP and Equation 2.3 and Equation 2.9, respectively. Table 5.2 provides the best-fit theoretical WSP data and corresponding computed local shear stresses and flow velocities. A plot of shear stress and flow velocity versus horizontal station is presented in Figure 5.2 and Figure 5.3 presents the hydraulic grade line and energy grade line versus horizontal station along the embankment. Normal depth was not achieved on the 20-ft long embankment. The maximum computed local shear stress and flow velocity was 4.49 lbs/ft² and 15.3 ft/s, respectively. For the purpose of quantifying hydraulic conditions experienced by individual blocks, shear-stress and flow-velocity values were averaged over a control volume length of one block located directly upstream of the last restrained block. For the Petraflex example, the block length along

the flow direction was 1.32 ft and thus the length of the control volume was 1.32 ft. Control volume averaged shear-stress and flow-velocity values for the Petraflex 1.0-ft overtopping test were 4.43 lbs/ft² and 15.2 ft/s, respectively.

Table 5.2: Water-surface Profile Data and Computed Hydraulics for Optimal Manning's n (0.020)

Horizontal Station (ft)	Bed Elevation (ft)	HGL (ft)	Vertical Flow Depth (ft)	Flow Depth (ft)	Flow Velocity (ft/s)	EGL (ft)	Local EGL Slope (ft/ft)	Shear-stress Momentum (lbs/ft ²)
17.80	101.48	101.81	0.32	0.29	8.67	102.91	n/a	n/a
17.90	101.43	101.75	0.32	0.28	8.85	102.90	n/a	n/a
18.00	101.38	101.69	0.31	0.28	9.01	102.90	0.08	1.28
18.10	101.33	101.64	0.30	0.27	9.18	102.89	0.09	1.33
18.20	101.28	101.58	0.30	0.27	9.33	102.88	0.09	1.39
18.30	101.23	101.53	0.29	0.26	9.48	102.87	0.10	1.44
18.40	101.18	101.47	0.29	0.26	9.63	102.86	0.10	1.50
18.50	101.13	101.42	0.29	0.26	9.77	102.85	0.11	1.55
18.60	101.08	101.37	0.28	0.25	9.91	102.84	0.11	1.60
18.70	101.03	101.31	0.28	0.25	10.04	102.82	0.12	1.66
18.80	100.98	101.26	0.27	0.25	10.17	102.81	0.12	1.71
18.90	100.93	101.21	0.27	0.24	10.29	102.80	0.13	1.76
19.00	100.88	101.15	0.27	0.24	10.42	102.78	0.13	1.81
19.10	100.83	101.10	0.27	0.24	10.54	102.77	0.14	1.86
19.20	100.78	101.05	0.26	0.23	10.65	102.76	0.14	1.90
19.30	100.73	100.99	0.26	0.23	10.76	102.74	0.15	1.95
19.40	100.68	100.94	0.26	0.23	10.87	102.73	0.16	2.00
19.50	100.63	100.89	0.25	0.23	10.98	102.71	0.16	2.05
19.60	100.58	100.84	0.25	0.23	11.08	102.69	0.17	2.09
19.70	100.53	100.78	0.25	0.22	11.18	102.68	0.17	2.14
19.80	100.48	100.73	0.25	0.22	11.28	102.66	0.18	2.18
19.90	100.43	100.68	0.25	0.22	11.38	102.64	0.18	2.23
20.00	100.38	100.63	0.24	0.22	11.47	102.62	0.19	2.27
20.10	100.33	100.57	0.24	0.22	11.56	102.60	0.19	2.31
20.20	100.28	100.52	0.24	0.21	11.65	102.58	0.20	2.36
20.30	100.23	100.47	0.24	0.21	11.73	102.56	0.20	2.40
20.40	100.18	100.42	0.24	0.21	11.82	102.54	0.21	2.44
20.50	100.13	100.37	0.23	0.21	11.90	102.52	0.21	2.48
20.60	100.08	100.32	0.23	0.21	11.98	102.50	0.22	2.52
20.70	100.03	100.26	0.23	0.21	12.06	102.48	0.22	2.56
20.80	99.98	100.21	0.23	0.21	12.14	102.46	0.23	2.60
20.90	99.93	100.16	0.23	0.20	12.21	102.43	0.23	2.64
21.00	99.88	100.11	0.23	0.20	12.28	102.41	0.23	2.67
21.10	99.83	100.06	0.23	0.20	12.35	102.38	0.24	2.71
21.20	99.78	100.01	0.23	0.20	12.42	102.36	0.24	2.75
21.30	99.73	99.96	0.22	0.20	12.49	102.34	0.25	2.78

Horizontal Station (ft)	Bed Elevation (ft)	HGL (ft)	Vertical Flow Depth (ft)	Flow Depth (ft)	Flow Velocity (ft/s)	EGL (ft)	Local EGL Slope (ft/ft)	Shear-stress Momentum (lbs/ft ²)
21.40	99.68	99.90	0.22	0.20	12.56	102.31	0.25	2.82
21.50	99.63	99.85	0.22	0.20	12.62	102.28	0.26	2.85
21.60	99.58	99.80	0.22	0.20	12.69	102.26	0.26	2.88
21.70	99.53	99.75	0.22	0.20	12.75	102.23	0.27	2.92
21.80	99.48	99.70	0.22	0.20	12.81	102.20	0.27	2.95
21.90	99.43	99.65	0.22	0.19	12.87	102.18	0.27	2.98
22.00	99.38	99.60	0.22	0.19	12.92	102.15	0.28	3.01
22.10	99.33	99.55	0.22	0.19	12.98	102.12	0.28	3.05
22.20	99.28	99.49	0.21	0.19	13.03	102.09	0.29	3.08
22.30	99.23	99.44	0.21	0.19	13.09	102.06	0.29	3.11
22.40	99.18	99.39	0.21	0.19	13.14	102.03	0.29	3.14
22.50	99.13	99.34	0.21	0.19	13.19	102.00	0.30	3.16
22.60	99.08	99.29	0.21	0.19	13.24	101.97	0.30	3.19
22.70	99.03	99.24	0.21	0.19	13.29	101.94	0.31	3.22
22.80	98.98	99.19	0.21	0.19	13.34	101.91	0.31	3.25
22.90	98.93	99.14	0.21	0.19	13.38	101.88	0.31	3.27
23.00	98.88	99.09	0.21	0.19	13.43	101.85	0.32	3.30
23.10	98.83	99.04	0.21	0.19	13.47	101.82	0.32	3.33
23.20	98.78	98.99	0.21	0.18	13.52	101.78	0.32	3.35
23.30	98.73	98.94	0.21	0.18	13.56	101.75	0.33	3.38
23.40	98.68	98.88	0.21	0.18	13.60	101.72	0.33	3.40
23.50	98.63	98.83	0.20	0.18	13.64	101.68	0.33	3.43
23.60	98.58	98.78	0.20	0.18	13.68	101.65	0.34	3.45
23.70	98.53	98.73	0.20	0.18	13.72	101.62	0.34	3.47
23.80	98.48	98.68	0.20	0.18	13.76	101.58	0.34	3.49
23.90	98.43	98.63	0.20	0.18	13.79	101.55	0.35	3.52
24.00	98.38	98.58	0.20	0.18	13.83	101.51	0.35	3.54
24.10	98.33	98.53	0.20	0.18	13.87	101.48	0.35	3.56
24.20	98.28	98.48	0.20	0.18	13.90	101.44	0.36	3.58
24.30	98.23	98.43	0.20	0.18	13.93	101.41	0.36	3.60
24.40	98.18	98.38	0.20	0.18	13.97	101.37	0.36	3.62
24.50	98.13	98.33	0.20	0.18	14.00	101.33	0.37	3.64
24.60	98.08	98.28	0.20	0.18	14.03	101.30	0.37	3.66
24.70	98.03	98.23	0.20	0.18	14.06	101.26	0.37	3.68
24.80	97.98	98.18	0.20	0.18	14.09	101.22	0.37	3.70
24.90	97.93	98.13	0.20	0.18	14.12	101.18	0.38	3.72
25.00	97.88	98.07	0.20	0.18	14.15	101.15	0.38	3.73
25.10	97.83	98.02	0.20	0.18	14.18	101.11	0.38	3.75
25.20	97.78	97.97	0.20	0.18	14.20	101.07	0.38	3.77
25.30	97.73	97.92	0.20	0.18	14.23	101.03	0.39	3.79
25.40	97.68	97.87	0.20	0.18	14.26	100.99	0.39	3.80
25.50	97.63	97.82	0.20	0.18	14.28	100.95	0.39	3.82
25.60	97.58	97.77	0.20	0.17	14.31	100.91	0.39	3.83
25.70	97.53	97.72	0.20	0.17	14.33	100.87	0.40	3.85
25.80	97.48	97.67	0.19	0.17	14.36	100.84	0.40	3.86
25.90	97.43	97.62	0.19	0.17	14.38	100.80	0.40	3.88

Horizontal Station (ft)	Bed Elevation (ft)	HGL (ft)	Vertical Flow Depth (ft)	Flow Depth (ft)	Flow Velocity (ft/s)	EGL (ft)	Local EGL Slope (ft/ft)	Shear-stress Momentum (lbs/ft ²)
26.00	97.38	97.57	0.19	0.17	14.40	100.76	0.40	3.89
26.10	97.33	97.52	0.19	0.17	14.42	100.71	0.40	3.91
26.20	97.28	97.47	0.19	0.17	14.45	100.67	0.41	3.92
26.30	97.23	97.42	0.19	0.17	14.47	100.63	0.41	3.94
26.40	97.18	97.37	0.19	0.17	14.49	100.59	0.41	3.95
26.50	97.13	97.32	0.19	0.17	14.51	100.55	0.41	3.96
26.60	97.08	97.27	0.19	0.17	14.53	100.51	0.41	3.97
26.70	97.03	97.22	0.19	0.17	14.55	100.47	0.42	3.99
26.80	96.98	97.17	0.19	0.17	14.57	100.43	0.42	4.00
26.90	96.93	97.12	0.19	0.17	14.58	100.38	0.42	4.01
27.00	96.88	97.07	0.19	0.17	14.60	100.34	0.42	4.02
27.10	96.83	97.02	0.19	0.17	14.62	100.30	0.42	4.03
27.20	96.77	96.97	0.19	0.17	14.64	100.26	0.42	4.05
27.30	96.72	96.92	0.19	0.17	14.65	100.21	0.43	4.06
27.40	96.67	96.86	0.19	0.17	14.67	100.17	0.43	4.07
27.50	96.62	96.81	0.19	0.17	14.69	100.13	0.43	4.08
27.60	96.57	96.76	0.19	0.17	14.70	100.09	0.43	4.09
27.70	96.52	96.71	0.19	0.17	14.72	100.04	0.43	4.10
27.80	96.47	96.66	0.19	0.17	14.73	100.00	0.43	4.11
27.90	96.42	96.61	0.19	0.17	14.75	99.96	0.44	4.12
28.00	96.37	96.56	0.19	0.17	14.76	99.91	0.44	4.13
28.10	96.32	96.51	0.19	0.17	14.78	99.87	0.44	4.14
28.20	96.27	96.46	0.19	0.17	14.79	99.82	0.44	4.15
28.30	96.22	96.41	0.19	0.17	14.80	99.78	0.44	4.16
28.40	96.17	96.36	0.19	0.17	14.82	99.73	0.44	4.16
28.50	96.12	96.31	0.19	0.17	14.83	99.69	0.44	4.17
28.60	96.07	96.26	0.19	0.17	14.84	99.65	0.44	4.18
28.70	96.02	96.21	0.19	0.17	14.85	99.60	0.45	4.19
28.80	95.97	96.16	0.19	0.17	14.87	99.56	0.45	4.20
28.90	95.92	96.11	0.19	0.17	14.88	99.51	0.45	4.20
29.00	95.87	96.06	0.19	0.17	14.89	99.47	0.45	4.21
29.10	95.82	96.01	0.19	0.17	14.90	99.42	0.45	4.22
29.20	95.77	95.96	0.19	0.17	14.91	99.38	0.45	4.23
29.30	95.72	95.91	0.19	0.17	14.92	99.33	0.45	4.23
29.40	95.67	95.86	0.19	0.17	14.93	99.28	0.45	4.24
29.50	95.62	95.81	0.19	0.17	14.94	99.24	0.45	4.25
29.60	95.57	95.76	0.19	0.17	14.95	99.19	0.46	4.25
29.70	95.52	95.71	0.19	0.17	14.96	99.15	0.46	4.26
29.80	95.47	95.66	0.19	0.17	14.97	99.10	0.46	4.27
29.90	95.42	95.61	0.19	0.17	14.98	99.06	0.46	4.27
30.00	95.37	95.56	0.19	0.17	14.99	99.01	0.46	4.28
30.10	95.32	95.51	0.19	0.17	15.00	98.97	0.46	4.29
30.20	95.27	95.46	0.19	0.17	15.01	98.92	0.46	4.29
30.30	95.22	95.40	0.19	0.17	15.02	98.87	0.46	4.30
30.40	95.17	95.35	0.19	0.17	15.02	98.83	0.46	4.30
30.51	95.12	95.30	0.19	0.17	15.03	98.78	0.46	4.31

Horizontal Station (ft)	Bed Elevation (ft)	HGL (ft)	Vertical Flow Depth (ft)	Flow Depth (ft)	Flow Velocity (ft/s)	EGL (ft)	Local EGL Slope (ft/ft)	Shear-stress Momentum (lbs/ft ²)
30.61	95.07	95.25	0.19	0.17	15.04	98.73	0.47	4.31
30.71	95.02	95.20	0.19	0.17	15.05	98.69	0.47	4.32
30.81	94.97	95.15	0.19	0.17	15.06	98.64	0.47	4.32
30.91	94.92	95.10	0.19	0.17	15.06	98.59	0.47	4.33
31.01	94.87	95.05	0.19	0.17	15.07	98.54	0.47	4.33
31.11	94.82	95.00	0.19	0.17	15.08	98.50	0.47	4.34
31.21	94.77	94.95	0.19	0.17	15.08	98.45	0.47	4.34
31.31	94.72	94.90	0.19	0.17	15.09	98.40	0.47	4.35
31.40	94.67	94.85	0.19	0.17	15.10	98.36	0.47	4.35
31.50	94.62	94.80	0.19	0.17	15.10	98.31	0.47	4.36
31.60	94.57	94.75	0.19	0.17	15.11	98.26	0.47	4.36
31.71	94.52	94.70	0.18	0.17	15.12	98.22	0.47	4.37
31.81	94.47	94.65	0.18	0.17	15.12	98.17	0.47	4.37
31.91	94.42	94.60	0.18	0.17	15.13	98.12	0.47	4.37
32.01	94.37	94.55	0.18	0.17	15.13	98.07	0.47	4.38
32.11	94.32	94.50	0.18	0.17	15.14	98.03	0.48	4.38
32.21	94.27	94.45	0.18	0.17	15.14	97.98	0.48	4.38
32.31	94.22	94.40	0.18	0.17	15.15	97.93	0.48	4.39
32.41	94.17	94.35	0.18	0.16	15.15	97.88	0.48	4.39
32.51	94.12	94.30	0.18	0.16	15.16	97.83	0.48	4.40
32.61	94.06	94.25	0.18	0.16	15.16	97.79	0.48	4.40
32.71	94.01	94.20	0.18	0.16	15.17	97.74	0.48	4.40
32.81	93.97	94.15	0.18	0.16	15.17	97.69	0.48	4.41
32.90	93.92	94.10	0.18	0.16	15.18	97.64	0.48	4.41
33.00	93.87	94.05	0.18	0.16	15.18	97.60	0.48	4.41
33.10	93.82	94.00	0.18	0.16	15.19	97.55	0.48	4.41
33.20	93.77	93.95	0.18	0.16	15.19	97.50	0.48	4.42
33.30	93.72	93.90	0.18	0.16	15.20	97.45	0.48	4.42
33.40	93.67	93.85	0.18	0.16	15.20	97.40	0.48	4.42
33.51	93.61	93.80	0.18	0.16	15.20	97.35	0.48	4.43
33.61	93.56	93.75	0.18	0.16	15.21	97.31	0.48	4.43
33.71	93.51	93.70	0.18	0.16	15.21	97.26	0.48	4.43
33.81	93.46	93.65	0.18	0.16	15.22	97.21	0.48	4.43
33.91	93.41	93.60	0.18	0.16	15.22	97.16	0.48	4.44
34.00	93.36	93.55	0.18	0.16	15.22	97.11	0.48	4.44
34.10	93.31	93.50	0.18	0.16	15.23	97.07	0.48	4.44
34.20	93.27	93.45	0.18	0.16	15.23	97.02	0.49	4.44
34.30	93.21	93.40	0.18	0.16	15.23	96.97	0.49	4.45
34.40	93.16	93.35	0.18	0.16	15.24	96.92	0.49	4.45
34.51	93.11	93.30	0.18	0.16	15.24	96.87	0.49	4.45
34.61	93.06	93.25	0.18	0.16	15.24	96.82	0.49	4.45
34.71	93.01	93.20	0.18	0.16	15.25	96.77	0.49	4.45
34.80	92.96	93.15	0.18	0.16	15.25	96.72	0.49	4.46
34.90	92.91	93.10	0.18	0.16	15.25	96.68	0.49	4.46
35.00	92.86	93.05	0.18	0.16	15.25	96.63	0.49	4.46
35.10	92.81	93.00	0.18	0.16	15.26	96.58	0.49	4.46

Horizontal Station (ft)	Bed Elevation (ft)	HGL (ft)	Vertical Flow Depth (ft)	Flow Depth (ft)	Flow Velocity (ft/s)	EGL (ft)	Local EGL Slope (ft/ft)	Shear-stress Momentum (lbs/ft ²)
35.20	92.76	92.95	0.18	0.16	15.26	96.53	0.49	4.46
35.30	92.72	92.90	0.18	0.16	15.26	96.48	0.49	4.47
35.40	92.67	92.85	0.18	0.16	15.27	96.43	0.49	4.47
35.50	92.62	92.80	0.18	0.16	15.27	96.39	0.49	4.47
35.59	92.57	92.75	0.18	0.16	15.27	96.34	0.49	4.47
35.69	92.52	92.70	0.18	0.16	15.27	96.29	0.49	4.47
35.80	92.47	92.65	0.18	0.16	15.28	96.24	0.49	4.47
35.90	92.42	92.60	0.18	0.16	15.28	96.19	0.49	4.48
36.00	92.37	92.55	0.18	0.16	15.28	96.14	0.49	4.48
36.10	92.32	92.50	0.18	0.16	15.28	96.09	0.49	4.48
36.20	92.27	92.45	0.18	0.16	15.28	96.04	0.49	4.48
36.30	92.22	92.40	0.18	0.16	15.29	95.99	0.49	4.48
36.39	92.17	92.35	0.18	0.16	15.29	95.95	0.49	4.48
36.49	92.12	92.30	0.18	0.16	15.29	95.90	0.49	4.49
36.59	92.07	92.25	0.18	0.16	15.29	95.85	0.49	4.49
36.70	92.02	92.20	0.18	0.16	15.29	95.80	0.49	4.49

HGL = hydraulic grade line; EGL = energy grade line; n/a = not available

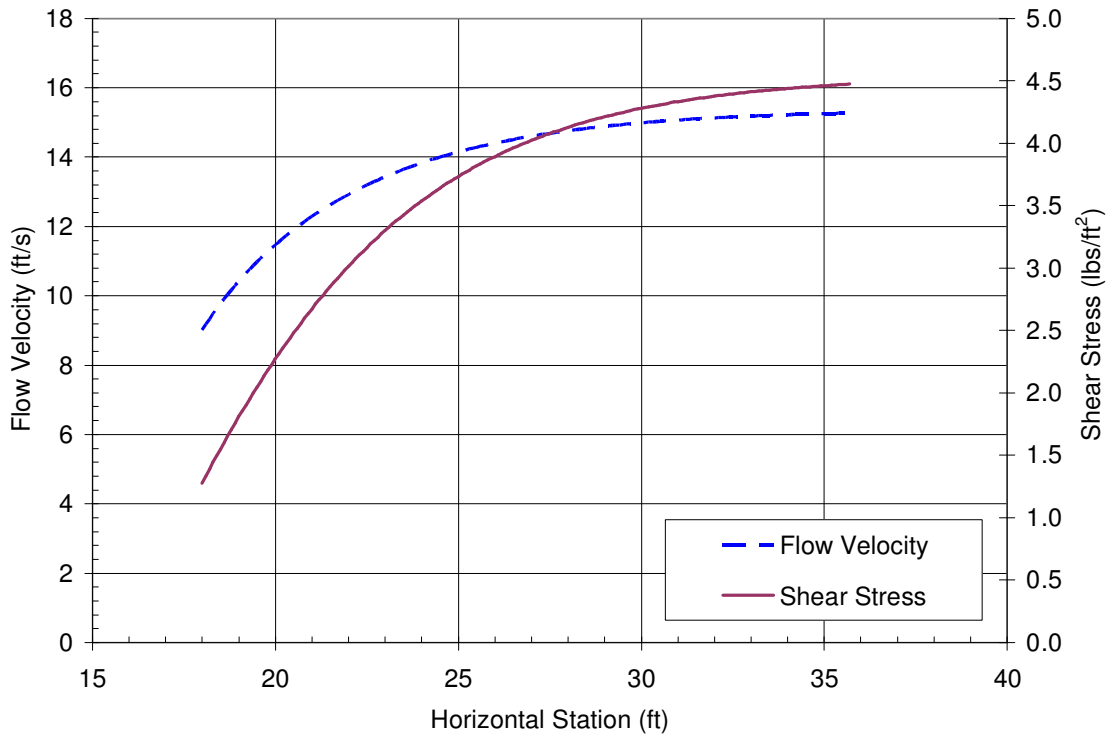


Figure 5.2: Flow Velocity and Shear Stress versus Horizontal Station

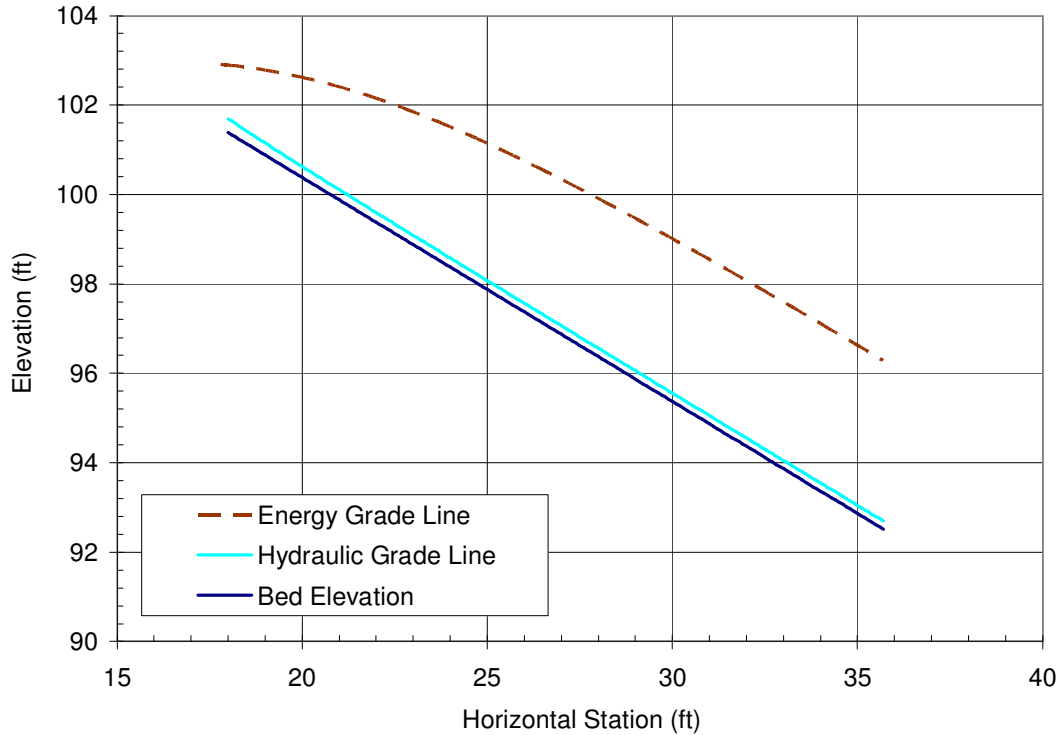


Figure 5.3: Energy Grade Line and Hydraulic Grade Line versus Horizontal Station

5.2 ASTM D7276 (2008) HYDRAULIC ANALYSIS OF 30S AND PETRAFLEX DATA

The ASTM D7276 (2008) standard guide for interpretation was used to compute control volume averaged shear-stress and flow-velocity values from all available WSP data. Table 5.3 and Table 5.4 provide the results of the ASTM D7276 hydraulic analysis for the 30S and Petraflex, respectively. Figure 5.4 provides a graphical comparison of the shear-stress values computed from the ASTM D7276 (2008) standard and the shear-stress values reported in Clopper and Chen (1988). Additionally, Figure 5.5 provides a plot of the percent difference between the ASTM D7276 computed shear stresses and the reported shear-stress values in Clopper and Chen (1988) as a function of overtopping

depth. For the 1.0-ft and 2.0-ft overtopping FHWA 30S tests, the computed ASTM D7276 shear-stress values were 1% greater and 14% less than the reported FHWA shear-stress values, respectively. However, shear stresses computed for the 4.0-ft overtopping FHWA 30S and Petraflex tests were an average of 72% less than the values reported by Clopper and Chen (1988). Shear stresses and flow velocities for the FHWA Petraflex 1.0-ft and 2.0-ft overtopping tests were approximated by using the 0.029 Manning's n value computed from the 4.0-ft overtopping depth test with a theoretical 1.0-ft and 2.0-ft overtopping depth flow profile. Shear-stress discrepancies at higher overtopping depths illustrate the sensitivity of computed shear-stress values to the computation method, embankment length, and associated draw-down toward normal depth. With advancements in computing technology and the resulting capability to perform complex forewater computations, the necessity to obtain a best-fit profile and compute shear stress using the momentum equation is clear.

Table 5.3: ASTM D7276 (2008) Hydraulic Results for 30S Testing

Test ID No.	Block Name	Overtopping Depth (ft)	Test Date	S_0 (ft/ft)	Q (cfs)	Flow Depth ^a (ft)	V^a (ft/s)	τ_0^a (lbs/ft ²)	Manning's n	System Condition
1	30S	1.0	9/1/1987	0.442	13.8	0.29	12.1	7.1	0.035	Stable
2	30S	2.0	9/9/1987	0.442	34.0	0.57	14.9	10.3	0.039	Stable
3	30S	4.0	9/11/1987	0.442	90.5	1.11	20.4	12.6	0.035	Unstable
4	30S	1.0	8/11/2000	0.499	10.0	0.14	17.6	2.5	0.013	Unstable
5	30S	1.0	6/14/2009	0.230	10.0	0.24	10.5	3.3	0.026	Stable
6	30S	1.6	6/15/2009	0.230	20.0	0.34	14.7	4.0	0.022	Stable
7	30S	2.0	6/15/2009	0.230	30.0	0.44	17.2	4.7	0.021	Unstable
8	30S	0.9	6/25/2009	0.431	8.0	0.15	13.7	3.6	0.020	Stable
9	30S	1.2	6/25/2009	0.431	12.0	0.20	15.0	4.9	0.022	Unstable

^a Values averaged over a control volume length of one block located directly upstream of the last restrained block

Table 5.4: ASTM D7276 (2008) Hydraulic Results for Petraflex Testing

Test ID No.	Block Name	Overtopping Depth (ft)	Test Date	S_0 (ft/ft)	Q (cfs)	Flow Depth ^a (ft)	V^a (ft/s)	τ_0^a (lbs/ft ²)	Manning's n	System Condition
10	Petraflex	1.0	n/a	0.437	13.5	0.27 ^b	12.3 ^b	5.0 ^b	0.029 ^b	Stable
11	Petraflex	2.0	n/a	0.437	34.0	0.55 ^b	15.3 ^b	6.2 ^b	0.029 ^b	Stable
12	Petraflex	4.0	9/22/1987	0.437	96.0	1.26	19.0	7.0	0.029	Stable
13	Petraflex	1.0	8/21/2000	0.501	10.0	0.16	15.2	4.5	0.020	Stable
14	Petraflex	2.0	8/21/2000	0.501	28.4	0.40	17.8	10.2	0.031	Unstable

n/a = not available

^a Values averaged over a control volume length of one block located directly upstream of the last restrained block

^b Values approximated using theoretical 1.0-ft and 2.0-ft overtopping depth flow profiles with the 4.0-ft overtopping depth Manning's n value of 0.029

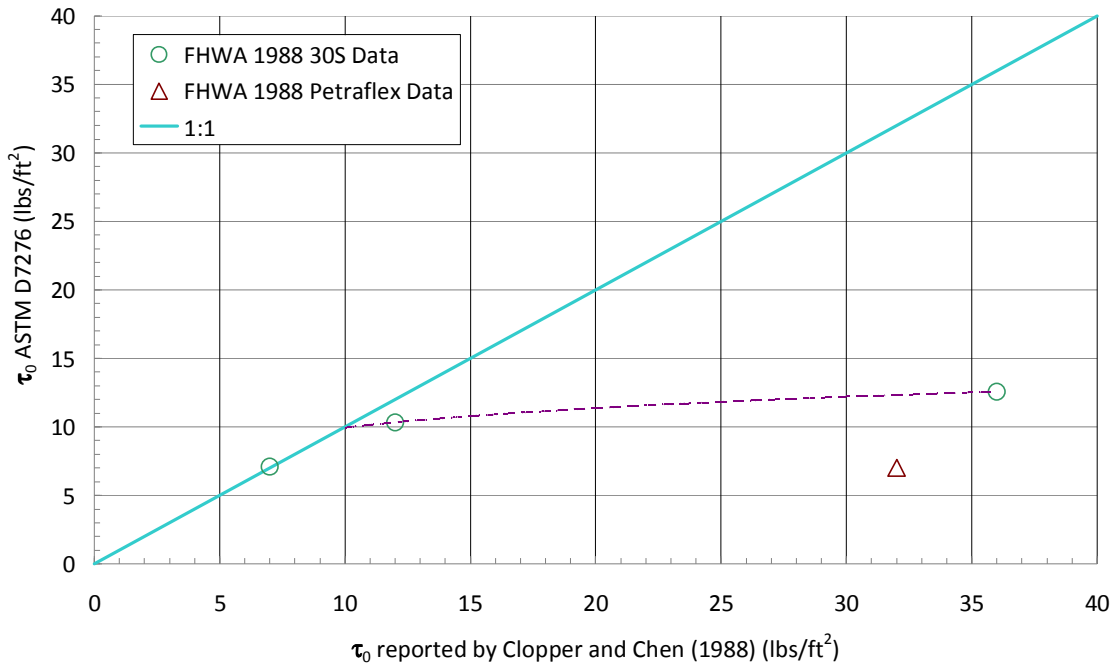


Figure 5.4: Comparison of Shear Stresses Computed from ASTM D7276 (2008) to Shear Stresses Reported in Clopper and Chen (1988)

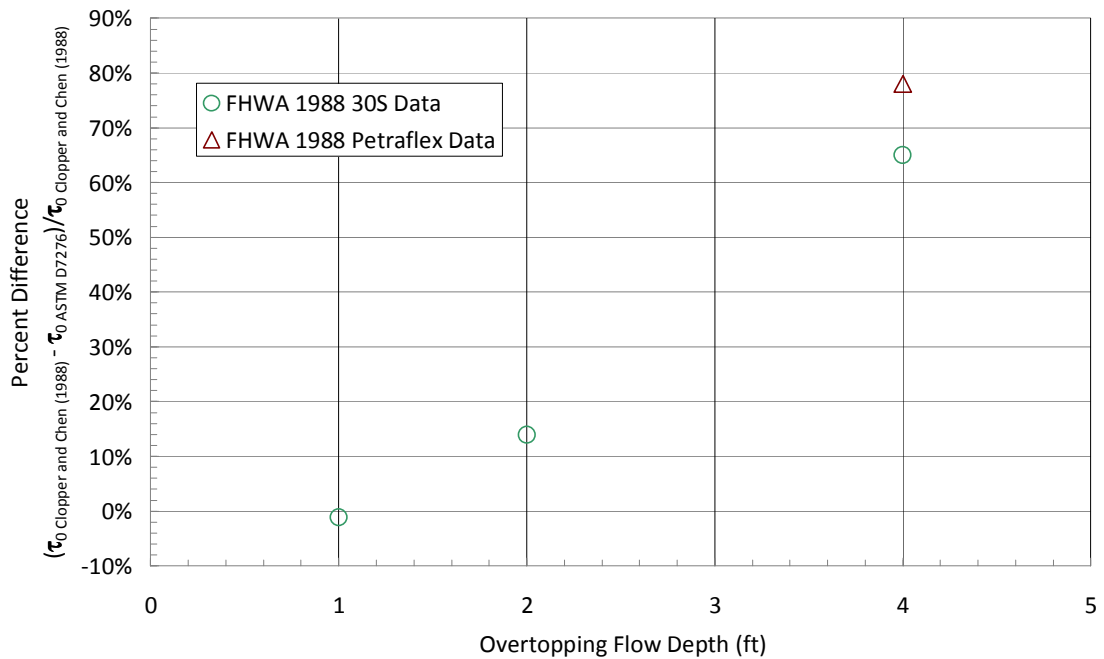


Figure 5.5: Percent Difference between ASTM D7276 (2008) Shear Stresses and Reported Values from Clopper and Chen (1988) versus Overtopping Flow Depth

5.3 HYDRAULIC ANALYSIS OF CORPS BLOCK DATA

Water-surface profile and bed-elevation data were not reported in Abt *et al.* (2001). Therefore, conducting the ASTM D7276 (2008) analysis standard on the Corps Block dataset was not possible. Abt *et al.* (2001) computed shear stress using Equation 5.1 for both the overtopping and channelized data analysis:

$$\tau_0 = \gamma d S_f \quad \text{Equation 5.1}$$

where

τ_0 = shear stress (lbs/ft²);

γ = unit weight of water (62.4 lbs/ft³);

d = flow depth (ft); and

S_f = slope of the energy grade line (friction slope) (ft/ft).

Shear-stress and flow-velocity values for the overtopping tests reported in Abt *et al.* (2001) were used in the assessment of the Clopper (1991) and NCMA (2006) safety factor equation. For the 1.2-ft overtopping test, the block system failed prior to acquisition of flow data and Abt *et al.* (2001) do not report flow-depth or shear-stress values for the 1.2-ft overtopping test. To obtain a 1.2-ft overtopping shear-stress value for the Clopper (1991) and NCMA (2006) safety factor assessment, a linear interpolation of the shear-stress values reported for the 1.0-ft and 2.0-ft overtopping flow depths was conducted based on discharge. The linear interpolation resulted in a shear-stress value of 2.65 lbs/ft² for the 1.2-ft overtopping test.

Shear-stress values for the channelized testing were recomputed using Equation 5.2 from the reported Abt *et al.* (2001) data:

$$\tau_0 = \gamma R S_f \quad \text{Equation 5.2}$$

where

τ_0 = shear stress (lbs/ft²);

γ = unit weight of water (62.4 lbs/ft³);

R = hydraulic radius (ft); and

S_f = slope of the energy grade line (friction slope) (ft/ft).

The hydraulic radius in Equation 5.2 was computed using Equation 5.3:

$$R = \frac{A}{P} \quad \text{Equation 5.3}$$

where

R = hydraulic radius (ft);

A = cross-section flow area (ft²); and

P = wetted (roughened) perimeter (ft).

Since the ACB system roughness was considerably greater than the concrete flume wall roughness, the length corresponding to the concrete flume wall was not included in the wetted perimeter. Table 5.5 provides the final hydraulic analysis results for both the overtopping and channelized Corps Block tests. The 125.0-cfs channelized test was excluded from the data used in the Clopper (1991) and NCMA (2006) safety factor assessment since flow-depth and shear-stress data were not available and the system was previously identified as unstable at the 112.0-cfs test.

Table 5.5: Results of the Corps Block Hydraulic Analysis

Test ID No.	Test Condition	S_0 (ft/ft)	Side Slope (H/V)	Q (cfs)	Flow Depth (ft)	Flow Velocity (ft/s)	Shear Stress (lbs/ft ²)	System Condition
15	Overtopping	0.200	n/a	11.0	0.28	13.6	3.5	Stable
16	Overtopping	0.200	n/a	28.5	0.49	17.3	4.9	Unstable
17	Overtopping	0.143	n/a	9.8	0.25	12.8	2.1	Stable
18	Overtopping	0.143	n/a	25.0	0.65	16.5	4.8	Unstable
19	Overtopping	0.143	n/a	13.0	-	14.5	2.7 ^a	Unstable
20	Channel	0.030	2.0	29.0	2.0	6.5	2.2	Stable
21	Channel	0.030	2.0	50.0	2.1	7.9	2.3	Stable
22	Channel	0.030	2.0	80.0	2.3	11.5	2.5	Stable
23	Channel	0.030	2.0	100.0	2.3	13.2	2.5	Stable
24	Channel	0.030	2.0	112.0	2.5	14.0	2.6	Unstable

n/a = not applicable

^a Computed from linear interpolation, based on discharge, of 1.0-ft and 2.0-ft overtopping data on 0.143 ft/ft embankment

5.4 SUMMARY

Hydraulic analysis was conducted on the database to provide shear-stress and flow-velocity values for the assessment of the NCMA (2006) safety factor equation. An example of the ASTM D7276 (2008) analysis was presented using data from the CSU 1.0-ft overtopping Petraflex test. Using the ASTM D7276 (2008) analysis standard, flow-velocity and shear-stress values were computed for the 30S and Petraflex datasets. Due to lack of water-surface profile data for the Corps Block testing, hydraulic values reported by Abt *et al.* (2001) were retained for the overtopping testing. Shear-stress values for the channelized tests were recomputed using hydraulic radius, instead of flow depth, in the simplified shear-stress equation. A combined summary of the 30S, Petraflex, and Corps Block hydraulic analysis results is provided in Table 5.6. The hydraulic analysis results were used in the evaluation of the NCMA (2006) safety factor method presented in Chapter 6.

Table 5.6: Hydraulic Analysis Results for ACB Database

Test ID No.	Block Name	Test Condition	Over-topping Depth (ft)	Test Date	S_0 (ft/ft)	Side Slope (H/V)	Q (cfs)	Flow Depth (ft)	V (ft/s)	τ_0 (lbs/ft ²)	Manning's n	System Condition
1	30S	Overtopping	1.0	9/1/1987	0.442	n/a	13.8	0.29	12.1	7.1	0.035	Stable
2	30S	Overtopping	2.0	9/9/1987	0.442	n/a	34.0	0.57	14.9	10.3	0.039	Stable
3	30S	Overtopping	4.0	9/11/1987	0.442	n/a	90.5	1.11	20.4	12.6	0.035	Unstable
4	30S	Overtopping	1.0	8/11/2000	0.499	n/a	10.0	0.14	17.6	2.5	0.013	Unstable
5	30S	Overtopping	1.0	6/14/2009	0.230	n/a	10.0	0.24	10.5	3.3	0.026	Stable
6	30S	Overtopping	1.6	6/15/2009	0.230	n/a	20.0	0.34	14.7	4.0	0.022	Stable
7	30S	Overtopping	2.0	6/15/2009	0.230	n/a	30.0	0.44	17.2	4.7	0.021	Unstable
8	30S	Overtopping	0.9	6/25/2009	0.431	n/a	8.0	0.15	13.7	3.6	0.020	Stable
9	30S	Overtopping	1.2	6/25/2009	0.431	n/a	12.0	0.20	15.0	4.9	0.022	Unstable
10	Petraflex	Overtopping	1.0	N/A	0.437	n/a	13.5	0.27	12.3	5.0	0.029	Stable
11	Petraflex	Overtopping	2.0	N/A	0.437	n/a	34.0	0.55	15.3	6.2	0.029	Stable
12	Petraflex	Overtopping	4.0	9/22/1987	0.437	n/a	96.0	1.26	19.0	7.0	0.029	Stable
13	Petraflex	Overtopping	1.0	8/21/2000	0.501	n/a	10.0	0.16	15.2	4.5	0.020	Stable
14	Petraflex	Overtopping	2.0	8/21/2000	0.501	n/a	28.4	0.40	17.8	10.2	0.031	Unstable
15	Corps Block	Overtopping	1.0	N/A	0.200	n/a	11.0	0.28	13.6	3.5	N/A	Stable
16	Corps Block	Overtopping	2.0	N/A	0.200	n/a	28.5	0.49	17.3	4.9	N/A	Unstable
17	Corps Block	Overtopping	1.0	N/A	0.143	n/a	9.8	0.25	12.8	2.1	N/A	Stable
18	Corps Block	Overtopping	2.0	N/A	0.143	n/a	25.0	0.65	16.5	4.8	N/A	Unstable
19	Corps Block	Overtopping	1.2	N/A	0.143	n/a	13.0	n/a	14.5	2.7	N/A	Unstable
20	Corps Block	Channel	n/a	N/A	0.030	2.0	29.0	2.0	6.5	2.2	N/A	Stable
21	Corps Block	Channel	n/a	N/A	0.030	2.0	50.0	2.1	7.9	2.3	N/A	Stable
22	Corps Block	Channel	n/a	N/A	0.030	2.0	80.0	2.3	11.5	2.5	N/A	Stable
23	Corps Block	Channel	n/a	N/A	0.030	2.0	100.0	2.3	13.2	2.5	N/A	Stable
24	Corps Block	Channel	n/a	N/A	0.030	2.0	112.0	2.5	14.0	2.6	N/A	Unstable

n/a = not applicable; N/A = not available

6 EVALUATION OF CLOPPER (1991) AND NCMA (2006) METHODS USING ACB TEST DATA

NCMA (2006) provides a safety factor equation which represents the state-of-the-practice for ACB system design. However, the Clopper (1991) safety factor design method has been extensively employed for ACB system design as well. Previously, limited data have been available for assessing the validity of the Clopper (1991) and NCMA (2006) safety factor equations. Available datasets were exclusively for overtopping tests and primarily had 2H:1V embankment slopes. Three ACB systems were included in the developed database: 1) 30S, 2) Petraflex, and 3) the Corps Block. Twenty-four tests encompassing both overtopping and channelized conditions composed the database.

Clopper (1991) safety factors for channelized conditions were computed using Equation 6.1:

$$SF = \frac{(\ell_2 / \ell_1) \cos \theta}{\sin \theta \cos \beta + (\ell_2 / \ell_1) \eta'} \quad \text{Equation 6.1}$$

where

SF = factor of safety;

θ = side-slope angle;

η' = stability number defined by Equation 2.48;

- β = block rotation angle defined by Equation 2.59 (radians);
- ℓ_2 = block length measured from the block center to the block corner (ft); and
- ℓ_1 = one-half of the block height (ft).

Additionally, NCMA (2006) safety factors for channelized conditions were computed using Equation 6.2:

$$SF = \frac{(\ell_2 / \ell_1) a_\theta}{\sqrt{1 - a_\theta^2} \cos \beta + (\ell_2 / \ell_1) \eta_1} \quad \text{Equation 6.2}$$

where

- SF = factor of safety;
- a_θ = weight force component defined by Equation 2.107;
- η_1 = stability number defined by Equation 2.118;
- β = block rotation angle defined by Equation 2.126 (radians);
- ℓ_2 = block length measured from the block center to the block corner (ft); and
- ℓ_1 = one-half of the block height (ft).

Since the database was developed from tests conducted in a controlled laboratory setting, Equation 6.1 and Equation 6.2 exclude the additional lift and drag forces attributed to protrusion on an individual block above adjacent blocks.

For overtopping conditions, the Clopper (1991) and NCMA (2006) safety factor equations are identical. Equation 6.3 provides the Clopper (1991) and NCMA (2006) safety factor equation for blocks on a channel bed:

$$SF = \frac{(\ell_2 / \ell_1) \cos \theta}{\sin \theta + (\ell_2 / \ell_1) \eta} = \frac{(\ell_2 / \ell_1) \cos \theta}{\sin \theta + (\ell_2 / \ell_1) (\tau_0 / \tau_c)} \quad \text{Equation 6.3}$$

where

SF = factor of safety;

θ = bed-slope angle = $\arctan(S_0)$ (radians);

η = stability number for blocks on a channel bed;

τ_0 = boundary shear stress (lbs/ft²);

τ_c = block critical shear stress on a horizontal plane (lbs/ft²);

ℓ_2 = one-half of the block length along the flow direction (ft); and

ℓ_1 = one-half of the block height (ft).

Consistent with the channelized testing, Equation 6.3 excludes the additional lift and drag forces attributed to protrusion on an individual block above adjacent blocks.

Critical shear stress at horizontal values, τ_c , were computed for each stable test directly preceding an unstable test. Equation 6.3 was set equal to a safety factor of 1 and solved for τ_c to derive the expression for computing a critical shear-stress value at horizontal as presented in Equation 6.4:

$$\tau_c = \tau_0 \left[\frac{(\ell_2/\ell_1)}{(\ell_2/\ell_1)\cos\theta - \sin\theta} \right] \quad \text{Equation 6.4}$$

where

τ_c = block critical shear stress on a horizontal plane (lbs/ft²);

τ_0 = boundary shear stress on a sloped embankment (lbs/ft²);

ℓ_2 = one-half of the block length along the flow direction (ft);

ℓ_1 = one-half of the block height (ft); and

θ = bed-slope angle (radians).

6.1 30S CLOPPER (1991) AND NCMA (2006) *SF* ANALYSIS

Using Equation 6.3, the Clopper (1991) and NCMA (2006) safety factor equation for overtopping conditions, safety factors were computed for each test presented in Table 5.3. Initially, critical shear-stress values at horizontal, τ_c , were computed using Equation 6.4 for each stable test preceding an unstable test. Table 6.1 provides the computed τ_c 30S values. Computed critical shear-stress values for the 30S on a horizontal plane ranged from 4.5 to 13.5 lbs/ft². According to Clopper (1991) and NCMA (2006), a unique value of critical shear stress on a horizontal plane should exist.

Table 6.1: Computed Critical Shear-stress Values for the 30S on a Horizontal Plane

Test ID No.	Block Name	Overtopping Depth (ft)	Test Date	S_0 (ft/ft)	Q (cfs)	V (ft/s)	τ_0 (lbs/ft ²)	NCMA τ_c (lbs/ft ²)
2	30S	2.0	9/9/1987	0.442	34.0	14.9	10.3	13.5
6	30S	1.6	6/15/2009	0.230	20.0	14.7	4.0	4.5
8	30S	0.9	6/25/2009	0.431	8.0	13.7	3.6	4.7

Safety factors were computed for the 30S data using each of the critical shear-stress values presented in Table 6.1. Table 6.2 provides a summary of the computed safety factor values. Plots of bed slope versus 30S computed safety factors for the 13.5, 4.5, and 4.7 lbs/ft² τ_c values are presented in Figure 6.1, Figure 6.2, and Figure 6.3, respectively. The following summarizes the ability of each critical shear-stress value to predict system stability for the 30S dataset:

- $\tau_c = 13.5 \text{ lbs/ft}^2$ correctly predicted the point of instability for 25% of the tested installations:
 - Computed safety factor values for stable tests ranged from 1.00 to 2.96
 - Correctly predicted 100% of stable tests
 - Computed safety factor values for unstable tests ranged from 0.85 to 2.59
 - Correctly predicted 25% of unstable tests
- $\tau_c = 4.5 \text{ lbs/ft}^2$ correctly predicted the point of instability for 25% of the tested installations:
 - Computed safety factor values for stable tests ranged from 0.38 to 1.19
 - Correctly predicted 40% of stable tests
 - Computed safety factor values for unstable tests ranged from 0.31 to 1.27
 - Correctly predicted 75% of unstable tests
- $\tau_c = 4.7 \text{ lbs/ft}^2$ correctly predicted the point of instability for 50% of the tested installations:
 - Computed safety factor values for stable tests ranged from 0.39 to 1.22
 - Correctly predicted 60% of stable tests
 - Computed safety factor values for unstable tests ranged from 0.32 to 1.30
 - Correctly predicted 75% of unstable tests

Table 6.2: Computed 30S *SF* for Clopper (1991) and NCMA (2006) Method

Test ID No.	Block Name	Overtopping Depth (ft)	S_0 (ft/ft)	V (ft/s)	τ_0 (lbs/ft ²)	System Condition	<i>SF</i> ($\tau_c = 13.5$ lbs/ft ²)	<i>SF</i> ($\tau_c = 4.5$ lbs/ft ²)	<i>SF</i> ($\tau_c = 4.7$ lbs/ft ²)
1	30S	1.0	0.442	12.1	7.1	Stable	1.36	0.54	0.55
2	30S	2.0	0.442	14.9	10.3	Stable	1.00	0.38	0.39
3	30S	4.0	0.442	20.4	12.6	Unstable	0.85	0.31	0.32
4	30S	1.0	0.499	17.6	2.5	Unstable	2.59	1.27	1.30
5	30S	1.0	0.230	10.5	3.3	Stable	2.96	1.19	1.22
6	30S	1.6	0.230	14.7	4.0	Stable	2.55	1.00	1.03
7	30S	2.0	0.230	17.2	4.7	Unstable	2.25	0.87	0.89
8	30S	0.9	0.431	13.7	3.6	Stable	2.22	0.98	1.00
9	30S	1.2	0.431	15.0	4.9	Unstable	1.81	0.75	0.77

Orange cells identify tests used to calibrate τ_c values

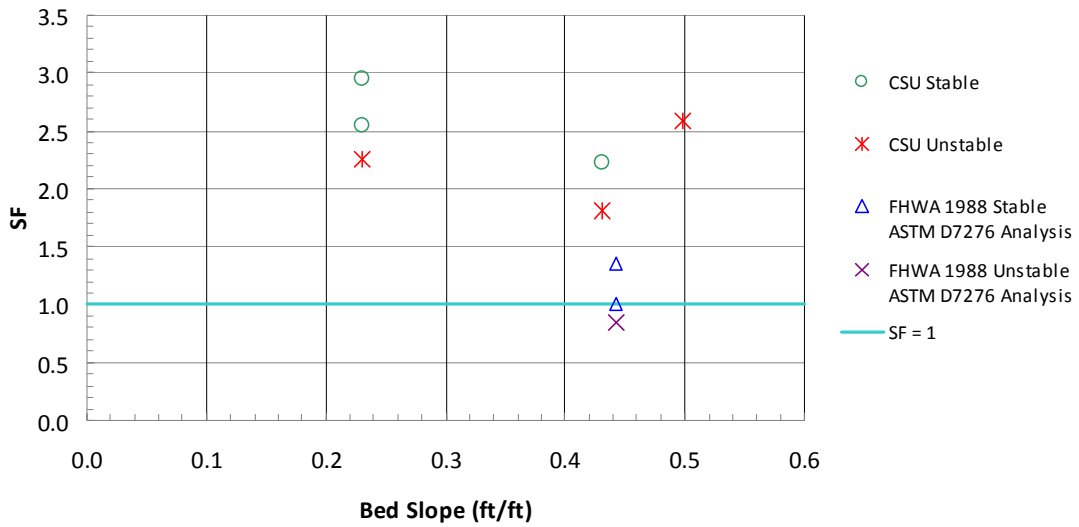


Figure 6.1: 30S SF Computed from Clopper (1991) and NCMA (2006) Method with $\tau_c = 13.5 \text{ lbs/ft}^2$ Calibrated from Clopper and Chen (1988) Data with ASTM D7276 (2008) Analysis

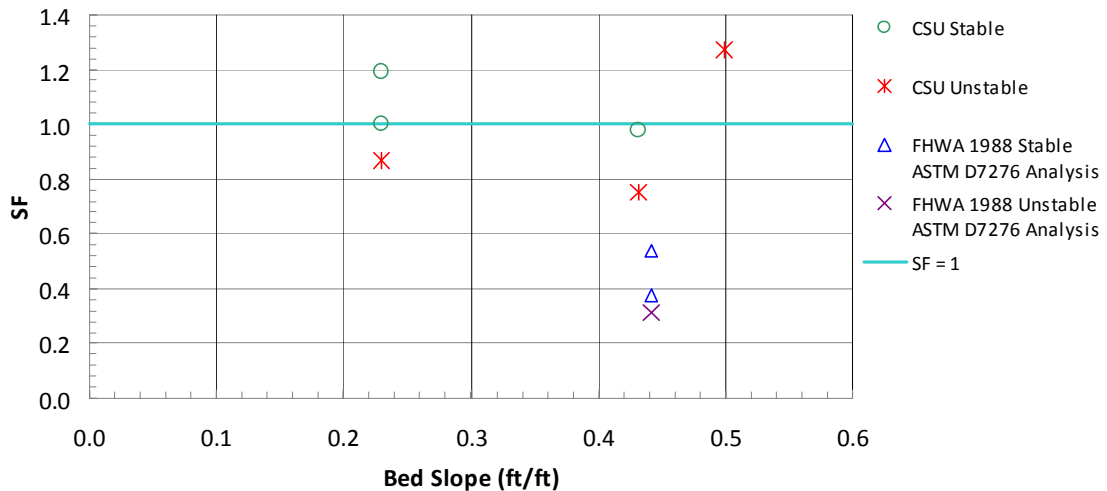


Figure 6.2: 30S SF Computed from Clopper (1991) and NCMA (2006) Method with $\tau_c = 4.5 \text{ lbs/ft}^2$ Calibrated from CSU Data at 0.230 Embankment Slope

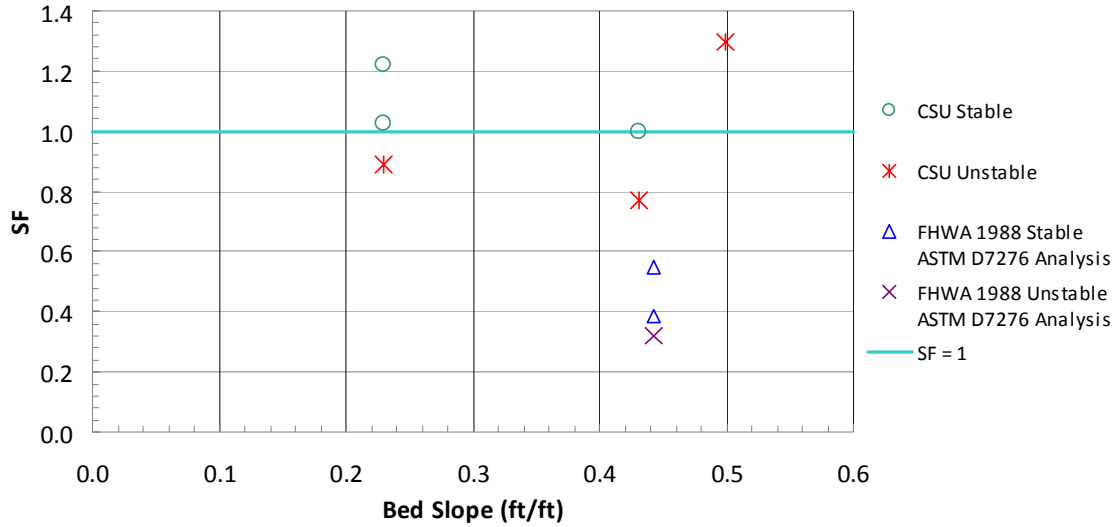


Figure 6.3: 30S SF Computed from Clopper (1991) and NCMA (2006) Method with $\tau_c = 4.7 \text{ lbs/ft}^2$ Calibrated from CSU Data at 0.431 Embankment Slope

6.2 PETRAFLEX CLOPPER (1991) AND NCMA (2006) SF

ANALYSIS

Using Equation 6.3, the Clopper (1991) and NCMA (2006) safety factor equation for overtopping conditions, safety factors were computed for each test presented in Table 5.4. Initially, critical shear-stress values at horizontal, τ_c , were computed using Equation 6.4 for each stable test preceding an unstable test. Table 6.3 provides the computed Petraflex τ_c values. Computed critical shear-stress values for the Petraflex system on a horizontal plane ranged from 5.7 to 8.6 lbs/ft^2 .

Table 6.3: Computed Critical Shear-stress Values for the Petraflex on a Horizontal Plane

Test ID No.	Block Name	Overtopping Depth (ft)	Test Date	S_0 (ft/ft)	Q (cfs)	V (ft/s)	τ_0 (lbs/ft^2)	NCMA
								τ_c (lbs/ft^2)
12	Petraflex	4.0	9/22/1987	0.437	96.0	19.0	7.0	8.6
13	Petraflex	1.0	8/21/2000	0.501	10.0	15.2	4.5	5.7

Safety factors were computed for the Petraflex data using both of the critical shear-stress values. Table 6.4 provides a summary of the computed safety factor values. Plots of bed slope versus computed safety factors for the 8.6 and 5.7 lbs/ft² τ_c values are presented in Figure 6.4 and Figure 6.5, respectively. The following summarizes the ability of each critical shear-stress value to predict system stability for the Petraflex dataset:

- $\tau_c = 8.6$ lbs/ft² correctly predicted the point of instability for 100% of the tested installations:
 - Computed safety factor values for stable tests ranged from 1.00 to 1.42
 - The computed safety factor value for the unstable test was 0.69
- $\tau_c = 5.7$ lbs/ft² correctly predicted the point of instability for 50% of the tested installations:
 - Computed safety factor values for stable tests ranged from 0.69 to 1.00
 - The computed safety factor value for the unstable test was 0.47

Table 6.4: Computed Petraflex *SF* for Clopper (1991) and NCMA (2006) Method

Test ID No.	Block Name	Over-topping Depth (ft)	S_0 (ft/ft)	V (ft/s)	τ_0 (lbs/ft ²)	System Condition	<i>SF</i>	<i>SF</i>
							($\tau_c = 8.6$ lbs/ft ²)	($\tau_c = 5.7$ lbs/ft ²)
10	Petraflex	1.0	0.437	12.3	5.0	Stable	1.34	0.93
11	Petraflex	2.0	0.437	15.3	6.2	Stable	1.12	0.77
12	Petraflex	4.0	0.437	19.0	7.0	Stable	1.00	0.69
13	Petraflex	1.0	0.501	15.2	4.5	Stable	1.42	1.00
14	Petraflex	2.0	0.501	17.8	10.2	Unstable	0.69	0.47

Orange cells identify tests used to calibrate τ_c values

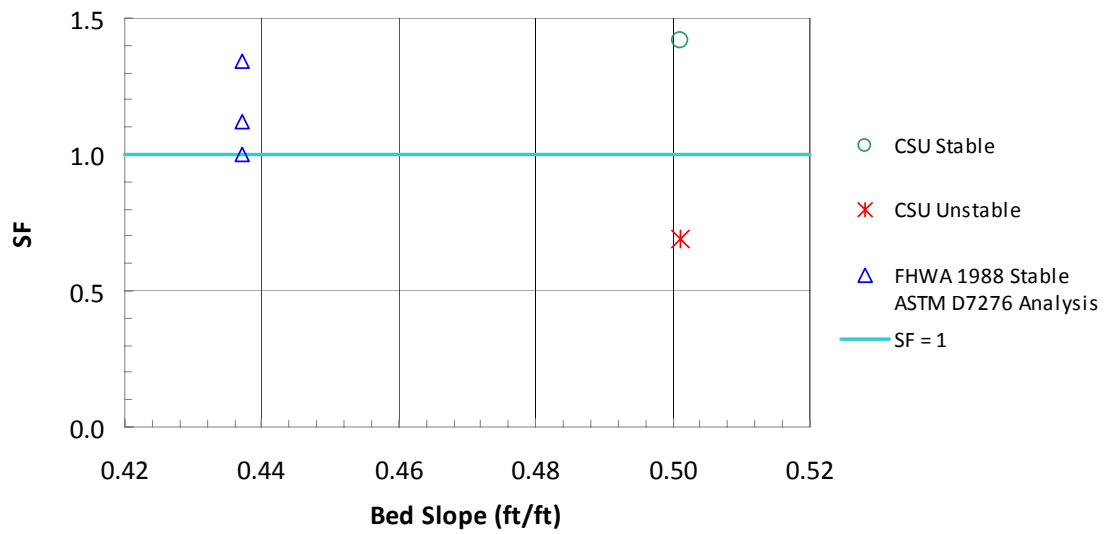


Figure 6.4: Petraflex SF Computed from Clopper (1991) and NCMA (2006) Method with $\tau_c = 8.6 \text{ lbs/ft}^2$ Calibrated from Clopper and Chen (1988) Data and ASTM D7276 (2008) Analysis

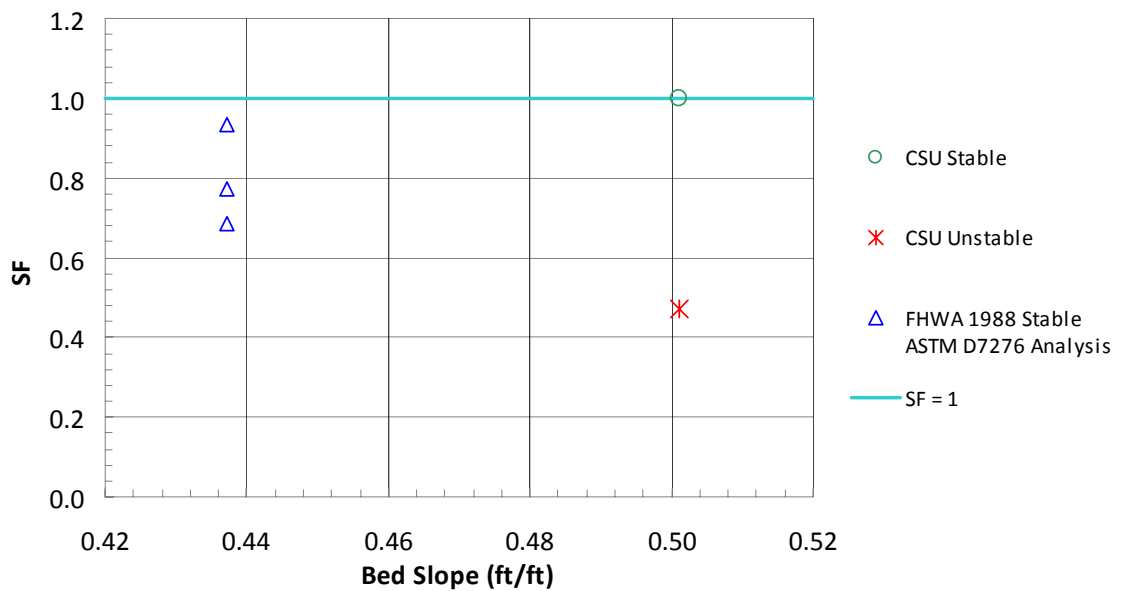


Figure 6.5: Petraflex SF Computed from Clopper (1991) and NCMA (2006) Method with $\tau_c = 5.7 \text{ lbs/ft}^2$ Calibrated from CSU Petraflex Data

6.3 CORPS BLOCK CLOPPER (1991) AND NCMA (2006) SF

ANALYSIS

Safety factors were computed for the tests presented in Table 5.5 using the Clopper (1991) safety factor equation for channel conditions, Equation 6.1; the NCMA (2006) safety factor equation for channel conditions, Equation 6.2; and the Clopper (1991) and NCMA (2006) safety factor equation for overtopping conditions, Equation 6.3. Initially, critical shear-stress values at horizontal, τ_c , were computed for each stable test preceding an unstable test. Table 6.5 provides the computed Corps Block τ_c values. Computed critical shear-stress values for the Corps Block system on a horizontal plane ranged from 2.2 to 3.7 lbs/ft².

Table 6.5: Computed Critical Shear-stress Values for the Corps Block on a Horizontal Plane

Test ID No.	Block Name	Over-topping Depth (ft)	S ₀ (ft/ft)	Side Slope (H/V)	Q (cfs)	V (ft/s)	τ_0 (lbs/ft ²)	NCMA τ_c (lbs/ft ²)
15	Corps Block	1.0	0.200	n/a	11.0	13.6	3.5	3.7
17	Corps Block	1.0	0.143	n/a	9.8	12.8	2.1	2.2
23	Corps Block	n/a	0.030	2.0	100.0	13.2	2.5	2.9

n/a = not applicable

Safety factors were computed for the Corps Block data using each of the critical shear-stress values. Table 6.6 provides a summary of the Corps Block computed safety factor values for the overtopping tests. Additionally, Table 6.7 and Table 6.8 provide computed safety factors for the channelized tests for the Clopper (1991) and NCMA (2006) methods, respectively. Plots of bed slope versus computed safety factors for the 3.7, 2.2, and 2.9 lbs/ft² τ_c values are presented in Figure 6.6, Figure 6.7, and Figure 6.8,

respectively. The following summarizes the ability of each critical shear-stress value to predict system stability for the Corps Block dataset:

- $\tau_c = 3.7 \text{ lbs/ft}^2$ correctly predicted the point of instability for 33% of the tested installations:
 - Computed safety factor values for stable tests ranged from 1.00 to 1.67
 - Correctly predicted 100% of stable tests
 - Computed safety factor values for unstable tests ranged from 0.71 to 1.32
 - Correctly predicted 50% of unstable tests
- $\tau_c = 2.2 \text{ lbs/ft}^2$ correctly predicted the point of instability for 33% of the tested installations:
 - Computed safety factor values for stable tests ranged from 0.60 to 1.00
 - Correctly predicted 17% of stable tests
 - Computed safety factor values for unstable tests ranged from 0.42 to 0.79
 - Correctly predicted 100% of unstable tests
- $\tau_c = 2.9 \text{ lbs/ft}^2$ correctly predicted the point of instability for 33% of the tested installations:
 - Computed safety factor values for stable tests ranged from 0.78 to 1.30
 - Correctly predicted 83% of stable tests
 - Computed safety factor values for unstable tests ranged from 0.55 to 1.03
 - Correctly predicted 75% of unstable tests

Table 6.6: Computed Corps Block SF for Overtopping Tests for Clopper (1991) and NCMA (2006) Method

Test ID No.	Block Name	S_0 (ft/ft)	V (ft/s)	τ_0 (lbs/ft ²)	System Condition	SF ($\tau_c = 3.7$ lbs/ft ²)	SF ($\tau_c = 2.2$ lbs/ft ²)	SF ($\tau_c = 2.9$ lbs/ft ²)
15	Corps Block	0.200	13.6	3.5	Stable	1.00	0.60	0.78
16	Corps Block	0.200	17.3	4.9	Unstable	0.71	0.42	0.55
17	Corps Block	0.143	12.8	2.1	Stable	1.67	1.00	1.30
18	Corps Block	0.143	16.5	4.8	Unstable	0.75	0.44	0.58
19	Corps Block	0.143	14.5	2.7	Unstable	1.32	0.79	1.03

Orange cells identify tests used to calibrate τ_c values

Table 6.7: Computed Corps Block SF for Channel Tests for Clopper (1991) Method

Test ID No.	Block Name	S_0 (ft/ft)	Side Slope (H/V)	V (ft/s)	τ_0 (lbs/ft ²)	System Condition	SF ($\tau_c = 3.7$ lbs/ft ²)	SF ($\tau_c = 2.2$ lbs/ft ²)	SF ($\tau_c = 2.9$ lbs/ft ²)
20	Corps Block	0.030	2.0	6.5	2.2	Stable	1.69	0.99	1.30
21	Corps Block	0.030	2.0	7.9	2.3	Stable	1.63	0.95	1.25
22	Corps Block	0.030	2.0	11.5	2.5	Stable	1.51	0.88	1.16
23	Corps Block	0.030	2.0	13.2	2.5	Stable	1.51	0.88	1.16
24	Corps Block	0.030	2.0	14.0	2.6	Unstable	1.41	0.82	1.08

Table 6.8: Computed Corps Block *SF* for Channel Tests for NCMA (2006) Method

Test ID No.	Block Name	S_0 (ft/ft)	Side Slope (H/V)	V (ft/s)	τ_0 (lbs/ft ²)	System Condition	SF ($\tau_c = 3.7$ lbs/ft ²)	SF ($\tau_c = 2.2$ lbs/ft ²)	SF ($\tau_c = 2.9$ lbs/ft ²)
20	Corps Block	0.030	2.0	6.5	2.2	Stable	1.41	0.86	1.11
21	Corps Block	0.030	2.0	7.9	2.3	Stable	1.36	0.83	1.07
22	Corps Block	0.030	2.0	11.5	2.5	Stable	1.27	0.77	1.00
23	Corps Block	0.030	2.0	13.2	2.5	Stable	1.27	0.77	1.00
24	Corps Block	0.030	2.0	14.0	2.6	Unstable	1.19	0.72	0.94

Orange cell identifies test used to calibrate τ_c value

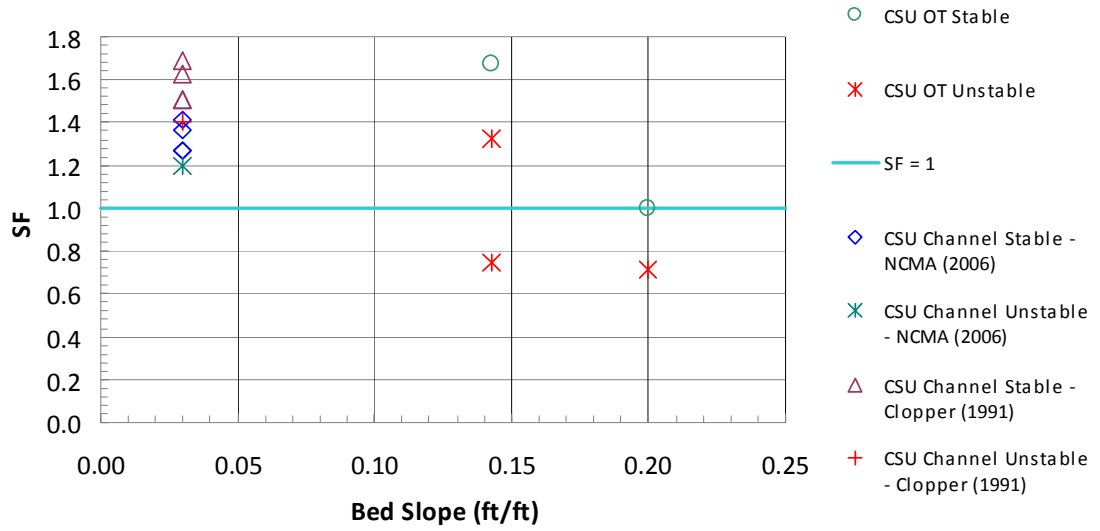


Figure 6.6: Corps Block SF Computed from Clopper (1991) and NCMA (2006) Methods with $\tau_c = 3.7 \text{ lbs/ft}^2$ Calibrated from 0.200 ft/ft Bed-slope Data

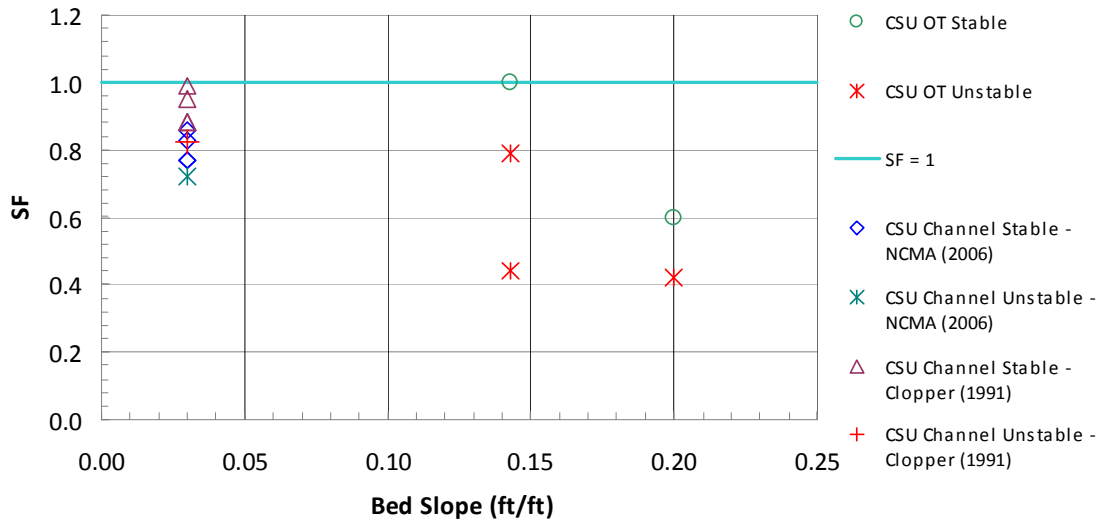


Figure 6.7: Corps Block SF Computed from Clopper (1991) and NCMA (2006) Methods with $\tau_c = 2.2 \text{ lbs/ft}^2$ Calibrated from 0.143 ft/ft Bed-slope Data

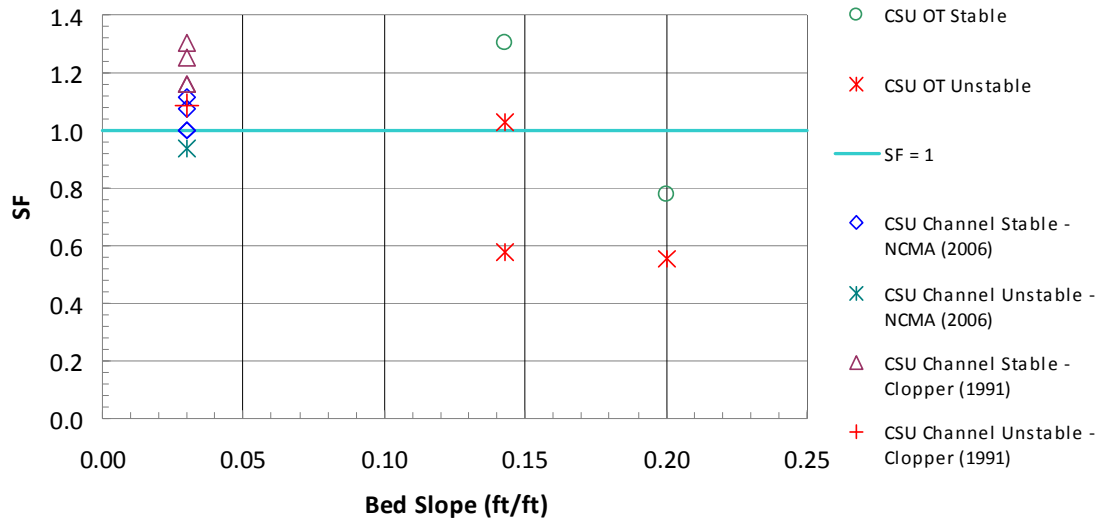


Figure 6.8: Corps Block *SF* Computed from Clopper (1991) and NCMA (2006) Methods with $\tau_c = 2.9 \text{ lbs/ft}^2$ Calibrated from Channelized Corps Data

6.4 SUMMARY

Safety factors were computed using the Clopper (1991) and NCMA (2006) safety factor equations for the tests within the database. The Clopper (1991) and NCMA (2006) safety factor equations proved inadequate at predicting system stability for the 30S and Corps Block datasets. For the Petraflex dataset, which was limited to tested embankments slopes of 0.437 and 0.501 ft/ft, the Clopper (1991) and NCMA (2006) method was successful at predicting stability with the τ_c value of 8.6 lbs/ft². Based on the results of the Clopper (1991) and NCMA (2006) safety factor calculations for ACB data, the need to develop a design methodology capable of predicting ACB system stability for both high-velocity, steep-slope and channelized applications was identified.

7 DERIVATION OF NEW SAFETY FACTOR METHOD

A new factor of safety equation was derived by investigating the ratio of the sum of resisting moments (moments that work to stabilize the block) to the sum of overturning moments (moments that work to set the block in motion). Results from the investigation of assumptions related to existing safety factor equations identified the most influential assumption as the non-conservative assumption of equal lift and drag forces. Therefore, a lift coefficient was employed to compute the lift force in a new safety factor equation. Other assumptions, including the weight force distribution simplification and computation of the rotation angle, were excluded in the derivation of a new safety factor equation.

A right-hand coordinate system was applied to the block system as defined by Figure 7.1 for the factor of safety analysis. Weight force components acting along the x, y, and z axis were derived and used during the safety factor derivations. Factor of safety equations were derived for incipient motion rotating about three separate points: 1) pivot Point P in the positive x direction, 2) pivot Point O in the positive z direction, and 3) pivot Point M on the corner of the block as illustrated in Figure 7.2. Subsequent sections present the derivation of the weight force components and the derivation of the new safety factor equation.

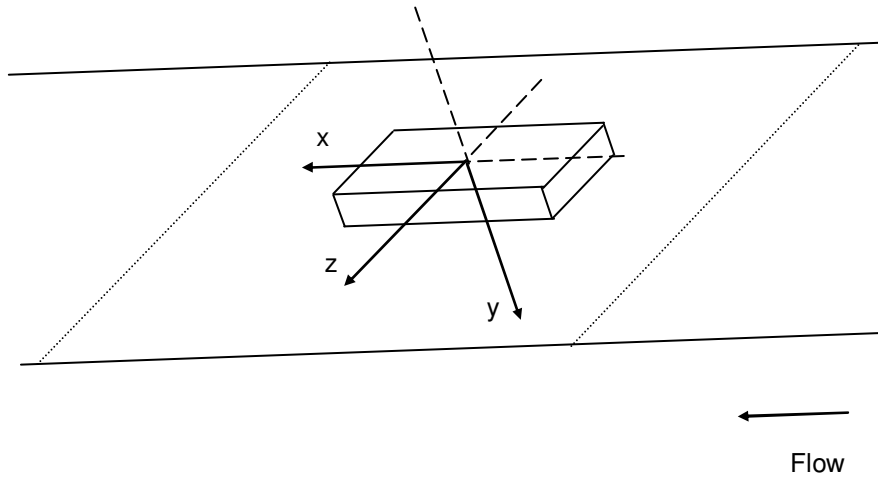


Figure 7.1: Coordinate System for Factor of Safety Equation Derivations

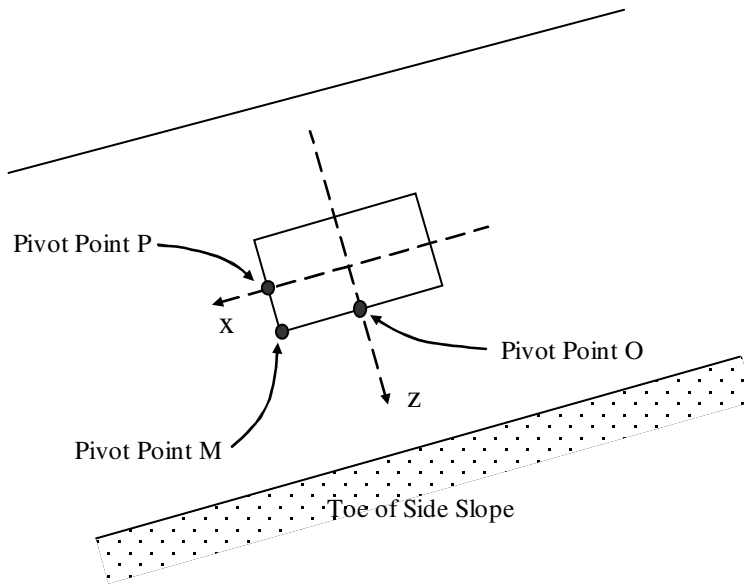


Figure 7.2: View of Block Normal to Side-slope Plane with Identified Pivot Points

7.1 DERIVATION OF SUBMERGED WEIGHT FORCE COMPONENTS

For the moment analysis, the components of the submerged weight in each of the directions of the three-dimensional coordinate system (x, y, and z) were derived:

- a. W_{SX} – weight force component parallel to the side-slope plane in the x direction:

$$W_{SX} = W_S \sin \theta_0 \quad \text{Equation 7.1}$$

where θ_0 is the angle of the bed slope.

- b. W_{SY} – weight force component normal to the side-slope plane in the y direction:

$$W_{SY} = W_S \cos \theta_0 \cos \theta_2 \quad \text{Equation 7.2}$$

where θ_2 is the angle resulting from the projection of the bed slope (θ_0) on the side-slope face and is mathematically defined by Equation 7.3:

$$\theta_2 = \arctan(\tan \theta_1 \cos \theta_0) \quad \text{Equation 7.3}$$

where θ_0 is the bed-slope angle and θ_1 is the side-slope angle.

- c. W_{SZ} – weight force component parallel to the side-slope plane in the positive z direction:

$$W_{SZ} = W_S \cos \theta_0 \sin \theta_2 \quad \text{Equation 7.4}$$

Derivations for each of the submerged weight components are presented in this section.

The weight force component acts in the negative vertical direction from the center of mass of the block as illustrated in Figure 7.3. Two components can be used to represent the total weight force: one along the direction of the bed slope and one normal to the bed slope. As shown in Figure 7.3, the weight force component in the x direction, W_{sx} , is $W_s \sin \theta_0$.

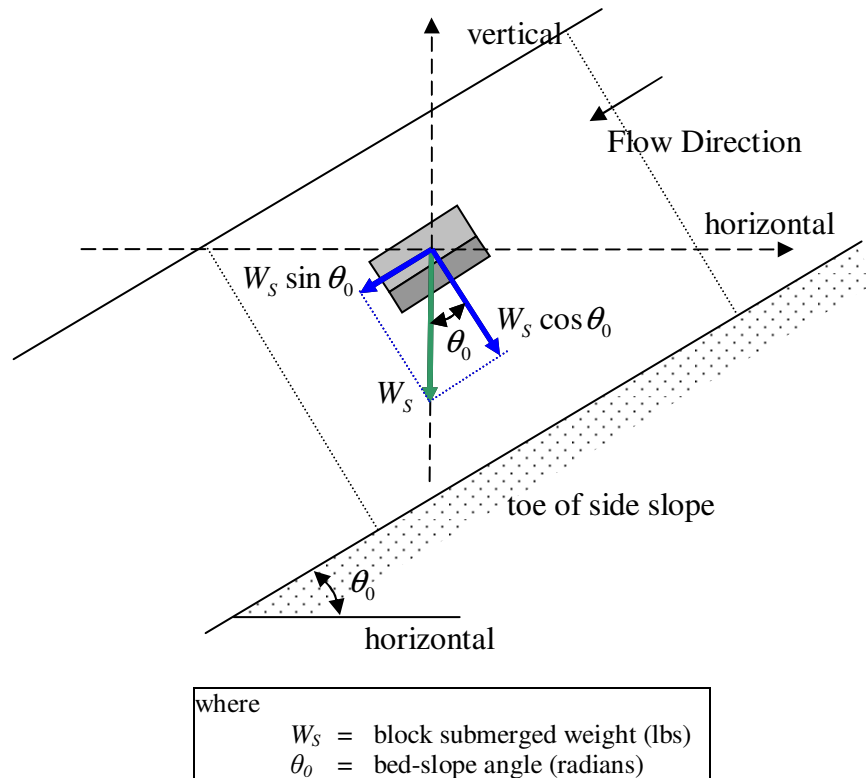
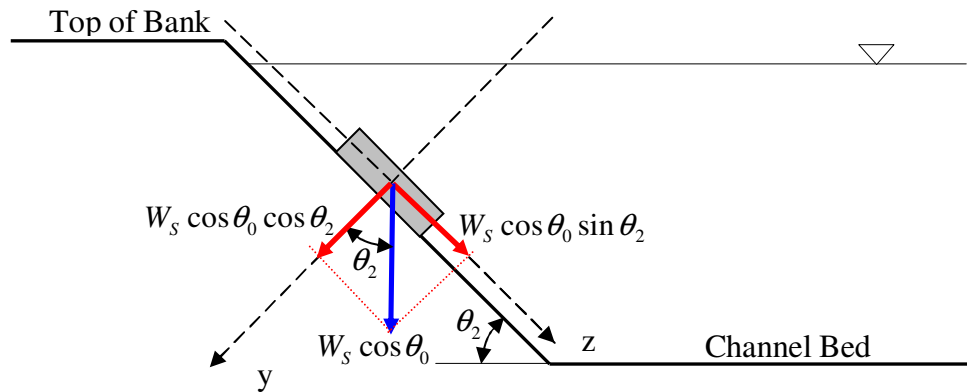


Figure 7.3: Weight Force Components Normal and Perpendicular to the Direction of the Bed Slope

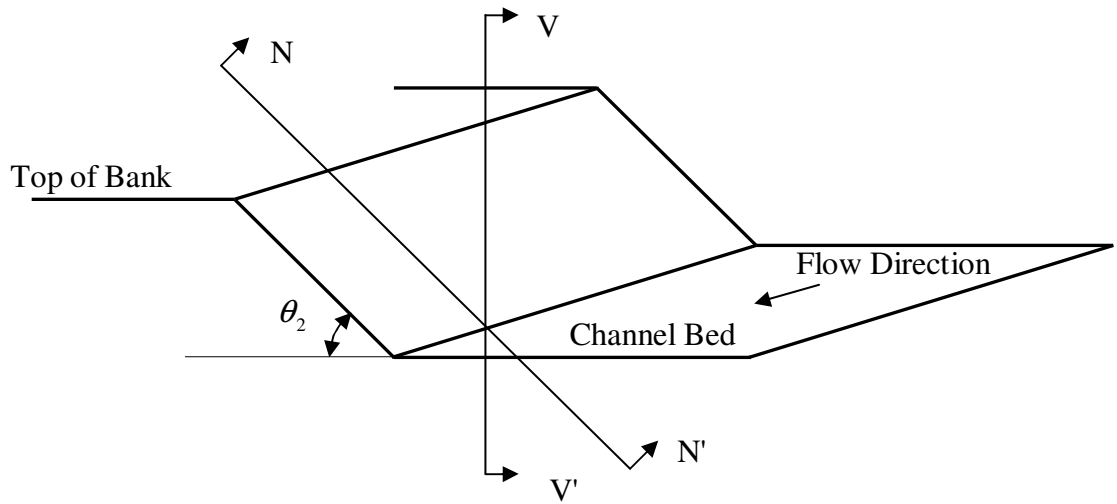
To obtain an expression for the weight force components in the y and z direction, W_{sy} and W_{sz} , respectively, the component perpendicular to the direction of flow in the horizontal-vertical plane, $W_s \cos \theta_0$ (Figure 7.3), was further investigated. Figure 7.4 presents the $W_s \cos \theta_0$ component in the z-y plane. $W_s \sin \theta_0$ is not shown in Figure 7.4 since it is located solely in the x axis which is normal to the z-y plane. As Figure 7.4

illustrates, $W_{SY} = W_S \cos \theta_0 \cos \theta_2$ and $W_{SZ} = W_S \cos \theta_0 \sin \theta_2$, where θ_2 is the angle between the bed slope and the side slope from a cross section normal to the bed-slope surface. Figure 7.5 illustrates the location of the θ_2 dimension.



where	
W_S	= block submerged weight (lbs)
θ_0	= bed-slope angle (radians)
θ_2	= side-slope angle measured along a cross section normal to the bed-slope (radians)
y, z	= y and z axes of the three-dimensional coordinate system

Figure 7.4: Channel Cross Section Normal to the Bed-slope View



<p>where</p> <p>V-V' = vertical cross-section</p> <p>N-N' = cross-section normal to the bed-slope plane</p> <p>θ_2 = angle between the bed-slope and the side-slope from a cross section normal to the bed-slope plane (radians)</p>
--

Figure 7.5: Definition of θ_2

7.2 DERIVATION OF SIDE-SLOPE ANGLE PERPENDICULAR TO BED SLOPE

An equation for the side-slope angle normal to the bed slope, θ_2 , as an expression of the side slope, θ_1 and the bed slope, θ_0 , was derived. Figure 7.6 presents a vertical cross-section view (V-V' from Figure 7.5) of the channel and defines the location of the side slope, θ_1 . Figure 7.7 presents a cross-section view normal to the bed slope (N-N' from Figure 7.5) and defines the location of θ_2 . Given the lengths adjacent, A , and opposite, O , of the angle θ_1 , as defined by Figure 7.6, the relationship presented in Equation 7.5 can be produced:

$$\tan \theta_1 = \frac{O}{A} \quad \text{Equation 7.5}$$

Furthermore, given the length adjacent, A , and opposite, O' , of the angle θ_2 , as defined by Figure 7.7, the relationship presented in Equation 7.6 can be produced:

$$\tan \theta_2 = \frac{O'}{A} \quad \text{Equation 7.6}$$

Solving Equation 7.5 for A and substituting into Equation 7.6 generates Equation 7.7:

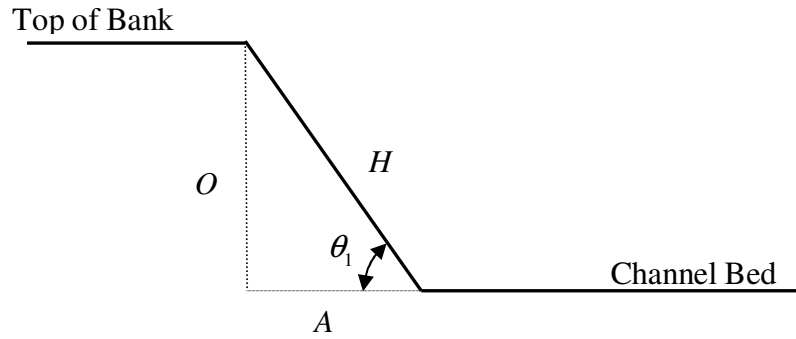
$$\tan \theta_2 = \frac{O' \tan \theta_1}{O} \quad \text{Equation 7.7}$$

As shown in Figure 7.8, the relationship presented in Equation 7.8 exists between the lengths opposite of θ_1 and θ_2 :

$$O' = O \cos \theta_0 \quad \text{Equation 7.8}$$

Substituting Equation 7.8 into Equation 7.7 and solving for θ_2 provides Equation 7.9, which is an expression for the side-slope angle normal to the bed slope, θ_2 , in terms of the bed-slope angle, θ_0 , and the vertical side-slope angle, θ_1 :

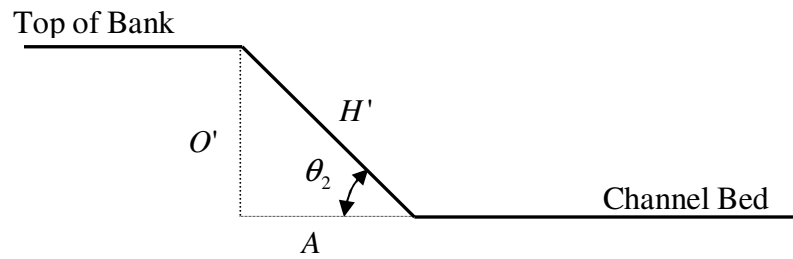
$$\theta_2 = \arctan(\cos \theta_0 \tan \theta_1) \quad \text{Equation 7.9}$$



where

- A = length adjacent of angle θ_1
- H = hypotenuse of right triangle created by θ_1
- O = length opposite of angle θ_1
- θ_1 = vertical side-slope angle (radians)

Figure 7.6: Cross-section V-V' View (vertical)



where

- A = length adjacent of angle θ_2
- H' = hypotenuse of right triangle created by θ_2
- O' = length opposite of angle θ_2
- θ_2 = angle between the bed-slope and the side-slope from a cross section normal to the bed-slope plane (radians)

Figure 7.7: Cross-section N-N' View (normal to the bed slope)

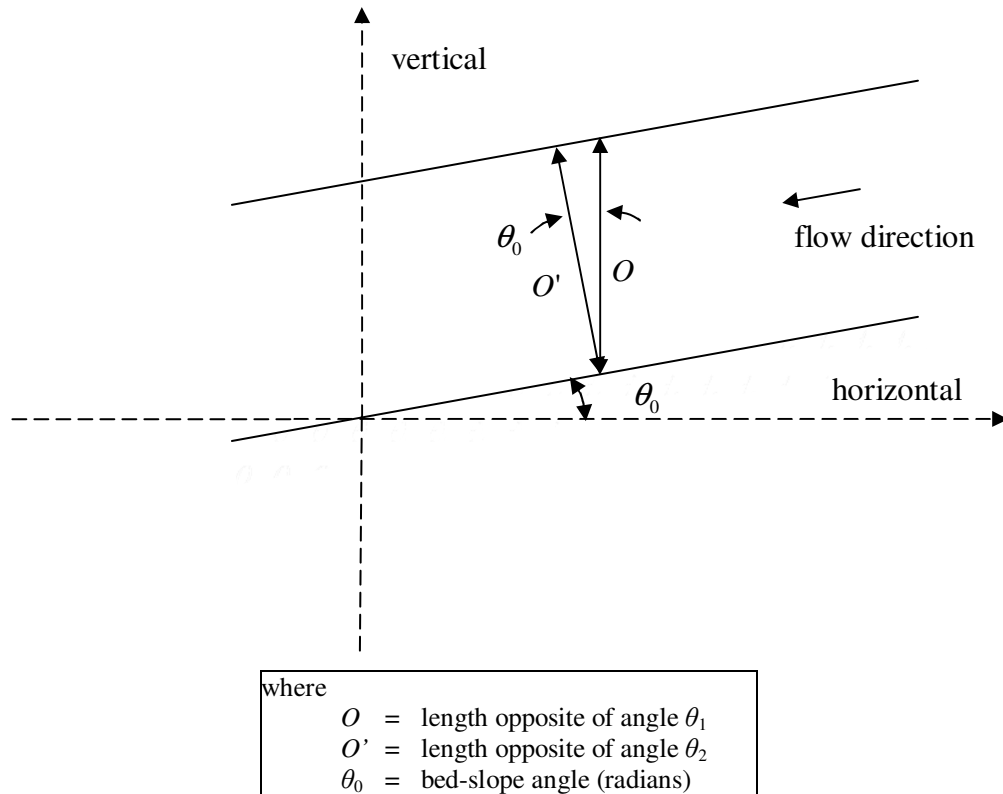


Figure 7.8: Channel Profile View Including Lengths O and O' for θ_1 and θ_2 , Respectively

7.3 DERIVATION OF SAFETY FACTOR EQUATIONS

Factor of safety equations were derived for rotation about the three points illustrated in Figure 7.2. For a given block and flow conditions, the three safety factor equations can be used to determine the critical rotation point.

Drag and lift force values for each derivation are computed by the same method. An expression for the drag force exerted on a block was obtained from the average boundary shear-stress equation and the block surface area. The drag force acting on the block surface was calculated by the product of the average boundary shear stress, τ_0 , and

surface area of the block face parallel to direction of flow, A_B . Equation 7.10 presents the expression for drag force exerted on a block.

$$F_D = \tau_0 A_B \quad \text{Equation 7.10}$$

where

F_D = drag force (lbs);

τ_0 = boundary shear stress (lbs/ft²); and

A_B = block area parallel to direction of flow (ft²).

According to dimensional analysis, the lift force is defined by Equation 7.11 (Wilcox, 2000):

$$F_L = \frac{1}{2} C_L \rho A_B V^2 \quad \text{Equation 7.11}$$

where

F_L = lift force (lbs);

C_L = lift coefficient;

ρ = mass density of water (slugs/ft³);

A_B = block area parallel to direction of flow (ft²); and

V = flow velocity (ft/s).

Additional lift and drag forces caused by a protruding block were computed using Equation 7.12, which is consistent with the method presented in NCMA (2006):

$$F_D' = F_L' = 0.5 \Delta Z b \rho V^2 \quad \text{Equation 7.12}$$

where

F'_D = additional drag force caused by block protrusion (lbs);

F'_L = additional lift force caused by block protrusion (lbs);

ΔZ = height of block protrusion above ACB system (ft);

b = block width normal to the flow direction (ft);

ρ = mass density of water (slugs/ft³); and

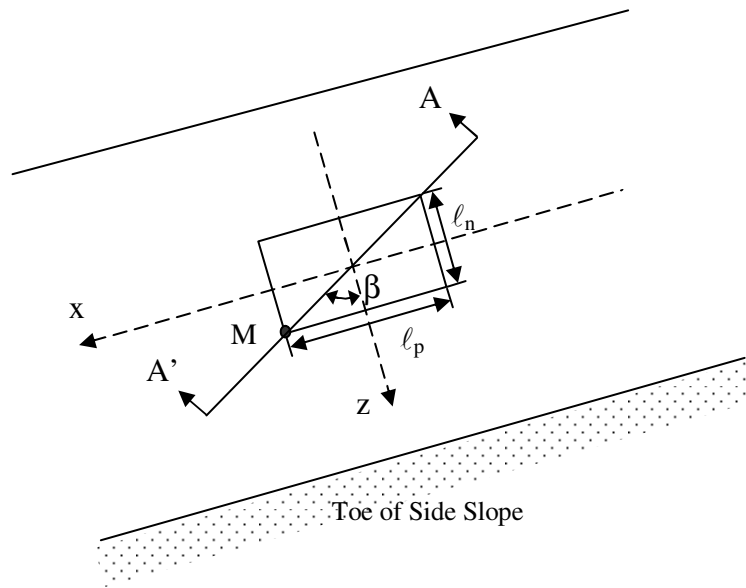
V = flow velocity (ft/s).

7.3.1 SAFETY FACTOR EQUATION FOR ROTATION ABOUT BLOCK CORNER (POINT M)

The location of the cross section used to calculate the safety factor equation for movement about the block corner (Point M), A-A', is presented in Figure 7.9. The angle β can be calculated from given block dimensions as expressed by Equation 7.13:

$$\beta = \arctan\left(\frac{\ell_p}{\ell_n}\right) \quad \text{Equation 7.13}$$

where ℓ_p is the block length parallel to the bed slope and ℓ_n is the block length normal to the bed slope as illustrated in Figure 7.9.



where	A-A'	=	cross section along block rotation path for rotation about the block corner
	l_n	=	block length normal to the bed-slope (ft)
	l_p	=	block length parallel to the bed-slope (ft)
	M	=	point of rotation for rotation about the block corner
	β	=	angle of block rotation measured in the side-slope plane (radians)
	x, z	=	x and z axes of the three-dimensional coordinate system

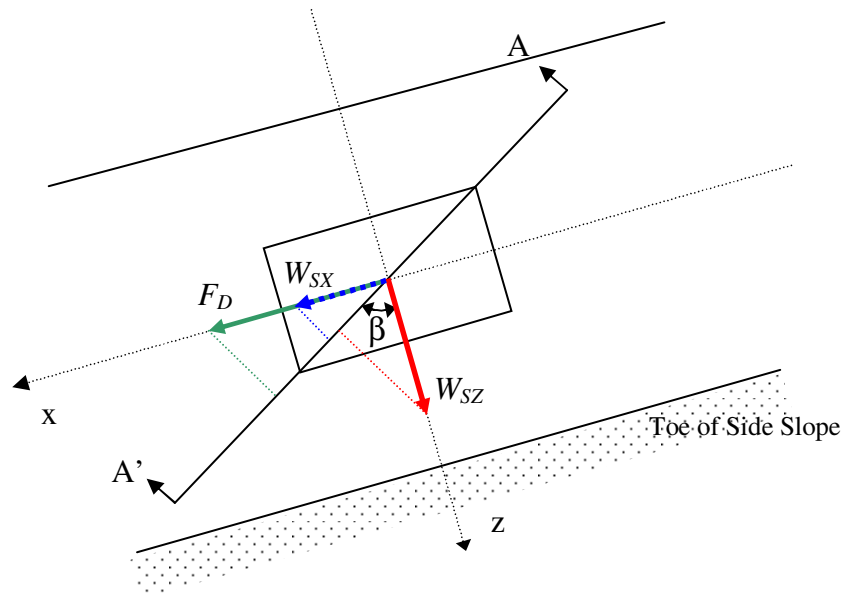
Figure 7.9: View of Block Normal to Side-slope Plane with Identified Cross-section A-A' and Angle β

The drag force acts in the direction of flow along the x axis. As illustrated by Figure 7.10, the components of the W_{SX} , W_{SZ} , and F_D forces in the direction of Cross-section A-A' were calculated and are expressed by Equation 7.14, Equation 7.15, and Equation 7.16, respectively:

$$W_{SX(A-A')} = W_{SX} \sin(\beta) \quad \text{Equation 7.14}$$

$$W_{SZ(A-A')} = W_{SZ} \cos(\beta) \quad \text{Equation 7.15}$$

$$F_{D(A-A')} = F_D \sin(\beta) \quad \text{Equation 7.16}$$



where	
A-A'	= cross section along block rotation path for rotation about the block corner
F_D	= drag force (lbs)
W_{SX}	= block submerged weight component along the x axis (lbs)
W_{SZ}	= block submerged weight component along the z axis (lbs)
β	= angle of block rotation measured in the side-slope plane (radians)
x, z	= x and z axes of the three-dimensional coordinate system

Figure 7.10: View of Block Normal to Side-slope Plane with Identified Force Components

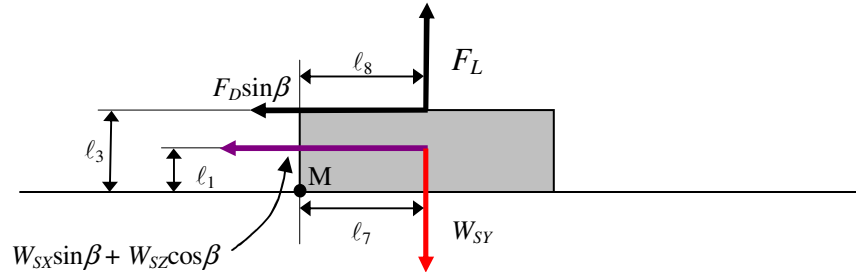
A free-body diagram of the block Cross-section A-A' is presented in Figure 7.11 with corresponding moment arms. The moment arm between the block corner and the W_{SY} weight force component, l_7 , which acts along the direction of the A-A' can be calculated from the block dimensions using Equation 7.17:

$$l_7 = 0.5\sqrt{l_p^2 + l_n^2} \qquad \text{Equation 7.17}$$

where

l_p = block length parallel to the bed slope (ft); and

l_n = block length normal to the bed slope as illustrated in Figure 7.9 (ft).



where

- β = angle of block rotation measured in the side-slope plane (radians)
- F_D = drag force (lbs)
- F_L = lift force (lbs)
- l_1 = moment arm for submerged weight force component parallel to the side-slope plane (ft)
- l_3 = block height and moment arm for the drag force component along the path of motion (ft)
- l_7 = moment arm for the weight force component normal to the side-slope plane (ft)
- l_8 = moment arm for the lift force (ft)
- M = rotation point about the block corner
- W_{SX} = block submerged weight component along the x axis (lbs)
- W_{SY} = block submerged weight component along the y axis (lbs)
- W_{SZ} = block submerged weight component along the z axis (lbs)

Figure 7.11: Free-body Diagram for Rotation about Point M

Equation 7.18 presents the safety factor equation for rotation about pivot Point M, which was derived by taking the ratio of resisting moments to overturning moments illustrated in Figure 7.11:

$$SF_M = \frac{M_{resisting}}{M_{overturning}} = \frac{l_7 W_{SY}}{l_1 (W_{SX} \sin \beta + W_{SZ} \cos \beta) + l_3 (F_D + F_D') \sin \beta + l_8 (F_L + F_L')}$$

Equation 7.18

where

W_{SX} = block submerged weight component along the x axis (lbs);

W_{SY} = block submerged weight component along the y axis (lbs);

W_{SZ} = block submerged weight component along the z axis (lbs);

F_D = drag force (lbs);

F_D' = additional drag force due to block protruding above adjacent blocks
(lbs);

F_L = lift force (lbs);

F_L' = additional lift force due to block protruding above adjacent blocks (lbs);

and

ℓ_i = corresponding moment arms as illustrated in Figure 7.11 (ft).

After substituting Equation 7.1, Equation 7.2, and Equation 7.4 for W_{SX} , W_{SY} , and W_{SZ} in Equation 7.18, respectively, Equation 7.19 is derived as the safety factor equation for rotation about Point M:

$$SF_M = \frac{\ell_7 W_S \cos \theta_0 \cos \theta_2}{\ell_1 (W_S \sin \theta_0 \sin \beta + W_S \cos \theta_0 \sin \theta_2 \cos \beta) + \ell_3 (F_D + F_D') \sin \beta + \ell_8 (F_L + F_L')}$$

Equation 7.19

where

W_S = block submerged weight (lbs);

θ_0 = bed-slope angle (radians); and

θ_2 = side-slope angle normal to the bed slope as defined by Equation 7.3
(radians).

7.3.2 SAFETY FACTOR EQUATION FOR ROTATION IN THE FLOW DIRECTION (POINT P)

A free-body diagram for incipient failure in the positive x direction, rotation about Point P, is presented in Figure 7.12. Equation 7.20, which conservatively ignores inter-block restraint, is the safety factor equation for rotation in the x-y plane:

$$SF_P = \frac{M_{resisting}}{M_{overturning}} = \frac{\ell_2 W_{SY}}{\ell_1 W_{SX} + \ell_3 (F_D + F'_D) + \ell_4 (F_L + F'_L)} \quad \text{Equation 7.20}$$

where

W_{SX} = block submerged weight component along the x axis (lbs);

W_{SY} = block submerged weight component along the y axis (lbs);

F_D = drag force (lbs);

F'_D = additional drag force due to block protruding above adjacent blocks (lbs);

F_L = lift force (lbs);

F'_L = additional lift force due to block protruding above adjacent blocks (lbs);
and

ℓ_i = corresponding moment arms as illustrated in Figure 7.12 (ft).

After substituting Equation 7.1 and Equation 7.2 for W_{SX} and W_{SY} in Equation 7.20, respectively, Equation 7.21 is derived as the safety factor equation for rotation about Point P:

$$SF_P = \frac{\ell_2 W_S \cos \theta_0 \cos \theta_2}{\ell_1 W_S \sin \theta_0 + \ell_3 (F_D + F'_D) + \ell_4 (F_L + F'_L)} \quad \text{Equation 7.21}$$

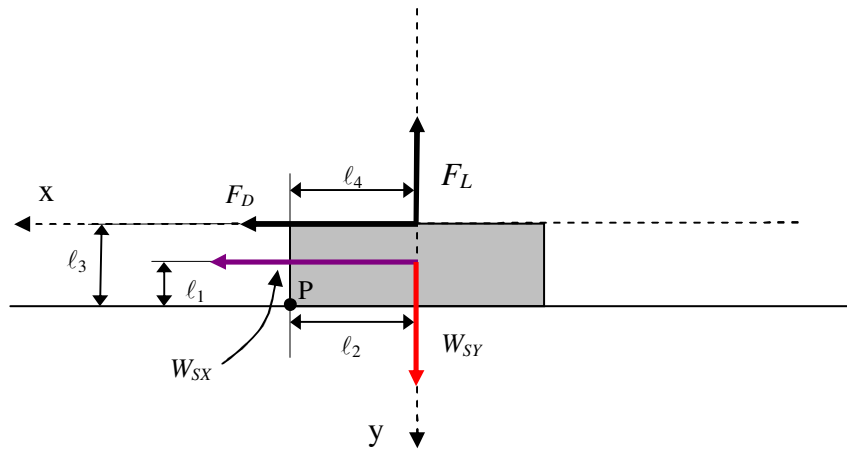
where

W_S = block submerged weight (lbs);

θ_0 = bed-slope angle (radians); and

θ_2 = side-slope angle normal to the bed slope as defined by Equation 7.3 (radians).

The moment arm associated with the lift force, l_4 , is equal to the moment arm for the weight force in the y direction, l_2 , where $l_2 = \frac{1}{2} \times l_p$.



where

F_D = drag force (lbs)

F_L = lift force (lbs)

l_1 = moment arm for submerged weight force component parallel to the side-slope plane (ft)

l_2 = moment arm for submerged weight force component normal to the side-slope plane (ft)

l_3 = block height and moment arm for the drag force (ft)

l_4 = moment arm for the lift force (ft)

P = rotation point about the block edge in the downstream direction

W_{SX} = block submerged weight component along the x axis (lbs)

W_{SY} = block submerged weight component along the y axis (lbs)

x, y = x and y axes of the three-dimensional coordinate system

Figure 7.12: Free-body Diagram for Rotation about Point P

7.3.3 SAFETY FACTOR EQUATION FOR ROTATION PERPENDICULAR TO THE FLOW DIRECTION (POINT O)

A free-body diagram for incipient failure in the positive z direction, rotation about Point O, is presented in Figure 7.13. Equation 7.22, which conservatively ignores inter-block restraint, represents the safety factor equation for rotation in the z-y plane:

$$SF_O = \frac{M_{resisting}}{M_{overturning}} = \frac{\ell_5 W_{SY}}{\ell_1 W_{SZ} + \ell_6 (F_L + F'_L)} \quad \text{Equation 7.22}$$

where

W_{SZ} = block submerged weight component in the z direction (lbs);

W_{SY} = block submerged weight component in the y direction (lbs);

F_L = lift force (lbs);

F'_L = additional lift force due to protruding block (lbs); and

ℓ_i = corresponding moment arms as illustrated in Figure 7.13 (ft).

After substituting Equation 7.1 and Equation 7.4 for W_{SX} and W_{SZ} in Equation 7.22, respectively, Equation 7.23 is derived as the safety factor equation for rotation about Point O:

$$SF_O = \frac{\ell_5 W_S \cos \theta_0 \cos \theta_2}{\ell_1 W_S \cos \theta_0 \sin \theta_2 + \ell_6 (F_L + F'_L)} \quad \text{Equation 7.23}$$

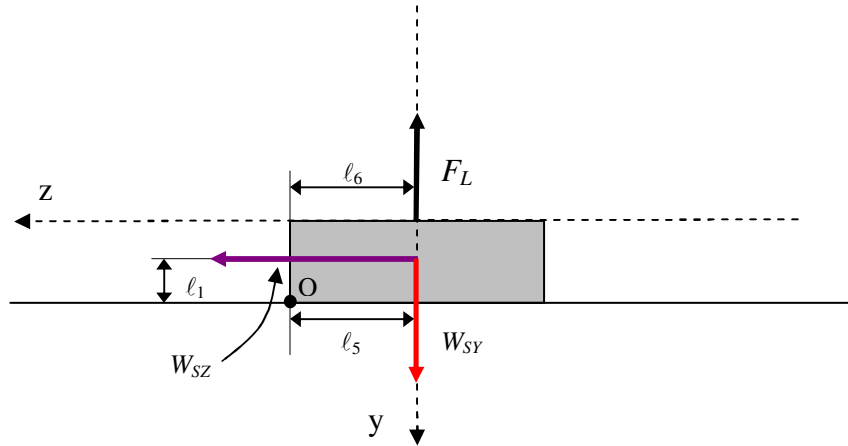
where

W_S = block submerged weight (lbs);

θ_0 = bed-slope angle (radians); and

θ_2 = side-slope angle normal to the bed slope as defined by Equation 7.3 (radians).

The moment arm associated with the lift force, l_6 , is equal to the moment arm for the weight force in the y direction, l_5 , where $l_5 = \frac{1}{2} \times l_n$.



where	
F_L	= lift force (lbs)
l_1	= moment arm for submerged weight force component parallel to the side-slope plane (ft)
l_5	= moment arm for the weight force component in the y direction (ft)
l_6	= moment arm for the lift force (ft)
O	= rotation point about the block edge laterally into the channel
W_{SY}	= block submerged weight component along the y axis (lbs)
W_{SZ}	= block submerged weight component in the z direction (lbs)
x, y	= x and y axes of the three-dimensional coordinate system

Figure 7.13: Free-body Diagram for Rotation about Point O

7.4 SAFETY FACTOR EQUATION FOR BLOCKS ON A CHANNEL BED

The factor of safety equation for a block on the channel bed can be directly derived from Equation 7.21 by setting the side-slope angle, θ_1 , to 0. When the side-slope

angle is 0, the corresponding side-slope angle normal to the bed slope is 0 as illustrated in Equation 7.24:

$$\theta_2 = \arctan(\tan(0)\cos\theta_0) = \arctan(0) = 0 \quad \text{Equation 7.24}$$

Equation 7.25, Equation 7.26 and Equation 7.27 present the W_{SX} , W_{SY} , and W_{SZ} weight force components, respectively, for a block on the channel bed which can be derived by substituting 0 for θ_2 in Equation 7.1, Equation 7.2, and Equation 7.4:

$$W_{SX} = W_S \sin\theta_0 \quad \text{Equation 7.25}$$

$$W_{SY} = W_S \cos\theta_0 \quad \text{Equation 7.26}$$

$$W_{SZ} = 0 \quad \text{Equation 7.27}$$

Rotation about Point P is the critical concern for incipient failure for a block on the channel bed since that rotation is in the direction of flow and in the plane of the only weight force components. Substituting 0 for θ_2 in Equation 7.21 results in Equation 7.28, which is the SF equation for a block on the channel bed:

$$SF_{BED} = \frac{\ell_2 W_S \cos\theta_0}{\ell_1 W_S \sin\theta_0 + \ell_3 (F_D + F_D') + \ell_4 (F_L + F_L')} \quad \text{Equation 7.28}$$

where

W_S = block submerged weight (lbs);

θ_0 = bed-slope angle (radians);

F_D = drag force (lbs);

F'_D = additional drag force due to block protruding above adjacent blocks
(lbs);

F_L = lift force (lbs);

F'_L = additional lift force due to block protruding above adjacent blocks (lbs);
and

ℓ_i = corresponding moment arms as illustrated in Figure 7.12 (ft).

7.5 SUMMARY

Safety factor equations were derived for stability of a rectangular particle on a channel side slope and stability on a channel bed. Computation of the lift force for the safety factor method uses the flow velocity with a lift coefficient specific to a given rectangular particle. Additionally, expressions for computation of the weight force distribution which correctly account for the bed-slope contribution are utilized. Channel side-slope safety factor equations were derived for rotation about three locations on the block: 1) rotation about the block corner (Point M), 2) rotation about the block edge in the downstream direction (Point P), and 3) rotation about the block edge laterally into the channel (Point O). To derive the safety factor equation for blocks on a channel bed, the side-slope angle was set to 0 in the channel side-slope safety factor equation for rotation about Point P. Table 7.1 provides a summary of the derived safety factor equations. Values for bed slope, side slope, block geometry, block weight, specific gravity of block material, design velocity, design shear stress, and calibrated lift coefficient are required to use the new safety factor method. Since the only calibrated parameter within the derived

safety factor equation is the lift coefficient, it accounts for inter-block friction which is not represented in the moment stability model.

Table 7.1. Summary of New Safety Factor Equations

	Equation	Equation Number
	$\theta_2 = \arctan(\tan \theta_1 \cos \theta_0)$	Equation 7.3
	$F_D = \tau_0 A_B$	Equation 7.10
	$F_L = \frac{1}{2} C_L \rho A_B V^2$	Equation 7.11
	$F'_D = F'_L = 0.5 \Delta Z b \rho V^2$	Equation 7.12
	$\beta = \arctan\left(\frac{\ell_p}{\ell_n}\right)$	Equation 7.13
Channel Side-slope SF Equation for Rotation about the Block Corner (Point M):	$SF_M = \frac{\ell_7 W_S \cos \theta_0 \cos \theta_2}{\ell_1 (W_S \sin \theta_0 \sin \beta + W_S \cos \theta_0 \sin \theta_2 \cos \beta) + \ell_3 (F_D + F'_D) \sin \beta + \ell_8 (F_L + F'_L)}$	Equation 7.19
Channel Side-slope SF Equation for Rotation about the Block Edge in the Flow Direction (Point P):	$SF_P = \frac{\ell_2 W_S \cos \theta_0 \cos \theta_2}{\ell_1 W_S \sin \theta_0 + \ell_3 (F_D + F'_D) + \ell_4 (F_L + F'_L)}$	Equation 7.21
Channel Side-slope SF Equation for Rotation about the Block Edge Laterally into the Channel (Point O):	$SF_O = \frac{\ell_5 W_S \cos \theta_0 \cos \theta_2}{\ell_1 W_S \cos \theta_0 \sin \theta_2 + \ell_6 (F_L + F'_L)}$	Equation 7.23
Channel Bed SF Equation for Rotation about the Block Edge in the Flow Direction (Point P):	$SF_{BED} = \frac{\ell_2 W_S \cos \theta_0}{\ell_1 W_S \sin \theta_0 + \ell_3 (F_D + F'_D) + \ell_4 (F_L + F'_L)}$	Equation 7.28

Table 7.1 (continued): Summary of New Safety Factor Equations

where

θ_2	=	side-slope angle perpendicular to the bed-slope plane (radians);
θ_0	=	vertical side-slope angle = $\arctan(1/z)$ (radians);
θ_1	=	bed-slope angle = $\arctan(S_0)$ (radians);
F_D	=	drag force (lbs);
τ_0	=	boundary shear stress (lbs/ft ²);
A_B	=	block area parallel to direction of flow (ft ²);
F_L	=	lift force (lbs);
C_L	=	lift coefficient;
ρ	=	mass density of water (slugs/ft ³);
V	=	flow velocity (ft/s);
F_D'	=	additional drag force caused by block protrusion (lbs);
F_L'	=	additional lift force caused by block protrusion (lbs);
ΔZ	=	height of block protrusion above ACB system (ft);
b	=	block width normal to the flow direction (ft);
β	=	angle to block corner (radians);
l_p	=	block length parallel to the bed slope (ft);
l_n	=	block length normal to the bed slope (ft);
W_S	=	block submerged weight (lbs); and
l_i	=	moment arms corresponding to forces (ft).

8 ANALYSIS OF NEW SAFETY FACTOR EQUATIONS

An assessment of the safety factor equations developed in Chapter 7 was conducted using the database presented in Chapter 4. A lift coefficient was calibrated for each block and safety factors were computed for all tests using the equations presented in Table 7.1.

For overtopping hydraulic test conditions, Equation 7.28 was used to determine the value of C_L for each block. Lift coefficients were calculated by setting the SF equal to 1 and using the flow velocity and boundary shear stress measured for the stable test condition prior to identified failure. Substituting Equation 7.11 into Equation 7.28 and setting SF equal to 1 generates Equation 8.1 for C_L :

$$SF_{BED} = 1 = \frac{\ell_2 W_s \cos \theta_0}{\ell_1 W_s \sin \theta_0 + \ell_3 (F_D) + \ell_4 \left(\frac{1}{2} C_L \rho A_B V^2 \right)} \quad \text{Equation 8.1}$$

Since the database was developed from tests conducted in a controlled laboratory setting, Equation 8.1 excludes the additional lift and drag forces attributed to block protrusion above adjacent blocks. Equation 8.2 presents the formula for computing a lift coefficient, C_L , which was derived by solving Equation 8.1:

$$C_L = \frac{\ell_2 W_s \cos \theta_0 - \ell_1 W_s \sin \theta_0 - \ell_3 F_D}{0.5 \ell_4 \rho A_B V^2} \quad \text{Equation 8.2}$$

For channelized hydraulic test conditions, the critical point of rotation was initially identified by evaluating Equation 7.19, Equation 7.21, and Equation 7.23 for the minimum safety factor using lift coefficients determined from the overtopping data assessment. Subsequently, a lift coefficient was computed from the safety factor equation with the minimum computed safety factor by setting the safety factor equal to 1 and solving for C_L .

8.1 30S NEW *SF* ANALYSIS

Using the derived safety factor calculation equations provided in Table 7.1, safety factors were computed for each 30S test presented in Table 5.3. Initially, the lift coefficient, C_L , was computed for all stable tests which directly preceded an unstable test by using the computed shear stress and flow velocity on the embankment and assuming a safety factor value of 1. A lift coefficient value of 0.0972 was determined to be the optimum value to represent the stability conditions within the dataset.

Safety factors were computed for the 30S data using the 0.0972 lift coefficient value. Table 8.1 provides a summary of the computed safety factor values. A plot of bed slope versus 30S computed safety factors is presented in Figure 8.1. The following summarizes the ability of the new safety factor equation to predict system stability for the 30S dataset:

- $C_L = 0.0972$ correctly predicted the point of instability for 75% of the tested installations:
 - Computed safety factor values for stable tests ranged from 0.74 to 1.71
 - Correctly predicted 80% of stable tests

- Computed safety factor values for unstable tests ranged from 0.46 to 0.84
- Correctly predicted 100% of unstable tests

The new safety factor equation proved successful in predicting stability for eight out of the nine 30S tests.

Table 8.1: Computed 30S SF for the New SF Method

Test ID No.	Block Name	Overtopping Depth (ft)	S_0 (ft/ft)	V (ft/s)	τ_0 (lbs/ft ²)	System Condition	SF ($C_L = 0.0972$)
1	30S	1.0	0.442	12.1	7.1	Stable	1.05
2	30S	2.0	0.442	14.9	10.3	Stable	0.74
3	30S	4.0	0.442	20.4	12.6	Unstable	0.46
4	30S	1.0	0.499	17.6	2.5	Unstable	0.66
5	30S	1.0	0.230	10.5	3.3	Stable	1.71
6	30S	1.6	0.230	14.7	4.0	Stable	1.00
7	30S	2.0	0.230	17.2	4.7	Unstable	0.76
8	30S	0.9	0.431	13.7	3.6	Stable	1.00
9	30S	1.2	0.431	15.0	4.9	Unstable	0.84

Orange cell identifies test used to calibrate C_L value

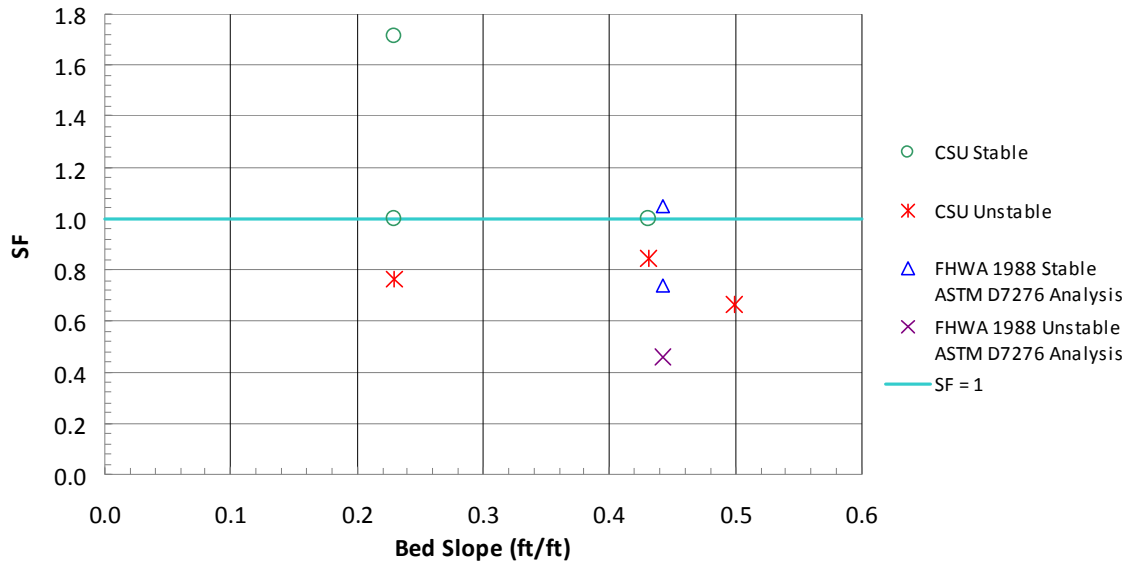


Figure 8.1: 30S SF Computed from the New SF Method with $C_L = 0.0972$ Calibrated from CSU 30S 0.230 ft/ft Bed-slope Data

8.2 PETRAFLEX NEW *SF* ANALYSIS

Using the new safety factor calculation equations provided in Table 7.1, safety factors were computed for the Petraflex tests. Initially, the lift coefficient, C_L , was computed for all stable tests which directly preceded an unstable test by using the computed shear stress and flow velocity on the embankment and assuming a safety factor value of 1. A lift coefficient value of 0.0207 was determined to be the optimum value to represent the stability conditions within the dataset.

Safety factors were computed for the Petraflex data using the 0.0207 lift coefficient value. Table 8.2 provides a summary of the computed safety factor values. A plot of bed slope versus Petraflex computed safety factor is presented in Figure 8.2. The following summarizes the ability of the new safety factor equation to predict system stability for the Petraflex dataset:

- $C_L = 0.0207$ correctly predicted the point of instability for 100% of the tested installations:
 - Computed safety factor values for stable tests ranged from 1.00 to 1.76
 - The computed safety factor values for the unstable test was 0.91

The new safety factor equation proved successful in predicting stability for all of the Petraflex tests.

Table 8.2: Computed Petraflex SF for the New SF Method

Test ID No.	Block Name	Over-topping Depth (ft)	S_0 (ft/ft)	V (ft/s)	τ_0 (lbs/ft ²)	System Condition	SF ($C_L = 0.0207$)
10	Petraflex	1.0	0.437	11.7	5.8	Stable	1.76
11	Petraflex	2.0	0.437	15.0	7.5	Stable	1.33
12	Petraflex	4.0	0.437	19.0	7.0	Stable	1.00
13	Petraflex	1.0	0.501	15.2	4.5	Stable	1.41
14	Petraflex	2.0	0.501	17.8	10.2	Unstable	0.91

Orange cell identifies test used to calibrate C_L value

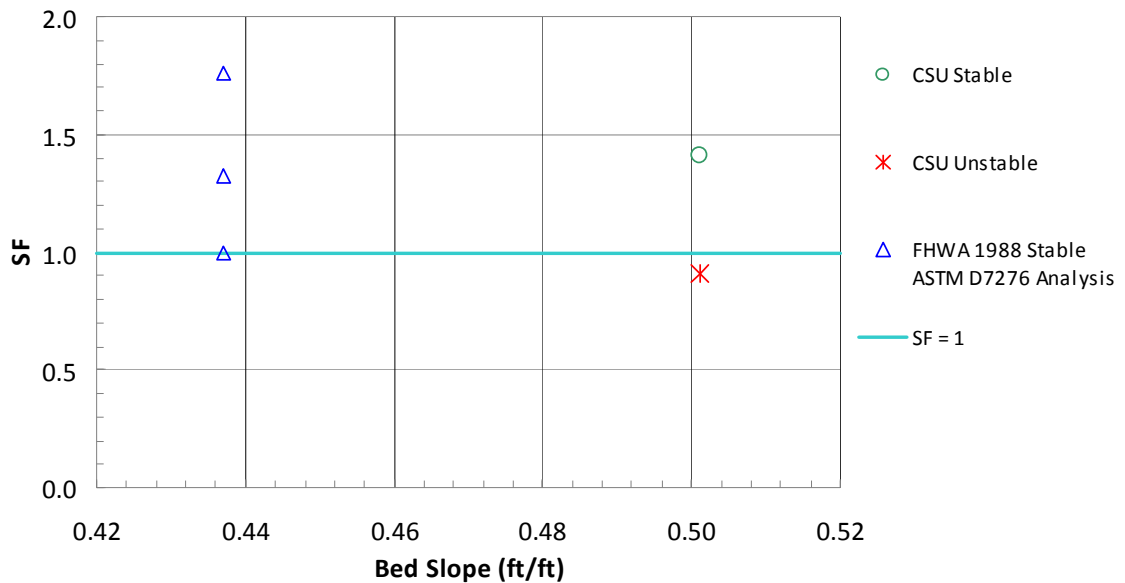


Figure 8.2: Petraflex SF Computed from the New SF Method with $C_L = 0.0207$ Calibrated from Clopper and Chen (1988) Data and ASTM D7276 (2008) Analysis

8.3 CORPS BLOCK NEW SF ANALYSIS

Using the derived safety factor equations provided in Table 7.1, safety factors were computed for the Corps Block tests. Initially, the lift coefficient, C_L , was computed for all stable tests which directly preceded an unstable test by using the computed shear stress and flow velocity on the embankment and assuming a safety factor value of 1. A

lift coefficient value of 0.115 was determined to be the optimum value to represent the stability conditions within the dataset.

Safety factors were computed for the Corps Block data using the 0.115 lift coefficient value. Table 8.3 provides a summary of the computed safety factor values. A plot of bed slope versus Corps Block computed safety factors is presented in Figure 8.3. The following summarizes the ability of the new safety factor equation to predict system stability for the Corps Block dataset:

- $C_L = 0.115$ correctly predicted the point of instability for 100% of the tested installations:
 - Computed safety factor values for stable tests ranged from 1.00 to 2.95
 - Computed safety factor values for unstable tests ranged from 0.66 to 0.96

The new safety factor equation proved successful in predicting stability for all of the Corps Block tests.

Table 8.3: Computed Corps Block SF for the New SF Method

Test ID No.	Block Name	S_0 (ft/ft)	Over-topping Depth (ft)	Side Slope (H/V)	V (ft/s)	τ_0 (lbs/ft ²)	System Condition	SF ($C_L = 0.115$)
15	Corps Block	0.200	1.0	n/a	13.6	3.5	Stable	1.03
16	Corps Block	0.200	2.0	n/a	17.3	4.9	Unstable	0.66
17	Corps Block	0.143	1.0	n/a	12.8	6.8	Stable	1.22
18	Corps Block	0.143	2.0	n/a	16.5	12.0	Unstable	0.73
19	Corps Block	0.143	1.2	n/a	14.5	7.9	Unstable	0.96
20	Corps Block	0.030	n/a	2.0	6.5	2.2	Stable	2.95
21	Corps Block	0.030	n/a	2.0	7.9	2.3	Stable	2.27
22	Corps Block	0.030	n/a	2.0	11.5	2.5	Stable	1.27
23	Corps Block	0.030	n/a	2.0	13.2	2.5	Stable	1.00
24	Corps Block	0.030	n/a	2.0	14.0	2.6	Unstable	0.90

n/a = not applicable

Orange cell identifies test used to calibrate C_L value

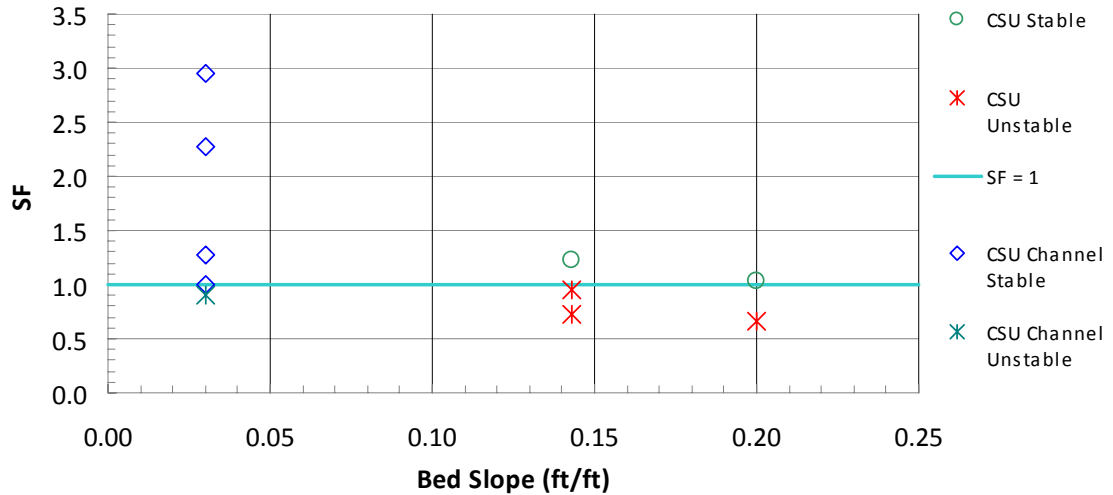


Figure 8.3: Corps Block SF Computed from the New SF Method with $C_L = 0.115$ Calibrated from Channel Data

8.4 DISCUSSION OF CONSIDERATIONS, RECOMMENDATIONS AND LIMITATIONS

The moment stability analysis approach is a simplified model of a complex physical phenomenon. Inter-block friction is not represented in the moment stability analysis and is encompassed within the calibrated lift coefficient, C_L . Therefore, coefficient extrapolations based on varying block thicknesses, block footprints, and block weights should not be employed without further research and verification.

Performance testing at overtopping depth intervals smaller than 1.0 ft is recommended based on the database safety factor evaluation. As illustrated by the CSU Petreflex data in Figure 8.2 where the 1.0-ft and 2.0-ft overtopping test safety factors were 1.41 and 0.91, respectively, there can be a large gap between safety factors computed from 1.0-ft overtopping depth intervals. Since the system critical condition is within these two overtopping depths and lift coefficients must be computed from a stable

condition, testing at smaller intervals, such as 0.5-ft, would provide a more precise identification of the lift coefficient.

Verification of the developed safety factor equation was limited to the database limitations. A summary of the database limitations is provided by the following:

- Overtopping embankment slopes ranged from 0.230 to 0.501 ft/ft;
- Overtopping depths ranged from 1.0 to 4.0 ft;
- One channelized condition with a side slope of 2H:1V; and
- Exclusively non-vertical interlocking blocks.

8.5 SUMMARY

Safety factors were computed using the safety factor method developed in Chapter 7 for the tests within the database. Calibrated lift coefficients for the 30S, Petraflex, and Corps Block systems were 0.0972, 0.0207, and 0.115, respectively. The new safety factor equations proved successful in predicting system stability for twenty-three out of the total twenty-four tests, which is a 96% success rate. The stable 2.0-ft overtopping FHWA 30S test was conservatively predicted as unstable.

9 CONCLUSIONS AND RECOMMENDATIONS

9.1 OVERVIEW

The focus of the presented research was to evaluate existing ACB design methods with a full-scale database and develop a comprehensive design methodology applicable to channelized and overtopping hydraulic conditions. Existing ACB design methods, Clopper (1991) and NCMA (2006), compute a safety factor using a moment stability analysis approach. To date, verification of the Clopper (1991) and NCMA (2006) method has not been conducted with a database encompassing both channelized data and overtopping data with a range of bed slopes and embankment lengths.

A literature review revealed that testing and evaluation of ACB protection systems has been conducted by CIRIA, FHWA, USACE, and CSU dating back to the late 1980s. Overtopping hydraulic conditions were the primary form of testing ACB armored embankments with the exception of Abt *et al.* (2001) which tested channelized flow conditions. Further results from the literature review include the identification of ASTM D7277 (2008) and ASTM D7276 (2008) as the current state-of-the-practice for testing and evaluation of ACB protection systems and NCMA (2006) as the current state-of-the-practice for ACB system hydraulic design.

Clopper (1991) and NCMA (2006) present extrapolations of safety factor methods developed by Stevens and Simons (1971), Julien (1998) and Julien and Anthony (2002) for mild-slope, low-velocity hydraulic conditions to high-velocity, steep-slope conditions

associated with embankment overtopping environments. Through the investigation of assumptions, the most unsuitable assumption for the high-velocity, steep-slope example was identified as the assumption of equal lift and drag forces, which was determined to be non-conservative for velocity values greater than approximately 10 ft/s. Trigonometric simplifications and the computation of the angle β were also identified as inapt assumptions for the investigated example.

A database was developed for the purpose of evaluating the Clopper (1991) and NCMA (2006) safety factor design methods. The database included three ACB systems: 1) 30S, 2) Petraflex, and 3) the Corps Block. The 30S dataset was composed of nine total overtopping tests on four different installations. Discharges ranged from 8.0 to 90.5 cfs, embankment slopes ranged from 0.230 to 0.499 ft/ft, and embankment lengths ranged from 13 ft to 40 ft for the combined 30S dataset.

The Petraflex dataset was composed of five total overtopping tests on two different installations. Discharges ranged from 10.0 to 93.0 cfs, embankment slopes ranged from 0.437 to 0.501 ft/ft, and embankment lengths ranged from 13 ft to 20 ft for the combined Petraflex dataset.

The Corps Block dataset was composed of eleven total tests including five overtopping tests and six channelized tests. Discharges ranged from 9.8 to 28.5 cfs, embankment slopes ranged from 0.143 to 0.200 ft/ft, and a constant 20-ft embankment length for the Corps Block overtopping dataset. The Corps Block channelized dataset had discharges ranging from 29.0 to 125.0 cfs.

Hydraulic analysis was conducted on the database to provide shear-stress and flow-velocity values for the assessment of the Clopper (1991) and NCMA (2006) safety

factor equations. Subsequently, safety factors were computed using the Clopper (1991) and NCMA (2006) safety factor equations for the tests within the database. Both the Clopper (1991) and NCMA (2006) safety factor equations proved inadequate at predicting system stability for the 30S and Corps Block datasets. The Clopper (1991) and NCMA (2006) methods were both successful at predicting stability for 100% of the Petraflex dataset, which was a limited dataset with tested embankments slopes of 0.437 and 0.501 ft/ft. Both the Clopper (1991) and NCMA (2006) safety factor methods predicted the point of instability correctly for five out of the nine tested installations, which is a 56% success rate.

A new methodology for safety factor computation was developed for stability of a rectangular particle on a channel side slope and on a channel bed. Computation of the lift force for the safety factor method uses the flow velocity with a calibrated lift coefficient. Additionally, expressions for computation of the weight force distribution which correctly account for the bed-slope contribution were utilized. Table 7.1 provided a summary of the new safety factor equations.

Safety factors were computed using the new safety factor method for the tests within the database. Calibrated lift coefficients for the 30S, Petraflex, and Corps Block systems were determined to be 0.0972, 0.0207, and 0.115, respectively. Collectively, the new safety factor method predicted the point of instability correctly for eight out of the nine tested installations, which is an 89% success rate. Additionally, the new safety factor equations proved successful at predicting system stability for 96% of the individual tests; twenty-three tests were predicted correctly out of the total twenty-four tests.

9.2 CONCLUSIONS

Conclusions for the ACB safety factor research are as follows:

- The shear-stress value computed using the current state-of-the-practice analysis method (ASTM D7276, 2008) was less than 1% different than the shear-stress value reported for the 30S 1.0-ft overtopping test in Clopper and Chen (1988).
- The shear-stress value computed using the current state-of-the-practice analysis method (ASTM D7276, 2008) was 14% less than the shear-stress value reported for the 30S 2.0-ft overtopping test in Clopper and Chen (1988).
- Shear-stress values computed using the current state-of-the-practice analysis method (ASTM D7276, 2008) were an average of 72% less than the shear-stress values reported for the 30S and Petraflex 4.0-ft overtopping tests in Clopper and Chen (1988).
- Clopper (1991) and NCMA (2006) safety factor equations proved inadequate at predicting system stability for the 30S dataset by correctly predicting the point of instability for a maximum of two out of the four 30S installations.
- Clopper (1991) and NCMA (2006) safety factor equations proved successful at predicting system stability for the Petraflex dataset by correctly predicting the point of instability for each of the two Petraflex installations.
- Clopper (1991) and NCMA (2006) safety factor equations proved inadequate at predicting system stability for the Corps Block dataset by correctly predicting the point of instability for a maximum of one out of the three Corps Block installations.

- New safety factor equations were developed which incorporated a lift coefficient for the computation of the lift force. A summary of the new safety factor equations was provided in Table 7.1.
- The new safety factor equations proved successful at predicting system stability by correctly predicting the point of instability for eight out of the nine total combined 30S, Petraflex, and Corps Block installations.
- Performance testing at overtopping depth intervals smaller than 1.0 ft is recommended to allow for lift coefficient determination with greater precision.

9.3 RESEARCH RECOMMENDATIONS

The developed safety factor equation provides a tool for design and assessment of ACB stability; however, as technology evolves and environmental conditions change, the applicability of the design method should be reevaluated. Several areas of further related research have been identified from this study. Although the database used for evaluating the safety factor equations included multiple blocks and varying hydraulic conditions, a more detailed database could provide further advancements in the moment stability analysis assessment. Specifically, the addition of more channelized performance data would improve the existing database.

Furthermore, lift coefficient extrapolations based on varying block thicknesses, block footprints, and block weights should be further researched. Theoretical extrapolations could be developed similar to the extrapolations presented in NCMA

(2006). However, considering the context of the lift coefficient within the safety factor equation, developed extrapolations should be verified using test data.

Another area of recommended research is evaluating the sensitivity of ACB system performance to varying underlying filter layers. Filter layers can be composed of geotextile, graded granular media, or both. Effects of varying filter designs are not addressed in current literature.

Finally, further research is recommended on the hydraulic evaluation of overtopping data. Multiple ACB tests have been conducted and reported shear-stress values were observed to vary more than 200% dependent upon the overtopping flow depth and analysis method. Research providing “typical” shear-stress values for a range of embankment lengths, Manning’s roughnesses, and overtopping flow depth would prove invaluable for engineers interpreting reported performance data.

REFERENCES

- Abt, S.R., Leech, J.R., Thornton, C.I., Lipscomb, C.M. (2001). Articulated Concrete Block Stability Testing. *Journal of the American Water Resources Association*, 37(1):27-34, February.
- ASTM D698 (2007). Standard Test Methods for Laboratory Compaction Characteristics of Soil Using Standard Effort (12 400 ft-lbf/ft³ (600 kN-m/m³)).
- ASTM D7276 (2008). Guide for Analysis and Interpretation of Test Data for Articulating Concrete Block (ACB) Revetment Systems in Open Channel Flow.
- ASTM D7277 (2008). Test Method for Performance Testing of Articulating Concrete Block (ACB) Revetment Systems for Hydraulics Stability in Open Channel Flow.
- Clopper, P.E., Chen, Y.H. (1988). Minimizing Embankment Damage During Overtopping Flow. FHWA Report No. FHWA-RD-88-181.
- Clopper, P.E. (1989). Hydraulic Stability of Articulated Concrete Block Revetment Systems during Overtopping Flow. FHWA Report No. FHWA-RD-89-199.
- Clopper, P.E. (1991). Protecting Embankment Dams with Concrete Block Systems. *Hydro Review*, X(2), April.
- Gessler, J. (1971). Critical Shear Stress for Sediment Mixtures. Trans. XIV Congress IAHR, Paris, Vol. III.
- Harris County Flood Control District (HCFCD) (2001). Design manual for Articulating Concrete Block Systems. September, 66 p.

- Hewlett, H.W.M., Borman, L.A., Bramley, M.E. (1987). Design of Reinforced Grass Waterways. Construction Industry Research and Information Association, Report 116, London, UK.
- Julien, P.Y. (1998). Erosion and Sedimentation. Cambridge University Press, Cambridge, UK.
- Julien, P.Y., Anthony, D.J. (2002). Bed Load Motion and Grain Sorting in a Meandering Stream. *Journal of Hydraulic Research*, 40(2):125-134.
- Leech, J.R., Abt, S.R., Thornton, C.I., Lipscomb, C.M. (1999a). Development of a Circular Shaped, Articulated Concrete Block and Uniform Testing Procedures for Articulated Concrete Blocks. Draft Technical Report, U.S. Army Engineer Waterways Experiment Station, Vicksburg, Mississippi.
- Leech, J.R., Abt, S.R., Thornton, C.I., Combs, P.G. (1999b). Developing Confidence in Concrete Revetment Products for Bank Stabilization. *Journal of the American Water Resources Association*, 35(4):877-885, August.
- Meyer-Peter, E., Müller, R. (1948). Formulas for Bed-load Transport. Proceedings of 3rd Meeting IAHR, Stockholm, pp. 39-64.
- National Concrete Masonry Association (NCMA) (2006). Design Manual for Articulating Concrete Block (ACB) Revetment Systems. 76 p.
- Robeson, M.D., Thornton, C.I., Lipscomb, C.M. (2002). Articulated Concrete Block Data Report. Colorado State University Report submitted to Armortec Erosion Control Solutions, January.

Stevens, M.A., Simons, D.B. (1971). Stability Analyses for Coarse Granular Material on Slopes. In: Vol. 1, Chapter A, River Hydraulics, H.W. Shen (Ed.), Water Resources Publications, Littleton, Colorado.

Wilcox, D.C. (2000). Basic Fluid Mechanics. Second Edition, DWC Industries, Inc., La Canada, CA.

APPENDIX A

HYDRAULIC DATA FROM CLOPPER AND CHEN (1988)

Table A.1: Available Data for FHWA Petraflex Testing (Clopper and Chen, 1988)

Run Number : 49 Date of Test : 09-22-87 Start Time : 10:00 AM
 Soil Type : TYPE I, w/ PETRAFLEX Duration : 10 Hours End Time : 8:00 PM
 Overtopping Depth : 4.0 ft Water Surface Drop: FF Photographs: YES
 Side Slope : 2:1 Discharge : 96.0 CFS Video Tape : YES

Time (hr)	Station Number	Embankment Elev. (ft)	Water Surface Elev. (feet)	Meas Flow Depth (ft)	Corr Flow Depth (ft)	Ave Vel (ft/s)	EGL Elev (ft)
0.0	16.0	5.47	9.55	4.08	4.08	5.882	10.087
0.0	18.0	6.06	9.30	3.24	3.24	7.407	10.152
0.0	20.0	6.06	9.10	3.04	3.04	7.895	10.068
0.0	22.0	6.01	8.70	2.69	2.69	8.922	9.936
0.0	24.0	6.04	8.50	2.46	2.46	9.756	9.978
0.0	26.0	6.05	8.25	2.20	2.20	10.909	10.098
0.0	28.0	5.96	8.20	2.24	2.24	10.714	9.983
0.0	30.0	5.89	8.10	2.21	2.21	10.860	9.931
0.0	32.0	5.91	8.00	2.09	2.09	11.483	10.048
0.0	34.0	5.96	7.75	1.79	1.79	13.408	10.541
0.0	36.0	5.72	7.55	1.83	1.83	13.115	10.221
0.0	38.0	5.05	6.90	1.85	1.85	14.511	10.170
0.0	40.0	4.04	5.76	1.72	1.54	15.608	9.543
0.0	42.0	3.08	4.64	1.56	1.39	17.209	9.238
0.0	44.0	2.10	3.61	1.51	1.35	17.779	8.518
0.0	46.0	1.29	2.67	1.38	1.23	19.453	8.546
0.0	48.0	0.78	2.05	1.29	1.15	20.811	8.775
1.0	16.0	5.39	9.60	4.21	4.21	5.701	10.105
1.0	18.0	6.07	9.35	3.28	3.28	7.317	10.181
1.0	20.0	6.42	9.00	2.58	2.58	9.302	10.344
1.0	22.0	6.04	8.70	2.66	2.66	9.023	9.964
1.0	24.0	6.01	8.35	2.34	2.34	10.256	9.983
1.0	26.0	5.98	8.15	2.17	2.17	11.060	10.049
1.0	28.0	5.97	8.10	2.13	2.13	11.268	10.071
1.0	30.0	5.90	8.10	2.20	2.20	10.909	9.948
1.0	32.0	5.88	8.00	2.12	2.12	11.321	9.990
1.0	34.0	5.95	7.90	1.95	1.95	12.308	10.252
1.0	36.0	5.83	7.55	1.72	1.72	13.953	10.573
1.0	38.0	4.97	6.69	1.72	1.54	15.608	10.473
1.0	40.0	3.93	5.62	1.69	1.51	15.885	9.538
1.0	42.0	2.98	4.60	1.62	1.45	16.571	8.864
1.0	44.0	2.12	3.69	1.57	1.40	17.099	8.230
1.0	46.0	1.14	2.80	1.46	1.31	18.387	7.850
1.0	48.0	0.78	2.10	1.32	1.18	20.338	8.523

Note : A value of -0- indicates data point not taken

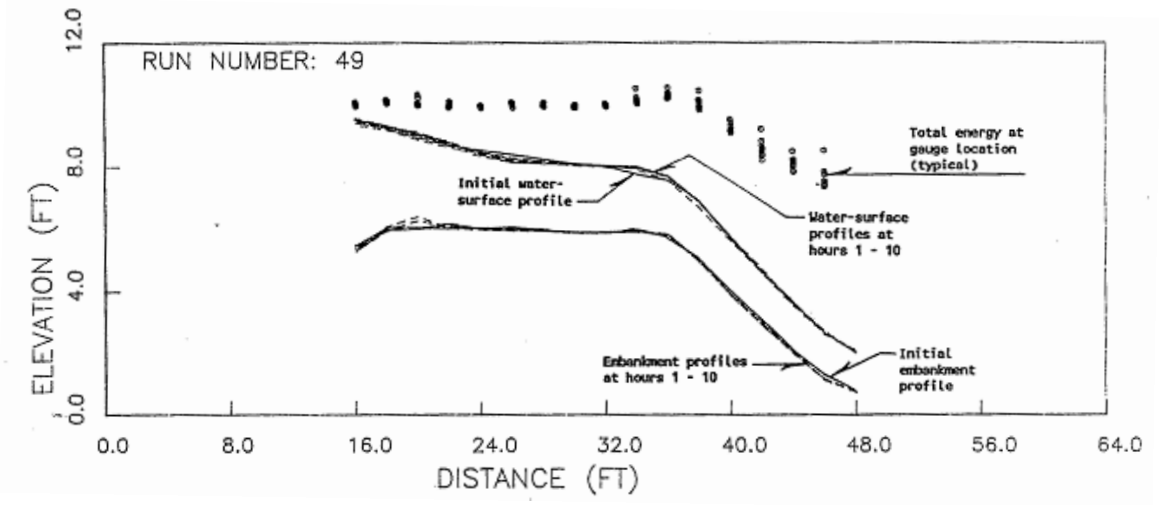


Figure A.1: FHWA Petraflex 4.0-ft Overtopping Water-surface Profile (Clopper and Chen, 1988)

Table A.4 (continued): FHWA 30S 1.0-ft Overtopping Data (Clopper and Chen, 1988)

Time (hr)	Station Number	Embankment Elev. (ft)	Water Surface Elev. (feet)	Meas Flow Depth (ft)	Corr Flow Depth (ft)	Ave Vel (ft/s)	EGL Elev (ft)
1.0	48.0	0.52	0.90	0.38	0.34	10.155	2.501
1.0	50.0	0.45	0.80	0.35	0.31	11.026	2.688
2.0	16.0	5.58	7.06	1.48	1.48	2.331	7.144
2.0	18.0	5.86	6.99	1.13	1.13	3.053	7.135
2.0	20.0	5.97	6.97	1.00	1.00	3.450	7.155
2.0	22.0	5.84	6.95	1.11	1.11	3.108	7.100
2.0	24.0	6.06	6.84	0.78	0.78	4.423	7.144
2.0	26.0	6.03	6.63	0.60	0.60	5.750	7.143
2.0	28.0	5.97	6.57	0.60	0.60	5.750	7.083
2.0	30.0	5.91	6.53	0.62	0.62	5.565	7.011
2.0	32.0	5.90	6.55	0.65	0.65	5.308	6.987
2.0	34.0	5.90	6.55	0.65	0.65	5.308	6.987
2.0	36.0	5.79	6.28	0.49	0.49	7.041	7.050
2.0	38.0	4.92	5.30	0.38	0.34	10.155	6.901
2.0	40.0	3.83	4.28	0.45	0.40	8.576	5.422
2.0	42.0	2.97	3.32	0.35	0.31	11.026	5.208
2.0	44.0	2.00	2.29	0.29	0.26	13.307	5.040
2.0	46.0	1.17	1.46	0.29	0.26	13.307	4.210
2.0	48.0	0.56	0.87	0.31	0.28	12.449	3.276
3.0	16.0	5.54	7.06	1.52	1.52	2.270	7.140
3.0	18.0	5.85	6.99	1.14	1.14	3.026	7.132
3.0	20.0	5.90	6.96	1.06	1.06	3.255	7.124
3.0	22.0	5.82	6.95	1.13	1.13	3.053	7.095
3.0	24.0	6.06	6.83	0.77	0.77	4.481	7.142
3.0	26.0	6.03	6.62	0.59	0.59	5.847	7.151
3.0	28.0	5.97	6.55	0.58	0.58	5.948	7.099
3.0	30.0	5.91	6.52	0.61	0.61	5.656	7.017
3.0	32.0	5.90	6.56	0.66	0.66	5.227	6.984
3.0	34.0	5.90	6.54	0.64	0.64	5.391	6.991
3.0	36.0	5.79	6.30	0.51	0.51	6.765	7.011
3.0	38.0	4.92	5.31	0.39	0.35	9.895	6.830
3.0	40.0	3.83	4.27	0.44	0.39	8.771	5.464
3.0	42.0	2.97	3.31	0.34	0.30	11.350	5.310
3.0	44.0	2.00	2.29	0.29	0.26	13.307	5.040
3.0	46.0	1.17	1.46	0.29	0.26	13.307	4.210
3.0	48.0	0.56	0.87	0.31	0.28	12.449	3.276
4.0	16.0	5.52	7.06	1.54	1.54	2.240	7.138
4.0	18.0	5.82	6.99	1.17	1.17	2.949	7.125
4.0	20.0	5.85	6.97	1.12	1.12	3.080	7.117
4.0	22.0	5.81	6.96	1.15	1.15	3.000	7.100
4.0	24.0	6.06	6.82	0.76	0.76	4.539	7.140
4.0	26.0	6.03	6.61	0.58	0.58	5.948	7.159
4.0	28.0	5.97	6.55	0.58	0.58	5.948	7.099

Note : A value of -0- indicates data point not taken

Table A.5 (continued): FHWA 30S 1.0-ft Overtopping Data (Clopper and Chen, 1988)

Time (hr)	Station Number	Embankment Elev. (ft)	Water Surface Elev. (feet)	Meas Flow Depth (ft)	Corr Flow Depth (ft)	Ave Vel (ft/s)	EGL Elev (ft)
4.0	30.0	5.91	6.51	0.60	0.60	5.750	7.023
4.0	32.0	5.90	6.57	0.67	0.67	5.149	6.982
4.0	34.0	5.90	6.53	0.63	0.63	5.476	6.996
4.0	36.0	5.79	6.30	0.51	0.51	6.765	7.011
4.0	38.0	4.92	5.30	0.38	0.34	10.155	6.901
4.0	40.0	3.83	4.26	0.43	0.38	8.975	5.511
4.0	42.0	2.97	3.30	0.33	0.30	11.694	5.423
4.0	44.0	2.00	2.28	0.28	0.25	13.782	5.230
4.0	46.0	1.17	1.45	0.28	0.25	13.782	4.400
4.0	48.0	0.55	0.86	0.31	0.28	12.449	3.266
5.0	16.0	5.52	7.04	1.52	1.52	2.270	7.120
5.0	18.0	5.82	7.00	1.18	1.18	2.924	7.133
5.0	20.0	5.81	6.97	1.16	1.16	2.974	7.107
5.0	22.0	5.82	6.97	1.15	1.15	3.000	7.110
5.0	24.0	6.06	6.85	0.79	0.79	4.367	7.146
5.0	26.0	6.02	6.63	0.61	0.61	5.656	7.127
5.0	28.0	5.96	6.56	0.60	0.60	5.750	7.073
5.0	30.0	5.91	6.54	0.63	0.63	5.476	7.006
5.0	32.0	5.90	6.57	0.67	0.67	5.149	6.982
5.0	34.0	5.89	6.54	0.65	0.65	5.308	6.977
5.0	36.0	5.79	6.31	0.52	0.52	6.635	6.994
5.0	38.0	4.92	5.30	0.38	0.34	10.155	6.901
5.0	40.0	3.83	4.25	0.42	0.38	9.188	5.561
5.0	42.0	2.97	3.31	0.34	0.30	11.350	5.310
5.0	44.0	2.00	2.27	0.27	0.24	14.293	5.442
5.0	46.0	1.17	1.45	0.28	0.25	13.782	4.400
5.0	48.0	0.54	0.85	0.31	0.28	12.449	3.256
6.0	16.0	5.53	7.05	1.52	1.52	2.270	7.130
6.0	18.0	5.83	6.99	1.16	1.16	2.974	7.127
6.0	20.0	5.79	6.97	1.18	1.18	2.924	7.103
6.0	22.0	5.77	6.98	1.21	1.21	2.851	7.106
6.0	24.0	5.86	6.79	0.93	0.93	3.710	7.024
6.0	26.0	6.02	6.61	0.59	0.59	5.847	7.141
6.0	28.0	5.97	6.55	0.58	0.58	5.948	7.099
6.0	30.0	5.91	6.53	0.62	0.62	5.565	7.011
6.0	32.0	5.90	6.54	0.64	0.64	5.391	6.991
6.0	34.0	5.90	6.54	0.64	0.64	5.391	6.991
6.0	36.0	5.79	6.27	0.48	0.48	7.188	7.072
6.0	38.0	4.90	5.29	0.39	0.35	9.895	6.810
6.0	40.0	3.85	4.26	0.41	0.37	9.412	5.636
6.0	42.0	2.97	3.32	0.35	0.31	11.026	5.208
6.0	44.0	2.02	2.34	0.32	0.29	12.060	4.598
6.0	46.0	1.15	1.52	0.37	0.33	10.430	3.209
6.0	48.0	0.53	0.88	0.35	0.31	11.026	2.768

Note: A value of -0- indicates data point not taken

Table A.6 (continued): FHWA 30S 1.0-ft Overtopping Data (Clopper and Chen, 1988)

Time (hr)	Station Number	Embankment Elev. (ft)	Water Surface Elev. (feet)	Meas Flow Depth (ft)	Corr Flow Depth (ft)	Ave Vel (ft/s)	EGL Elev (ft)
7.0	16.0	5.53	7.04	1.51	1.51	2.285	7.121
7.0	18.0	5.83	6.99	1.16	1.16	2.974	7.127
7.0	20.0	5.82	6.97	1.15	1.15	3.000	7.110
7.0	22.0	5.76	6.95	1.20	1.20	2.875	7.088
7.0	24.0	6.06	6.85	0.79	0.79	4.367	7.146
7.0	26.0	6.02	6.60	0.58	0.58	5.948	7.149
7.0	28.0	5.97	6.55	0.58	0.58	5.948	7.099
7.0	30.0	5.91	6.53	0.62	0.62	5.565	7.011
7.0	32.0	5.90	6.54	0.64	0.64	5.391	6.991
7.0	34.0	5.90	6.53	0.65	0.65	5.308	6.987
7.0	36.0	5.79	6.26	0.47	0.47	7.340	7.097
7.0	38.0	4.90	5.28	0.38	0.34	10.155	6.881
7.0	40.0	3.85	4.27	0.42	0.38	9.188	5.581
7.0	42.0	2.97	3.31	0.34	0.30	11.350	5.310
7.0	44.0	2.02	2.33	0.31	0.28	12.449	4.736
7.0	46.0	1.15	1.52	0.37	0.33	10.430	3.209
7.0	48.0	0.52	0.87	0.35	0.31	11.026	2.758
8.0	16.0	5.52	7.04	1.52	1.52	2.270	7.120
8.0	18.0	5.83	6.99	1.16	1.16	2.974	7.127
8.0	20.0	5.82	6.97	1.15	1.15	3.000	7.110
8.0	22.0	5.76	6.95	1.19	1.19	2.899	7.081
8.0	24.0	6.06	6.84	0.78	0.78	4.423	7.144
8.0	26.0	6.02	6.61	0.59	0.59	5.847	7.141
8.0	28.0	5.97	6.55	0.58	0.58	5.948	7.099
8.0	30.0	5.91	6.52	0.61	0.61	5.656	7.017
8.0	32.0	5.90	6.54	0.64	0.64	5.391	6.991
8.0	34.0	5.90	6.54	0.64	0.64	5.391	6.991
8.0	36.0	5.79	6.27	0.48	0.48	7.188	7.072
8.0	38.0	4.90	5.28	0.38	0.34	10.155	6.881
8.0	40.0	3.85	4.27	0.42	0.38	9.188	5.581
8.0	42.0	2.97	3.30	0.33	0.30	11.694	5.423
8.0	44.0	2.01	2.33	0.32	0.29	12.060	4.588
8.0	46.0	1.15	1.52	0.37	0.33	10.430	3.209
8.0	48.0	0.53	0.88	0.35	0.31	11.026	2.768
9.0	16.0	5.52	7.04	1.52	1.52	2.270	7.120
9.0	18.0	5.83	6.99	1.16	1.16	2.974	7.127
9.0	20.0	5.82	6.97	1.15	1.15	3.000	7.110
9.0	22.0	5.75	6.95	1.20	1.20	2.875	7.078
9.0	24.0	6.06	6.85	0.79	0.79	4.367	7.146
9.0	26.0	6.02	6.61	0.59	0.59	5.847	7.141
9.0	28.0	5.97	6.54	0.57	0.57	6.053	7.109
9.0	30.0	5.91	6.53	0.62	0.62	5.565	7.011
9.0	32.0	5.90	6.54	0.64	0.64	5.391	6.991
9.0	34.0	5.90	6.50	0.60	0.60	5.750	7.013

Note: A value of -0- indicates data point not taken

Table A.7 (continued): FHWA 30S 1.0-ft Overtopping Data (Clopper and Chen, 1988)

Time (hr)	Station Number	Embankment Elev. (ft)	Water Surface Elev. (feet)	Meas Flow Depth (ft)	Corr Flow Depth (ft)	Ave Vel (ft/s)	EGL Elev (ft)
9.0	36.0	5.79	6.27	0.48	0.48	7.188	7.072
9.0	38.0	4.90	5.27	0.37	0.33	10.430	6.959
9.0	40.0	3.85	4.26	0.41	0.37	9.412	5.636
9.0	42.0	2.97	3.30	0.33	0.30	11.694	5.423
9.0	44.0	2.01	2.32	0.31	0.28	12.449	4.726
9.0	46.0	1.15	1.50	0.35	0.31	11.026	3.388
9.0	48.0	0.53	0.87	0.34	0.30	11.350	2.870
10.0	16.0	5.52	7.04	1.52	1.52	2.270	7.120
10.0	18.0	5.83	6.99	1.16	1.16	2.974	7.127
10.0	20.0	5.82	6.97	1.15	1.15	3.000	7.110
10.0	22.0	5.75	6.96	1.21	1.21	2.851	7.086
10.0	24.0	6.06	6.85	0.79	0.79	4.367	7.146
10.0	26.0	6.02	6.60	0.58	0.58	5.948	7.149
10.0	28.0	5.97	6.54	0.57	0.57	6.053	7.109
10.0	30.0	5.91	6.53	0.62	0.62	5.565	7.011
10.0	32.0	5.90	6.53	0.63	0.63	5.476	6.936
10.0	34.0	5.90	6.53	0.63	0.63	5.476	6.936
10.0	36.0	5.79	6.27	0.48	0.48	7.188	7.072
10.0	38.0	4.90	5.27	0.37	0.33	10.430	6.959
10.0	40.0	3.85	4.26	0.41	0.37	9.412	5.636
10.0	42.0	2.97	3.31	0.34	0.30	11.350	5.310
10.0	44.0	2.01	2.33	0.32	0.29	12.060	4.588
10.0	46.0	1.15	1.50	0.35	0.31	11.026	3.388
10.0	48.0	0.53	0.87	0.34	0.30	11.350	2.870

Note : A value of -0- indicates data point not taken

Table A.4: FHWA 30S 1.0-ft Overtopping Velocity Data (Clopper and Chen, 1988)

Run Number : 44	Date of Test : 09-01-87	Start Time : 7:00 AM
Soil Type : TYPE I, ARMORFLEX	Duration : 10 Hours	End Time : 5:00 PM
Overtopping Depth : 1.0 ft	Water Surface Drop: FF	Photographs: YES
Side Slope : 2:1	Discharge : 13.8 CFS	Video Tape : YES

Time (hr)	Station Number	Velocity (ft/s)		
		0.2 depth	0.6 depth	0.8 depth
0.0	16.0	2.30	2.40	2.20
0.0	20.0	4.00	4.10	-0-
0.0	24.0	4.40	4.40	-0-
0.0	28.0	5.60	5.60	-0-
0.0	32.0	5.60	5.60	-0-
0.0	36.0	7.00	7.00	-0-
0.0	40.0	11.60	11.60	-0-

Note : A value of -0- indicates data point not taken

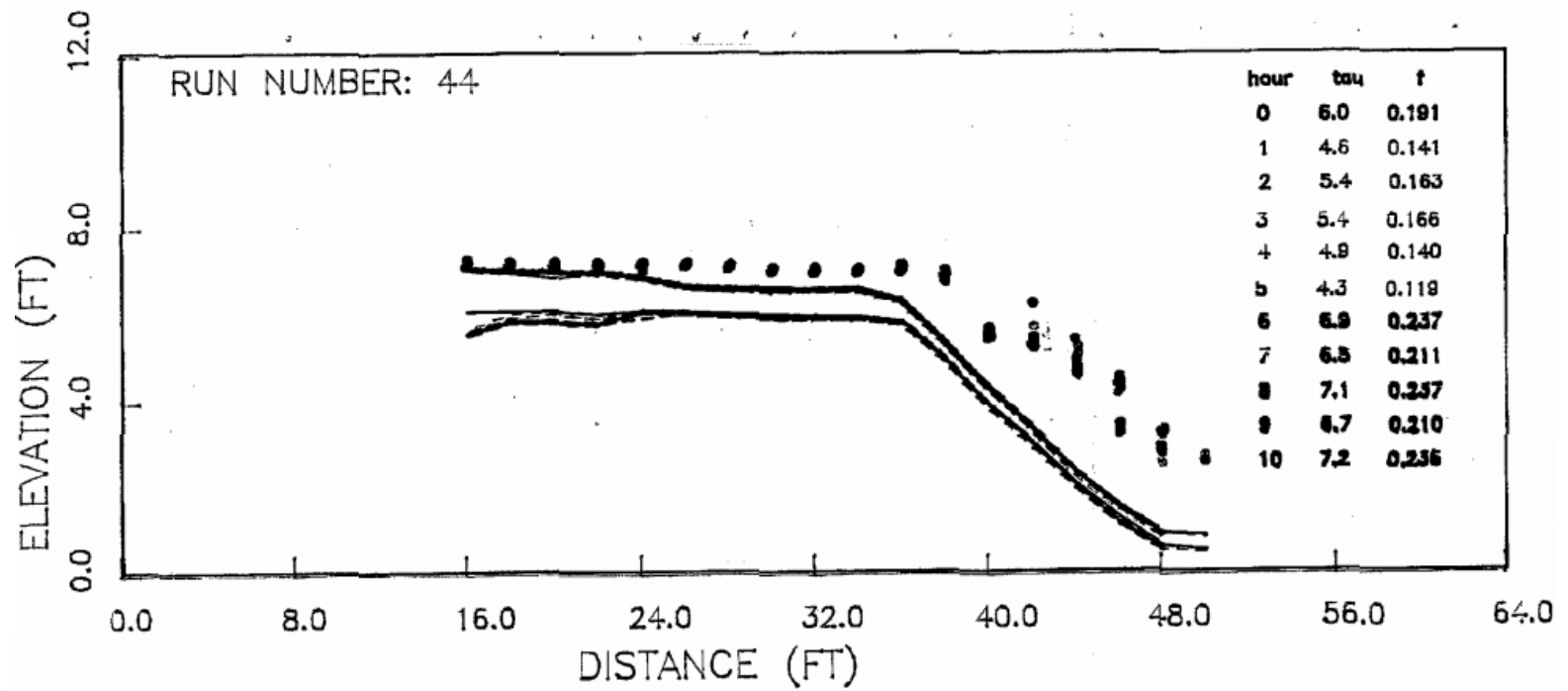


Figure A.2: FHWA 30S 1.0-ft Overtopping Water-surface Profile (Clopper and Chen, 1988)

Table A.5: FHWA 30S 2.0-ft Overtopping Data (Clopper and Chen, 1988)

Run Number : 45 Date of Test : 09-09-87 Start Time : 7:00 AM
 Soil Type : TYPE I, ARMORFLEX Duration : 10 Hours End Time : 5:00 PM
 Overtopping Depth : 2.0 ft Water Surface Drop: FF Photographs: YES
 Side Slope : 2:1 Discharge : 34.0 CFS Video Tape : YES

Time (hr)	Station Number	Embankment Elev. (ft)	Water Surface Elev. (feet)	Meas Flow Depth (ft)	Corr Flow Depth (ft)	Ave Vel (ft/s)	EGL Elev (ft)
0.0	16.0	6.01	7.97	1.96	1.96	4.668	8.308
0.0	18.0	6.02	7.84	1.82	1.82	5.027	8.232
0.0	20.0	6.06	7.80	1.74	1.74	5.259	8.229
0.0	22.0	6.10	7.83	1.73	1.73	5.289	8.264
0.0	24.0	6.12	7.62	1.50	1.50	6.100	8.198
0.0	26.0	6.04	7.43	1.39	1.39	6.583	8.103
0.0	28.0	6.01	7.15	1.14	1.14	8.026	8.150
0.0	30.0	5.88	7.16	1.28	1.28	7.148	7.953
0.0	32.0	5.88	7.13	1.25	1.25	7.320	7.962
0.0	34.0	5.88	7.04	1.16	1.16	7.888	8.006
0.0	36.0	5.76	6.76	1.00	1.00	9.150	8.060
0.0	38.0	4.91	5.90	0.99	0.89	10.338	7.560
0.0	40.0	3.88	4.82	0.94	0.84	10.888	6.661
0.0	42.0	2.99	3.60	0.61	0.55	16.779	7.971
0.0	44.0	2.04	2.64	0.60	0.54	17.058	7.158
0.0	46.0	1.23	1.81	0.58	0.52	17.646	6.645
0.0	48.0	0.59	1.18	0.59	0.53	17.347	5.853
0.0	50.0	0.50	-0-	-0-	-0-	-0-	-0-
1.0	16.0	5.74	7.95	2.21	2.21	4.140	8.216
1.0	18.0	5.82	7.84	2.02	2.02	4.530	8.159
1.0	20.0	5.76	7.80	2.04	2.04	4.485	8.112
1.0	22.0	5.70	7.85	2.15	2.15	4.256	8.131
1.0	24.0	6.04	7.64	1.60	1.60	5.719	8.148
1.0	26.0	6.00	7.42	1.42	1.42	6.444	8.065
1.0	28.0	5.94	7.16	1.22	1.22	7.500	8.033
1.0	30.0	5.92	7.17	1.25	1.25	7.320	8.002
1.0	32.0	5.91	7.15	1.24	1.24	7.379	7.995
1.0	34.0	5.91	7.04	1.13	1.13	8.097	8.058
1.0	36.0	5.78	6.78	1.00	1.00	9.150	8.000
1.0	38.0	4.85	5.87	1.02	0.91	10.034	7.433
1.0	40.0	3.80	4.70	0.98	0.88	11.372	6.708
1.0	42.0	2.86	3.55	0.69	0.62	14.833	6.967
1.0	44.0	1.94	2.61	0.67	0.60	15.276	6.234
1.0	46.0	1.20	1.84	0.64	0.57	15.992	5.811

Note : A value of -0- indicates data point not taken

Table A.5 (continued): FHWA 30S 2.0-ft Overtopping Data (Clopper and Chen, 1988)

Time (hr)	Station Number	Embankment Elev. (ft)	Water Surface Elev. (feet)	Meas Flow Depth (ft)	Corr Flow Depth (ft)	Ave Vel (ft/s)	EGL Elev (ft)
1.0	48.0	0.62	1.19	0.57	0.51	17.956	6.196
2.0	16.0	5.40	7.94	2.54	2.54	3.602	8.142
2.0	18.0	5.77	7.84	2.07	2.07	4.420	8.143
2.0	20.0	5.76	7.84	2.00	2.00	4.399	8.140
2.0	22.0	5.62	7.85	2.23	2.23	4.103	8.111
2.0	24.0	6.04	7.64	1.60	1.60	5.719	8.148
2.0	26.0	6.00	7.44	1.44	1.44	6.354	8.067
2.0	28.0	5.94	7.16	1.22	1.22	7.500	8.033
2.0	30.0	5.93	7.13	1.20	1.20	7.625	8.033
2.0	32.0	5.92	7.16	1.24	1.24	7.379	8.005
2.0	34.0	5.92	7.06	1.14	1.14	8.026	8.060
2.0	36.0	5.82	6.79	0.97	0.97	9.433	8.172
2.0	38.0	4.87	5.89	1.02	0.91	10.034	7.453
2.0	40.0	3.87	4.67	0.80	0.72	12.794	7.212
2.0	42.0	2.90	3.62	0.72	0.64	14.215	6.758
2.0	44.0	1.98	2.66	0.68	0.61	15.051	6.178
2.0	46.0	1.10	1.83	0.73	0.65	14.020	4.882
2.0	48.0	0.62	1.19	0.57	0.51	17.956	6.196
3.0	16.0	5.41	7.95	2.54	2.54	3.602	8.152
3.0	18.0	5.76	7.87	2.11	2.11	4.336	8.162
3.0	20.0	5.74	7.83	2.09	2.09	4.378	8.128
3.0	22.0	5.60	7.82	2.22	2.22	4.122	8.084
3.0	24.0	6.04	7.66	1.62	1.62	5.648	8.155
3.0	26.0	6.00	7.41	1.41	1.41	6.489	8.064
3.0	28.0	5.95	7.16	1.21	1.21	7.562	8.048
3.0	30.0	5.93	7.18	1.25	1.25	7.320	8.012
3.0	32.0	5.93	7.16	1.23	1.23	7.439	8.019
3.0	34.0	5.92	7.06	1.14	1.14	8.026	8.060
3.0	36.0	5.82	6.81	0.99	0.99	9.242	8.136
3.0	38.0	4.88	5.92	1.04	0.93	9.841	7.424
3.0	40.0	3.88	4.80	0.92	0.82	11.125	6.722
3.0	42.0	2.94	3.64	0.70	0.63	14.621	6.960
3.0	44.0	1.98	2.66	0.68	0.61	15.051	6.178
3.0	46.0	1.20	1.82	0.62	0.55	16.500	6.052
3.0	48.0	0.62	1.20	0.58	0.52	17.646	6.035
4.0	16.0	5.41	7.93	2.52	2.52	3.631	8.135
4.0	18.0	5.76	7.86	2.10	2.10	4.357	8.155
4.0	20.0	5.73	7.86	2.13	2.13	4.296	8.147
4.0	22.0	5.61	7.82	2.21	2.21	4.140	8.086
4.0	24.0	6.04	7.64	1.60	1.60	5.719	8.148
4.0	26.0	6.01	7.39	1.38	1.38	6.630	8.073
4.0	28.0	5.95	7.19	1.24	1.24	7.379	8.035
4.0	30.0	5.93	7.16	1.23	1.23	7.439	8.019

Note : A value of -0- indicates data point not taken

Table A.5 (continued): FHWA 30S 2.0-ft Overtopping Data (Clopper and Chen, 1988)

Time (hr)	Station Number	Embankment Elev. (ft)	Water Surface Elev. (feet)	Meas Flow Depth (ft)	Corr Flow Depth (ft)	Ave Vel (ft/s)	EGL Elev (ft)
4.0	32.0	5.92	7.16	1.24	1.24	7.379	8.005
4.0	34.0	5.92	7.06	1.14	1.14	8.026	8.060
4.0	36.0	5.82	6.79	0.97	0.97	9.433	8.172
4.0	38.0	4.91	5.96	1.05	0.94	9.748	7.435
4.0	40.0	3.86	4.76	0.90	0.80	11.372	6.768
4.0	42.0	2.95	3.66	0.71	0.63	14.415	6.887
4.0	44.0	2.00	2.67	0.67	0.60	15.276	6.294
4.0	46.0	1.20	1.86	0.66	0.59	15.507	5.594
4.0	48.0	0.62	1.21	0.59	0.53	17.347	5.883
5.0	16.0	5.41	7.96	2.55	2.55	3.588	8.160
5.0	18.0	5.71	7.90	2.19	2.19	4.178	8.171
5.0	20.0	5.73	7.90	2.17	2.17	4.217	8.176
5.0	22.0	5.60	7.86	2.26	2.26	4.049	8.115
5.0	24.0	6.04	7.69	1.65	1.65	5.545	8.168
5.0	26.0	6.01	7.49	1.48	1.48	6.182	8.084
5.0	28.0	5.96	7.23	1.27	1.27	7.205	8.036
5.0	30.0	5.94	7.18	1.24	1.24	7.379	8.025
5.0	32.0	5.93	7.17	1.24	1.24	7.379	8.015
5.0	34.0	5.92	7.09	1.17	1.17	7.821	8.040
5.0	36.0	5.82	6.82	1.00	1.00	9.150	8.120
5.0	38.0	4.88	5.96	1.08	0.97	9.477	7.355
5.0	40.0	3.87	4.78	0.91	0.81	11.247	6.744
5.0	42.0	2.94	3.66	0.72	0.64	14.215	6.798
5.0	44.0	2.00	2.68	0.68	0.61	15.051	6.198
5.0	46.0	1.21	1.91	0.70	0.63	14.621	5.230
5.0	48.0	0.62	1.22	0.60	0.54	17.058	5.738
6.0	16.0	5.40	7.97	2.57	2.57	3.560	8.167
6.0	18.0	5.70	7.90	2.20	2.20	4.159	8.169
6.0	20.0	5.73	7.89	2.16	2.16	4.236	8.169
6.0	22.0	5.59	7.86	2.27	2.27	4.031	8.112
6.0	24.0	6.04	7.69	1.65	1.65	5.545	8.168
6.0	26.0	6.01	7.49	1.48	1.48	6.182	8.084
6.0	28.0	5.96	7.22	1.26	1.26	7.262	8.039
6.0	30.0	5.94	7.19	1.25	1.25	7.320	8.022
6.0	32.0	5.93	7.17	1.24	1.24	7.379	8.015
6.0	34.0	5.92	7.09	1.17	1.17	7.821	8.040
6.0	36.0	5.82	6.82	1.00	1.00	9.150	8.120
6.0	38.0	4.88	5.95	1.07	0.96	9.565	7.371
6.0	40.0	3.87	4.77	0.90	0.80	11.372	6.778
6.0	42.0	2.94	3.67	0.73	0.65	14.020	6.722
6.0	44.0	2.00	2.68	0.68	0.61	15.051	6.198
6.0	46.0	1.21	1.90	0.69	0.62	14.833	5.317
6.0	48.0	0.62	1.22	0.60	0.54	17.058	5.738

Note : A value of -0- indicates data point not taken

Table A.5 (continued): FHWA 30S 2.0-ft Overtopping Data (Clopper and Chen, 1988)

Time (hr)	Station Number	Embankment Elev. (ft)	Water Surface Elev. (feet)	Meas Flow Depth (ft)	Corr Flow Depth (ft)	Ave Vel (ft/s)	EGL Elev (ft)
7.0	16.0	5.40	7.98	2.58	2.58	3.547	8.175
7.0	18.0	5.70	7.98	2.20	2.20	4.159	8.169
7.0	20.0	5.72	7.89	2.17	2.17	4.217	8.166
7.0	22.0	5.59	7.87	2.28	2.28	4.013	8.120
7.0	24.0	6.04	7.69	1.65	1.65	5.545	8.168
7.0	26.0	6.01	7.49	1.48	1.48	6.182	8.084
7.0	28.0	5.95	7.23	1.28	1.28	7.148	8.023
7.0	30.0	5.94	7.20	1.26	1.26	7.262	8.019
7.0	32.0	5.93	7.17	1.24	1.24	7.379	8.015
7.0	34.0	5.92	7.09	1.17	1.17	7.821	8.040
7.0	36.0	5.82	6.83	1.01	1.01	9.059	8.104
7.0	38.0	4.88	5.94	1.06	0.95	9.656	7.388
7.0	40.0	3.88	4.78	0.98	0.88	11.372	6.788
7.0	42.0	2.94	3.68	0.74	0.66	13.831	6.650
7.0	44.0	2.00	2.68	0.68	0.61	15.051	6.198
7.0	46.0	1.20	1.90	0.70	0.63	14.621	5.220
7.0	48.0	0.62	1.22	0.60	0.54	17.058	5.738
8.0	16.0	5.38	7.98	2.60	2.60	3.519	8.172
8.0	18.0	5.72	7.91	2.19	2.19	4.178	8.181
8.0	20.0	5.74	7.91	2.17	2.17	4.217	8.186
8.0	22.0	5.58	7.87	2.29	2.29	3.996	8.118
8.0	24.0	6.05	7.69	1.64	1.64	5.579	8.173
8.0	26.0	6.01	7.47	1.46	1.46	6.267	8.080
8.0	28.0	5.95	7.19	1.24	1.24	7.379	8.035
8.0	30.0	5.94	7.18	1.24	1.24	7.379	8.025
8.0	32.0	5.93	7.22	1.29	1.29	7.093	8.001
8.0	34.0	5.92	7.09	1.17	1.17	7.821	8.040
8.0	36.0	5.83	6.84	1.01	1.01	9.059	8.114
8.0	38.0	4.88	5.94	1.06	0.95	9.656	7.388
8.0	40.0	3.87	4.79	0.92	0.82	11.125	6.712
8.0	42.0	2.95	3.67	0.72	0.64	14.215	6.808
8.0	44.0	1.97	2.65	0.68	0.61	15.051	6.168
8.0	46.0	1.20	1.85	0.65	0.58	15.746	5.700
8.0	48.0	0.62	1.20	0.58	0.52	17.646	6.035
9.0	16.0	5.38	7.97	2.59	2.59	3.533	8.164
9.0	18.0	5.71	7.91	2.20	2.20	4.159	8.179
9.0	20.0	5.74	7.90	2.16	2.16	4.236	8.179
9.0	22.0	5.58	7.87	2.29	2.29	3.996	8.118
9.0	24.0	6.05	7.69	1.64	1.64	5.579	8.173
9.0	26.0	6.01	7.48	1.47	1.47	6.224	8.082
9.0	28.0	5.95	7.18	1.23	1.23	7.439	8.039
9.0	30.0	5.94	7.18	1.24	1.24	7.379	8.025
9.0	32.0	5.93	7.21	1.28	1.28	7.148	8.003
9.0	34.0	5.92	7.09	1.17	1.17	7.821	8.040
9.0	36.0	5.83	6.84	1.01	1.01	9.059	8.114

Note : A value of -0- indicates data point not taken

Table A.5 (continued): FHWA 30S 2.0-ft Overtopping Data (Clopper and Chen, 1988)

Time (hr)	Station Number	Embankment Elev. (ft)	Water Surface Elev. (feet)	Meas Flow Depth (ft)	Corr Flow Depth (ft)	Ave Vel (ft/s)	EGL Elev (ft)
9.0	38.0	4.88	5.93	1.05	0.94	9.748	7.405
9.0	40.0	3.87	4.80	0.93	0.83	11.005	6.681
9.0	42.0	2.95	3.66	0.71	0.63	14.415	6.887
9.0	44.0	1.98	2.65	0.67	0.60	15.276	6.274
9.0	46.0	1.20	1.85	0.65	0.58	15.746	5.700
9.0	48.0	0.62	1.21	0.59	0.53	17.347	5.883
10.0	16.0	5.38	7.98	2.60	2.60	3.519	8.172
10.0	18.0	5.71	7.90	2.19	2.19	4.178	8.171
10.0	20.0	5.72	7.88	2.16	2.16	4.236	8.159
10.0	22.0	5.56	7.86	2.30	2.30	3.978	8.106
10.0	24.0	6.04	7.69	1.65	1.65	5.545	8.168
10.0	26.0	6.01	7.46	1.45	1.45	6.310	8.078
10.0	28.0	5.95	7.19	1.24	1.24	7.379	8.035
10.0	30.0	5.93	7.20	1.27	1.27	7.205	8.006
10.0	32.0	5.93	7.18	1.25	1.25	7.320	8.012
10.0	34.0	5.92	7.08	1.16	1.16	7.888	8.046
10.0	36.0	5.82	6.83	1.01	1.01	9.059	8.104
10.0	38.0	4.88	6.01	1.13	1.01	9.057	7.284
10.0	40.0	3.87	4.74	0.87	0.78	11.764	6.889
10.0	42.0	2.98	3.69	0.71	0.63	14.415	6.917
10.0	44.0	1.98	2.68	0.70	0.63	14.621	6.000
10.0	46.0	1.21	1.90	0.69	0.62	14.833	5.317
10.0	48.0	0.62	1.22	0.60	0.54	17.058	5.738

Note : A value of -0- indicates data point not taken

Table A.6: FHWA 30S 2.0-ft Overtopping Velocity Data (Clopper and Chen, 1988)

Run Number : 45	Date of Test : 09-09-87	Start Time : 7:00 AM
Soil Type : TYPE I, ARMORFLEX	Duration : 10 Hours	End Time : 5:00 PM
Overtopping Depth : 2.0 ft	Water Surface Drop: FF	Photographs: YES
Side Slope : 2:1	Discharge : 34.0 CFS	Video Tape : YES

Time (hr)	Station Number	Velocity (ft/s)		
		0.2 depth	0.6 depth	0.8 depth
0.0	16.0	3.10	3.20	2.90
0.0	20.0	4.30	3.60	-0-
0.0	24.0	5.40	5.60	5.80
0.0	28.0	7.50	7.40	7.30
0.0	32.0	7.60	7.60	7.70
0.0	36.0	-0-	9.20	9.70
0.0	40.0	-0-	14.00	-0-
0.0	44.0	-0-	15.50	-0-
1.0	16.0	3.40	3.30	3.00
1.0	20.0	4.30	4.30	4.30
1.0	24.0	5.40	5.60	5.70
1.0	28.0	7.40	7.50	7.30
1.0	32.0	7.60	7.60	7.60
1.0	36.0	9.20	9.40	9.60
1.0	40.0	14.30	14.30	14.30
1.0	44.0	-0-	16.80	-0-
2.0	16.0	3.30	3.20	3.10
2.0	20.0	4.30	4.20	4.30
2.0	24.0	5.40	5.60	5.70
2.0	28.0	7.40	7.40	7.30
2.0	32.0	7.50	7.60	7.60
2.0	36.0	9.00	9.20	9.40
2.0	40.0	14.20	14.20	14.20
2.0	44.0	-0-	17.50	-0-
3.0	16.0	3.40	3.30	3.10
3.0	20.0	4.10	4.30	4.20
3.0	24.0	5.30	5.50	5.70
3.0	28.0	7.50	7.50	7.30
3.0	32.0	7.50	7.60	7.60
3.0	36.0	9.10	9.25	9.40

Note : A value of -0- indicates data point not taken

Table A.6 (continued): FHWA 30S 2.0-ft Overtopping Velocity Data (Clopper and Chen, 1988)

Time (hr)	Station Number	Velocity (ft/s)		
		0.2 depth	0.6 depth	0.8 depth
3.0	40.0	-0-	14.00	-0-
3.0	44.0	-0-	16.60	-0-
4.0	16.0	3.20	3.30	3.10
4.0	20.0	4.10	4.20	4.30
4.0	24.0	5.20	5.50	5.70
4.0	28.0	7.30	7.30	7.20
4.0	32.0	7.60	7.60	7.60
4.0	36.0	9.10	9.25	9.40
4.0	40.0	-0-	14.20	-0-
4.0	44.0	-0-	16.00	-0-
5.0	16.0	3.20	3.30	3.10
5.0	20.0	4.20	4.30	4.30
5.0	24.0	-0-	5.20	5.70
5.0	28.0	7.40	7.50	7.30
5.0	32.0	7.80	7.80	7.80
5.0	36.0	9.20	9.30	9.40
5.0	40.0	-0-	14.00	-0-
5.0	44.0	-0-	16.10	-0-
6.0	16.0	3.20	3.40	3.10
6.0	20.0	4.20	4.30	4.30
6.0	24.0	-0-	5.30	5.70
6.0	28.0	7.50	7.50	7.30
6.0	32.0	7.80	7.80	7.80
6.0	36.0	9.30	9.35	9.40
6.0	40.0	-0-	14.10	-0-
6.0	44.0	-0-	16.20	-0-
7.0	16.0	3.30	3.30	3.10
7.0	20.0	4.30	4.30	4.30
7.0	24.0	5.20	5.40	5.70
7.0	28.0	7.40	7.50	7.50
7.0	32.0	7.80	7.80	7.80
7.0	36.0	9.20	9.30	9.40
7.0	40.0	-0-	14.10	-0-
7.0	44.0	-0-	16.30	-0-
8.0	16.0	3.30	3.30	3.00
8.0	20.0	4.10	4.40	4.20
8.0	24.0	5.40	5.50	5.80
8.0	28.0	7.40	7.40	7.40
8.0	32.0	7.70	7.70	7.70

Note: A value of -0- indicates data point not taken

Table A.6 (continued): FHWA 30S 2.0-ft Overtopping Velocity Data (Clopper and Chen, 1988)

Time (hr)	Station Number	Velocity (ft/s)		
		0.2 depth	0.6 depth	0.8 depth
8.0	36.0	9.10	9.25	9.40
8.0	40.0	-0-	14.00	-0-
8.0	44.0	-0-	17.50	-0-
9.0	16.0	3.20	3.30	3.10
9.0	20.0	4.20	4.40	4.30
9.0	24.0	5.30	5.50	5.70
9.0	28.0	7.40	7.40	7.40
9.0	32.0	7.60	7.65	7.70
9.0	36.0	9.20	9.30	9.40
9.0	40.0	-0-	14.10	-0-
9.0	44.0	-0-	17.30	-0-
10.0	16.0	3.20	3.40	3.00
10.0	20.0	4.10	4.20	4.10
10.0	24.0	5.20	5.50	5.70
10.0	28.0	7.30	7.40	7.40
10.0	32.0	7.60	7.65	7.70
10.0	36.0	9.10	9.25	9.40
10.0	40.0	14.10	14.20	-0-
10.0	44.0	-0-	15.60	-0-

Note : A value of -0- indicates data point not taken

Page : 3

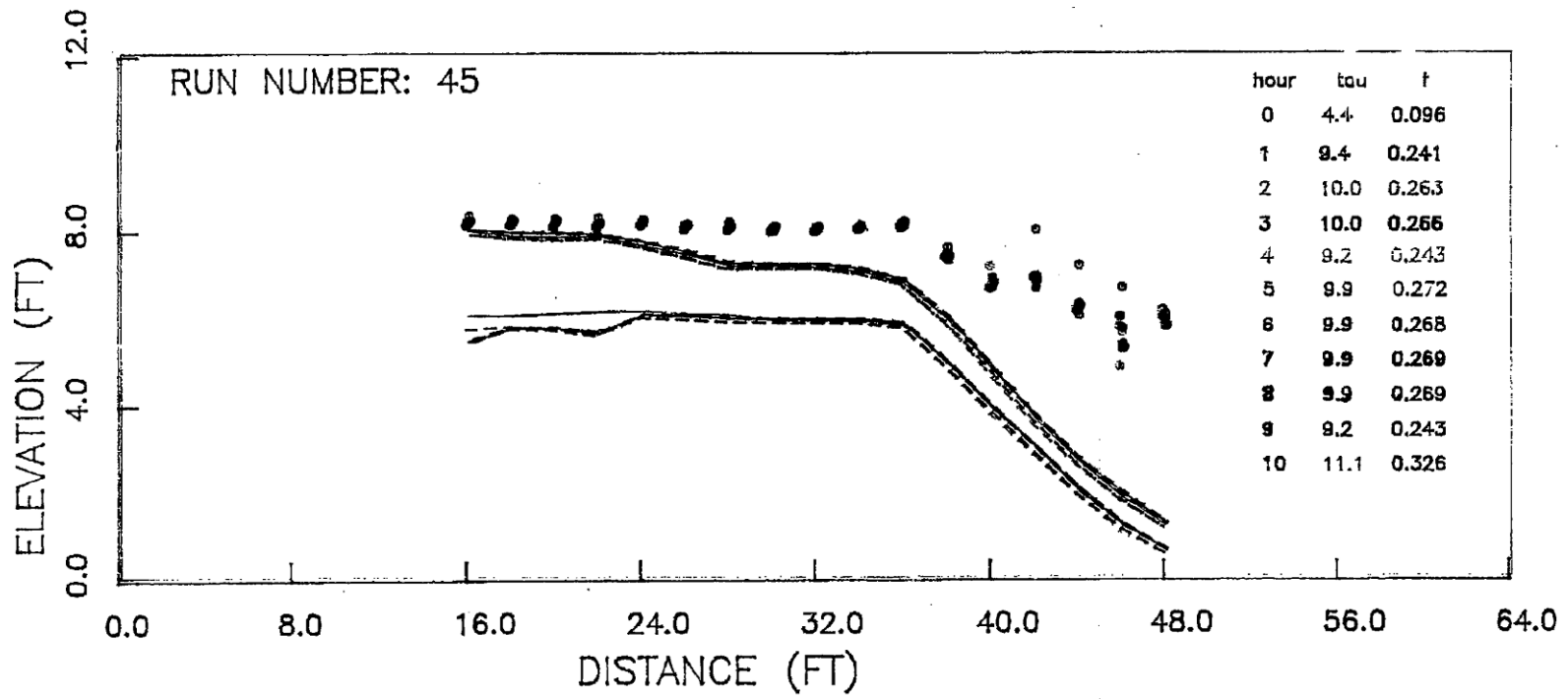


Figure A.3: FHWA 30S 2.0-ft Overtopping Water-surface Profile (Clopper and Chen, 1988)

Table A.7: FHWA 30S 4.0-ft Overtopping Data (Clopper and Chen, 1988)

Run Number : 46 Date of Test : 09-11-87 Start Time : 7:00 AM
 Soil Type : TYPE I, ARMORFLEX Duration : 5 Hours, FAILURE End Time : 2:45 PM
 Overtopping Depth : 4.0 ft Water Surface Drop: FF Photographs: YES
 Side Slope : 2:1 Discharge : 90.5 CFS Video Tape : NO

Time (hr)	Station Number	Embankment Elev. (ft)	Water Surface Elev. (feet)	Meas Flow Depth (ft)	Corr Flow Depth (ft)	Ave Vel (ft/s)	EGL Elev (ft)
0.0	16.0	6.00	9.50	3.50	3.50	6.464	10.149
0.0	18.0	6.10	9.25	3.15	3.15	7.183	10.051
0.0	20.0	6.08	8.90	2.82	2.82	8.023	9.900
0.0	22.0	5.96	8.70	2.74	2.74	8.257	9.759
0.0	24.0	6.14	8.60	2.46	2.46	9.197	9.913
0.0	26.0	6.03	8.40	2.37	2.37	9.546	9.815
0.0	28.0	5.98	8.25	2.27	2.27	9.967	9.793
0.0	30.0	5.89	8.15	2.26	2.26	10.011	9.706
0.0	32.0	5.90	8.10	2.20	2.20	10.284	9.742
0.0	34.0	5.91	7.95	2.04	2.04	11.091	9.860
0.0	36.0	5.80	7.60	1.80	1.80	12.569	10.053
0.0	38.0	4.87	6.77	1.90	1.70	13.320	9.525
0.0	40.0	3.90	5.60	1.70	1.52	14.887	9.041
0.0	42.0	2.98	4.50	1.52	1.35	16.650	8.805
0.0	44.0	2.03	3.44	1.41	1.26	17.949	8.442
0.0	46.0	1.25	2.66	1.41	1.26	17.949	7.662
0.0	48.0	0.59	1.94	1.35	1.21	18.746	7.397
1.0	16.0	5.60	9.50	3.90	3.90	5.801	10.023
1.0	18.0	5.70	9.25	3.55	3.55	6.373	9.881
1.0	20.0	6.08	9.15	3.07	3.07	7.370	9.993
1.0	22.0	5.92	9.10	3.18	3.18	7.115	9.886
1.0	24.0	6.07	9.00	2.93	2.93	7.722	9.926
1.0	26.0	6.04	8.65	2.61	2.61	8.669	9.817
1.0	28.0	5.98	8.50	2.52	2.52	8.978	9.752
1.0	30.0	5.91	8.25	2.34	2.34	9.669	9.702
1.0	32.0	5.92	8.15	2.23	2.23	10.146	9.748
1.0	34.0	5.92	8.00	2.08	2.08	10.877	9.837
1.0	36.0	5.80	7.60	1.80	1.80	12.569	10.053
1.0	38.0	4.93	6.75	1.82	1.63	13.905	9.752
1.0	40.0	3.86	5.67	1.81	1.62	13.982	8.706
1.0	42.0	2.89	4.46	1.57	1.40	16.119	8.495
1.0	44.0	2.03	3.45	1.42	1.27	17.822	8.382
1.0	46.0	1.34	2.71	1.37	1.22	18.473	8.009
1.0	48.0	0.60	2.13	1.53	1.37	16.541	6.378

Note : A value of -0- indicates data point not taken

Table A.7 (continued): FHWA 30S 4.0-ft Overtopping Data (Clopper and Chen, 1988)

Time (hr)	Station Number	Embankment Elev. (ft)	Water Surface Elev. (feet)	Meas Flow Depth (ft)	Corr Flow Depth (ft)	Ave Vel (ft/s)	EGL Elev (ft)
2.0	16.0	5.34	9.45	4.11	4.11	5.505	9.921
2.0	18.0	5.63	9.25	3.62	3.62	6.250	9.857
2.0	20.0	5.73	9.10	3.37	3.37	6.714	9.800
2.0	22.0	5.57	9.20	3.63	3.63	6.233	9.803
2.0	24.0	6.07	9.10	3.03	3.03	7.467	9.966
2.0	26.0	6.05	8.75	2.70	2.70	8.380	9.840
2.0	28.0	5.98	8.45	2.47	2.47	9.160	9.753
2.0	30.0	5.92	8.20	2.28	2.28	9.923	9.729
2.0	32.0	5.92	8.05	2.13	2.13	10.622	9.802
2.0	34.0	5.92	8.00	2.08	2.08	10.877	9.837
2.0	36.0	5.82	7.50	1.68	1.68	13.467	10.316
2.0	38.0	4.93	6.70	1.77	1.58	14.298	9.874
2.0	40.0	3.86	5.70	1.84	1.64	13.754	8.638
2.0	42.0	2.92	4.50	1.58	1.41	16.017	8.484
2.0	44.0	1.94	3.50	1.56	1.39	16.223	7.587
2.0	46.0	1.41	2.67	1.26	1.13	20.085	8.934
2.0	48.0	0.62	2.24	1.62	1.45	15.622	6.030
3.0	16.0	4.94	9.45	4.51	4.51	5.017	9.841
3.0	18.0	5.62	9.20	3.58	3.58	6.320	9.820
3.0	20.0	5.70	9.05	3.35	3.35	6.754	9.758
3.0	22.0	5.52	9.15	3.63	3.63	6.233	9.753
3.0	24.0	6.07	8.95	2.88	2.88	7.856	9.908
3.0	26.0	6.04	8.70	2.66	2.66	8.506	9.823
3.0	28.0	5.98	8.45	2.47	2.47	9.160	9.753
3.0	30.0	5.92	8.15	2.23	2.23	10.146	9.748
3.0	32.0	5.92	8.05	2.13	2.13	10.622	9.802
3.0	34.0	5.92	8.10	2.18	2.18	10.378	9.773
3.0	36.0	5.83	7.55	1.72	1.72	13.154	10.237
3.0	38.0	4.90	6.65	1.75	1.56	14.461	9.897
3.0	40.0	3.84	5.59	1.75	1.56	14.461	8.837
3.0	42.0	2.91	4.50	1.59	1.42	15.917	8.434
3.0	44.0	2.02	3.58	1.56	1.39	16.223	7.667
3.0	46.0	1.42	2.76	1.34	1.20	18.886	8.299
3.0	48.0	0.62	2.30	1.68	1.50	15.064	5.824
4.0	16.0	4.77	9.50	4.73	4.73	4.783	9.855
4.0	18.0	5.67	9.30	3.63	3.63	6.233	9.903
4.0	20.0	5.71	9.10	3.39	3.39	6.674	9.792
4.0	22.0	5.49	9.00	3.51	3.51	6.446	9.645
4.0	24.0	6.07	8.95	2.88	2.88	7.856	9.908
4.0	26.0	6.04	8.85	2.81	2.81	8.052	9.857
4.0	28.0	5.98	8.50	2.52	2.52	8.978	9.752
4.0	30.0	5.92	8.25	2.33	2.33	9.710	9.714
4.0	32.0	5.92	8.15	2.23	2.23	10.146	9.748

Note : A value of -0- indicates data point not taken

Table A.7 (continued): FHWA 30S 4.0-ft Overtopping Data (Clopper and Chen, 1988)

Time (hr)	Station Number	Embankment Elev. (ft)	Water Surface Elev. (feet)	Meas Flow Depth (ft)	Corr Flow Depth (ft)	Ave Vel (ft/s)	EGL Elev (ft)
4.0	34.0	5.92	8.05	2.13	2.13	10.622	9.802
4.0	36.0	5.85	7.70	1.85	1.85	12.230	10.022
4.0	38.0	4.98	6.65	1.67	1.49	15.154	10.216
4.0	40.0	3.84	5.60	1.76	1.57	14.379	8.811
4.0	42.0	2.97	4.59	1.62	1.45	15.622	8.380
4.0	44.0	1.97	3.55	1.58	1.41	16.017	7.534
4.0	46.0	1.55	2.86	1.31	1.17	19.319	6.655
4.0	48.0	0.63	2.57	1.94	1.73	13.045	5.212
5.0	16.0	4.65	9.45	4.80	4.80	4.714	9.795
5.0	18.0	5.65	9.20	3.55	3.55	6.373	9.831
5.0	20.0	5.72	9.10	3.38	3.38	6.694	9.796
5.0	22.0	5.50	9.25	3.75	3.75	6.033	9.815
5.0	24.0	6.10	8.95	2.85	2.85	7.939	9.929
5.0	26.0	6.05	8.70	2.65	2.65	8.538	9.832
5.0	28.0	5.99	8.50	2.51	2.51	9.014	9.762
5.0	30.0	5.92	8.15	2.23	2.23	10.146	9.748
5.0	32.0	5.92	8.05	2.13	2.13	10.622	9.802
5.0	34.0	5.92	8.10	2.18	2.18	10.378	9.773
5.0	36.0	5.80	7.55	1.75	1.75	12.929	10.145
5.0	38.0	5.11	6.65	1.54	1.38	16.434	10.843
5.0	40.0	4.50	-0-	-0-	-0-	-0-	-0-
5.0	42.0	4.16	-0-	-0-	-0-	-0-	-0-
5.0	44.0	2.88	-0-	-0-	-0-	-0-	-0-
5.0	46.0	3.17	-0-	-0-	-0-	-0-	-0-
5.0	48.0	0.77	-0-	-0-	-0-	-0-	-0-

Note : A value of -0- indicates data point not taken

Table A.8: FHWA 30S 4.0-ft Overtopping Velocity Data (Clopper and Chen, 1988)

Run Number : 45	Date of Test : 09-11-87	Start Time : 7:00 AM
Soil Type : TYPE I, ARMORFLEX	Duration : 10 Hours	End Time : 2:45 PM
Overtopping Depth : 4.0 ft	Water Surface Drop: FF	Photographs: YES
Side Slope : 2:1	Discharge : 90.5 CFS	Video Tape : YES

Time (hr)	Station Number	Velocity (ft/s)		
		0.2 depth	0.6 depth	0.8 depth
0.0	16.0	3.20	6.20	5.20
0.0	20.0	5.40	7.40	7.90
0.0	24.0	5.80	7.10	7.70
0.0	28.0	-0-	9.40	9.60
0.0	32.0	-0-	9.80	10.60
0.0	36.0	10.20	9.60	13.60
0.0	40.0	14.30	13.00	15.60
0.0	44.0	15.50	18.50	18.10
1.0	16.0	4.30	4.70	5.60
1.0	20.0	5.90	6.50	7.00
1.0	24.0	6.10	7.50	7.60
1.0	28.0	9.20	6.20	8.90
1.0	32.0	8.80	9.90	10.20
1.0	36.0	10.80	12.40	13.10
1.0	40.0	-0-	15.40	15.40
1.0	44.0	17.80	18.20	17.90
2.0	16.0	5.00	5.90	5.00
2.0	20.0	6.10	6.10	6.30
2.0	24.0	7.40	7.60	7.90
2.0	28.0	8.60	8.70	8.80
2.0	32.0	9.90	10.40	10.10
2.0	36.0	11.00	12.20	12.50
2.0	40.0	15.30	15.40	15.40
2.0	44.0	18.20	18.20	17.20
3.0	16.0	5.60	5.60	4.00
3.0	20.0	6.20	6.30	6.40
3.0	24.0	7.80	8.20	8.20
3.0	28.0	9.20	9.30	8.80
3.0	32.0	10.00	10.30	10.20
3.0	36.0	11.50	12.30	12.50

Note : A value of -0- indicates data point not taken

Table A.8 (continued): FHWA 30S 4.0-ft Overtopping Velocity Data (Clopper and Chen, 1988)

Time (hr)	Station Number	Velocity (ft/s)		
		0.2 depth	0.6 depth	0.8 depth
3.0	40.0	15.00	15.30	15.50
3.0	44.0	18.40	18.20	17.10
4.0	16.0	5.10	5.30	-0-
4.0	20.0	6.50	6.50	6.10
4.0	24.0	7.70	7.70	7.70
4.0	28.0	9.10	9.20	8.80
4.0	32.0	10.30	10.20	10.10
4.0	36.0	11.70	12.30	12.60
4.0	40.0	15.40	15.50	15.60
4.0	44.0	18.20	18.30	17.40
5.0	15.0	5.40	5.60	3.70
5.0	20.0	-0-	6.10	-0-

Note : A value of -0- indicates data point not taken

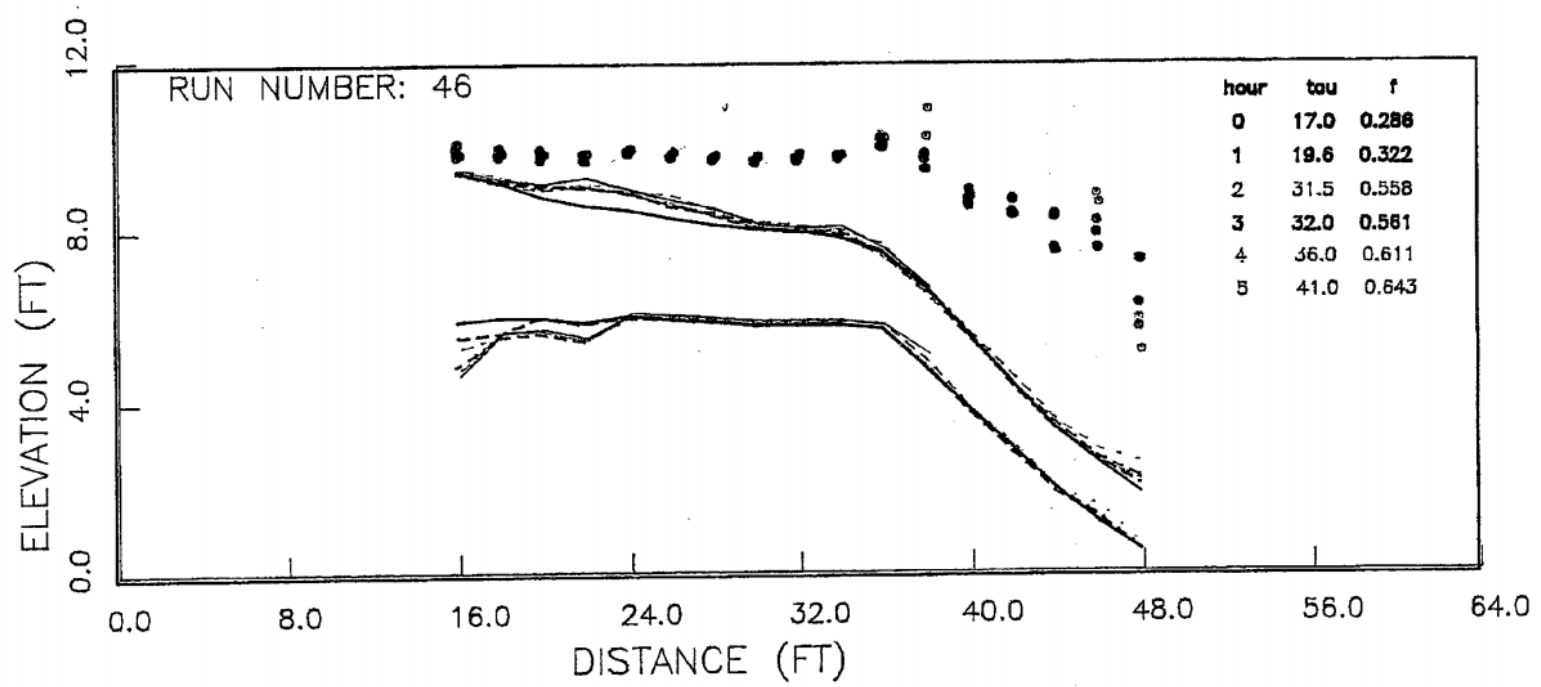


Figure A.4: FHWA 30S 4.0-ft Overtopping Water-surface Profile (Clopper and Chen, 1988)

Table A.9: FHWA 30S 96-cfs Overtopping Data (Clopper and Chen, 1988)

Run Number : 46A Date of Test :10-06-87 Start Time : 12:00 PM
 Soil Type : TYPE I, ARMORFLEX Duration :0.15 Hours End Time : 12:15 PM
 Overtopping Depth : 4.0 ft Water Surface Drop: FF Photographs: YES
 Side Slope : 2:1 Discharge : 96.0 CFS Video Tape : YES

Time (hr)	Station Number	Embankment Elev. (ft)	Water Surface Elev. (feet)	Meas Flow Depth (ft)	Corr Flow Depth (ft)	Ave Vel (ft/s)	EBL Elev (ft)
0.0	16.0	6.26	9.50	3.24	3.24	7.407	10.352
0.0	18.0	6.22	9.35	3.13	3.13	7.668	10.263
0.0	20.0	6.23	9.15	2.92	2.92	8.219	10.199
0.0	22.0	6.13	8.80	2.67	2.67	8.989	10.055
0.0	24.0	6.07	8.50	2.43	2.43	9.877	10.015
0.0	26.0	6.04	8.20	2.16	2.16	11.111	10.117
0.0	28.0	6.04	8.05	2.01	2.01	11.940	10.264
0.0	30.0	5.94	7.80	1.86	1.86	12.903	10.385
0.0	32.0	5.94	7.75	1.81	1.81	13.260	10.480
0.0	34.0	5.93	7.65	1.74	1.74	13.833	10.636
0.0	36.0	5.85	7.30	1.45	1.45	16.552	11.554
0.0	38.0	4.99	6.70	1.71	1.53	15.699	10.527
0.0	40.0	3.90	-0-	-0-	-0-	-0-	-0-
0.0	42.0	3.00	-0-	-0-	-0-	-0-	-0-
0.0	44.0	2.02	4.02	2.00	1.79	13.423	6.818
0.0	46.0	1.10	-0-	-0-	-0-	-0-	-0-
0.0	48.0	0.60	-0-	-0-	-0-	-0-	-0-
1.0	16.0	5.52	-0-	-0-	-0-	-0-	-0-
1.0	18.0	6.14	-0-	-0-	-0-	-0-	-0-
1.0	20.0	6.27	-0-	-0-	-0-	-0-	-0-
1.0	22.0	6.05	-0-	-0-	-0-	-0-	-0-
1.0	24.0	6.00	-0-	-0-	-0-	-0-	-0-
1.0	26.0	5.98	-0-	-0-	-0-	-0-	-0-
1.0	28.0	5.98	-0-	-0-	-0-	-0-	-0-
1.0	30.0	5.94	-0-	-0-	-0-	-0-	-0-
1.0	32.0	5.87	-0-	-0-	-0-	-0-	-0-
1.0	34.0	5.46	-0-	-0-	-0-	-0-	-0-
1.0	36.0	4.70	-0-	-0-	-0-	-0-	-0-
1.0	38.0	4.06	-0-	-0-	-0-	-0-	-0-
1.0	40.0	3.27	-0-	-0-	-0-	-0-	-0-
1.0	42.0	2.69	-0-	-0-	-0-	-0-	-0-
1.0	44.0	2.75	-0-	-0-	-0-	-0-	-0-
1.0	46.0	2.61	-0-	-0-	-0-	-0-	-0-
1.0	48.0	1.63	-0-	-0-	-0-	-0-	-0-

Note : A value of -0- indicates data point not taken

Table A.10: FHWA 30S 96-cfs Overtopping Velocity Data (Clopper and Chen, 1988)

Run Number : 46A	Date of Test : 10-05-87	Start Time : 12:00 PM
Soil Type : TYPE I, ARMORFLEX	Duration : 0.15 Hours	End Time : 12:15 PM
Overtopping Depth : 4.0 ft	Water Surface Drop: FF	Photographs: YES
Side Slope : 2:1	Discharge : 96.0 CFS	Video Tape : YES

Time (hr)	Station Number	Velocity (ft/s)		
		0.2 depth	0.6 depth	0.8 depth
0.0	18.0	-0-	-0-	-0-
0.0	16.0	-0-	5.40	5.40
0.0	20.0	-0-	-0-	-0-
0.0	22.0	-0-	-0-	-0-
0.0	24.0	-0-	-0-	-0-
0.0	26.0	-0-	-0-	-0-
0.0	28.0	-0-	-0-	-0-
0.0	30.0	-0-	-0-	-0-
0.0	32.0	-0-	-0-	-0-
0.0	34.0	-0-	-0-	-0-
0.0	36.0	-0-	-0-	-0-
0.0	38.0	-0-	-0-	-0-
0.0	40.0	-0-	-0-	-0-
0.0	42.0	-0-	-0-	-0-
0.0	44.0	-0-	-0-	-0-
0.3	16.0	-0-	-0-	-0-
0.3	20.0	-0-	-0-	-0-
0.3	22.0	-0-	-0-	-0-
0.3	24.0	-0-	-0-	-0-
0.3	26.0	-0-	-0-	-0-
0.3	28.0	-0-	-0-	-0-
0.3	30.0	-0-	-0-	-0-
0.3	32.0	-0-	-0-	-0-
0.3	34.0	-0-	-0-	-0-
0.3	36.0	-0-	-0-	-0-
0.3	38.0	-0-	-0-	-0-
0.3	40.0	-0-	-0-	-0-
0.3	42.0	-0-	-0-	-0-
0.3	44.0	17.90	17.90	18.00
0.3	46.0	-0-	-0-	-0-
0.3	48.0	-0-	-0-	-0-

Note : A value of -0- indicates data point not taken

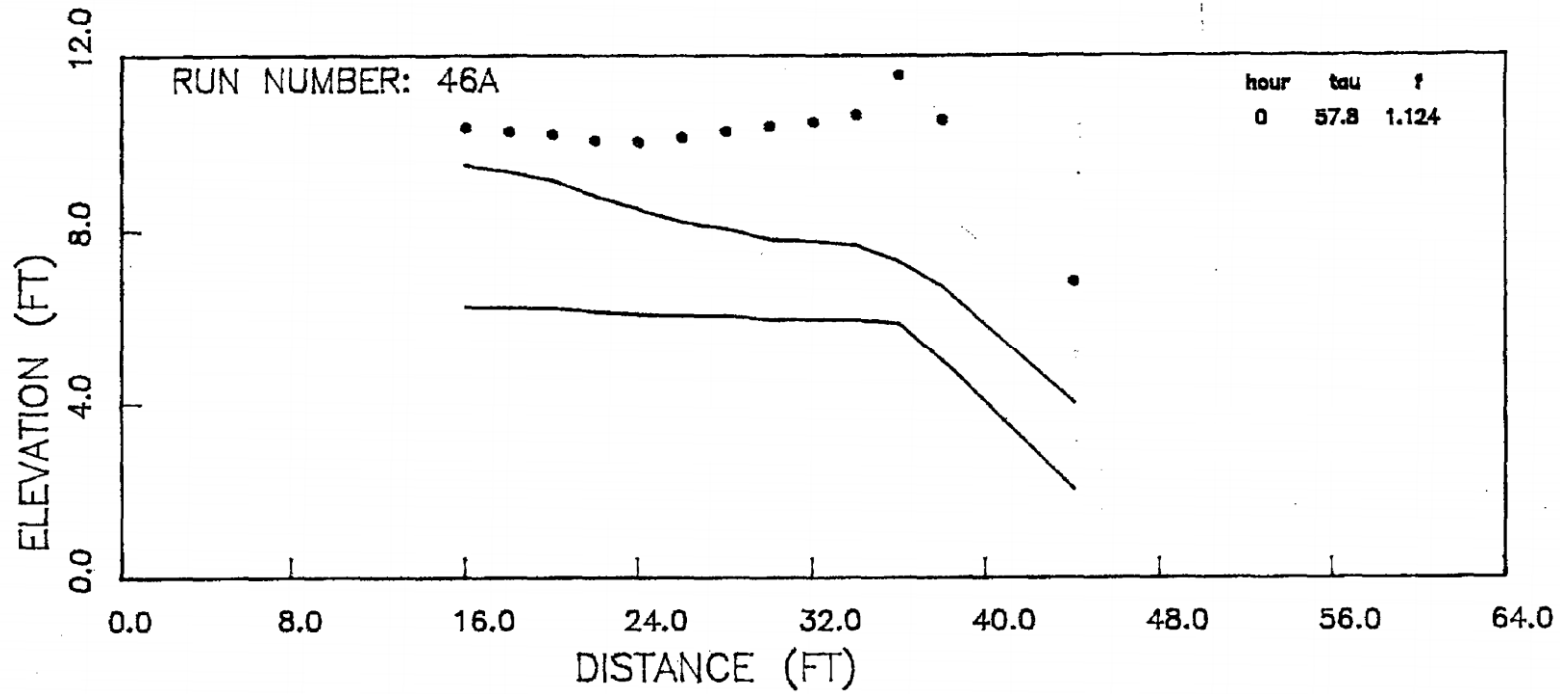
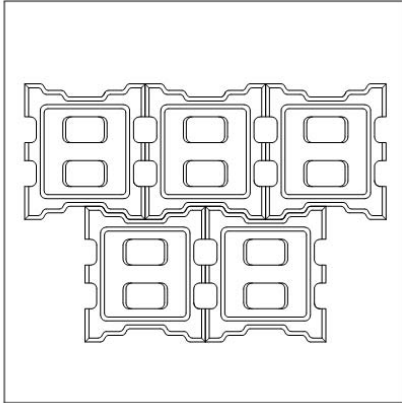


Figure A.5: FHWA 30S 96-cfs Overtopping Water-surface Profile (Clopper and Chen, 1988)

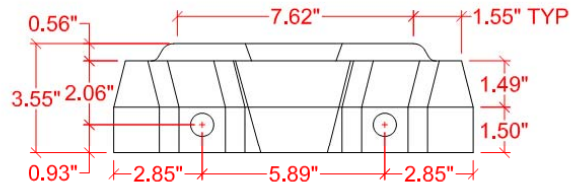
APPENDIX B

ACB BLOCK DIMENSIONS AND PHYSICAL PROPERTIES

30S BLOCK SPECIFICATIONS



BLOCK PROPERTIES	
DRY WEIGHT:	35.3 lbs
SUBMERGED WEIGHT:	19.8 lbs
VOLUME:	0.25 ft ³
VOID RATIO:	21 %



SAFETY FACTOR PROPERTIES	
A_B :	0.76 ft ²
C_L :	0.0972
l_1 :	0.20 ft
l_2 :	0.54 ft
$l_{3\text{ NCMA}}$:	0.32 ft
$l_{3\text{ New SF}}$:	0.40 ft
l_4 :	0.54 ft
l_5 :	0.48 ft
l_6 :	0.48 ft
l_7 :	0.73 ft
l_8 :	0.73 ft

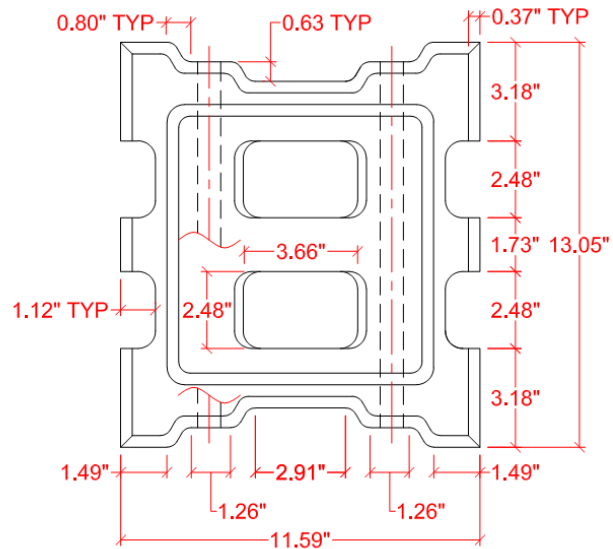
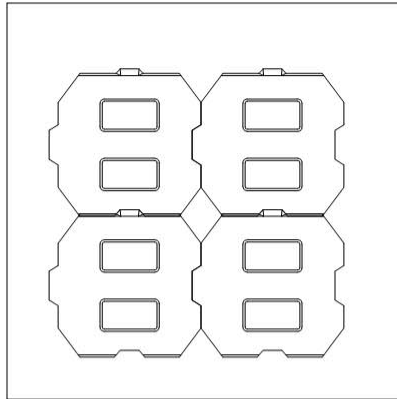
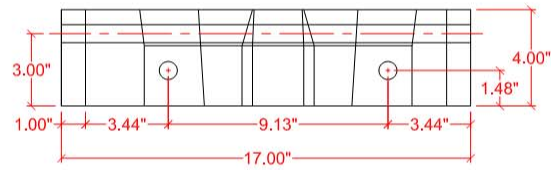


Figure B.1: 30S Block Dimensions and Physical Properties

PETRAFLEX BLOCK SPECIFICATIONS



BLOCK PROPERTIES	
DRY WEIGHT:	33.2 lbs
SUBMERGED WEIGHT:	18.6 lbs
VOLUME:	0.23 ft ³
VOID RATIO:	25 %



SAFETY FACTOR PROPERTIES

A_B :	1.40 ft ²
C_L :	0.0178
l_1 :	0.17 ft
l_2 :	0.66 ft
$l_{3 \text{ NCMA}}$:	0.27 ft
$l_{3 \text{ New SF}}$:	0.33 ft
l_4 :	0.66 ft
l_5 :	0.71 ft
l_6 :	0.71 ft
l_7 :	0.81 ft
l_8 :	0.81 ft

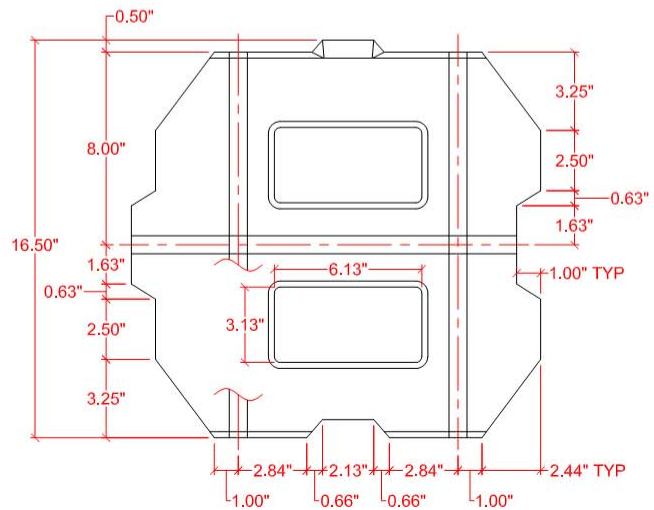
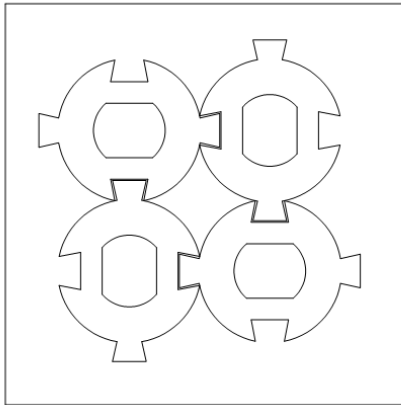
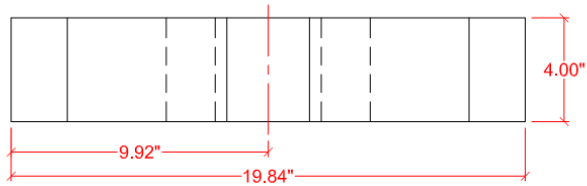


Figure B.2: Petraflex Block Dimensions and Physical Properties

USACE BLOCK SPECIFICATIONS



BLOCK PROPERTIES	
DRY WEIGHT:	50.7 lbs
SUBMERGED WEIGHT:	28.4 lbs
VOLUME:	0.36 ft ³
VOID RATIO:	36 %



SAFETY FACTOR PROPERTIES	
A_B :	1.14 ft ²
C_L :	0.115
l_1 :	0.17 ft
l_2 :	0.65 ft
$l_{3\text{ NCMA}}$:	0.26 ft
$l_{3\text{ New SF}}$:	0.33 ft
l_4 :	0.65 ft
l_5 :	0.83 ft
l_6 :	0.83 ft
l_7 :	0.65 ft
l_8 :	0.65 ft

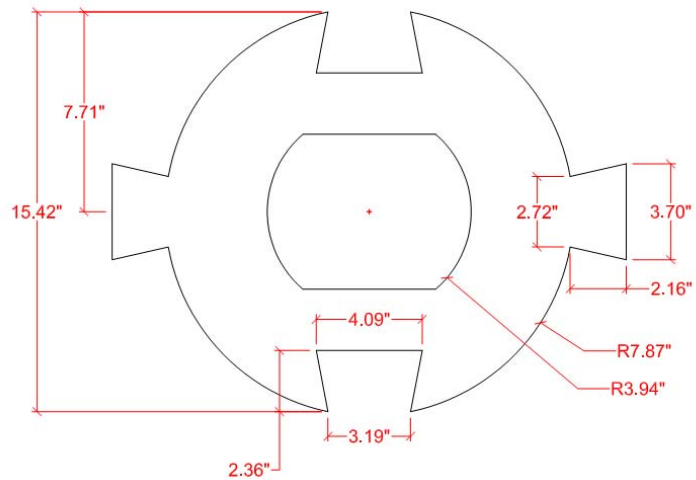


Figure B.3: Corps Block Dimensions and Physical Properties

APPENDIX C

HYDRAULIC DATA FOR CSU TESTING

Table C.1: Hydraulic Data for CSU 30S Test (Robeson *et al.*, 2002) on 0.499 Bed Slope at 10.0 cfs (8-11-2000)

Station along Slope (ft)	Horizontal Station (ft)	Bed Elevation (ft)	Flow Depth (ft)	Vertical Depth (ft)	Continuity Velocity (ft/s)
20.89	17.86	101.52	0.24	0.28	6.96
22.98	19.65	100.66	0.21	0.24	8.12
25.07	21.44	99.73	0.25	0.29	6.72
27.17	23.23	98.86	0.27	0.32	6.09
29.17	24.94	97.98	0.14	0.16	12.18
31.26	26.73	97.15	0.19	0.22	8.86
33.35	28.52	96.23	0.17	0.20	10.00
35.45	30.31	95.31	0.16	0.19	10.26
37.54	32.10	94.48	0.15	0.17	11.46
39.63	33.89	93.55	0.14	0.16	12.18
41.72	35.68	92.60	0.17	0.20	10.00

Table C.2: Hydraulic Data for CSU 30S Test on 0.431 Bed Slope at 8.0 cfs (6-25-2009)

Station along Slope (ft)	Horizontal Station (ft)	Bed Elevation (ft)	Flow Depth ^a (ft)	Vertical Depth (ft)	Continuity Velocity (ft/s)
55.32	49.57	90.43	0.27	0.30	5.03
57.40	51.44	89.63	0.28	0.31	4.73
59.40	53.23	88.83	0.26	0.29	5.21
61.42	55.04	88.04	0.23	0.25	5.84
63.45	56.85	87.28	0.22	0.24	6.13
65.45	58.65	86.52	0.22	0.25	6.04
67.50	60.48	85.72	0.23	0.26	5.76
69.50	62.27	84.96	0.22	0.25	5.96
71.55	64.11	84.15	0.23	0.25	5.92
73.55	65.90	83.41	0.22	0.24	6.08
75.60	67.74	82.58	0.22	0.24	6.08
77.59	69.53	81.80	0.23	0.25	5.92

^aAdjusted for point gage offset

Table C.3: Hydraulic Data for CSU 30S Test on 0.431 Bed Slope at 12.0 cfs (6-25-2009)

Station along Slope (ft)	Horizontal Station (ft)	Bed Elevation (ft)	Flow Depth ^a (ft)	Vertical Depth (ft)	Continuity Velocity (ft/s)
55.32	49.57	90.44	0.24	0.27	5.51
57.40	51.44	89.64	0.19	0.22	6.90
59.40	53.23	88.84	0.20	0.23	6.57
61.42	55.04	88.05	0.18	0.20	7.26
63.45	56.85	87.29	0.20	0.23	6.57
65.45	58.65	86.53	0.20	0.23	6.57
67.50	60.48	85.72	0.20	0.23	6.57
69.50	62.27	84.97	0.19	0.22	6.90
71.55	64.11	84.15	0.19	0.22	6.90
73.55	65.90	83.42	0.20	0.23	6.57
75.60	67.74	82.59	0.19	0.22	6.90
77.59	69.53	81.81	0.21	0.24	6.26

^aAdjusted for point gage offset

Table C.4: Hydraulic Data for CSU 30S Test on 0.230 Bed Slope at 10.0 cfs (6-14-2009)

Station along Slope (ft)	Horizontal Station (ft)	Bed Elevation (ft)	Flow Depth (ft)	Vertical Depth (ft)	Continuity Velocity (ft/s)
9.27	9.01	97.93	0.29	0.30	5.79
11.27	10.96	97.48	0.31	0.31	5.45
13.28	12.91	97.03	0.28	0.29	6.00
15.28	14.86	96.58	0.25	0.25	6.72
17.28	16.81	96.13	0.24	0.24	7.06
19.29	18.76	95.69	0.24	0.25	6.96
21.29	20.71	95.24	0.25	0.26	6.64
23.29	22.66	94.79	0.24	0.25	6.86
25.30	24.61	94.34	0.24	0.25	6.82
27.30	26.56	93.89	0.24	0.24	7.01
29.31	28.51	93.44	0.24	0.24	7.01
31.31	30.45	93.00	0.24	0.25	6.82
33.31	32.40	92.55	0.24	0.25	6.91
35.32	34.35	92.10	0.09	0.09	19.27

Table C.5: Hydraulic Data for CSU 30S Test on 0.230 Bed Slope at 20.0 cfs (6-15-2009)

Station along Slope (ft)	Horizontal Station (ft)	Bed Elevation (ft)	Flow Depth (ft)	Vertical Depth (ft)	Continuity Velocity (ft/s)
9.27	9.01	97.93	0.53	0.55	3.14
11.27	10.96	97.48	0.53	0.54	3.17
13.28	12.91	97.03	0.46	0.48	3.59
15.28	14.86	96.58	0.38	0.39	4.36
17.28	16.81	96.13	0.40	0.41	4.14
19.29	18.76	95.69	0.42	0.43	3.98
21.29	20.71	95.24	0.40	0.42	4.12
23.29	22.66	94.79	0.39	0.40	4.32
25.30	24.61	94.34	0.37	0.38	4.51
27.30	26.56	93.89	0.34	0.35	4.91
29.31	28.51	93.44	0.33	0.34	5.11
31.31	30.45	93.00	0.33	0.34	5.06
33.31	32.40	92.55	0.34	0.35	4.91
35.32	34.35	92.10	0.36	0.37	4.62

Table C.6: Hydraulic Data for CSU 30S Test on 0.230 Bed Slope at 30.0 cfs (6-15-2009)

Station along Slope (ft)	Horizontal Station (ft)	Bed Elevation (ft)	Flow Depth (ft)	Vertical Depth (ft)	Continuity Velocity (ft/s)
9.27	9.01	97.93	0.80	0.83	2.07
11.27	10.96	97.48	0.70	0.72	2.37
13.28	12.91	97.03	0.63	0.65	2.65
15.28	14.86	96.58	0.56	0.57	2.98
17.28	16.81	96.13	0.53	0.54	3.15
19.29	18.76	95.69	0.53	0.54	3.15
21.29	20.71	95.24	-	-	-
23.29	22.66	94.79	-	-	-
25.30	24.61	94.34	-	-	-
27.30	26.56	93.89	-	-	-
29.31	28.51	93.44	-	-	-
31.31	30.45	93.00	-	-	-
33.31	32.40	92.55	-	-	-
35.32	34.35	92.10	-	-	-

Table C.7: Hydraulic Data for CSU Petraflex Test (Robeson *et al.*, 2002) on 0.501 Bed Slope at 10.0 cfs (8-21-2000)

Station along Slope (ft)	Horizontal Station (ft)	Bed Elevation (ft)	Flow Depth (ft)	Vertical Depth (ft)	Continuity Velocity (ft/s)
20.85	17.80	101.50	0.28	0.32	6.05
22.86	19.51	100.64	0.23	0.27	7.30
25.04	21.38	99.67	0.16	0.19	10.41
27.05	23.09	98.82	0.16	0.19	10.27
29.23	24.95	97.89	0.17	0.20	9.76
31.24	26.67	97.03	0.16	0.19	10.41
33.42	28.53	96.11	0.17	0.20	9.64
35.43	30.25	95.28	0.15	0.18	11.00
37.61	32.11	94.35	0.15	0.18	10.85
39.62	33.83	93.47	0.17	0.19	10.10
41.80	35.69	92.47	0.15	0.18	10.85

Table C.8: Hydraulic Data for CSU 30S Test (Robeson *et al.*, 2002) on 0.501 Bed Slope at 28.4 cfs (8-21-2000)

Station along Slope (ft)	Horizontal Station (ft)	Bed Elevation (ft)	Flow Depth (ft)	Vertical Depth (ft)	Continuity Velocity (ft/s)
20.85	17.80	101.48	0.64	0.75	2.60
22.86	19.51	100.62	0.55	0.65	3.00
25.04	21.38	99.65	0.47	0.55	3.55
27.05	23.09	98.81	0.46	0.54	3.62
29.23	24.95	97.89	0.43	0.50	3.90
31.24	26.67	96.95	0.27	0.32	6.10
33.42	28.53	96.11	0.30	0.35	5.58
35.43	30.25	95.29	0.28	0.33	5.92
37.61	32.11	94.35	0.37	0.43	4.54
39.62	33.83	93.48	0.43	0.50	3.90
41.80	35.69	92.49	0.51	0.60	3.25